

ABSTRACT

Inhibitors of Human Cathepsin L and Cruzain as Therapeutic Agents

Wara Milenka Arispe Angulo, Ph.D.

Mentor: Mary Lynn Trawick, Ph.D.

Increased human cathepsin L activity is linked to invasive and metastatic cancers where it promotes degradation of the extracellular matrix. This major cysteine protease found in cell lysosomes and secreted from tissues, also plays a role in the pathology of degenerative cartilage and neurological disorders, and is reported to be required for the SARS coronavirus infection. A library of 59 small non-peptidic thiosemicarbazone and α , β -unsaturated carbonyl derivatives of benzophenone, propiophenone, α - and β -tetralone, 4-chromanone, and 4-thiochromenone were evaluated as inhibitors of human cathepsin L. While most of the compounds had IC₅₀ values in the range of 0.4 μ M or greater, four were very effective inhibitors of cathepsin L: the benzophenone thiosemicarbazones **2** (IC₅₀= 1.5 nM), **55** (IC₅₀= 44 nM), **38** (IC₅₀= 60 nM), **32** (IC₅₀= 66 nM), and **37** (IC₅₀= 140 nM) and a sulfone analog of the bromo substituted thiochroman-4-one **22** (IC₅₀= 1 nM). Kinetics studies were used to gain understanding in enzyme-inhibitor interactions of the most potent compounds (**2** and **22**) and they were found to be reversible, slow, tight binding inhibitors of cathepsin L. These data support formation of a transient covalent intermediate between thiosemicarbazone inhibitors and the cathepsin

L active site thiolate. Ten of the most promising lead compounds were also tested for cytotoxicity in HEK-293 cells and generated no toxicity after 24 hours. Exposure of the prostate cancer cell line DU-145 to the most promising lead compounds successfully decreased the invasiveness and mobility properties of these cells in vitro. The non-peptidic nature of these inhibitors, coupled with their cell-based activity, makes these compounds very promising leads for the development of selective cathepsin L inhibitors. A separate research project consisted of recombinant cruzain purification and evaluation of thiosemicarbazone derivatives as potential inhibitors of this parasitic cysteine protease. Cruzain is the major cysteine protease of *Trypanosoma cruzi* organism and is a validated therapeutic target for the development of new chemotherapy. Chagas disease, a result of *Trypanosoma cruzi* infection, is the third largest parasitic disease challenge worldwide after malaria and leishmania and there is an urgent need for development of new therapeutic agents against Chagas disease. From the same library of thiosemicarbazone derivatives evaluated against cathepsin L, 25 compounds were evaluated against cruzain from which six compounds were in the nanomolar range with IC_{50} values ranging from 170 nM to 622 nM.

Inhibitors of Human Cathepsin L and Cruzain as Therapeutic Agents

by

Wara Milenka Arispe Angulo, Licentiate

A Dissertation

Approved by the Department of Chemistry and Biochemistry

David E. Pennington, Ph.D., Interim Chairperson

Submitted to the Graduate Faculty of
Baylor University in Partial Fulfillment of the
Requirements for the Degree
of
Doctor of Philosophy

Approved by the Dissertation Committee

Mary Lynn Trawick, Ph.D., Chairperson

Lizbeth Souza-Fuertes, Ph.D.

Gouri S. Jas, Ph.D.

Kevin G. Pinney, Ph.D.

Sung-Kun Kim, Ph.D.

Accepted by the Graduate School
December 2008

J. Larry Lyon, Ph.D., Dean

Copyright © 2008 by Wara Milenka Arispe Angulo

All rights reserved

TABLE OF CONTENTS

List of Figures	vii
List of Tables	xi
List of Schemes	xii
List of Abbreviations	xiv
Acknowledgements.....	xvi
Dedication.....	xviii
Chapter One	1
Statement of the Problem and Significance	1
Chapter Two.....	5
Introduction to Cysteine Proteases.....	5
Papain-Like Cysteine Proteases.....	6
Amino Acid Sequence	6
Fold and Topology.....	9
Substrate-Binding Sites.....	11
Catalytic Mechanism	21
Cysteine Proteases's Intracellular and Tissue Distribution	23
The Stefin Family	26
Role of Cysteine Proteases in Pathological Conditions.....	28
Chapter Three.....	81
Experimental Procedures for the Biochemical and Biological Evaluation of Cathepsin L Inhibitors.....	81
Aminomethylcoumarin (AMC) Standard Curve	84
<i>K_M</i> and <i>V_{max}</i> Determination of Cathepsin L.....	85

IC ₅₀ Determination (Cuvette Assay Formate).....	86
Microplate Assay for IC ₅₀ Determination.....	88
Time Dependent Inhibition Study of the best Thiosemicarbazone Inhibitors against Cathepsin L.....	88
Reversibility Studies.....	89
Cell Culture Media Supplementation.....	92
Maintenance of Cell Culture in Dishes and Flasks.....	93
Cell Subculture Procedure.....	94
Cell Freezing Procedure.....	94
Cell Thawing Procedure.....	95
Trypan Blue Exclusion Assay.....	95
Preliminary Cytotoxicity Studies.....	97
Determination of Cathepsin L Activity on DU-145 Cell Culture.....	97
Cell Invasion and Motility Studies.....	98
DC Assay for Total Protein Concentration Determination.....	100
Western Blot Protocol for DU 145 Cells.....	101
Sample Preparation Protocol.....	101
SDS-PAGE Protocol.....	102
Western Blot Protocol.....	103
Chapter Four.....	106
Results and Discussion.....	106
Biochemical Evaluation of Potential Cathepsin L Inhibitors.....	106
Cathepsin L Assay.....	107
Thiosemicarbazones (TSC) as Inhibitors of Cathepsin L.....	121
Advanced Kinetic Studies.....	132
Advanced Cell Culture Studies.....	141

General Considerations	141
Preliminary Cytotoxicity Studies	141
Determination of Cathepsin L Activity on Mammalian Cell Culture.....	142
Cell Invasion and Motility Studies	143
Western Blot Analysis for Cathepsin L in DU 145 Cells	150
Chapter Five.....	154
General Section for Chemical Sources and Materials	154
Recombinant Cruzain Purification Procedure	158
Protein Expression	159
Cell Lysis and Isolation of Inclusion Bodies	160
Protein Refolding	160
Cruzain Purification and Analysis of Column Fractions	160
Analysis of Column Fractions	161
Activity Determination	162
Total Protein Concentration	162
SDS-PAGE	163
Activation of rCruzain	164
K_M and V_{max} Determination of Cruzain.....	165
IC_{50} Determination of Potential Cruzain Inhibitors	166
Chapter Six.....	168
Recombinant Cruzain Purification Results.....	168
Cruzain Purification and Analysis of Column Fractions Results	169
V_{max} and K_M Results of Cruzain	173
IC_{50} Determination Results.....	174
Thiosemicarbazones as Inhibitors of Cruzain Results	175

Chapter Seven	184
Conclusions and Future Directions	184
Appendix A	189
Appendix B	256
Appendix C	257
Appendix D	292
References	296

LIST OF FIGURES

Figure 1.	Amino acid sequence alignment of human lysosomal cathepsins and related parasite cysteine proteases.	8
Figure 2.	Superimposition of cathepsin L (blue) and cruzain (red).	9
Figure 3.	Fold of cathepsin L.	10
Figure 4.	Fold of procathepsin L.	11
Figure 5.	Diagrammatic representation of peptide substrate interaction with the active site pockets of a cysteine protease.	12
Figure 6.	Substrate-binding sites.	14
Figure 7.	Low molecular weight inhibitor binding geometry.	16
Figure 8.	Schemes of three most frequent reactive groups before and after binding to the reactive-site cysteine.	17
Figure 9.	Epoxysuccinyl derivatives.	18
Figure 10.	Evolution of 'Smith-Kline' compounds.	19
Figure 11.	A detailed view of the binding pocket of cathepsin L.	20
Figure 12.	Catalytic mechanism of cysteine proteases.	22
Figure 13.	Stabilization of the oxyanion generated by the cysteine protease catalytic reaction.	22
Figure 14.	Binding of protein inhibitors.	26
Figure 15.	Diagrammatic representation of metastasis.	30
Figure 16.	Diagrammatic representation of extracellular matrix components.	31
Figure 17.	Diagrammatic representation of a cell invasion assay.	34
Figure 18.	Structure of benznidazole (Bnz) and nifurtimox (Nfx).	36
Figure 19.	Diagram of <i>T. cruzi</i> morphologies.	37
Figure 20.	Overview of <i>Trypanosoma cruzi</i> stages.	38

Figure 21.	Diagram of the cruzain genomic organization of the gene as a tandem repeat of at least six copies.	41
Figure 22.	Plasmid vector used to express the <i>T. cruzi</i> cysteine protease in bacteria.	42
Figure 23.	Scheme of the processing events to yield active cruzain.	43
Figure 24.	Typical Michaelis-Menten Plot.....	46
Figure 25.	General kinetic scheme for competitive inhibition.....	48
Figure 26.	Plot of initial velocity of a simple Michaelis-Menten reaction of a competitive inhibitor [I].....	49
Figure 27.	General kinetic model of mixed inhibition.....	50
Figure 28.	Plot of initial velocity of a simple Michaelis-Menten reaction of a mixed inhibitor [I].....	51
Figure 29.	General kinetic model for uncompetitive inhibition.....	52
Figure 30.	Plot of initial velocity of a simple Michaelis-Menten reaction of an uncompetitive inhibitor [I].....	53
Figure 31.	The Lineweaver-Burk graph as a tool to distinguish types of reversible inhibition.	54
Figure 32.	Time dependent inhibitor profile.	56
Figure 33.	Kinetic schemes for three mechanisms of slow inhibition.	58
Figure 34.	Representative examples of slow binding progress curves.....	60
Figure 35.	A typical Williams-Morrison plot.....	63
Figure 36.	Typical IC ₅₀ curve for competitive inhibitors.....	64
Figure 37.	Odanacatib chemical structure.	66
Figure 38.	Functional groups of reported cysteine proteases inhibitors.....	67
Figure 39.	Binding modes of epoxysuccinyl derivative.....	70
Figure 40.	Cathepsin L inhibitor Katunuma (CLIK)	71
Figure 41.	Schematic representation of aziridinyl peptides	73
Figure 42.	Inhibition of cathepsin B and L by 6-substituted oxapenam.....	74

Figure 43.	Effect of the oxidation state of sulfur in 6-substituted penams on the inhibition of cathepsin.....	74
Figure 44.	Cyanamides as inhibitors of cathepsin K and L.....	76
Figure 45.	Homophenylalanine containing vinyl sulfones are highly potent inhibitors of papain-like enzymes.....	77
Figure 46.	Ethacrynic acid derivatives inhibit cysteine proteases.....	78
Figure 47.	Thiosemicarbazone scaffold.	79
Figure 48.	Inhibition of a cysteine protease with a thiosemicarbazone.	80
Figure 49.	Scheme of cell number determination with the hemocytometer.	96
Figure 50.	Assembled transfer stack for Western blot experiments.....	104
Figure 51.	Non-fluorescent peptide substrate Z-FR-AMC reaction.....	108
Figure 52.	Monitoring of the Z-FR-AMC hydrolysis by cathepsin L in the presence of increasing concentrations of inhibitor.	108
Figure 53.	Dependence of cathepsin L activity on substrate concentration.	110
Figure 54.	Typical IC ₅₀ determination using the dose-response sigmoid model from the GraphPad Prism 4.03 software.....	112
Figure 55.	Plot of initial velocity of a simple Michaelis-Menten reaction versus the substrate concentration [S] in the presence of different concentrations of a inhibitor [I].	136
Figure 56.	Time-dependent inhibition kinetics of compound 2 and 22	137
Figure 57.	Michaelis-Menten plot compound 2 and 22	138
Figure 58.	Williams-Morrison equation as the fitting model of compounds 2 and 22 kinetic data.	139
Figure 59.	Cathepsin L inhibitors tested for cytotoxicity.....	146
Figure 60.	Cell viability using the trypan blue exclusion assay.	146
Figure 61.	Inhibition of cathepsin L activity in DU-145 cell conditioned media by compounds 2 and 22	147
Figure 62.	Inhibition of cathepsins L activity in DU-145 cell lysates by compounds 2 and 22	147

Figure 63.	Invasiveness studies with DU-145 cells.	149
Figure 64.	Motility assay results.	150
Figure 65.	Immunodetection of cathepsin L in DU 145 cell lysates and cell conditioned media.	152
Figure 66.	Immunodetection of cathepsin L in DU 145 cell lysates and cell conditioned media compared to commercial human liver cathepsin L.	152
Figure 67.	Immunodetection of cathepsin L in concentrated DU 145 cell lysates and cell conditioned media.	153
Figure 68.	Elution gradient used for cruzain purification.	161
Figure 69.	Elution profile of four proteins from a Bio-Rad column standard kit.	169
Figure 70.	Elution profile of sample run in Q Sepharose Fast Flow column.	170
Figure 71.	Cruzain auto-activation monitoring profile.	171
Figure 72.	SDS-PAGE analysis of two purified and concentrated recombinant cruzain samples.	172
Figure 73.	SDS-PAGE Calibration curve.	173
Figure 74.	Dependence of cathepsin L activity on substrate concentration.	174

LIST OF TABLES

Table 1.	Inhibitor Serial Dilution Preparation.	83
Table 2.	Preparation Table for AMC Standards.	85
Table 3.	Preparation of Z-FR-AMC Stock Solutions.	86
Table 4.	Preparation of Z-FR-AMC Solutions in 7% DMSO.....	86
Table 5.	Preparation Table for IC ₅₀ Determination Experiment.	87
Table 6.	Preparation Table for Time Dependence Inhibition Studies.....	89
Table 7.	Preparation Table for Reversibility Studies.....	90
Table 8.	Inhibition of Cathepsin L by TSC Analogues and other Novel Cyclic Compounds.....	113
Table 9.	Comparison between IC ₅₀ and % Cell Invasion and %Motility	148
Table 10.	Inhibitor Serial Dilution Preparation.	158
Table 11.	Preparation of Z-FR-AMC Stock Solutions.	165
Table 12.	Preparation of Z-FR-AMC Solutions in 7% DMSO.....	166
Table 13.	Preparation Table for IC ₅₀ Determination Experiment.....	167
Table 14.	Inhibition of Cruzain by TSC Analogues and other Novel Cyclic Compounds.	181

LIST OF SCHEMES

Scheme 1.	Benzophenone thiosemicarbazone derivatives.	121
Scheme 2.	Para-linked m-bromobenzophenone derivatives.....	122
Scheme 3.	Para-substitution in both aromatic rings of bromobenzophenone derivatives	123
Scheme 4.	Halogen monosubstitution in bromobenzophenone derivatives.	124
Scheme 5.	Comparison between bromobenzophenone TSC derivatives.	124
Scheme 6.	Propiophenone thiosemicarbazone derivatives.....	125
Scheme 7.	Potency trend in α -tetralone monobromo derivatives.....	126
Scheme 8.	Potency trend in α -tetralone derivatives	126
Scheme 9.	Thiosemicarbazone derivatives of the sulfone analog of a substituted thiochroman-4-one.....	127
Scheme 10.	Potency trend in halogenated and unhalogenated substituted α -tetralone series.	128
Scheme 11.	Potency trends related to the bromination effect in β -tetralone thiosemicarbazone derivatives.....	129
Scheme 12.	Indaone and connected ring systems thiosemicarbazone derivatives evaluated.	130
Scheme 13.	Potency trends in naphthalene derivatives.....	131
Scheme 14.	Evaluated aziridine derivatives and other cyclic compounds.	131
Scheme 15.	Benzophenone thiosemicarbazone derivatives	176
Scheme 16.	Para-substitution in both aromatic rings of bromobenzophenone derivatives.....	177
Scheme 17.	Comparison between mono and disubstitution in bromobenzophenone TSC derivatives.....	178
Scheme 18.	Thiosemicarbazone derivatives of the sulfone analog of a substituted thiochroman-4-one.....	179

Scheme 19.	Potency trend in halogenated α -tetralone compounds.	180
Scheme 20.	Evaluated aziridine derivatives and other cyclic compounds.	180

LIST OF ABBREVIATIONS

°C	Degrees Celsius
PI	Propidium iodide
Z-FR-AMC	Substrate benzyloxycarbonyl-L-phenylalaninyl-L-argininyl-7-amido-4-methylcoumarin
AMC	7-Amino-4-methylcoumarin
E-64	<i>L-trans</i> -Epoxy succinyl-leucylamido(4-guanidino)butane
NaOAc	Anhydrous sodium acetate
EDTA	Ethylenediaminetetraacetic acid
DMSO	Dimethyl sulfoxide
DU-145	Human prostate carcinoma cell line
HEK-293	Human epithelial kidney cell line
ATCC	American Type Culture Collection
DMSO	Dimethyl sulfoxide
IC ₅₀	Inhibitor concentration when the activity of a given enzyme is reduced to 50%
KM	Michaelis-Menten constant
ECL	Enhanced chemiluminescence
IPTG	Isopropyl β-D-1-thiogalactopyranoside
HRP	Horseradish peroxidase
NaCl	Sodium chloride
PMSF	Phenylmethylsulphonyl fluoride
Amp	Ampicillin

MW	Molecular weight (in g/mol)
NaOAc	Sodium acetate
TSC	Thiosemicarbazone
DMEM	Dulbecco's Modified Eagle's Medium
PBS	Phosphate Buffer Solution
DTT	Dithiothreitol

ACKNOWLEDGEMENTS

I thank God for my life on this earth and for giving me strength to overcome adversity.

I am grateful to my advisor Dr. Mary Lynn Trawick for the opportunity she gave me to work in her research group. I am deeply appreciative for her suggestions and guidance along my graduate career.

I am greatly thankful to all of my committee members, Dr. Gouri Jas, Dr. Kevin Pinney, Dr. Kim Sung-Kun, and Dr. Lizbeth Souza-Fuertes for their encouragement, guidance, and advice throughout this process. I would like also to offer my everlasting gratitude to Dr. Carlos Manzanares for giving me the opportunity to pursue my graduate studies at Baylor University and for always being willing to listen. Thank you so much Dr. Manzanares, I am truly grateful and indebted.

I am uniquely and foremost grateful to my family for their love, motivation, and understanding that sustained me to complete this work. I have been always looking to my parents as a model, and trying to follow their footsteps in academic career and integrity.

I wish to thank my dear friend Yani Perez for her support and understanding that sustained me to complete this work and for sharing with me unforgettable “tiempitos de calidad”. I am so lucky to be your friend.

I am deeply grateful to my beloved friend Herman Meza for his love, support, and encouragement. His contribution throughout my studies is beyond words of recognition.

I would like to thank all the former and current members of the Trawick's research group with whom I had the privilege of working together. Special thanks go to Amanda Charlton-Sevcik and John Hall for their friendship and encouragement. I am also deeply grateful to Gustavo Chavarria, Maryuri Roca, Benon Mugabe, Sam Chen, and Francisco Gonzalez. I would like to especially thank to my undergraduate research assistants: Julio Osorio, Lauren Adamson and Stephanie Li for their hard work towards our research projects.

I would like to thank to my dear friends: Tessa Coronado, Jigna Patel, Helena Diez y Riega, Gerardo Elguezabal, Monica Elguezabal, Vanessa Castleberry and Jose Boquin for all the love, encouragement, and friendship they gave to me and for making the graduate school an experience I will never forget.

My appreciation also goes to Dr. Diane Wycuff for being such a good role model of women in science.

I would like to thank Nancy Kallus, Andrea Johnson, Adonna Cook, Virginia Hynek, and Patricia Diamond for all their help during these years. I am also thankful to the staff at the International Student and Scholar Services Office for their valuable support and guidance.

I wish to thank Dr. Kishore Gaddale, Dr. Ming Zhou, Rogelio Siles, Freeland Ackley, Jiangli Song, and Lindsay Jones for the synthesis of the compounds evaluated in this study.

Last but certainly not least, I thank Baylor University and OXiGENE Inc. for the generous financial support of my research.

DEDICATION

To

My beloved parents, Miguel and Maria Luisa

My adored grandmother, Casimira

My wonderful sisters, Karen and Tania

My favorite brother, Victor

With love and gratitude

CHAPTER ONE

Statement of the Problem and Significance

Cysteine proteases are widely distributed among living organisms, the most abundant being the papain family (clan CA, family C1). The family consists of papain and related plant proteases, of cruzipain and related parasite proteases and of lysosomal cathepsins.^{2, 3} These enzymes degrade polypeptides and are characterized by having a common catalytic mechanism that involves a nucleophilic cysteine thiol in the catalytic triad.⁴

Within the past decade, the view of papain-like cysteine proteases has shifted from house-keeping enzymes of little if any diagnostic and therapeutic value to a large protease family of highly diversified and specific functions. Initially lysosomal cysteine proteases were believed to be mainly involved in non-selective intracellular protein degradation, but now it has become more evident that these enzymes must be involved in a range of specific cellular tasks much broader than simple housekeeping tasks. Papain-like cysteine proteases fulfill specific functions in extracellular matrix turnover, antigen presentation and processing events.⁵

Consequently, they may represent viable drug targets for major diseases such as cardiovascular, inflammatory, neurological, respiratory, immunological, musculoskeletal, viral, cancer, and for a wide variety of parasitic infections such as Chagas disease.^{2, 4}

Their redundancy, in higher life forms at least, often makes the function of a particular enzyme ambiguous.

In simpler organisms, a cysteine protease may take on more crucial roles, such as the cathepsin L-like enzyme, cruzain, from the parasite *Trypanosoma cruzi*, which is required for parasite replication and survival.⁶

Currently, no drug targeted towards papain-like cysteine protease is in use; however, many are in development. The development of selective inhibitors of the papain-family proteases as potential therapeutic agents has been difficult because of the high degree of similarity in the primary S₂ substrate-recognition pocket of these proteases.^{7, 8}

Also, a considerable number of potent cysteine protease inhibitors are not suitable as drugs because they have been developed from peptide-like lead compounds, thus displaying (i) low stability to non-selective proteolytic degradation, (ii) inadequate lipophilicity to achieve good oral bioavailability, and (iii) negative side effects due to their lack of selectivity in some cases.⁹

To solve these issues, a structurally diverse variety of non-peptidic inhibitors have been proposed. However, many of these known inhibitors are not considered suitable for use as therapeutic agents in humans because although they can be very selective and demonstrate high affinity, they suffer from various shortcomings including cytotoxicity, poor solubility, and overly rapid plasma clearance.

Cathepsin L, although less well studied than cathepsin B, has been linked to tumor invasion and metastasis,¹⁰ and the inhibition of cathepsin L is expected to be a promising anticancer strategy.¹¹ Currently, relatively few selective inhibitors for cathepsin L exist and the *in vivo* selectivity of most existing compounds is still unclear.¹²

Equally important is the inhibition of crucial parasite proteases as a potential strategy to develop new chemotherapy for the parasitic diseases that are major health problems in under-developed parts of the world because they are involved in parasite survival, replication, and the production of disease.¹³ Very promising preliminary data with cysteine protease inhibitors indicate that the inhibition of papain-like proteases might be highly beneficial for the treatment of pandemic diseases such as malaria, Chagas disease, amebiasis, leishmaniasis or African sleeping sickness.^{14, 15}

The flagellated protozoan parasite, *Trypanosoma cruzi*, is the etiologic agent of Chagas disease, a life-long chronic disease that is the leading cause of heart disease in Latin America where it affects millions of individuals. Chagas disease affects primarily the heart and the nervous system. After a brief acute phase, patients develop a chronic infection resulting in neurological disorders which manifest in the formation of mega-organs (megacolon or megaesophagus) and in the damage of the heart muscle.^{16, 17, 18, 19}

Due to the toxicity of current chemotherapy that was designed decades ago and emerging drug resistance; there is an urgent need for developing an effective therapy against Chagas disease.¹⁴ Cruzipain or its recombinant form cruzain, is pivotal for the parasite's development and survival within the host as is demonstrated when cysteine protease inhibitors are added to a cell culture model of the parasite life cycle and they block the development of *T. cruzi* disrupting its replicative cycle.^{13, 20, 21}

In this context, the overall goal of this project is the biochemical and biological evaluation of compounds, synthesized in Dr. Kevin G. Pinney's laboratory at Baylor University, as novel cathepsin L and cruzain inhibitors in order to treat cancer and the parasitic disease American Trypanosomiasis, also known as Chagas disease.

This strategy has been accomplished through the evaluation of a library of 60 synthetic small non-peptidic thiosemicarbazone (TSC) and α,β -unsaturated carbonyl derivatives of benzophenone, propiophenone, α - and β -tetralone, 4-chromanone, and 4-thiochromenone for inhibition of cruzain and cathepsin L. The main purpose of this research was to explore the structure-activity relationships of these compounds. In addition, kinetic studies (reversibility, time dependence and K_I value determination) were used to characterize the enzyme-inhibitor interactions.

Another objective was to explore if the most potent cathepsin L inhibitors from the evaluated library were able to retain their activity while in contact with cancer cells utilizing advanced cell studies. The biological evaluation included the determination of cytotoxicity and anti-invasiveness properties of the most potent cathepsin L inhibitors in the prostate cancer cell line DU-145.

It is recognized that cancer cells secrete elevated amounts of cathepsins L to degrade the extracellular matrix, thus promoting tumor invasion and metastasis. However, very little information is available concerning the secreted forms of cathepsins L and their role in cancer. Immunoblotting analysis was carried out to determine if a form of cathepsin L is directly secreted from cancer cell lines or if it is a product processed from procathepsin L after secretion into the cell culture medium.

CHAPTER TWO

Introduction to Cysteine Proteases

Proteases make up the largest class of enzymes, with over 1600 proteases identified from over 1700 organisms. Human proteases account for approximately 500 of that number and represent an attractive area for novel drug discovery.²² Proteases are involved in virtually all biological functions and dysfunctions as they regulate numerous biochemicals and disease processes by controlling protein synthesis and degradation.²³

Proteases can be categorized based on their substrate specificities or mechanisms of catalysis. Enzymes cleaving within a polypeptide chain are named endopeptidases, and those cleaving at the ends of polypeptides are named exopeptidases. Four major protease classes are known: serine, cysteine, aspartic, and metalloproteases.^{24, 25}

Aspartic proteases use two catalytic aspartic acid residues in the active site to coordinate the nucleophilic attack of the peptide bond by a water molecule. Serine proteases have a hydroxyl group at the active site that acts as the nucleophile that attacks the peptide bond. In the case of cysteine proteases, a thiolate ion at the active site is used to attack the peptide bond. Metalloproteases use a metal atom to coordinate the substrate and catalyze the nucleophilic attack of a water molecule on the peptide bond.²²

The present discussion will focus on papain-like cysteine proteases, the largest subfamily among the cysteine protease class (clan CA, family C1), making special emphasis in the mammalian cathepsin L and the parasitic cysteine protease cruzain.

This family is widely expressed throughout the animal and plant kingdoms, viruses and bacteria.²⁶ Lysosomal mammalian papain-like cysteine proteases are also known as thiol-dependent cathepsins.

Cathepsins are distributed among four classes of proteases: cysteine (the majority of cathepsins), aspartyl (cathepsins D and E), serine (cathepsins A and G) and metallo (cathepsin III).^{26, 22} Several dozens of cysteine proteases have been identified in various parasitic organisms, and they all share the common amino acid sequence and fold of a papain-like structure as well.

Papain-Like Cysteine Proteases: Sequence, Structure, Mechanism, Expression, Substrate Specificity, and Physiological Functions

Lysosomal cysteine proteases comprise a group of papain-like enzymes, sharing similar amino acid sequences and folds. They are optimally active under the slightly acidic conditions and their molecular weights are usually in the 20-30 kDa range, not including the proregion, which extends from approximately 60-100 kDa. The mature forms of these enzymes are mostly monomeric.

Amino Acid Sequence

Eleven papain-like cathepsins are expressed in the human genome (B, H, L, S, C, K, O, F, V, X and W).⁵ All cysteine proteases have a conserved active site in common, consisting of cysteine, histidine, and asparagine residues.

The cysteine residue (Cys-25, papain numbering) is embedded in a highly conserved peptide sequence, CGSCWAFS. Similar to the area around the active site cysteine residues, the vicinities of the histidine and asparagine residues are also conserved.

The histidine residue (His-159) is adjacent to small amino acid residues such as glycine or alanine followed by four aliphatic hydrophobic residues (valine, leucine, isoleucine and glycine).²⁷

The catalytic domains of most papain-like cysteine proteases are between 220 and 260 amino acids in length, with the exception of several parasite-derived cysteine proteases which contain a C-terminal extension of unknown function.

The amino acid alignment of 11 human cathepsins and 5 parasitic cathepsins of major human and animal pathogens is shown in Figure 1.

The human cathepsin L gene encodes a 333-amino acid cysteine protease that contains a 17-amino acid signal peptide, a 96-amino-acid propeptide, and a 220-amino acid mature region.

The 38-kDa procathepsin L is processed to mature, active cathepsin L, and exists either as a single chain form of 30 kDa or as a two-chain form of 25 and 5 kDa.²⁶⁻²⁹

There is a high structural similarity between cathepsin L and the parasitic cysteine protease cruzain.

The sizes of the mature forms of cathepsin L (220 residues) and cruzain (216 residues) are close and the sequence identity has 47.9% similarity.

Superimposition of the cathepsin L and cruzain backbones is shown in Figure 2. The backbones of cathepsin L and cruzain align with each other except for some of the loop regions.³⁰

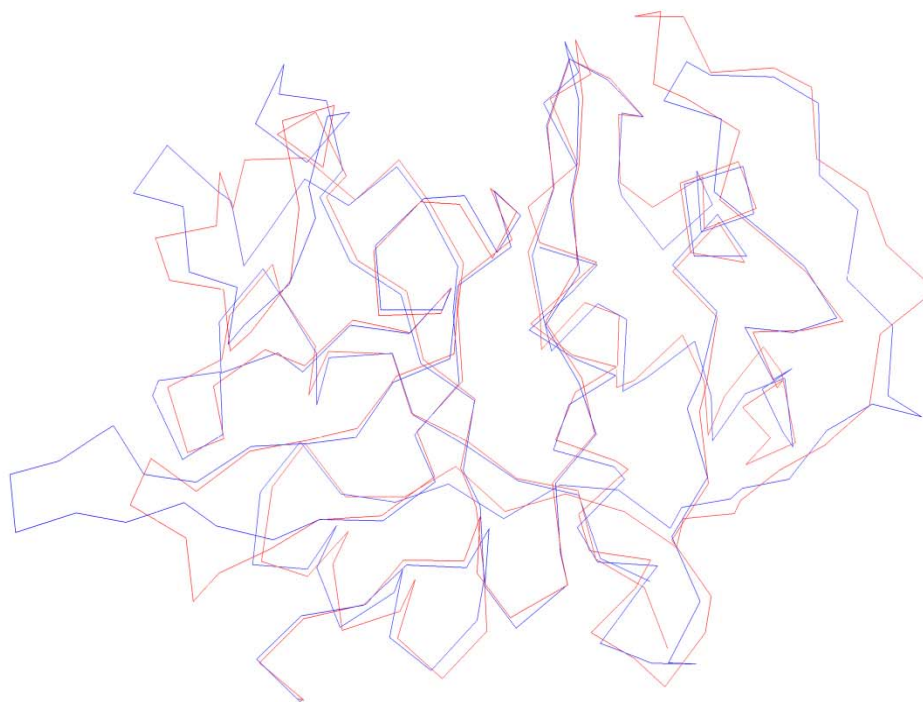


Figure 2. Superimposition of cathepsin L (blue) and cruzain (red). Reproduced with kind permission from Chen.³⁰

Fold and Topology

A papain-like fold consists of two domains, reminiscent of a closed book with the spine located at the front. The domains separate at the “top” in a V-shaped active-site cleft, in the center of which, residues Cys-25 and His-159 of each domain form the catalytic site of the enzyme.^{3, 11, 27} Substrate can then bind in an extended conformation along the active site cleft.

The structure consists of an L and R domain of similar size. The L-domain has three helical regions, the longest being the central helix, about 30-40 residues long, having the catalytic Cys-25 perched at its N terminus. The fold of the R-domain is based on a β -barrel motif of five to six strands and includes a shorter α -helical motif (Figure 3).⁶ Although the left domain is mainly comprised of the N-terminal half of the enzyme, the polypeptide chain actually starts on the distal right side of the right domain.

Similarly, the mostly C-terminal right domain ends in a strand that extends into the left domain. For many enzymes in this group, two disulfide linkages add stability to the left domain, whereas one is found in the right domain.⁶

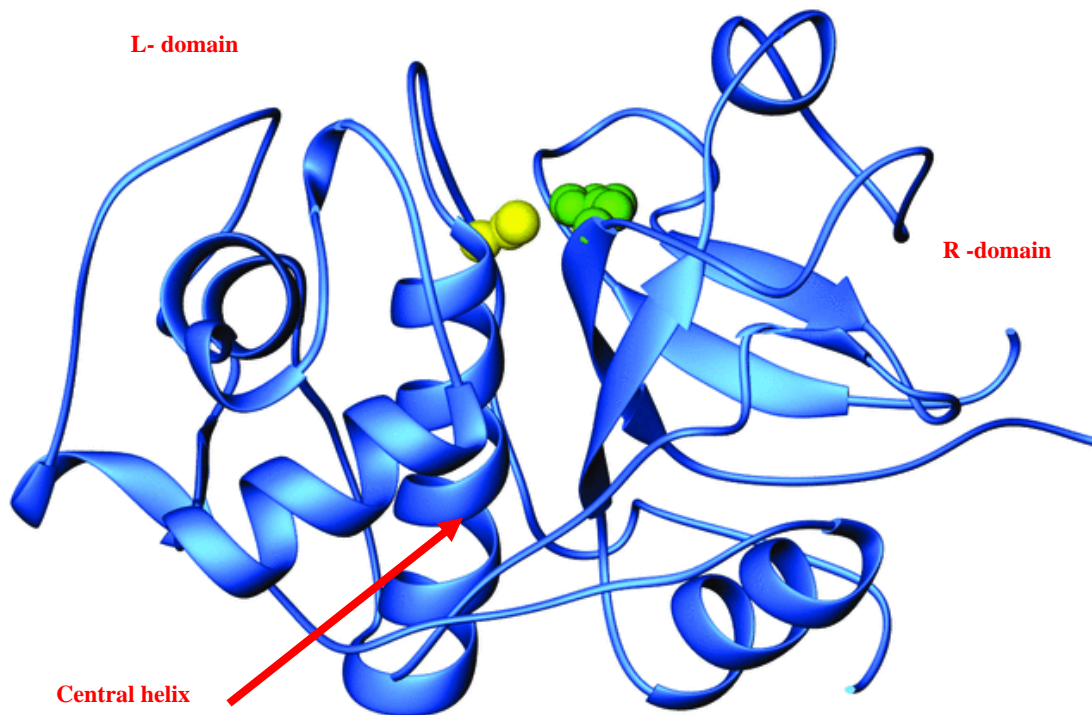


Figure 3. Fold of cathepsin L viewed along the two-domain interface and the active site at the top. The side chains of the catalytic residues Cys-25 and His-159 (papain numbering) are shown as yellow and green atom spheres, respectively. Reproduced with kind permission from Turk.²⁷

The propeptide is less structured and runs in the inverse orientation through the substrate binding cleft (as shown in Figure 4).²⁷ The crystal structures of the proenzymes showed that the structure of the mature enzyme is already formed in the zymogen form.³¹ The propeptide chain builds an α -helical domain, which continues along the active-site cleft toward the N-terminus of the mature enzyme in a predominantly extended conformation in a direction opposite to substrate binding, which blocks access to the active site (Figure 4).²⁷

The activation process is triggered by a pH drop that presumably weakens the interactions between the propeptide and the catalytic site. As a consequence, the proenzyme most likely adopts a looser conformation, where the propeptide is less tightly bound to the active site without the loss of the secondary structure making it more accessible to proteolytic cleavage.²⁰

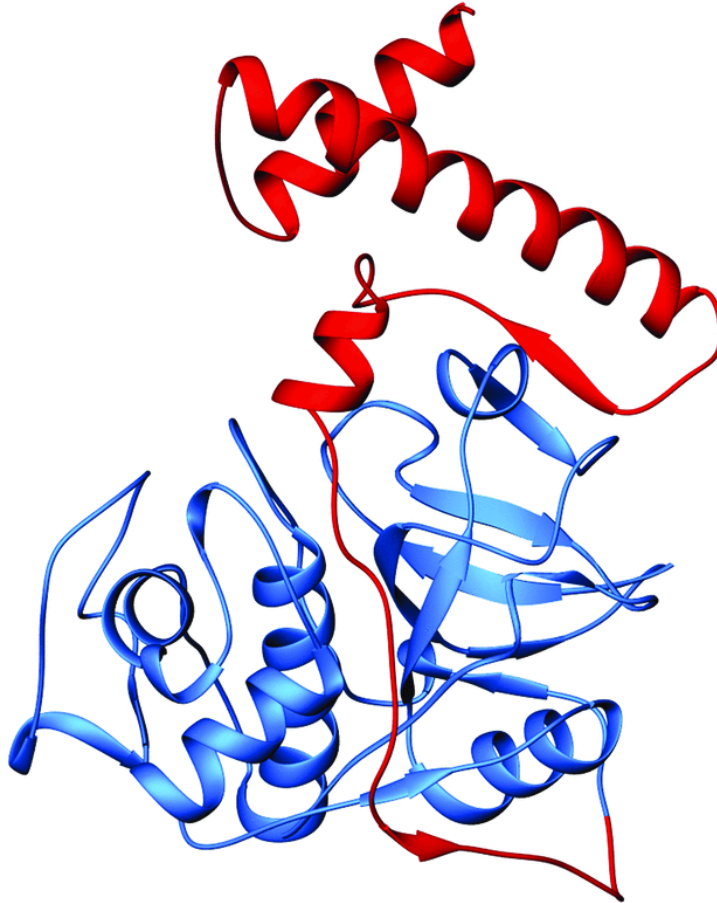


Figure 4. Fold of procathepsin L (1cj). The mature enzyme part of cathepsin L is shown in blue and the propeptide is shown in red. Reproduced with kind permission from Turk.²⁷

Substrate-Binding Sites

Seven possible substrate-binding sites, which bracket the catalytic dyad of Cys-25 and His-159, were first described for the endopeptidases by Schechter & Berger in 1967.

The carboxyl side of the peptide substrate and corresponding enzyme subsites are conventionally referred to as the prime side and are termed P_1' , P_2' , P_n' and S_1' , S_2' , and S_n' respectively. The amino side of the peptide and corresponding subsites assigned the non-prime side and are designated P_1 , P_2 , P_n and S_1 , S_2 and S_n , respectively (Figures 5 and 6a).²⁰

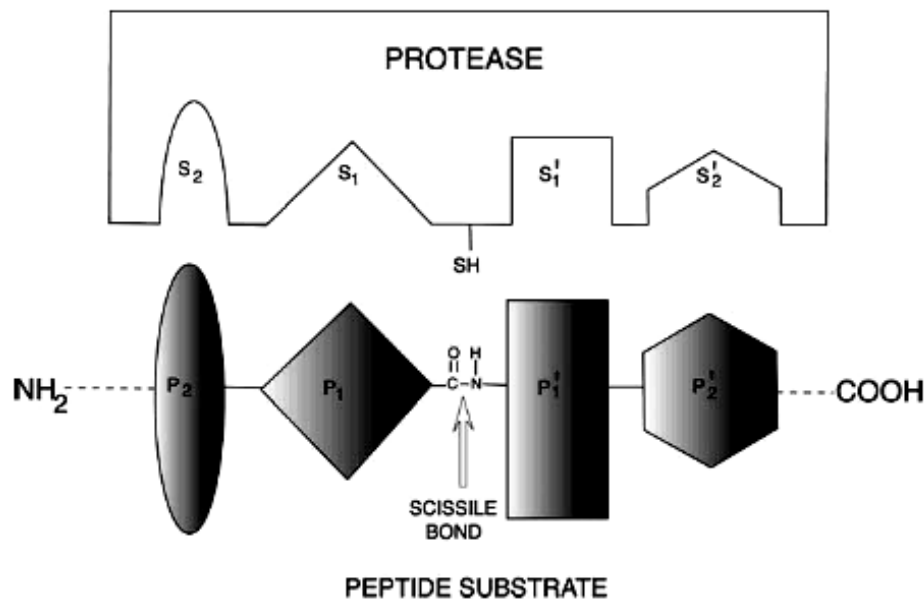


Figure 5. Diagrammatic representation of peptide substrate interaction with the active site pockets of a cysteine protease. Amino acid residues from the peptide substrate are denoted by 'P' and the sub-sites that the peptide interacts with are given the letter 'S'. The active site cysteine sulfhydryl nucleophile is represented as SH. Reproduced with kind permission from Sajid.²⁰

Cysteine proteases have rather short active-site clefts, comprising three well defined substrate-binding subsites (S_2 , S_1 and S_1'). Additionally they have comparatively broad binding areas (S_4 , S_3 , S_2' , S_3').²⁴ As shown in Figure 6, the loop formed by residues 59–67 constitutes the area where P_3 residues bind and is termed the S_3 binding area.

The form of the S₁ binding site is also a loop, but is constructed from parts of the loops embracing the S₃ and S₂' binding sites and is enclosed at the top by the conserved disulfide bridge Cys22–Cys63. The top of the R-domain is formed by two broad loops placed on top of each other. The lower loop (175–205) forms the base, on top of which rest residues 133–159 of the upper loop.

The substrate-binding sites exhibit no strict specificities.³¹ Their subsite preferences arise more from specific exclusions of substrate type, which presents a challenge for the design of inhibitors to target a specific cathepsin.²⁷ Cysteine proteases prefer bulky hydrophobic residues at P2.³² The S₂ binding site is a deep hydrophobic pocket.^{33, 34} The positioning of the P₃ residue is mediated only by side-chain interactions.

If human cathepsin L and cruzain substrate-binding sites are compared, it can be noticed that the active site of cathepsin L is more defined than that of cruzain. The S₁ pocket of cruzain is bigger than that of cathepsin L and the opening of the cathepsin L S₂ pocket is much smaller than that of cruzain. The S₂ pocket of cathepsin L is slightly narrower, longer and deeper in distance than that of cruzain. A more defined S₄ pocket is also seen in cathepsin L.³⁰ Cathepsin L may accommodate a more bulky group at the S₃ site³³ and has preference for positively charged residues at the S₁ and S₃ position.^{34, 27}

The superimposed structures of complexes of substrate-analogue inhibitors and a papain-like cysteine protease model (Figure 7) have revealed that substrate residues bind along the active-site cleft in an extended conformation with the side chains alternately oriented toward the L- and R-domains. Each substrate residue docks on the surface of an enzyme in a specific orientation (Figure 8).

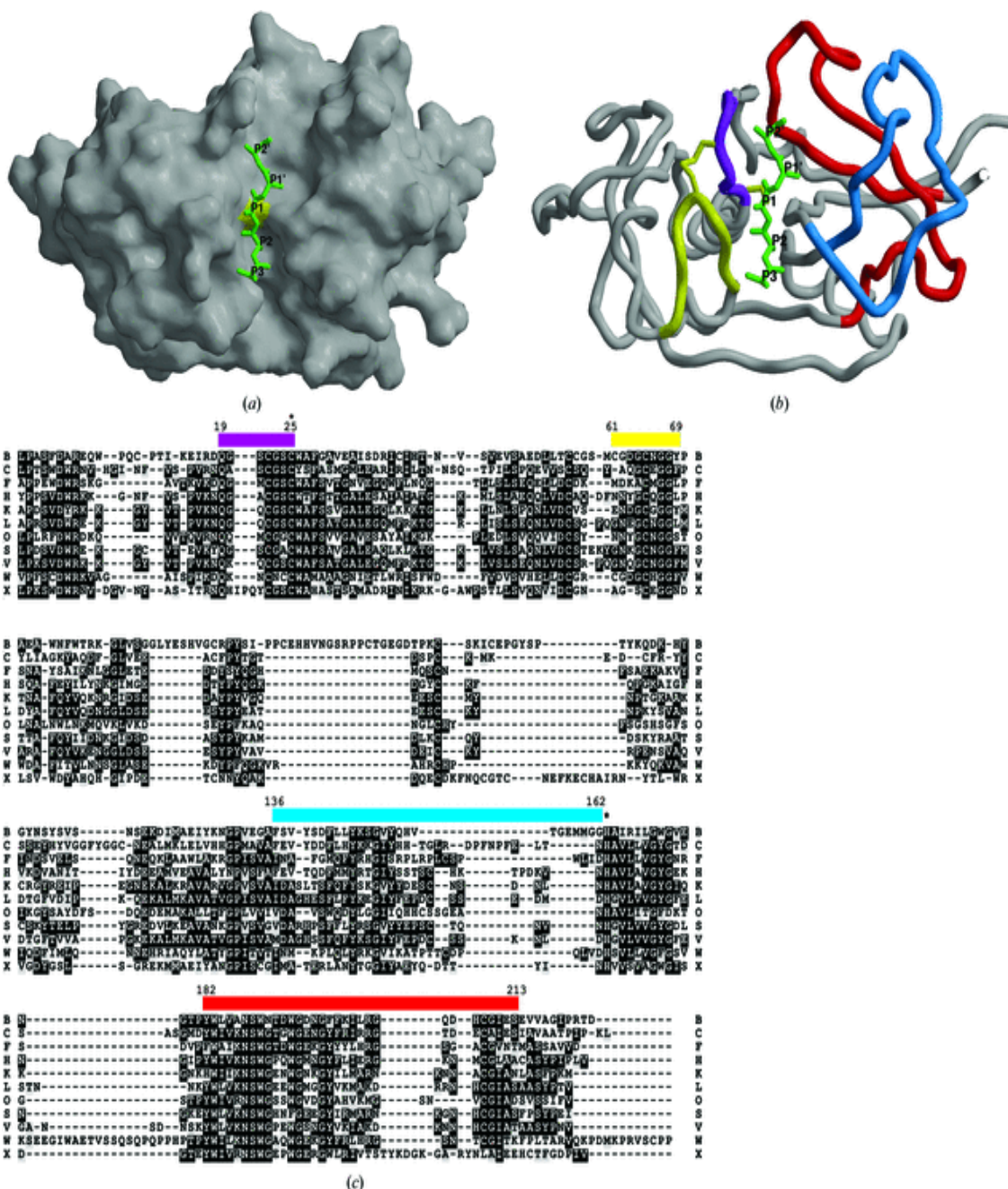


Figure 6. Substrate-binding sites. (a) Polyalanine substrate model (green sticks) bound in the active-site cleft of cathepsin L and denoted using the Schechter and Berger nomenclature. The surface of the catalytic cysteine side chain is yellow. (b) The same as (a), only that in this case cathepsin L is shown as a chain trace. The substrate-binding sites are color-coded: the L-domain loops (19-25 and 61-69) are purple and yellow and the R-domain loops (136-162 and 182-213) are blue and red. (c) Structure-based amino-acid alignment of sequences of papain-like domains of all known human cathepsins. The substrate-binding sites are marked at the top with stripes of the same color code as in Figure 5 (b). Reproduced with kind permission from Turk.²⁷

Structures of the irreversible cysteine protease inhibitor E-64 and its analogues (Figure 9) revealed that they bind into the non-primed region of the active site, but in the direction of propeptide binding and opposite to substrate binding (Figure 7b). Alternatively, the CA030 inhibitor in complex with cathepsin B, demonstrated that E-64 derivatives can also bind into the primed binding side in the direction of substrate binding.

The carboxylic group of the C-terminal residue of CA030 mimics the C-terminus of a substrate and docks to the occluding loop (Figure 7c).

Therefore, it was suggested that the substrate residue-binding regions beyond S_2 and S_2' should not be called sites but areas.²⁷ The S_1' binding site can also be reached with inhibitors using an exceptionally long side chain of a P_1 -mimicking residue of a chloromethyl or a vinylsulfone based inhibitor (Figures 7a and 7d).

The covalent interaction with the reactive-site cysteine is not mandatory as shown by a series of 'Smith-Kline' compounds (Figure 7e and Figure 10), which utilize various constructs to non-covalently block the reactive site tightly.²⁷

In conclusion, residues P_2 , P_1 and P_1' bind into well defined binding sites. The S_2 and S_1' substrate binding sites are responsible for the diversity and selectivity of the substrate and inhibitor binding.^{27, 32}

A detailed view of cathepsin L amino acid residue interactions is shown in Figure 11.³⁶ The S' region of the binding site encompasses S_1' and S_2' and represents the oxyanion hole. The oxyanion hole consists of the side chains of Gln-19, Trp-189, His-163 and the main chain of Cys-25. Below the active site is the S_2 subsite which is characterized by its deep, hydrophobic cleft usually present in most cysteine proteases.

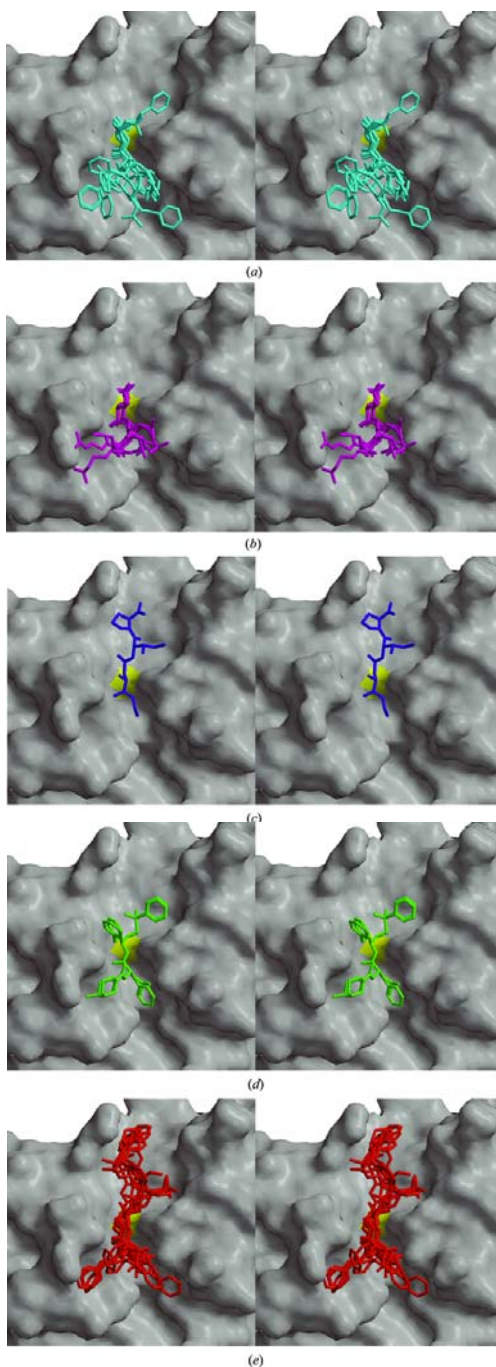


Figure 7. Low molecular weight inhibitor binding geometry. The inhibitors (shown as stick models) from structures of complexes with papain-like cysteine proteases are superimposed on top of the cathepsin L surface. The catalytic site Cys²⁵ surface is coloured yellow. (a) Substrate-analogue inhibitors: fluoro- and chloromethylketone-based inhibitors and leupeptin are shown in light green. (b) E-64 and derivative are shown in magenta. (c) The CA030 cathepsin B inhibitor is shown in blue. (d) Vinylsulfone-based inhibitors are shown in green. (e) A group of non-covalent cathepsin K and L inhibitors are shown in red. Reproduced with kind permission from Turk.²⁷

Surrounding the right hand side of the S_2 pocket are residues Asp-162, Met-161, Asp-71, and Ala-214. At the bottom of the S_2 subsite is Met-70 making the cleft shallower than that of cathepsin B.

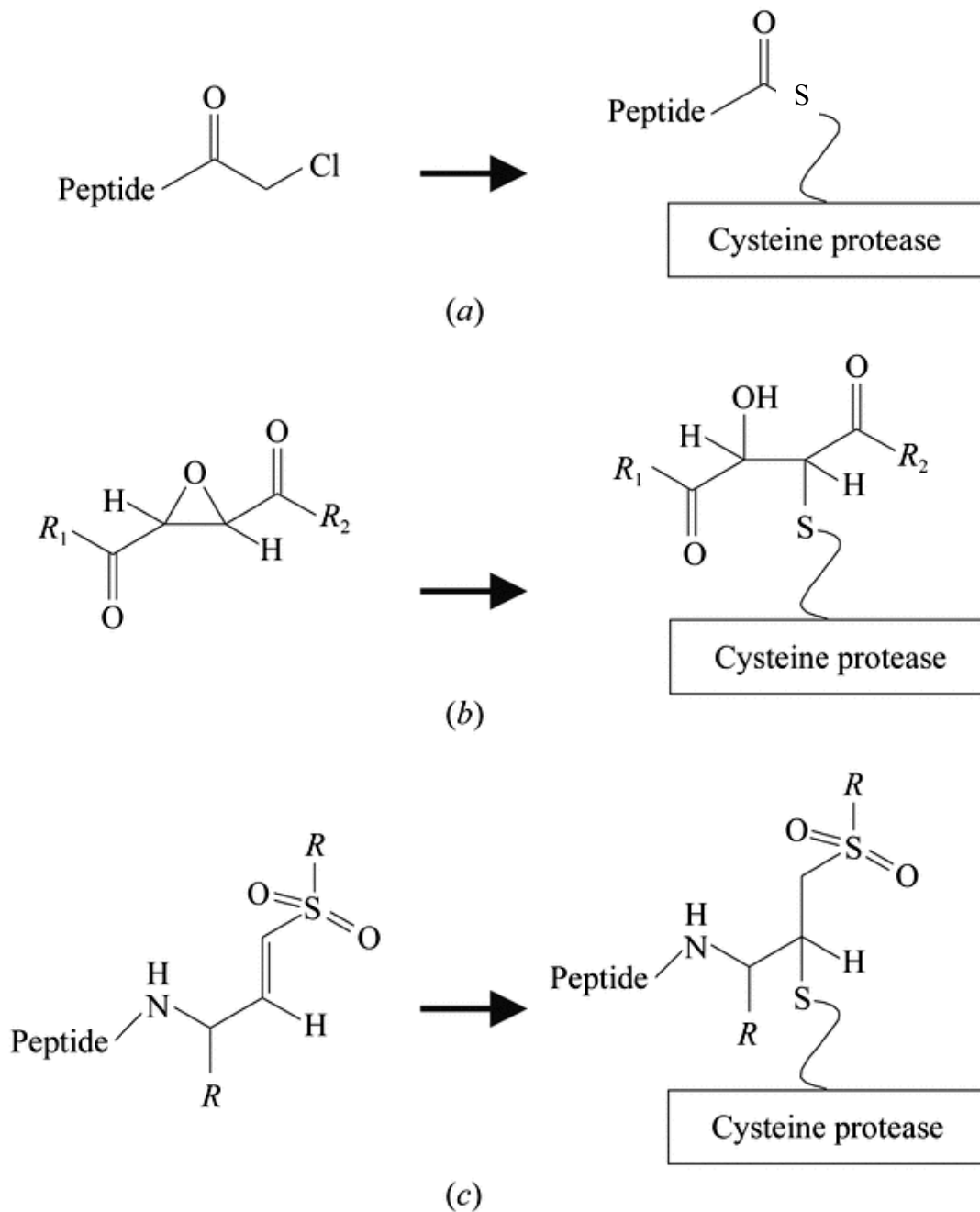


Figure 8. Schemes of three most frequent reactive groups before and after binding to the reactive-site cysteine. (a) chloromethylketone, (b) epoxysuccinyl, (c) vinylsulfone. Reproduced with kind permission from Turk.²⁷

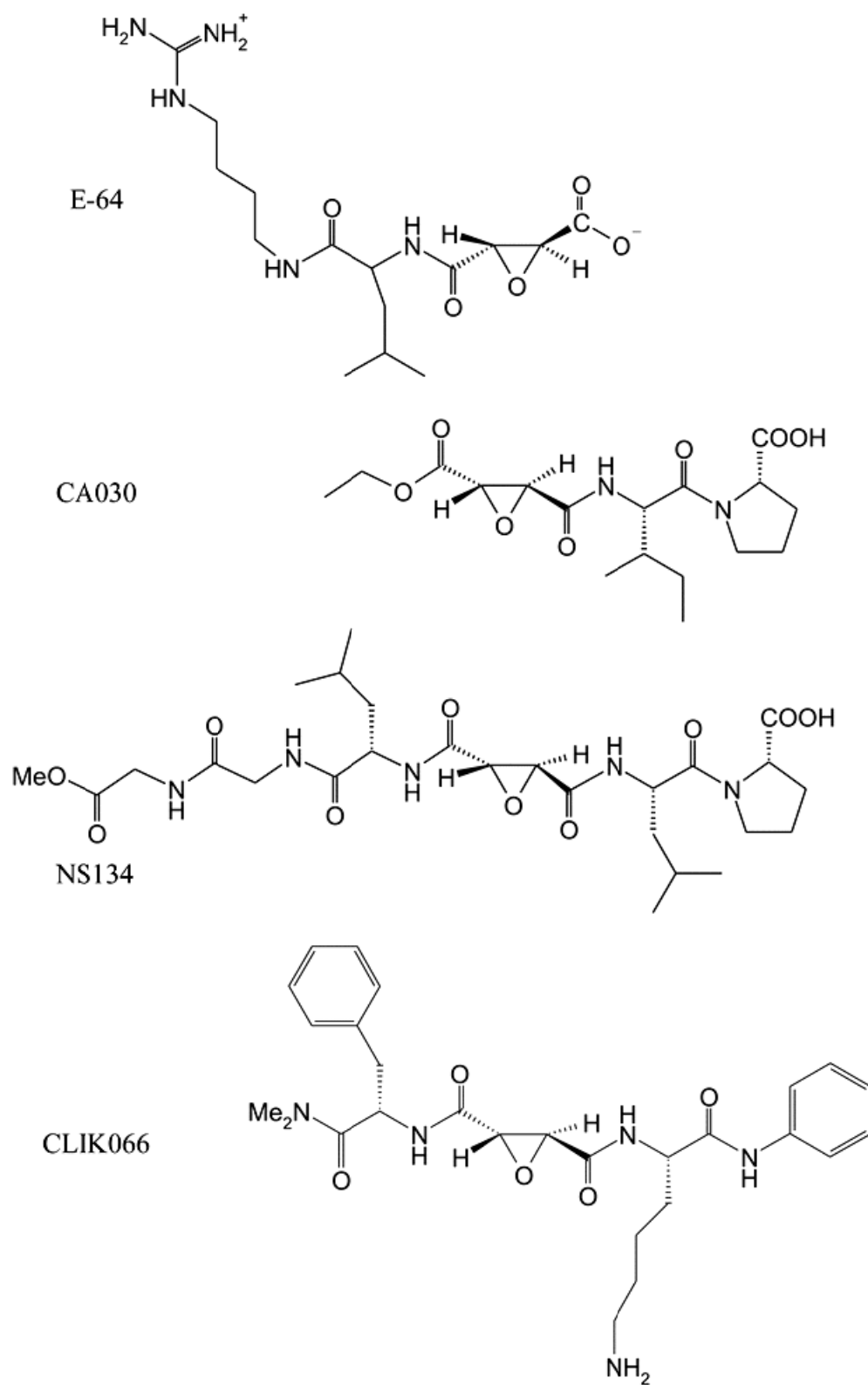


Figure 9. Epoxysuccinyl derivatives. Reproduced with kind permission from Turk.²⁷

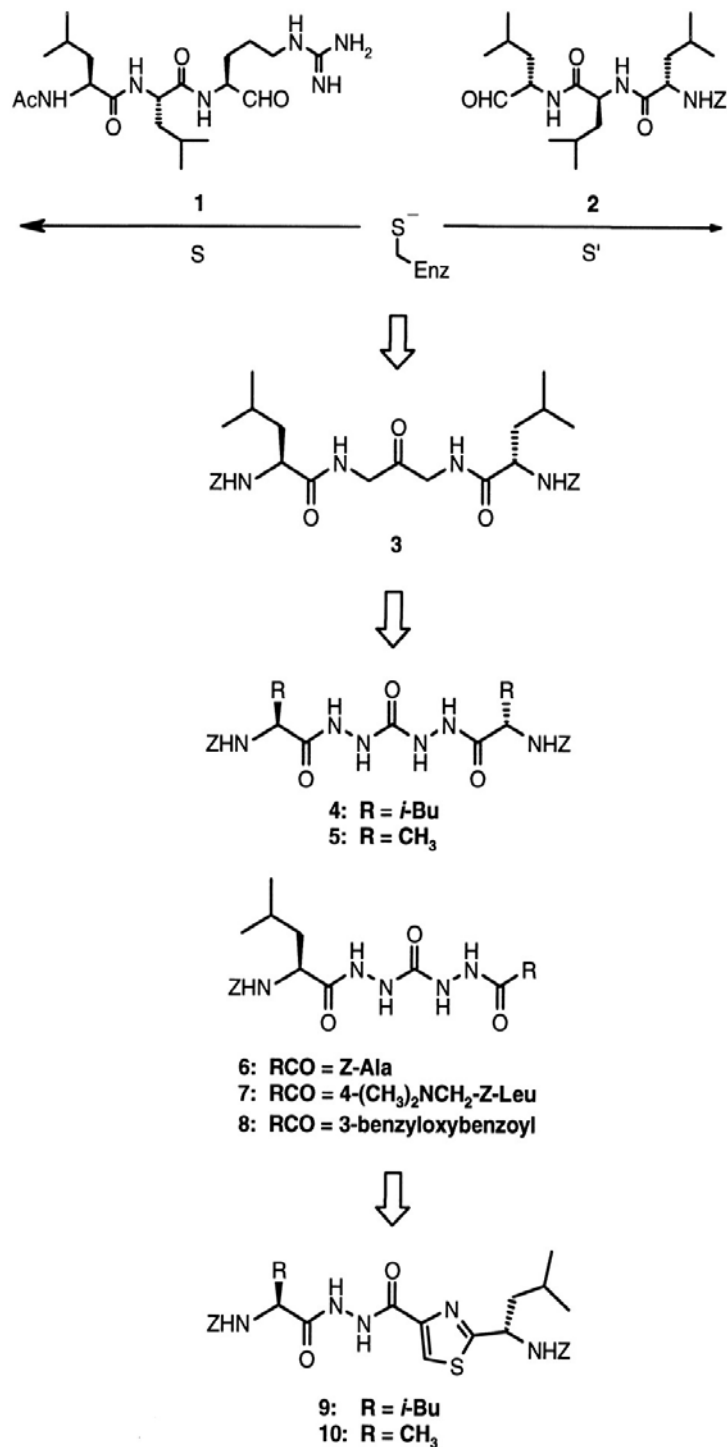


Figure 10. Evolution of 'Smith-Kline' compounds. Leupeptin (1) was observed to bind on the S side of the active site and the closely related aldehyde (2) was observed to bind only in the S' direction. The overlay of these two crystal structures led to the successful design of a potent class of selective inhibitors of cathepsin K that span both sides of its active site (3). Reproduced with kind permission from Thompson.³⁵

The S3 subsite is located just slightly below and to the left of the S₂ subsite. At the center of the subsite are residues Gly-67 and Gly-68 which are surrounded by the side chains of Asn-66, Glu-63, and Leu-69 as well as the carbonyl oxygen of Gly-61. Since the active enzyme begins with amino acid 114, all numbers used in the rest of the report will begin with residue 114 designated as the first amino acid.

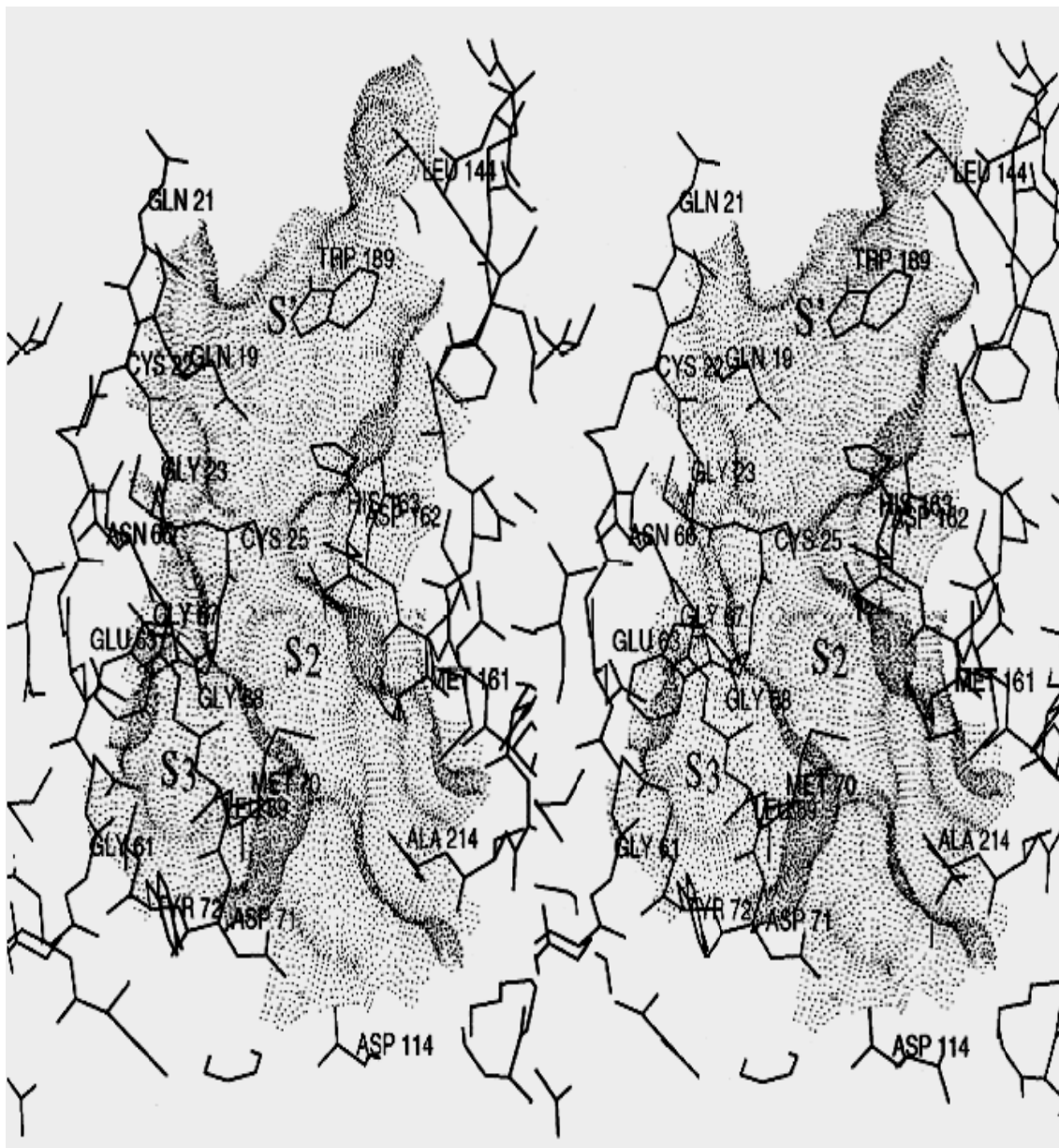


Figure 11. A detailed view of the binding pocket of cathepsin L. Reproduced with kind permission from Kakegawa.³⁶

Catalytic Mechanism

Cysteine proteases catalyze the hydrolysis of amide bonds in proteins through nucleophilic attack by the active site cysteine thiol on the amide carbonyl.³⁷ The catalytic site of papain-like cysteine proteases is highly conserved and formed by three residues: Cys-25, His-159, and Asn-175. Cys-25 and His-159 form an ion pair which is stabilized by Asn-175 via a hydrogen bond.^{38, 25}

The hydrolysis mechanism of cysteine proteases consist of an attack of a negatively charged thiolate group of a cysteine residue at the carbonyl carbon of the peptide bond leading to an acyl enzyme which is hydrolyzed in the second step (Figure 12).³⁹

During peptide hydrolysis, the nucleophilic thiolate cysteine attacks the carbonyl carbon of the scissile bond of the bound substrate and forms a tetrahedral intermediate which is stabilized by the so-called oxyanion hole, a crucial element in forming an electrophilic center to stabilize the tetrahedral intermediate during hydrolysis (Figure 13).^{20, 24-25, 38}

Cysteine proteases have mechanistic similarities to serine proteases, but they are better nucleophiles due to the extra shell of electrons present in the sulfur of the thiol group.

The thiol group is enhanced as a nucleophile due to the close proximity of an active site histidine residue which acts as a proton donor.

The two ionizable groups of the thiolate–imidazolium diad allow a broad pH range of enzymatic activity.

They consist of a pKa for cysteine of approximately 4.0 and a pKa for histidine ionization of approximately 8.5.^{20, 6}

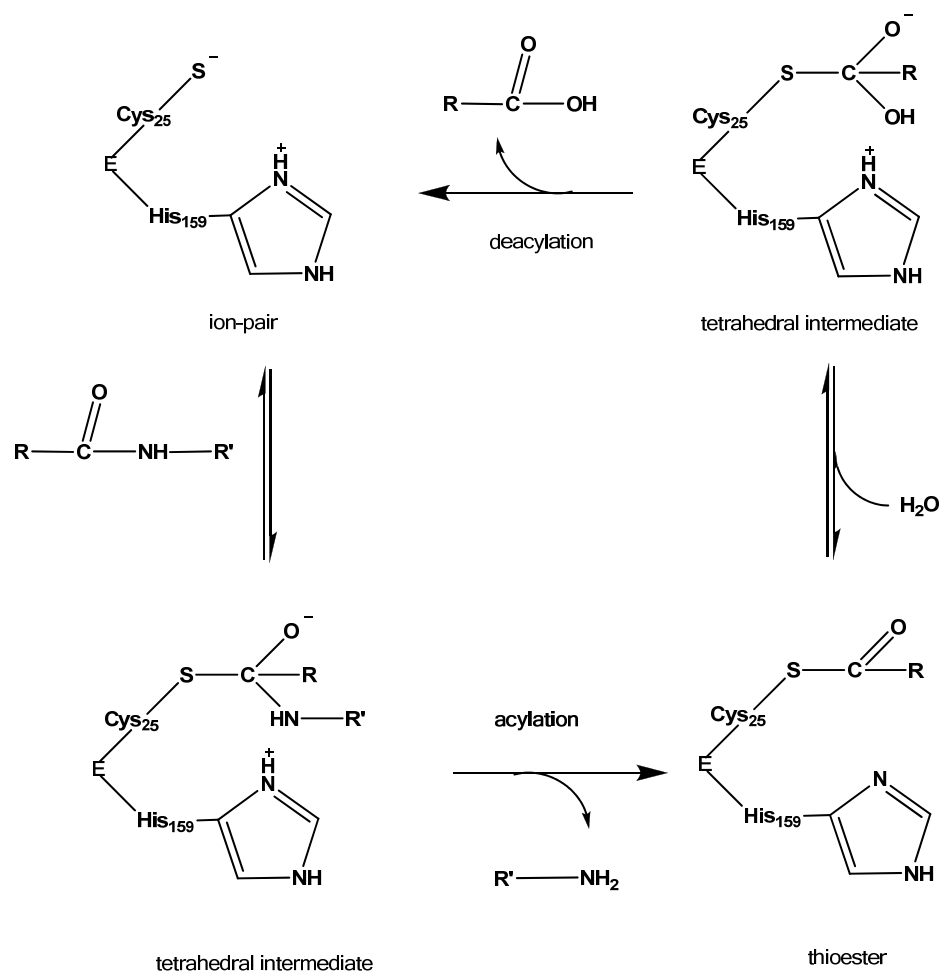


Figure 12. Catalytic mechanism of cysteine proteases. Their catalytic site has the Cys-25, His-159 and Asn-175 conserved in all of its members. In this triad, Cys-25 and His-159 form an ion pair which is stabilized by Asn-175 *via* a hydrogen bond allowing peptide hydrolysis.^{12, 40}

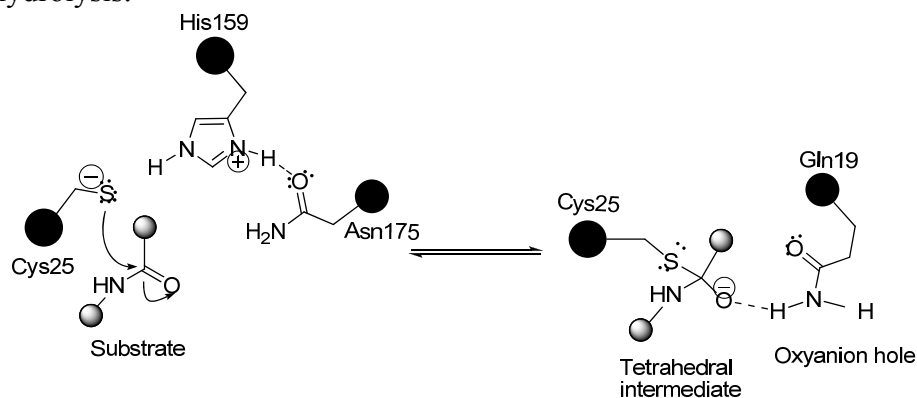


Figure 13. Stabilization of the oxyanion generated by the cysteine protease catalytic reaction. Reproduced with kind permission from Chen.³⁰

Cysteine Proteases's Intracellular and Tissue Distribution

The expression of cysteine proteases are either ubiquitous or tissue and cell specific.¹² The location of papain-like cysteine proteases is not strictly lysosomal; rather, the enzymes are trafficking between phagosomes, endosomes, and lysosomes. The individual proteases may accumulate in different organelles. Human cathepsins have an acidic pH optimum which allows for full activity within the lysosomal compartment. Cathepsin L displays a ubiquitous expression in lysosomes of most tissues and differs from other cathepsins in that it lacks exopeptidase activity and has the highest proteolytic activity in lysosomes.^{41-42, 3}

Cathepsin K is selectively expressed in osteoclasts (cells involved in bone resorption) and it is considered that inhibitors of cathepsin K can be potential therapeutic agents for the treatment of diseases characterised by excessive bone loss, including osteoporosis.⁴³

Cathepsin B is present and active intracellularly and extracellularly in almost all tissue types. Intracellularly, it is localized in the lysosomes, whereas extracellularly, it can be found both free and bound to the extracellular matrix proteins, where it has many important physiological functions such as thyroxine synthesis, site-selective cleavage of human prorenin, processing of antigens, and self-protection of cytotoxic T-lymphocytes during degranulation.^{44, 45}

Regulation of Lysosomal Cathepsin Activity

Proteolytic activity is important for normal functioning of an organism and must be rigorously controlled to avoid potentially dangerous excess protein degradation.

Lysosomal cysteine protease activity is regulated in a number of ways, the most important being zymogen activation and inhibition by endogenous protein inhibitors.

Zymogen Activation

Lysosomal cathepsins are synthesized as preproenzymes.¹¹ Following synthesis, the propeptide is removed during the passage to the endoplasmic reticulum. Procathepsin undergoes proteolytic processing to the active, mature enzyme form in the acidic environment of late endosomes or lysosomes.^{26, 41} Limited proteolysis is thus a crucial step in controlling the proteolytic activity of lysosomal cysteine proteases and numerous other proteases.

The propeptide, part or all of which is removed during activation, is responsible for proper targeting of the enzymes, for the stability and for the proper folding of the enzymes,^{28, 46} as well as, being able to specifically inhibit the activity of mature enzymes.¹¹

The proregions are tightly binding, highly selective and reversible inhibitors that occupy the cleft in a linear, but backwards orientation, preventing the premature activation of the catalytic domain of mature cathepsin with K_I values in the nanomolar range.^{6, 47} Usually, the inhibition obeys slow-binding kinetics, but the mechanism is also pH dependent.^{47, 46, 48} The K_I value for inhibition of human cathepsin L propeptide towards the mature cathepsin L is 0.088 nM at pH 5.5, but increases to 3.0 nM at pH 4.0.³¹

Conversion to the mature form occurs intracellularly in lysosomes at pH 3.0-3.5 by autocatalytic removal of the prosegment,^{46, 26} whereas extracellularly, at pH 5.5-6.0, maturation is supported by negatively charged matrix surfaces.¹¹

Autoactivation of cathepsin B and L was found to be substantially accelerated in the presence of various glycosaminoglycans up to pH 6.0.^{41, 49} Propeptides, after serving their role to prevent inappropriate protease activity, are thought to dissociate from the protease, unfold, and are proteolytically degraded.²⁶

Endogenous Cysteine Proteases Inhibitors

Once activated, lysosomal cysteine proteases have enormous disruptive potential, and inappropriate action is controlled by their endogenous protein inhibitors, the cystatins.

On the basis of sequence homology, the cystatin superfamily is divided into three subfamilies: stefins, cystatins and kininogens.

Stefins are intracellular inhibitors, whereas cystatins and kininogens are extracellular inhibitors.⁵⁰

They have in common their enormous stability at high temperatures (up to 100 °C) and at extreme pH (pH 2-12, kininogens pH 5-12) as well as their specificity for cysteine proteases, although they are only able to discriminate between endo and exopeptidases.

They inhibit endopeptidases in the picomolar range and the inhibition is rapid and tight, almost pseudo-irreversible reaction, while the inhibition of exopeptidases is much weaker with K_i values in the millimolar to nanomolar range⁵¹

The cystatin superfamily members bind in a non-substrate-like manner, inserting the hairpin loop and the N-terminal trunk region into the protease-binding cleft as observed in a complex of papain and stefin B (Figure 14).²⁷

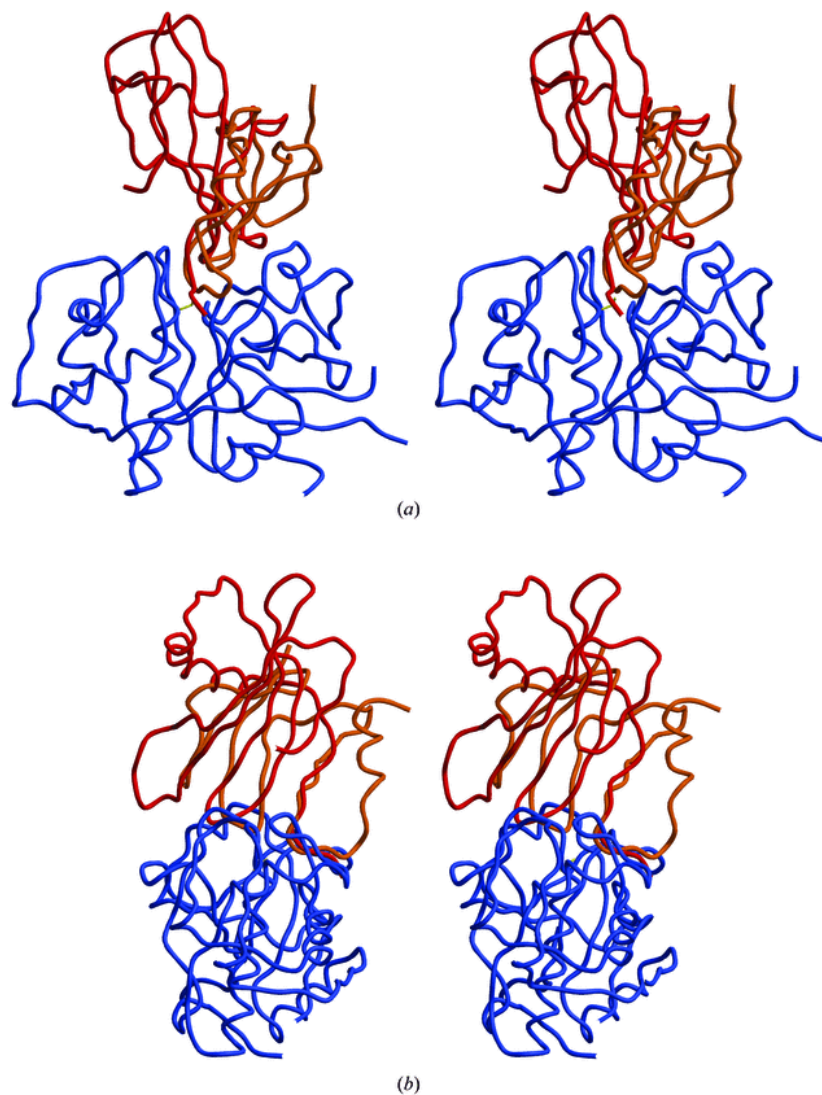


Figure 14. Binding of protein inhibitors. Stefin B superimposed on cathepsin L complex in views (a) across and (b) along the active-site cleft of cathepsin L. Chain traces of the steffin B and cathepsin L are shown in red and blue, respectively. Reproduced with kind permission from Turk.²⁷

The Stefin Family

These proteins lack disulfide bridges and carbohydrate residues. Members of this family are cystatins A and B, which have a molecular weight of approximately 11 kDa. Cystatin A (pI 4.5-5.0) is found mainly in epithelial cells and neutrophilic granulocytes while cystatin B (pI 6.0-6.6) is present in almost all cells and tissues.⁵⁰

The Cystatin Family

These proteins have molecular weights ranging from 12 to 13 kDa do not have carbohydrate residues (with the exception of cystatin C from rat197) but they do have two disulfide loops at the C-terminal end. Members of this family are cystatins C, D, and the three S-type cystatins (S, SN, SA). Cystatin C (pI 8.0-9.5) is widely distributed in the extracellular matrix and has also been found in cortical neurons, pancreatic islet cells, the thyroid gland.⁵⁰ Cystatin D was isolated from saliva.⁵² Cystatin S (pI 4.7) has been found in mammalian salivary glands, tear fluid, serum, gall, urine, pancreas, and bronchi.⁵³

The Kininogen Family

A high molecular weight (HMW) kininogen (120 kDa) and a low molecular weight (LMW) kininogen (50-80 kDa) are known in humans. Their principal characteristics include the presence of carbohydrate residues, signal peptide and disulfide bridges. HMW is produced by the liver together with prekallikrein. It acts mainly as a cofactor on coagulation and inflammation, and has no intrinsic catalytic activity. LMW is produced locally by numerous tissues, and secreted together with tissue kallikrein.⁵⁰

Cysteine Proteases Physiological Role

Human cysteine proteases mostly fulfill housekeeping functions, but they are also involved in more specialized processes. They play a role not only in protein catabolism, but also in hormone activation, antigen presentation, and tissue remodeling.^{54-55, 31} The major physiological role of cathepsins inside lysosomes is non-specific protein digestion,¹¹ whereas outside of lysosomes, they degrade proteins.²⁷

One of the most important precursors processed by cysteine proteases is thyroglobulin, a source of thyroid hormones.^{38, 33}

Analyses of gene knockouts suggested that cathepsin L is involved in epidermal homeostasis and hair follicle morphogenesis.²⁷ Cathepsins also participate in apoptosis, although the exact mechanism is not yet clear.⁵⁶

Papain-like cysteine proteases expressed in major human and domestic animal disease-causing parasites have been demonstrated to be essential for their life cycles and virulence.

In contrast to a simple digestive role, parasite derived cysteine proteases have been characterized to perform indispensable roles in the biology and life cycle of many species of parasites such as in replication, cell differentiation, signaling, and host invasion.^{20-21, 57}

Role of Cysteine Proteases in Pathological Conditions

Failure in biological control mechanisms of proteolytic activities and the consequent disturbance of the normal balance of enzymatic activity causes a wide range of pathological conditions.

A common factor in both processes is that the equilibrium between lysosomal enzymes and their endogenous inhibitors in the extracellular space is disturbed.

This imbalance may originate from reduced inhibitor activity due to saturation of the natural inhibitors by excess release of lysosomal enzymes, a change in the binding properties of the inhibitors and thus easier dissociation of the enzymes from the enzyme-inhibitor complexes and/or increased stability of lysosomal cathepsins which are normally inactive in the extracellular space (creation of microenvironments with low pH).

Papain-like cysteine proteases have been increasingly recognized as critical enzyme activities in degenerative, invasive, and immune system related disorders as well as in various parasitic infections.⁵⁸⁻⁶⁰

When secreted in excess, lysosomal cysteine proteases can be very harmful, resulting in pathological conditions. Free lysosomal proteases and uncontrolled proteolysis destroy proteins of the cell membrane and of connective and supportive tissues. Toxic peptides are produced by this process which inhibits the enzymes of the blood system.^{61, 59, 62, 8}

Cysteine proteases have been observed in a number of diseases such as cancer, apoptosis, rheumatoid arthritis, osteoarthritis, bone resorption,^{63, 54} Alzheimer's disease,⁷ multiple sclerosis, and muscular dystrophy.^{64, 27}

In many of these diseases, lysosomal enzymes were found to be present in the extracellular/extralyosomal environment in their proforms, which are substantially more stable than the mature enzymes.

Impaired cathepsin-L like activity may play a key role in the establishment of skin and gingival abnormalities seen in I-cell disease. In addition, reduced activities may play an important role in drug-induced gingival overgrowth.⁶⁵

In addition to the requirement of host cell receptors, lysosomal cysteine proteases are required for productive infection by some viruses. It has been reported that SARS coronavirus utilizes the enzymatic activity of cathepsin L to infect ACE2-expressing cells.⁶⁶

Cathepsin L also seems to be partly responsible for the degradation of cartilage⁴² and joints in osteoarthritis.^{33, 46}

In addition, monocyte-derived macrophages, mainly involved in tissue damage in chronic inflammatory diseases, have been shown to secrete fully processed and active forms of cathepsin B, L, and S into the extracellular milieu.

Role of Cathepsins in Cancer

Proteolytic activities from all major protease classes including papain-like cysteine proteases have been implicated in cancer metastasis. The ability of malignant tumor cells to invade normal surrounding tissue contributes in large part to the significant morbidity and mortality of cancers. Invasiveness requires several distinct cellular functions including adhesion, motility, detachment, and extracellular matrix proteolysis.

Tumor progression and metastasis require local proteolysis for the spatial expansion of tumors, the generation of tumor supporting blood vessels (angiogenesis), and the migration of transformed cells in and out of the vascular system (metastasis) (Figure 15).⁵

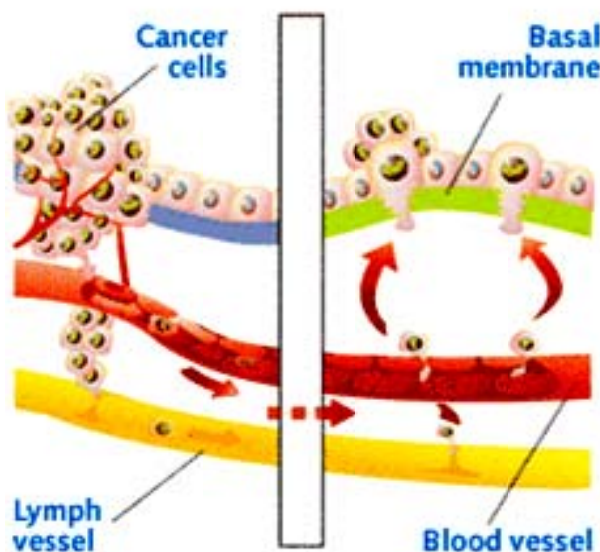


Figure 15. Diagrammatic representation of metastasis. Taken directly from <http://bh.sanofi-aventis.com>.¹³⁴

The largest structural barrier to formation of metastases and invasive growth of malignant tumors is the connective tissue of the extracellular matrix (ECM); the most important part being the basal membrane, which provides an immunological separation of different tissues, surrounding the blood and lymph vessels.⁶⁷ The basal lamina is composed of type IV collagen, proteoglycans, and the cell surface proteins fibronectin, laminin, and entactin (Figure 16).⁶⁸

A characteristic of malignant tumors is the destruction of the extracellular matrix (ECM).^{69, 60} It is now certain that the degradation of the ECM, which is necessary for metastasis formation and invasion of tumors into neighboring tissue, involves proteolytic enzymes such as plasminogen activators, cathepin B,⁴⁴ cathepsin L and collagenase^{69, 70,}⁵⁹⁻⁶⁰ in addition to metallo and serine proteases.⁶⁰

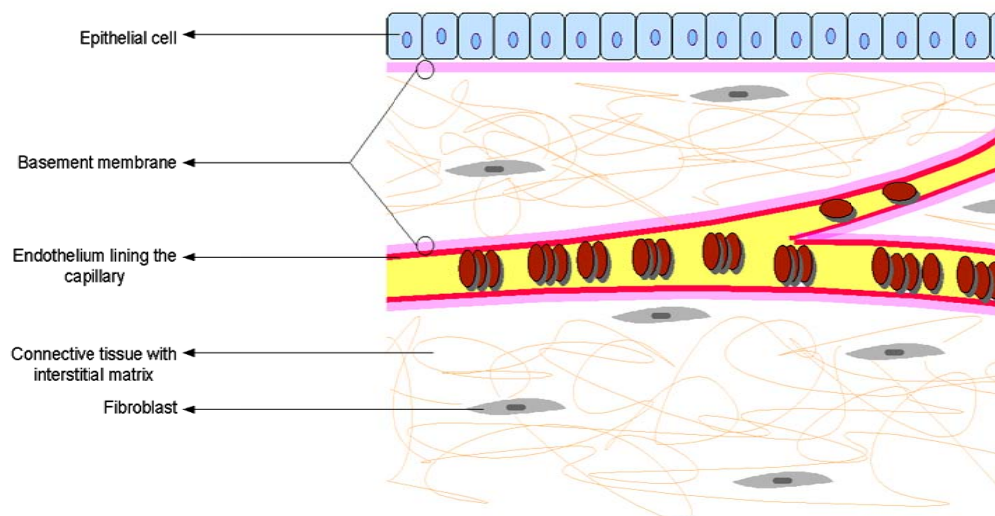


Figure 16. Diagrammatic representation of extracellular matrix components

It has been postulated that these activities are organized in activation cascades. For example, procathepsins B and L can be activated by cathepsin D, by tissue (tPA) and urokinase plasminogen activators (uPA), or by cathepsin G (serine protease).⁷¹

Active cathepsins B and L can then convert more uPA zymogen and plasminogen into their proteolytically active forms which in turn have matrix metalloproteinase activating properties.⁷² The role of cathepsin B in extracellular matrix degradation is supported by the findings that this protease undergoes intracellular redistribution from the apical region to the basal plasma membrane when compared with normal cells.⁷³

Proteases involved in tumor invasion and metastasis are not only expressed by tumor cells, but also by surrounding stromal cells. Tumor cells activate protease expression in stromal fibroblasts which then assist in the degradation of the extracellular matrix. It has been shown that fibroblasts neighboring tumor cells have elevated levels of gelatinase B (MMP9).⁷⁴

Most cathepsin-like proteases released by tumor cells have a higher molecular weight and unusual stability at neutral to alkaline pH, mainly due to their binding to the external cell surface proteins which increase their pH stability.⁷⁵ Tumor cathepsins do not differ from normal lysosomal cathepsins in their immunological and kinetic characteristics.⁶⁹

Alterations in the balance between endogenous inhibitors and the cathepsins have been postulated to contribute to malignant progression.⁶⁷ In various cancers, the level of cathepsin in the plasma membrane fraction is up to 30 times higher than that in nonpathological cells, indicating that these enzymes are protected from endogenous cysteine protease inhibitors and denaturation through membrane binding. For example, high expression levels of cathepsin B in colorectal cancer patients correlated with shorter survival,⁷⁶ and it has been reported that inhibition of cell-surface cathepsin B can prevent the activation of uPA, a well-known prognostic marker in cancer.⁷⁷

Previous studies have linked over-expression of cathepsin L to metastasis following ras transformation of NIH/3T3 cells. It has been reported that non-metastatic melanoma cells were converted to metastatic cells by over-expression of cathepsin L.¹⁰ Elevated expression levels of cathepsin L have also been reported in kidney and testicular tumors, meningiomas, non small cell carcinomas of the lung and in most cancers of the breast, ovary, colon, adrenal, bladder, prostate, and thyroid.^{69, 38, 25}

Increased expression levels of cathepsin B have been observed at the invasive edge of various tumors including bladder, colon, and prostate carcinomas,^{78,79,44} and cathepsin K has been associated with human breast carcinoma.⁶

Cell Invasion and Motility Assays

Commercially available Matrigel[®] invasion chambers provide cells with artificial conditions that allow assessment of their invasive property *in vitro*. Cell invasion chambers consist of polycarbonate membrane inserts (8 μm pore size) in a 24-well plate. The upper surface of the insert membrane is coated with a thin layer of Matrigel[®] basement membrane matrix, which acts as a reconstituted basement membrane *in vitro* and blocks non-invasive cells from migrating through the membrane.

In contrast, invasive cells are able to degrade the matrix proteins in the layer, invade through the Matrigel[®] matrix and ultimately pass through the pores of the polycarbonate membrane. Finally, non-invasive cells are removed from the top of the membrane and the invaded cells are stained and quantified (Figure 17).

Control inserts that contain only the 8 μm mesh without the Matrigel[®] coating are used in motility assays. Migration is measured as described in the invasion assay.

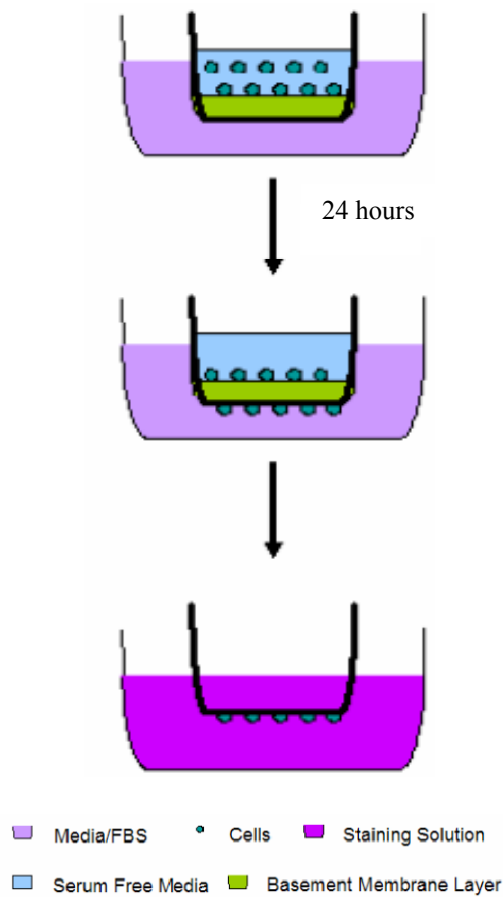


Figure 17. Diagrammatic representation of a cell invasion assay. Figure taken directly from www.cellbiolabs.com.¹³⁵

Role of Cruzain in Chagas Disease (American Trypanosomiasis)

As a result of the roles of many cathepsin L-like proteases in diseases such as malaria (falcipain), leishmaniasis (*Leishmania major* cathepsin L), Chagas disease (cruzipain), African trypanosomiasis (congopain), toxoplasmosis (*Toxoplasma gondii* cathepsin L), amoebiasis (histolysain), and sleeping sickness (rhodesain), inhibitors of human cathepsin L are proposed to be highly valuable as therapeutic treatments against these infectious diseases.⁸⁰

Parasitic papain-like cysteine proteases have been shown to be virulence factors by degrading components of the host immune system including immunoglobulins and components of the complement system. They are able to degrade extracellular matrix proteins and enhance the processing of various zymogens such as procollagenases and proenzymes of the clotting system, or exhibit a kininogenase activity and release bradykinin.⁸¹ In vitro studies demonstrated that cruzipain is involved in the activation of the kinin cascade, favoring parasite invasion in the host cells expressing kinin receptors.⁸²

Characterization of Chagas Disease

Chagas disease, caused by the parasitic protozoan *Trypanosoma cruzi*, is the leading cause of heart disease in Latin America and affects more than 12 million people, resulting in more than 50,000 deaths each year mainly because of chronic chagasic cardiomyopathy.⁸³ Large-scale population movements have increased the geographic distribution and changed the epidemiology of Chagas disease, with isolated cases reported in the United States.

T. cruzi is transmitted to humans either by triatomine vectors (kissing bug) or less commonly by blood transfusions or organ transplants. It has been established that the presence of *T. cruzi* is essential for the disease to persist and elimination of *T. cruzi* is a pre-requisite for the cure.^{84, 85}

Available chemotherapy for Chagas disease is unsatisfactory with current therapeutic molecules such as, nifurtimox (Nfx) and benznidazole (Bnz), which show limited efficacy and severe side effects for the treatment of chronic forms of the disease (Figure 18).⁸⁶⁻⁸⁸ Moreover, certain strands of *T. cruzi* have developed resistance to these two drugs.

Trypanosoma Cruzi

Throughout its life cycle five morphologies in reduviid vectors and four stages in mammalian hosts can be identified. The morphologies are sphaeromastigote, epimastigote mid log, epimastigote late log, metacyclic trypomastigote, and amastigote at different stages (Figure 19).

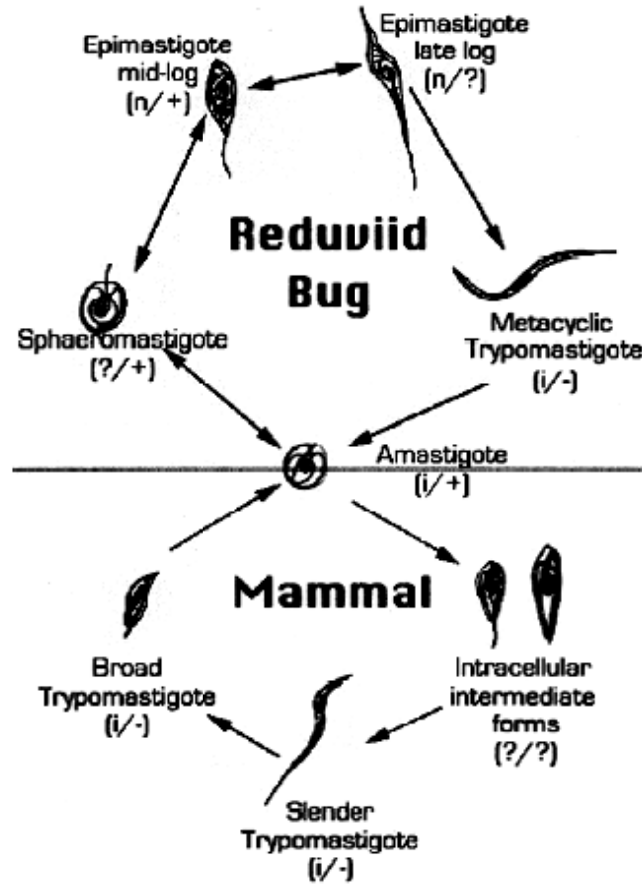


Figure 19. Diagram of *T. cruzi* morphologies in the vertebrate and invertebrate host. Not drawn to scale. (i) is an infective form; (n) is non-infective; (+) represents a proliferative form; and (-) is nonproliferative. Reproduced with kind permission from Tyler.⁹³

The amastigote is the intracellular replicate form of the parasite in the vertebrate host and the reduviid vectors during the transmission. As *T. cruzi* enters the mammal host, it shifts among broad trypomastigote, slender trypomastigote, and intracellular intermediate forms.

T. cruzi is found as an intracellular form, the amastigote, and as a trypomastigote form in the human blood. In the vector, noninfective dividing forms (epimastigotes) transform into metacyclic infective trypomastigotes in the insect's midgut. The infected bugs, while biting deposit feces which contain metacyclic trypomastigotes on the skin (human infections occurs through the bite wound or penetration of mucous membranes of the eyes, nose, or mouth) (Figure 20).⁹³

T. cruzi is the only human trypanosome that can be transmitted by the feces of its invertebrate vector, as most other trypanosomes are transmitted by saliva. After cell invasion, the vacuoles are disrupted and the parasite escapes into the cytoplasm of the cell, where it replicates into round-shaped amastigotes. After several binary divisions, infective trypomastigotes are released into the blood and tissue spaces.⁸⁸

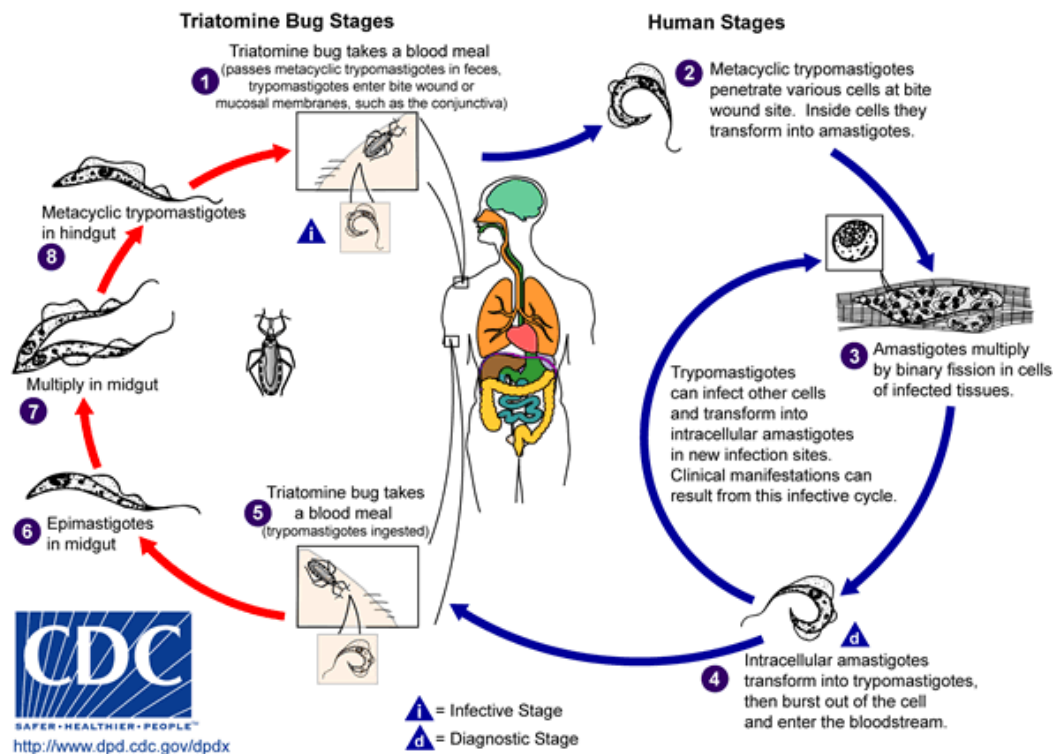


Figure 20. Overview of *Trypanosoma cruzi* infective and diagnostic stages. Figure taken directly from <http://www.dpd.cdc.gov/dpdx>.

Cruzipain

Cruzipain (also known as cruzain) is the major proteolytic enzyme present in all stages of the life cycle of *T. cruzi* with the highest expression levels in the epimastigote form.⁹⁴ This cysteine protease is crucial to *T. cruzi* throughout its life cycle including replication, metabolism, etc.^{95, 93}

The proteolytic activity of cruzain was suggested to contribute to the pathologic effects of Chagas disease. This cysteine protease participates in host tissue damage directly by secretion from the parasites, which may facilitate rupture of host cells or incidentally by leakage of the protease upon parasite death and lysis, thus stimulating the observed host immune response.^{89, 96}

Cruzipain is encoded by numerous polymorphic genes organized in tandem units (up to 130 in the Tul2 strain), resulting in relative complex isoforms with substrate specificity between those of cathepsins L and B.⁸⁷

The amino acid sequence data, coupled with enzymatic characterization classified this protease as a member of the papain superfamily of cysteine proteases with a sequence closely related to the major cysteine protease of *Trypanosoma brucei* (59.3%) and the murine cathepsin L (42.2%).⁹⁷

Inhibition of cruzipain has been shown to impair in vitro host cell invasion and to block amastigote replication as well as trypomastigote/amastigote differentiation, thereby arresting intracellular development. More recently, a novel class of irreversible cysteine protease inhibitors, vinyl sulfones, induced an accumulation of the proform of cruzipain in the Golgi apparatus resulting in the death of *T. cruzi* epimastigotes.¹⁴

Production of Recombinant Cruzain

Recombinant proteins are obtained by introduction of their expressed genes in the genome of a simpler organism (like yeast or bacterium), which will express those recombinant genes as if they were its own genes.

The potential for toxicity and instability of heterologously expressed proteolytic enzymes is great. The target protein can be conjugated with another known protein to be separated on the basis of the affinity of the second protein, and even the target proteins can be over-expressed in those organisms.

The expression of the cruzain gene in bacteria proved to be very difficult until the expression plasmid, pCheY15LOX was used. A possible explanation for the success of this plasmid in generating relatively large quantities of recombinant enzyme is that this system initially produces inactive and insoluble protein.

The inactivation of the protease by precipitation in inclusion bodies provides an extremely convenient purification step. The urea solubilization of the fusion protein and subsequent refolding steps allow the recovery of the fusion protein which is processed autocatalytically to yield mature cruzain.⁸⁹

It has been reported that this protease has the capability and specificity to process its proform to the fully active mature protease with the same NH₂ terminus as that found on the endogenous enzyme.⁹⁵

The processed form of the recombinant protease has a NH₂-terminal sequence identical to that of the mature form of the protease purified from *T.cruzi*.

Expression Plasmid Vector

Once a purified phage clone, containing an insert of approximately 20 kb of *T. cruzi* DNA, was digested with several different restriction endonucleases (i.e. PvuI, Sall, and EcoRV) generating the same size (1845 bp) fragment, it was found that six copies of the gene are present in the genome and are organized in a tandem array of copies which are identical in all restriction endonuclease sites tested as indicated by Figure 21.

The three developmental stages of *T. cruzi* are epimastigotes (insect forms), trypomastigotes (bloodstream forms), and amastigotes (intracellular forms) and the mRNA encoding the enzyme is present in all three developmental stages with mRNA levels approximately 2-fold higher in the intracellular amastigote form.⁸⁹

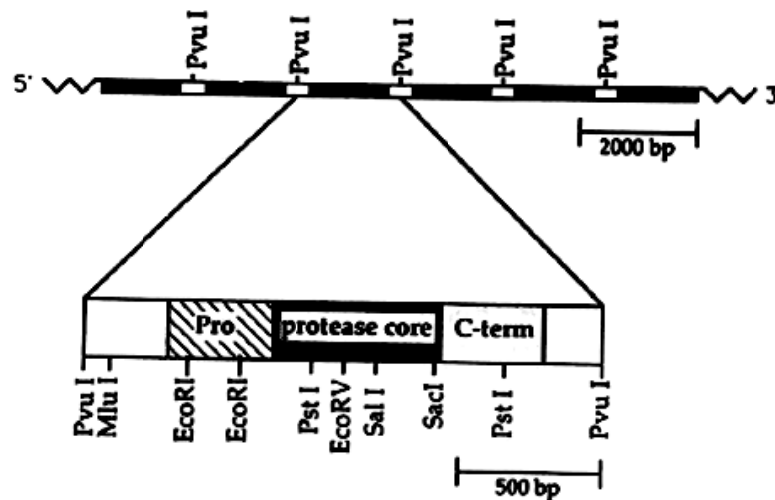


Figure 21. Diagram of the genomic organization of the gene as a tandem repeat of at least six copies. A restriction map is shown on the enlarged PvuI fragment to indicate the positions of the endonuclease sites which are conserved in each of the copies of the gene. Reproduced with kind permission from Eakin.⁸⁹

The gene encoding the proform (Cys-104 to Leu-342) of cruzain was ligated into the plasmid (pCheYTc) to permit expression of the proform of the protease as a fusion with the *E. coli* CheY protein under control of the lac promoter (Figure 22).

The proform of cruzain (beginning with amino acid Cys-104) was expressed as a fusion with 40 amino acids of the CheY protein of *E. coli*. An enteropeptidase site was included at the junction of this fusion to facilitate its removal after expression and isolation without altering the amino terminus of the *T. cruzi* protease.

The domains of the protease are demarcated and the sequences at the CheY-protease and protease domain junctions are shown above the Figure 22. The sites of autoproteolysis which remove the proregion and the COOH-terminal extension are indicated with arrows above the sequence. The active site Cys-25, His-159, and Asn-175 side chains are shown.⁸⁹

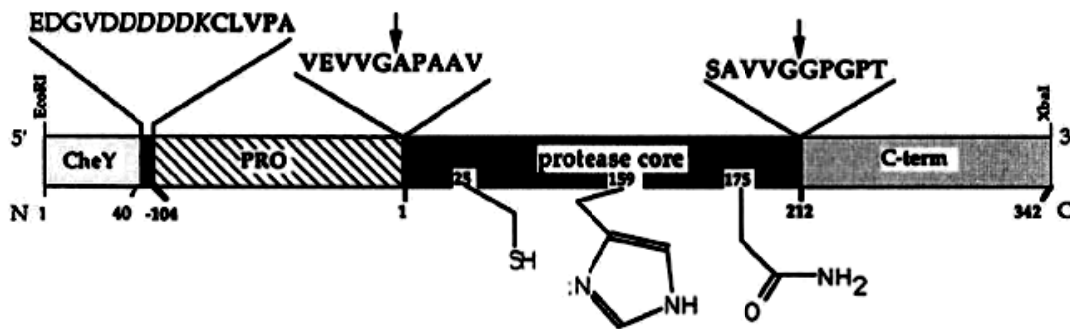


Figure 22. Plasmid vector used to express the *T. cruzi* cysteine protease in bacteria. The side chains of the amino acids of the catalytic triad are displayed below the diagram at their approximate positions within the protease core. The remainder of the expression plasmid (not shown) contains the lac promoter and the 3-lactamase gene, which confers resistance to ampicillin. Reproduced with kind permission from Eakin.⁸⁹

Autoproteolytic Processing

The incubation period activates the proteolytic processing events that remove the CheY fusion, the prodomain, and the COOH-terminal domain of the cruzain. These proteolytic events were assumed to be autoproteolytic, because a similar cleavage process was observed for the native protease purified from *T. cruzi* epimastigotes.¹³

As shown in Figure 23- sequence C, the first cleavage event to occur is the removal of the COOH-terminal domain by a bacterial protease or some other hydrolytic event. It occurs prior to the incubation period and as the polyprotein is bound to the anion exchange column (Q Fast Flow Sepharose).^{89, 13}

The subsequent processing events occur during the incubation period at 37°C for several hours. The second cleavage event releases the CheY fusion (Figure 23- sequence A) and takes place at two sites within the prodomain of the protease as determined by NH₂ terminal sequencing to yield protein with 90% of the sequence beginning at Ala-93 and 10% at Ser-87.

The final processing event is the removal of the remaining pro-domain (Figure 23- sequence B), resulting in fully active cruzain. At the same time, this incubation results in a reduction in the size of the fusion protein. The accurate molecular mass of the fully processed recombinant cruzain was determined by electrospray mass spectrometry to be 23.5 ± 6.6 kDa.¹³

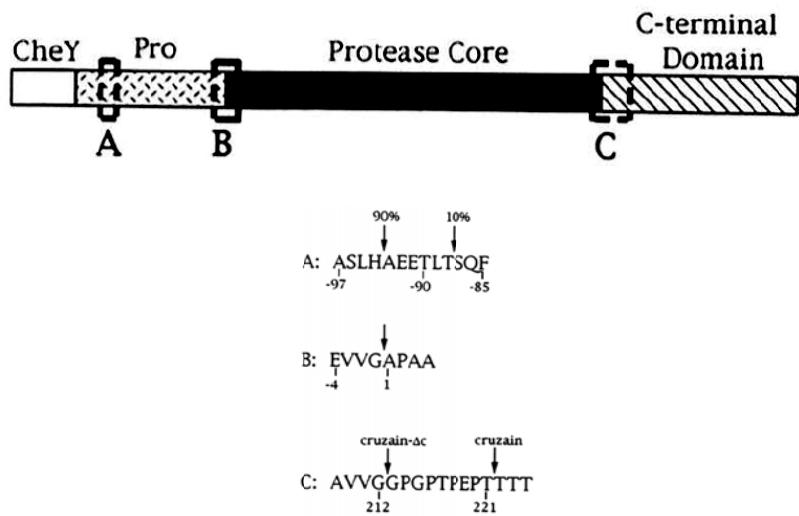


Figure 23. Scheme of the processing events that occur during purification and activation of the Che Y fusion protein to yield active cruzain. Reproduced with kind permission from Eakin.¹³

Basic Principles of Enzyme-Catalyzed Reactions

Steady State Kinetics

In biological systems, the rate of a reaction is determined by the enzyme that catalyzes the reaction. The conversion of substrate S to product P, catalyzed by enzyme E, under initial conditions (no P present) could proceed as:



Where, ES, k_1 , k_{-1} , and k_2 are the enzyme-substrate complex, ES forward rate constant, ES reverse rate constant, and the forward rate constant for product formation, respectively. The rate of this reaction is given by the well-known Michaelis-Menten expression and k_1 , k_2 are the initial velocity conditions and k_{-2} is neglected for initial velocity condition.

This equation was derived under the assumption that the substrate concentration [S] is much higher than that of enzyme [E], and the ES complex concentration is approximately constant until the substrate concentration is nearly depleted. The change in the ES complex concentration is zero and is represented as the following equation, where v_o is denoted as the initial velocity.

$$v_o = \frac{d[ES]}{dt} = 0 = k_1[E][S] - k_{-1}[ES] - k_2[ES]$$

Since the total enzyme $[E]_T$ is more readily determined than the free enzyme E or the enzyme-substrate complex ES , the relationship between the total enzyme $[E]_T$, the free enzyme E , and the ES complex is represented as,

$$[E]_T = [E] + [ES]$$

Substituting $[E] = [E]_T - [ES]$, the following equation can now be derived from the steady state assumption.

$$k_1([E]_T - [ES])[S] = (k_{-1} + k_2)[ES]$$

After dividing both sides by k_1 and solve for $[ES]$, the following result is obtained.

$$[ES] = \frac{[E]_T[S]}{\frac{k_{-1} + k_2}{k_1} + [S]}$$

To simplify the above equation, the Michaelis constant K_M is used to substitute for the constants of the denominator.

$$K_M = \frac{k_{-1} + k_2}{k_1}$$

And the equation becomes,

$$[ES] = \frac{[E]_T[S]}{K_M + [S]}$$

And v_o can now be represented as,

$$v_o = k_2[ES] = \frac{k_2[E]_T[S]}{K_M + [S]}$$

Since the maximal velocity V_{\max} occurs when the total enzyme is in the ES complex form $V_{\max} = k_2 [E]_T$, the above equation can be rewritten as the regular Michaelis-Menten expression.

$$v_o = k_2[ES] = \frac{V_{\max}[S]}{K_M + [S]}$$

The Michaelis-Menten plot is a hyperbola curve with an initial linear portion when the substrate concentration is small, and a plateau reaching V_{\max} when the substrate concentration is much greater than K_M , as shown in Figure 24.

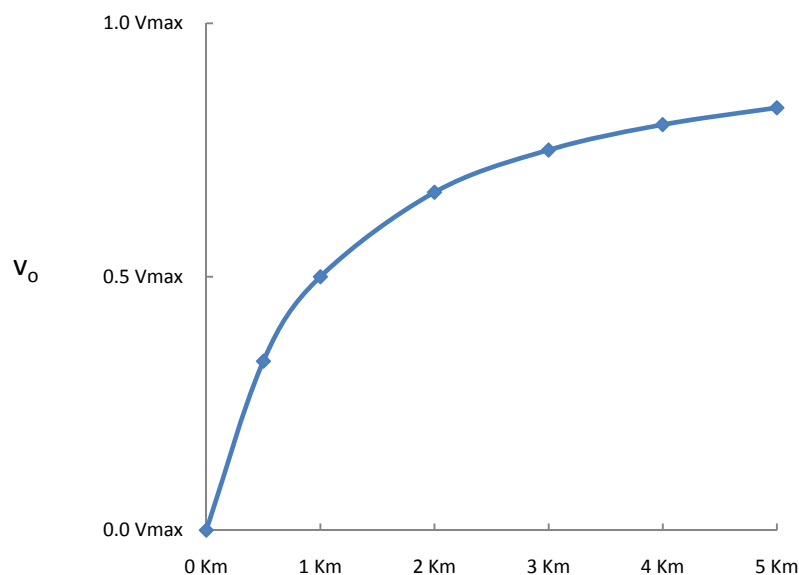


Figure 24. Typical Michaelis-Menten Plot.

Enzyme inhibitors are molecules that bind to enzymes and decrease their activity. Different types of enzyme inhibition are produced depending on whether the inhibitors bind the enzyme, the enzyme-substrate complex, or both.

The binding of an inhibitor can stop a substrate from entering the enzyme's active site and/or hinder the enzyme from catalyzing its reaction. Inhibitor binding is either reversible or irreversible.

Irreversible inhibitors usually react with the enzyme covalently and change it chemically. In contrast, reversible inhibitors usually can be classified as covalent or non-covalent.

Covalent inhibitors are characterized by the formation of a covalent bond, which is generally highly energetic, between inhibitor and protease. Non-covalent inhibitors interact with the protease solely through weaker bonds (hydrogen bonds and van der Waals forces).

Non-Covalent, Reversible Inhibition

Reversible inhibitors are characterized by their ability to dissociate (either rapidly or slowly) from the protease, allowing catalytic activity to be regained.

These inhibitors bind to enzymes with non-covalent interactions such as hydrogen bonds, hydrophobic interactions and ionic bonds.

Multiple weak bonds between the inhibitor and the active site combine to produce strong and specific binding.

Enzyme activity is restored by lowering the inhibitor concentration by dilution, dialysis or gel filtration. There are three major kinds of reversible enzyme inhibitors; competitive, mixed, and uncompetitive.²⁵

Competitive inhibition, in which the substrate and inhibitor cannot bind to the enzyme at the same time. This usually results from the inhibitor having an affinity for the active site of an enzyme where the substrate also binds; the substrate and inhibitor compete for access to the enzyme's active site.

This type of inhibition can be overcome by sufficiently high concentrations of substrate, i.e., by out-competing the inhibitor. Competitive inhibitors are often similar in structure to the real substrate and inhibit the substrate binding without affecting V_{max} for the reaction.⁹⁸

The following model describes that in addition to substrate binding, the free enzyme, E , can also bind a competitive inhibitor to form the enzyme-inhibitor complex EI .

However, the EI complex does not react with the substrate and therefore no reaction proceeds (Figure 25).

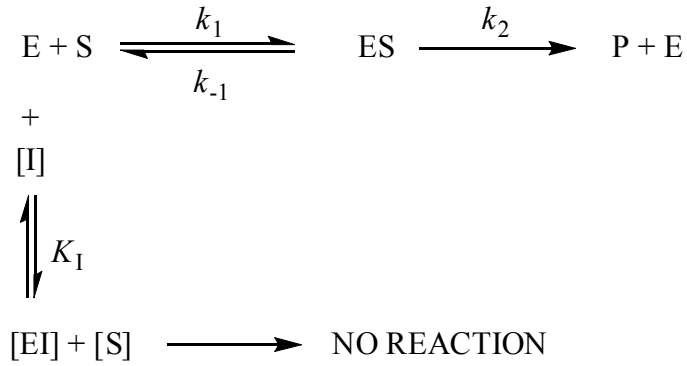


Figure 25. General kinetic scheme for competitive inhibition.

Here, the inhibitor I binds the enzyme reversibly and has a dissociation constant:

$$K_I = \frac{[\text{E}][\text{I}]}{[\text{EI}]}$$

Since $[\text{E}]_T = [\text{E}] + [\text{EI}] + [\text{ES}]$, and $[\text{E}]$ and $[\text{EI}]$ can be derived from the dissociation constants as:

$$\frac{K_M[\text{ES}]}{[\text{S}]} \text{ and } \frac{K_M[\text{ES}][\text{I}]}{[\text{S}]K_I} \text{ respectively}$$

$$[\text{E}]_T \text{ can be rewritten as } [\text{ES}] \left\{ \left(\frac{K_M}{[\text{S}]} \right) \left(1 + \frac{[\text{I}]}{K_I} \right) + 1 \right\}.$$

After solving for $[\text{ES}]$, the following equation is derived:

$$[\text{ES}] = \frac{[\text{E}]_T[\text{S}]}{K_M \left(1 + \frac{[\text{I}]}{K_I} \right) + [\text{S}]}$$

The initial velocity is expressed as,

$$v_o = k_2[\text{ES}] = \frac{k_2[\text{E}]_T[\text{S}]}{K_M \left(1 + \frac{[\text{I}]}{K_I} \right) + [\text{S}]}$$

If $1 + \frac{[\text{I}]}{K_I}$ is simplified to α , then the above equation can be rewritten as:

$$v_o = \frac{V_{\max}[\text{S}]}{\alpha K_M + [\text{S}]}$$

The double-reciprocal form is then:

$$\frac{1}{v_o} = \left(\frac{\alpha K_M}{V_{\max}}\right) \left(\frac{1}{[S]}\right) + \frac{1}{V_{\max}}$$

With a fixed enzyme and substrate concentration, the initial velocity decreases. A characteristic Michaelis-Menten plot for a competitive inhibitor is showed in Figure 26, in which initial velocities are plotted versus substrate concentration for various concentrations of inhibitor.

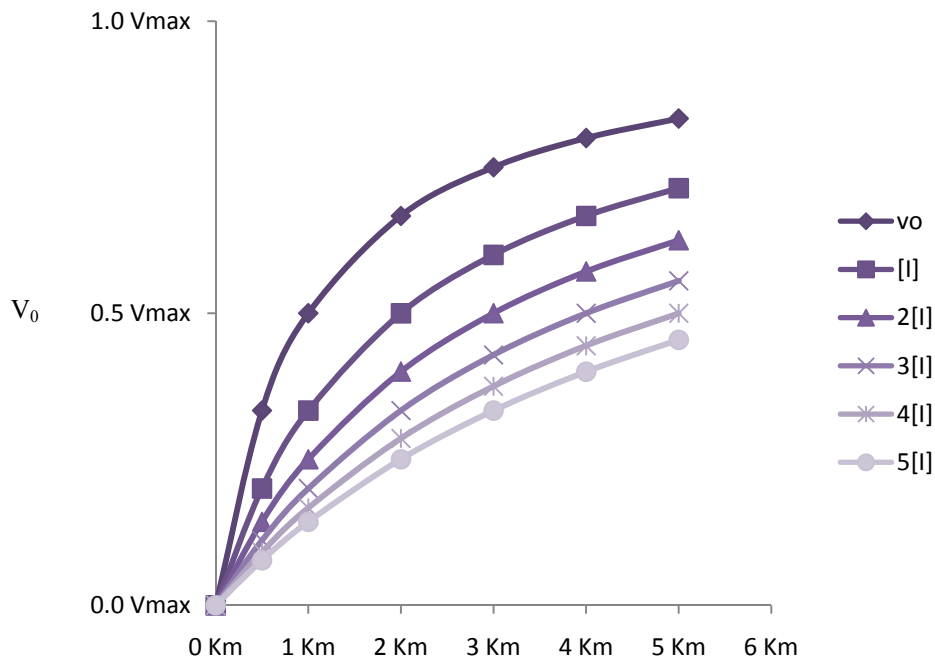


Figure 26. Plot of initial velocity of a simple Michaelis-Menten reaction versus the substrate concentration [S] in the presence of different concentrations of a competitive inhibitor [I].

Mixed inhibition, where the inhibitor can bind to the free enzyme at the same time as the enzyme-substrate complex; however, the binding of the inhibitor may affect the binding of the substrate (Figure 27). This type of inhibition may be reduced, but not overcome by increasing concentrations of substrate.

A typical Michaelis-Menten profile for a mixed inhibition is showed in Figure 28 and is similar to both competitive and uncompetitive inhibition.

Although it is possible for mixed-type inhibitors to bind in the active site, this type of inhibition generally results from an allosteric effect where the inhibitor binds to a different site on an enzyme.

Inhibitor binding to this allosteric site changes the conformation (i.e., tertiary structure or three-dimensional shape) of the enzyme so that the affinity of the substrate for the active site is reduced.⁹⁸

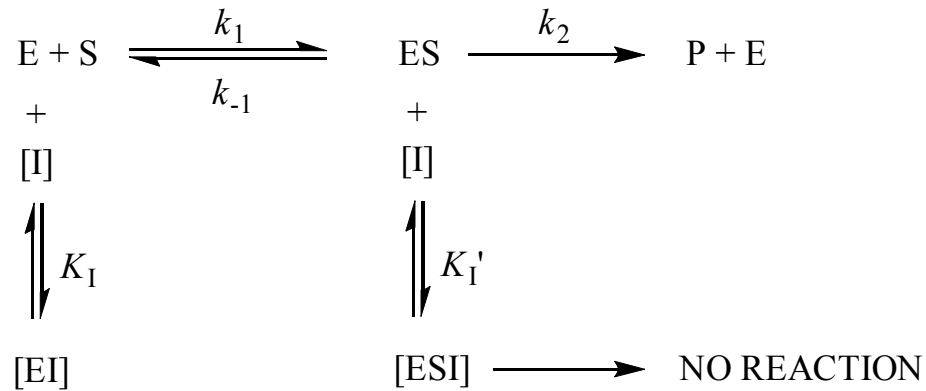


Figure 27. General kinetic model of mixed inhibition.

Using the same method as in the derivation of the previously derived competitive inhibition relationships, the initial velocity expression is demonstrated as,

$$v_o = \frac{V_{\max}[S]}{\alpha K_M + \alpha'[S]}$$

$$\alpha = 1 + \frac{[I]}{K_I}, \quad \alpha' = 1 + \frac{[I]}{K_I'}$$

The Lineweaver-Burk expression is the reciprocal of the above equation,

$$\frac{1}{v_o} = \left(\frac{\alpha K_M}{V_{\max}}\right) \left(\frac{1}{[S]}\right) + \frac{\alpha'}{V_{\max}}$$

Mixed inhibition makes the plot of initial velocities versus substrate concentration in the presence of inhibitor similar to both competitive inhibition and uncompetitive inhibition, but the Lineweaver-Burk plot is much different (Figure 31).

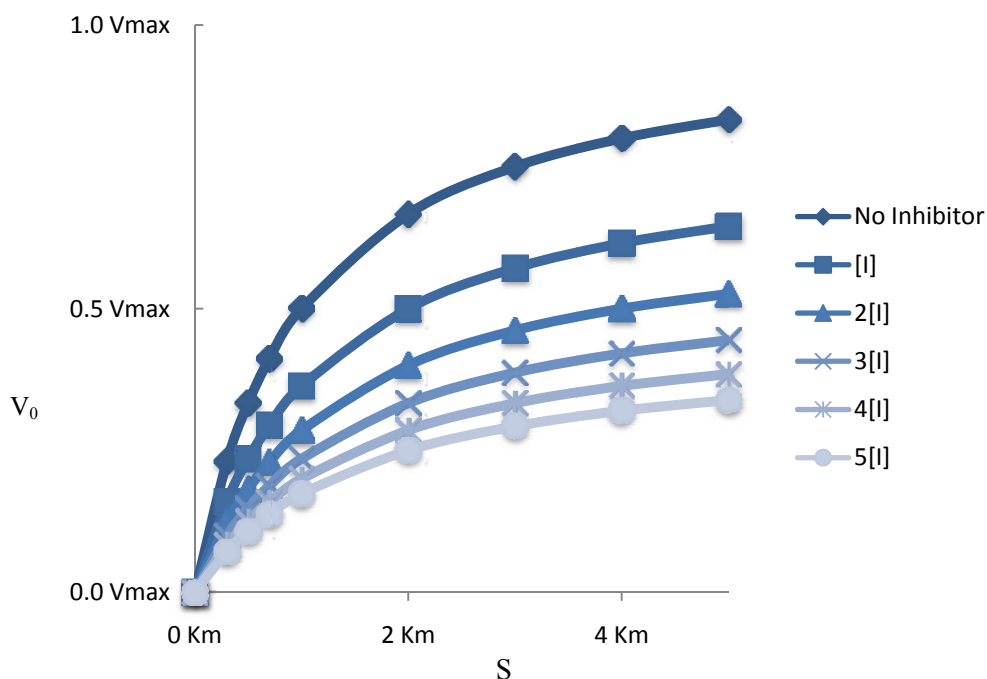


Figure 28. Plot of initial velocity of a simple Michaelis-Menten reaction versus the substrate concentration [S] in the presence of different concentrations of a mixed inhibitor [I].

Uncompetitive inhibition, takes place when an inhibitor binds only to the complex formed between the enzyme and the substrate but not to the free enzyme (Figure 29). This reduction in the effective concentration of the E-S complex increases the enzyme's apparent affinity for the substrate and decreases the maximum enzyme activity as it takes longer for the substrate or product to leave the active site.⁹⁸

The dissociation constant for the enzyme-substrate-inhibitor complex ESI is

$$K'_1 = \frac{[ES][I]}{[ESI]}$$

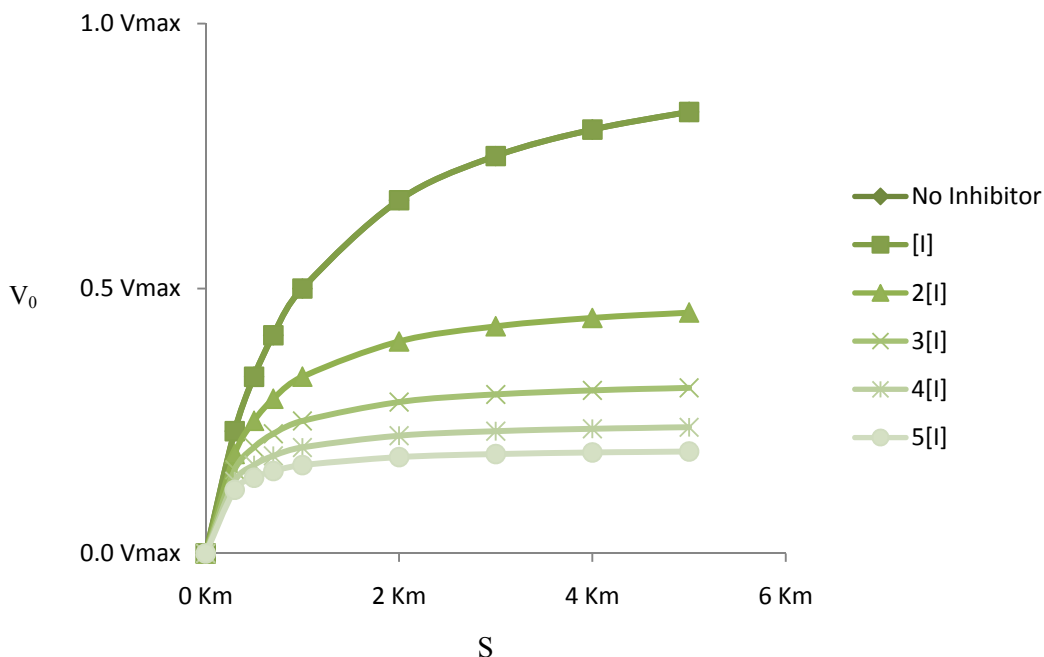


Figure 30. Plot of initial velocity of a simple Michaelis-Menten reaction versus the substrate concentration $[S]$ in the presence of different concentrations of an uncompetitive inhibitor $[I]$.

Although reactions are best fit directly to the Michaelis-Menten equation by non-linear regression analysis, the Lineweaver-Burk plot is a useful approximation to distinguish between different types of reversible inhibition (Figure 31).

The Lineweaver-Burk plot for competitive inhibition (Figure 31 A) is a series of lines intersecting at the y-axis. Indicative of competitive inhibition, V_{\max} is unchanged, but the apparent K_m ($K_{M,inh.}$ or αK_M) is increased according to the potency of the inhibitor.

The Lineweaver-Burk plot of uncompetitive inhibition is a series of parallel lines (Figure 31-B). Although the Lineweaver-Burk plot for mixed inhibition looks very similar to the one for a competitive inhibitor, the intersecting point of the individual lines is to the left of the y-axis. This indicates that the V_{\max} decreases in the presence of the inhibitor and the K_M value changes according to increasing concentrations of the inhibitor as shown in (Figure 31 D).

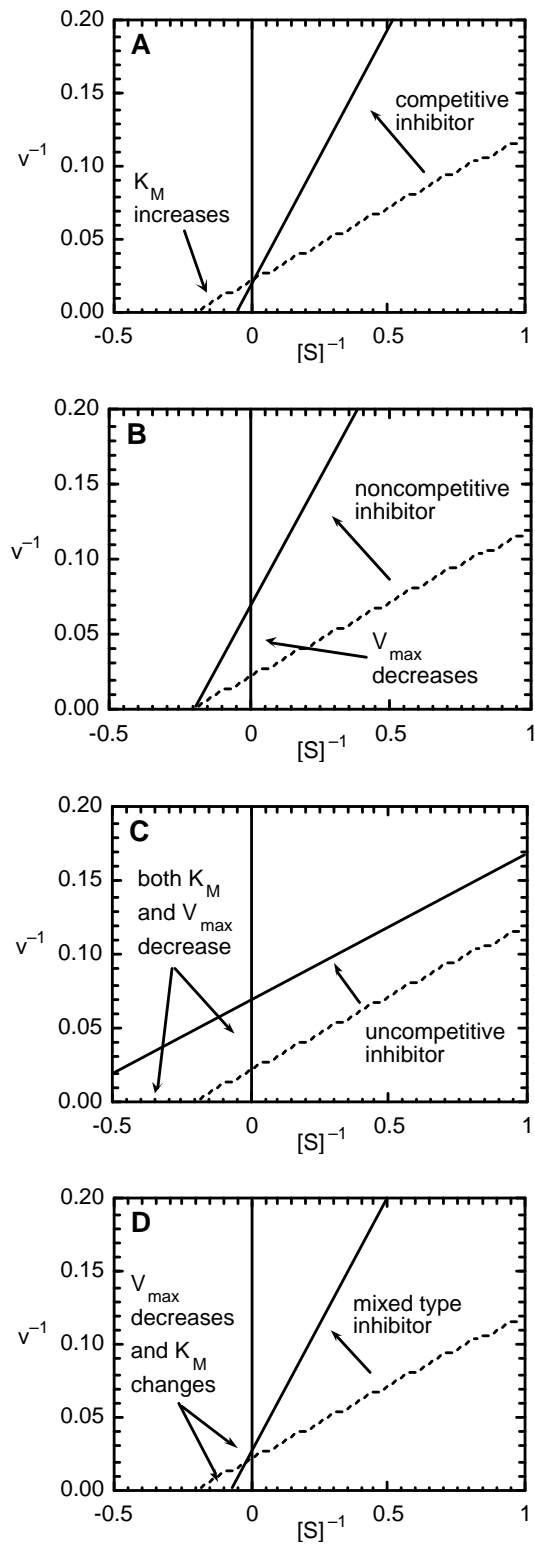


Figure 31. The Lineweaver-Burk graph as a tool to distinguish types of reversible inhibition. A. Competitive inhibition. B. Noncompetitive inhibition. C. Uncompetitive inhibition D. Mixed-type inhibition.

Irreversible Inhibition

Irreversible inhibitors usually covalently modify an enzyme with no reversal of inhibition observed upon decreasing the inhibitor concentration.

Due to the nature of a covalent bond, the bond between the inhibitor and enzyme is permanent resulting in the possibility of immunogenicity upon chronic exposure in therapeutics, or toxicity, because the inhibitor may form covalent bonds with other enzymes in the body.

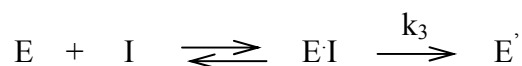
Development of drugs that irreversibly inactivate the targeted enzymes for chronic use is not usually an ideal objective. It is believed that long-term treatment of disease conditions using such irreversible inhibitors may lead to certain immune disorders, and/or increase the potential risk of haptensisation.

However, the short-term acute use of irreversible inhibitors for the treatment of certain disease conditions such as bacterial, viral, parasitic diseases, and cancer may be more readily acceptable.⁹

The binding and inactivation steps of an enzyme-inhibitor reaction are investigated by incubating the enzyme with inhibitor and assaying the amount of activity remaining over time.

The activity will decrease in a time-dependent manner, usually following exponential decay (Figure 32). Fitting these data to a rate equation gives the rate of inactivation at a specific concentration of inhibitor.

The expected reaction scheme for the formation of the irreversibly inactive enzyme is shown as the following:



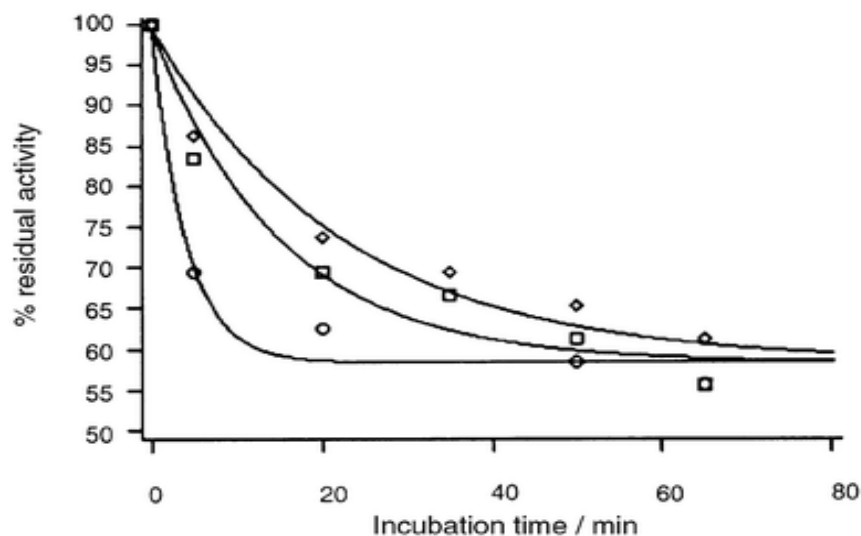


Figure 32. Time dependent inhibitor profile. Taken directly from <http://www.rsc.org/ej>.¹³⁶

Where, E is the free enzyme; I is the inhibitor; the enzyme is assumed to be in equilibrium with the reversible enzyme-inhibitor complex, E.I; and E' is the inactivated enzyme.

K_1 the equilibrium constant for the dissociation of the E.I complex, is equal to $[E][I]/[E.I]$; and k_3 is the rate constant (first order) for the conversion of the E.I complex to E'.

The total enzyme concentration, E° , is expressed as:

$$E^\circ = E + E.I + E' = \varepsilon + E'$$

The symbol ε represents the total remaining enzyme activity, so that $\varepsilon = E + E.I$

The rate of the inhibition is express as:

$$-\frac{d(\varepsilon)}{dt} = k_3[E.I] = k_3 \frac{[E][I]}{K_1}$$

$$\varepsilon = [E] + [E.I] = [E] + \frac{[E][I]}{K_1} = [E]\left(1 + \frac{[I]}{K_1}\right)$$

$$E = \left(\varepsilon - \frac{\varepsilon}{1 + [I]/K_I} \right)$$

$$-\frac{d(\varepsilon)}{dt} = k_3[E \cdot I] = k_3(\varepsilon - E) = k_3 \left(\varepsilon - \frac{\varepsilon}{1 + [I]/K_I} \right)$$

The solution is:

$$\ln \frac{\varepsilon}{E^\circ} = - \left(\frac{k_3}{1 + [I]/K_I} \right) t$$

This equation shows that irreversible inhibition is progressive with respect to time. For $[I] \gg E^\circ$, a plot of the $\ln \varepsilon/E^\circ$ versus time should give a straight line with a slope of:

$$k_{app} = \frac{k_3}{1 + K_I/[I]}$$

Then

$$-\frac{1}{k_{app}} = \frac{1}{k_3} + \frac{K_I}{k_3} * \frac{1}{[I]}$$

If K_I is very large or $[I]$ is very small, then the kinetics cannot be distinguished from a simple bimolecular reaction where k_3/K_I would be the second order rate constant for inactivation.¹⁰⁰

Special Cases

Slow-binding inhibitors, reversible inhibitors that inhibit enzyme activity very slowly due to conformational changes following enzyme-inhibitor complex formation; or irreversible inhibitors, which react with the enzyme via a non-covalent transition state that lead to rapid reduction of enzyme activity.

The initial enzyme–inhibitor complex undergoes isomerization to a second more tightly held complex, but the overall inhibition process is reversible.

Under these conditions, traditional Michaelis–Menten kinetics can give a false value for K_I , which is time–dependent. The true value of K_I can be obtained through more complex analysis.^{101, 102}

From the kinetic point of view, three possible mechanisms have been considered for slow binding inhibition (Figure 33). Binding between enzyme and inhibitor may either involve a single step, with small slow on ($k_{on[I]}$) and off rates (k_{off}) (Figure 33 a); have an initial fast-binding step, followed by a slow reversible transformation of EI to an intermediate, EI* (Figure 33b); or have an initial slow conformational change of the enzyme E into E*, prior to binding the inhibitor by a fast step (Figure 33 c).¹⁰³

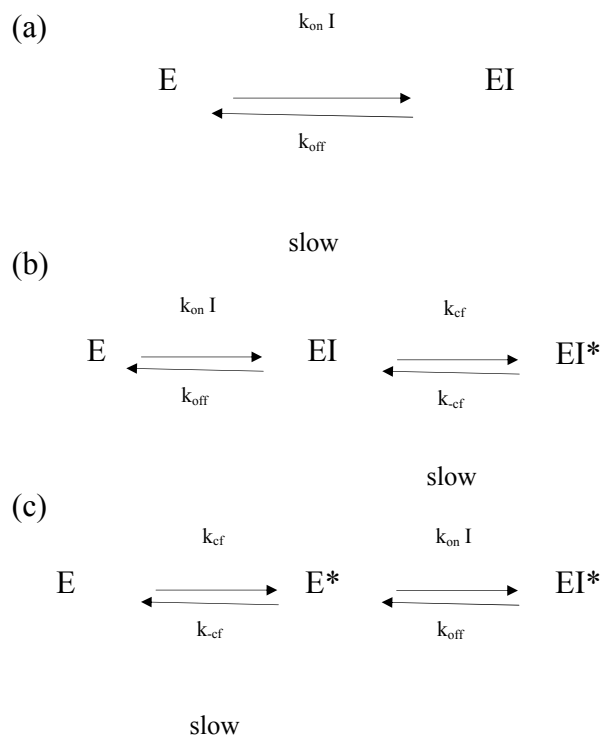


Figure 33. Kinetic schemes for three mechanisms of slow inhibition: (a) 'Direct binding' model, (b, c) two 'conformational change' models¹⁰³

For mechanism (33a) the time evolution is described by simultaneous differential equations $dP(t)/dt$ and $dE(t)/dt$. Under steady-state conditions, with respect to substrate, these are solved in closed form to yield the progress curve equation:

$$P(t) = A \left(1 - \frac{\alpha}{\beta}\right) t + \left(\frac{AC}{\beta}\right) [\exp(-\beta t) - 1]$$

where,

$$A = V_m \times \frac{s}{l+s}, s = \frac{[S]}{K_m}, \alpha = k_{on} \times \frac{[I]}{l+s}, \beta = \alpha + k_{off}, C = (ei)_{t=0} - \frac{\alpha}{\beta}, ei = [E_I]/[E_o]$$

For mechanism (33b), the progress curve for the above equation is also valid, but with different A, α and β coefficients:

$$A = V_m \times \frac{s}{(l+s+i)}, \alpha = k_{ef} \times \frac{i}{l+s+i}, \beta = \alpha + k_{-ef}, i = [I]/K_i$$

Also, mechanism (33c) has a progress curve that follows eqn. (1), but the A, α and β coefficients are:

$$A = V_m \times \frac{s}{(l+s)}, \alpha = k_{on} \times \frac{[I]}{l+s}, \beta = [k_{ef}/(l+s)] + [k_{-ef}/(l+i)]$$

For all the models the intrinsic $K_i = k_{off}/k_{on}$, although the progress curve data is given by the same equation for the three models, they can be distinguished by the dependence of the coefficients on the inhibitor concentration.

The coefficient of the linear term, the coefficient of the exponential term, and the apparent rate constant β can be determined by non-linear regression by fitting the experimental data to the progress curve equation.

The appearance of the progress curve will depend on the way the kinetic experiments are carried out. If enzyme and sufficient inhibitor are first preincubated, the constant $C > 0$ and as a result the progress curve will be upwards concave. In contrast, if no preincubation is performed, $C < 0$, and the progress curve will be upwards convex. Typical examples of slow binding progress curves and apparent rate constants (β) plots are presented in Figure 34.

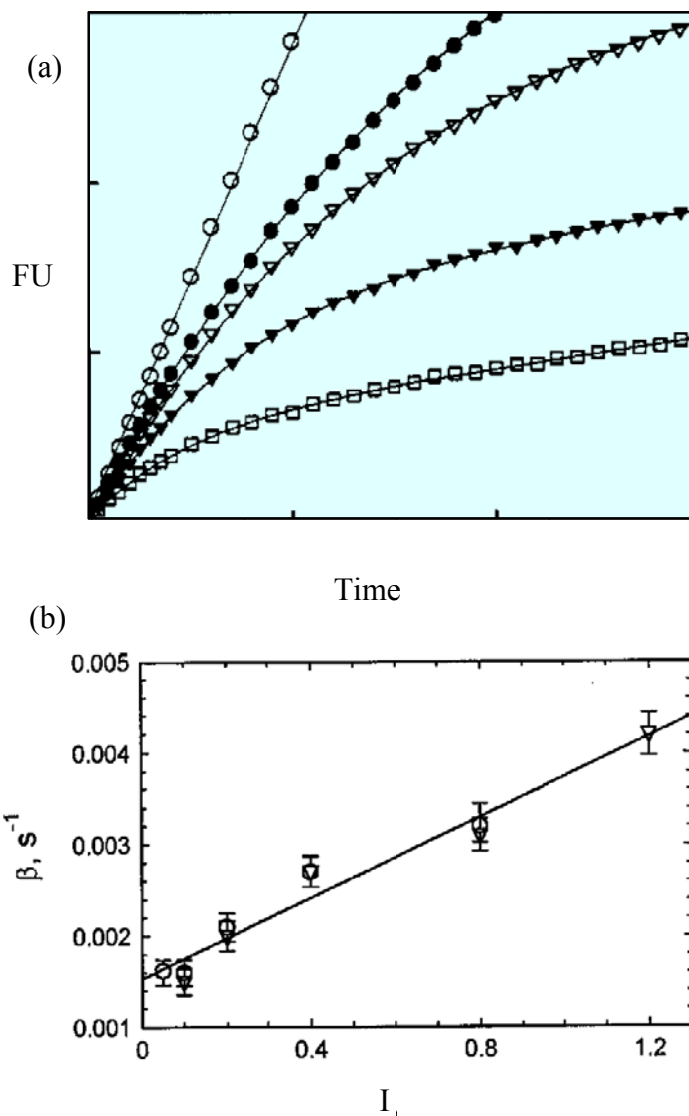


Figure 34. (a) Representative examples of slow binding progress curves. Reproduced with kind permission from Fox.¹⁰⁴ (b) Plots of the apparent rate constants β as a function of inhibitor concentration. Reproduced with kind permission from Lohse.¹⁰³

The apparent rate constant for mechanism (a) is a linear function of the inhibitor concentration represented by the following equation:

$$\beta = k_{on} \times [I] / \{(1+s) + k_{off}\}$$

The rate constants k_{on} and k_{off} can be determined from this rectilinear relationship.

The apparent rate constant is a monotonically increasing hyperbolic function of the inhibitor concentration for mechanism (b) and a decreasing hyperbolic function of $[I]$ for mechanism (c), having the form:

$$\beta = k_{ef} \times \frac{[I]}{\{(l + s)K_i + [I] + k_{-ef}\}}$$

Tight-binding inhibitors, reversible inhibitors that bind to the enzyme with high affinity and the enzyme inhibitor complex dissociate so slowly that it appears irreversible. These tight-binding inhibitors may show kinetics similar to covalent irreversible inhibitors.

In such cases, some of these inhibitors rapidly bind to the enzyme in a low-affinity enzyme-inhibitor complex which then undergoes a slower rearrangement to a very tightly bound enzyme-inhibitor complex.^{105,102}

The Williams-Morrison equation is applied for slow, tight-binding inhibitors and K_I is obtained from fitting the data sets to this equation. The Williams and Morrison equation is described below.

$$v = \frac{v_o}{2E_t} \sqrt{\left[\left(K_I \left(1 + \frac{S}{K_M} \right) + I_t - E_t \right)^2 + 4K_I \left(1 + \frac{S}{K_M} \right) E_t \right]} - \left[K_I \left(1 + \frac{S}{K_M} \right) + I_t - E_t \right]$$

In this equation, v is the the apparent velocity of the enzyme activity when substrate concentration is S , inhibitor concentration is I_t .

The total enzyme concentration is E_t . The dissociation enzyme-inhibitor constant and Michaelis-Menten constant are denoted as K_I and K_M , respectively.

The term $K_I \left(1 + \frac{S}{K_M}\right)$ is the apparent dissociation constant denoted as K_I^{app} .

In a given experiment, the dissociation constant K_I , Michaelis-Menten constant K_m , and the amount of total enzyme E_t remain the same.

Therefore, the above equation can be simplified as the following equation and used for non-linear regression analysis.¹⁰⁶

$$Y = \frac{v}{v_0} = \frac{E - X - K_I^{app} + \sqrt{\left((E - X - K_I^{app})^2 + 4 \times E \times K_I^{app}\right)}}{2 \times E}$$

Here, Y is the relative velocity of the enzyme, which is derived from the inhibited enzyme activity, v , divided by the uninhibited enzyme activity, v_0 . X is the inhibitor concentration used to inhibit the enzyme activity. E is the total enzyme concentration, which is also fixed for a given experiment. A typical plot is shown in Figure 35.

K_I^{app} is the apparent dissociation constant, which is obtained from the non-linear regression fit of this model. After the K_I^{app} is obtained from the model, the actual K_I can be obtained by solving the equation: $K_I^{app} = K_I \left(1 + \frac{S}{K_M}\right)$

IC₅₀ Values

The IC_{50} is a measure of the effectiveness of a drug candidate in inhibiting a biological or biochemical function and represents the concentration of a drug that is required for 50% inhibition *in vitro*. IC_{50} value is determined by three factors:

- The K_M . It takes more inhibitor to compete for a substrate with a low K_M than for a substrate with a high K_M .

- The concentration of the substrate. If a higher concentration of substrate is used, it will take a larger concentration of inhibitor to compete for 50% of the activity.
- The dissociation constant for binding of inhibitor to enzyme, the K_I . If this constant is low (the affinity is high), the IC_{50} will be low.

The experimental design to obtain this parameter will measure enzyme velocity at a single concentration of substrate with varying concentrations of an inhibitor.

Then, the initial velocity of these reactions is plotted against the logarithm of the inhibitor concentrations and often a sigmoid curve is obtained (Figure 36).²²

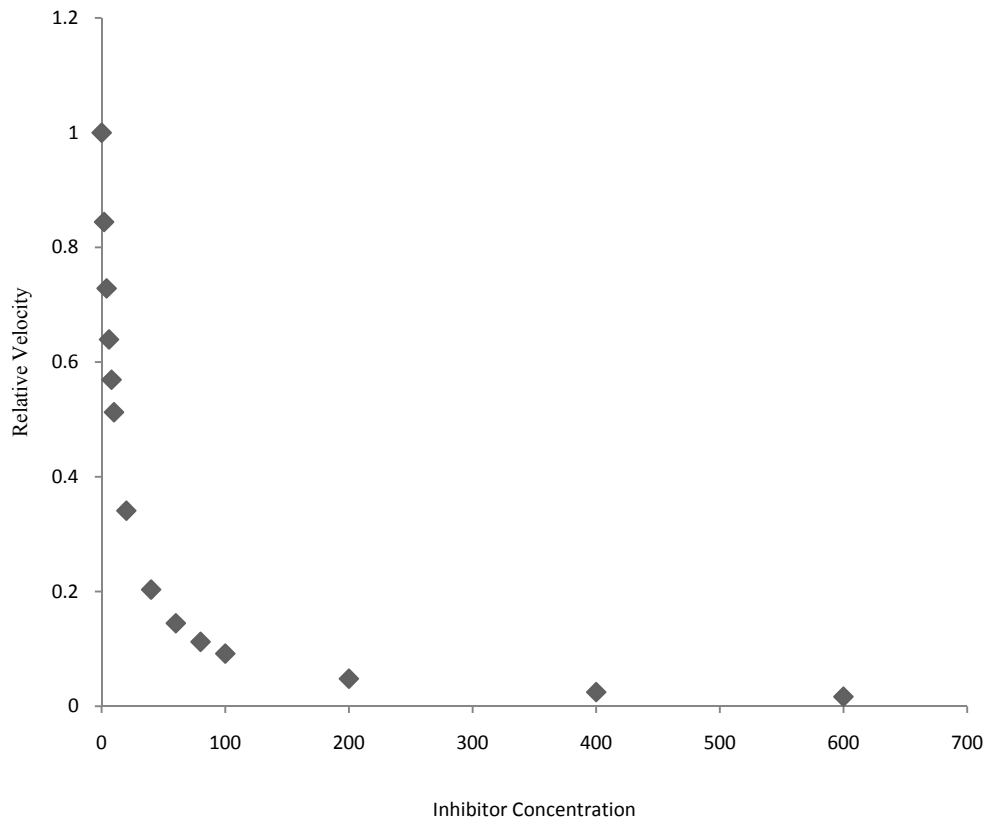


Figure 35. A typical Williams-Morrison plot.

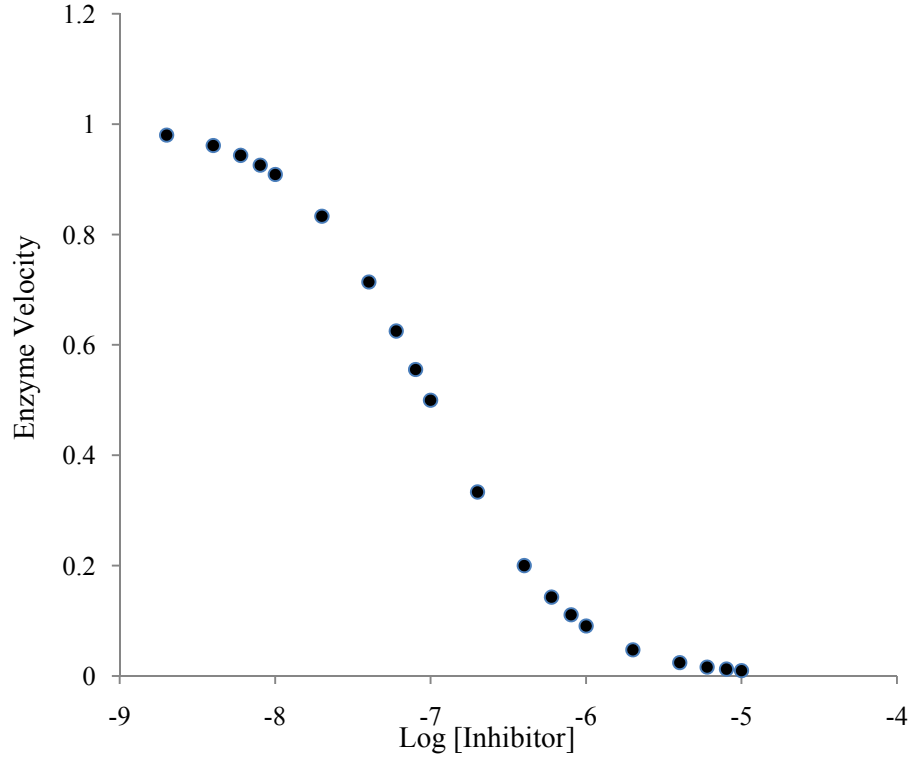


Figure 36. Typical IC₅₀ curve for competitive inhibitors.

Therefore, for a sigmoid-dose response with a variable slope, a modified version of the classical sigmoid model is used to fit the non-linear curve as follows:

$$Y = v_o = v_{Min} + \frac{v_{Max} - v_{Min}}{1 + 10^{(\text{LogIC}_{50} - X) \cdot \text{HillSlope}}}$$

Where, $Y = v_o$ is the initial enzyme velocity at various inhibitor concentrations. v_{Min} is the lowest enzyme activity when incubated with highest concentration of the inhibitor. v_{Max} is the highest enzyme activity without inhibition. X is the logarithm of the inhibitor concentration at which the initial enzyme velocity is Y , the Hill slope is the slope of the transition curve.

LogIC₅₀, which is logarithm of the IC₅₀ value of the inhibitor, can be determined visually, but is better to obtain this value from the non-linear regression fitting of the equation.

Basic Concepts of Drug Design

The implication of cathepsins in numerous vital processes and pathologies make them highly attractive targets for drug design. A medicinal enzyme inhibitor is often judged by its specificity (its lack of binding to other proteins) and its potency (its dissociation constant, which indicates the concentration needed to inhibit the enzyme). A high specificity and potency ensure that a drug will have few side effects and thus low toxicity.¹⁰⁷

All enzymes are regulated under normal conditions; however, proteases have the advantage of being regulated by endogenous competitive inhibitors. Endogenous protease inhibitors such as serpins, cystatins, and tissue inhibitor of metalloproteases (TIMP) bind to the substrate-binding pocket on their respective protease, but in such a way that the binding is not conducive to hydrolysis.

Therefore, the regulation of proteolytic activity by small-molecule inhibitors can mimic the natural regulation mechanisms. This fact has fostered the hope that proteases are amenable to inhibition by small-molecule drugs and that this inhibition can have desirable physiological effects.²²

There has been great success in developing inhibitors for a number of different proteases; however, this success has not been easily translated into clinically useful drugs. The limited substrate specificity of some proteases can make it more difficult to develop selective drugs that target only a single protease. This may be one of the reasons why relatively few proteases are clinically validated targets.²²

An exception of this fact is the potent and selective cathepsin K inhibitor, Odanacatib, currently in clinical development (phase III trial) for the treatment of postmenopausal osteoporosis (Figure 37).⁴³

Cathepsin K is the primary lysosomal cysteine protease that is highly expressed in osteoclasts, the cells responsible for bone degradation during bone remodeling. Osteoporosis is a disease in which the balance of bone resorption and formation has been pathologically disrupted by an inactive form of cathepsin K and there is an excessive bone breakdown. Thus, a specific cathepsin K inhibitor could restore this balance and improve bone health.^{6,35}

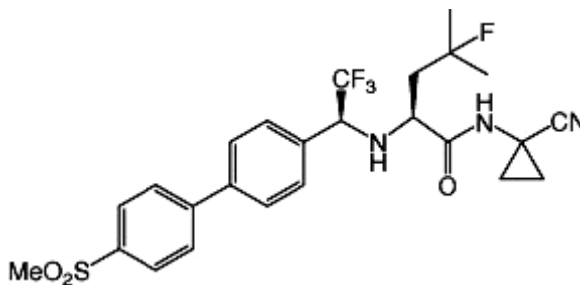


Figure 37. Odanacatib chemical structure. Odanacatib is very potent ($IC_{50}= 0.2$ nM) and highly selectivity against cathepsin B ($IC_{50}= 1034$ nM) and cathepsin L ($IC_{50}= 2995$ nM).⁴³

The most important concept in drug design is to understand the mechanisms by which the active site of the enzyme selectively restricts the binding of inappropriate structures.

Once this is known, combinations of chemical structures must be devised taking into account biological considerations for the development of new drugs to avoid chemical structures that are highly toxic to biological system.

Pharmacokinetic and pharamacodynamic considerations are not covered here in detail because they are outside the scope of this dicussion.

In general, the designed inhibitors should have “drug-like” properties such as minimal peptide character, high membrane permeability, long plasma half-lives, slow elimination, high selectivity for the protease target and good oral availability.

Important Low-Molecular-Weight Cysteine Protease Inhibitors

Cysteine proteases have proven to be good targets for the design of irreversible inhibitors because these enzymes use an active site residue (rather than a water molecule) to attack the carbonyl of the scissile bond of their substrates.

Irreversible inhibitors of proteases contain an electrophile that, upon reaction with the protease, forms a non-hydrolyzable adduct. Typical electrophiles that form non-hydrolyzable adducts include α -haloketones, diazoketones, and epoxide derivatives (Figure 38).²²

Since the utility of irreversible protease inhibitors as human therapeutics has caused concerns, recent research has been directed toward the identification of reversible inhibitors with hydrolyzable electrophiles, such as nitriles, aldehydes, and ketoheterocycles (Figure 38).²²

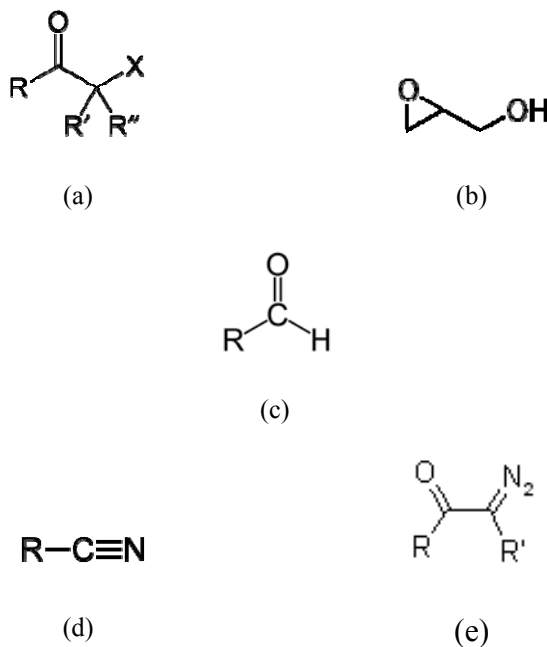


Figure 38. Functional groups of reported cysteine proteases inhibitors. (a) α -haloketones (b) epoxysuccinyl, (c) aldehyde, (d) nitrile, (e) diazoketones. R is an alkyl or aryl residue and X any one of the halogens

Peptidic Inhibitors of Cysteine Proteases

Most of the previously reported inhibitors of cathepsin L were peptidic in nature and irreversibly bind to the active site residues.¹⁰⁸

Since the discovery of E-64 in 1978 as a potent cysteine protease inhibitor a variety of inhibitors containing small rings as electrophilic building blocks responsible for enzyme inhibition have been developed. In this section peptidic and peptidomimetic inhibitors containing epoxide, aziridine, and β -lactam rings as electrophilic fragments are discussed.³⁹

It is suggested that an epoxysuccinyl fragment can be used as a building block that enables access to both the prime and non-prime substrate binding sites, in contrast to chloromethyl, fluoromethyl or aldehyde based inhibitors that would be active only in the non-prime subsites ((Figure 39).¹⁰⁹ A common feature of all inhibitors with three membered heterocycles bearing carboxylic acids or derivatives at the ring is the selective inhibition of cysteine proteases.³⁹

E-64 and Epoxysuccinyl Peptides Derivatives

E-64, a potent irreversible inhibitor with low toxicity,⁴² was isolated from an *Aspergillus japonicus* culture and became the prototype for cysteine protease inhibitors containing an electrophilic moiety.^{109, 39} E-64 utilizes an epoxysuccinyl group to covalently interact with the reactive-site cysteine. This compound is an irreversible inhibitor of cysteine proteases inactivating the enzymes by alkylation of the active site cysteine residues.^{39, 38}

E-64 inhibition is restricted to the papain superfamily of cysteine proteases but with little or no selectivity between the individual members of this enzyme clan.^{39, 42}

This is attributed to the fact that all these enzymes have similarly built non-primed substrate binding pockets. They have in common a P2-selectivity for hydrophobic residues, but larger differences between the enzymes can be found within the primed site.

It has been also proposed that inhibitors spanning both sides of the active site may improve selectivity. Addressing either this primed site or both primed and non-primed substrate binding pockets by means of so called "bispeptidyl derivatives" was therefore found to be a suitable strategy to develop selective inhibitors. For example, compounds CA-074 and NS-134 are cathepsin B selective inhibitors, while compounds of the CLIK series are cathepsin L selective (Figure 39).

When effective binding can be achieved in the S' direction by an inhibitor that binds in only one-half of the active site, selectivity seems unlikely despite any selectivity achieved by alternate binding in the S direction.³⁵

The CLIK series inhibitors, named after Katunuma and coworkers,¹⁰⁹ were designed based in their substrate-binding pockets using computer graphics and showed strong selectivity for individual cathepsins.⁴² It was reported that to show cathepsin L-specific inhibition, the trans-carbamoyl epoxysuccinyl carbamyl phenylalanine dimethyl amide group is essential for forming a thioether specifically with the active site of cathepsin L.⁴²

The characteristic aromatic derivatives in the left hand domain are bound directly to the epoxysuccinate-amide of the common fragment.¹⁰⁹ Furthermore, various residues are bound to the left side of carbamoyl group in order to protect from digestive enzymes and also show good penetration into the cell membranes.⁶¹

The modeling studies suggested that the fragment of CLIK group can fit optimally in the S₂ non-prime site of the protease, whereas the selectivity of the series is achieved by the fragments extending into the prime binding region.

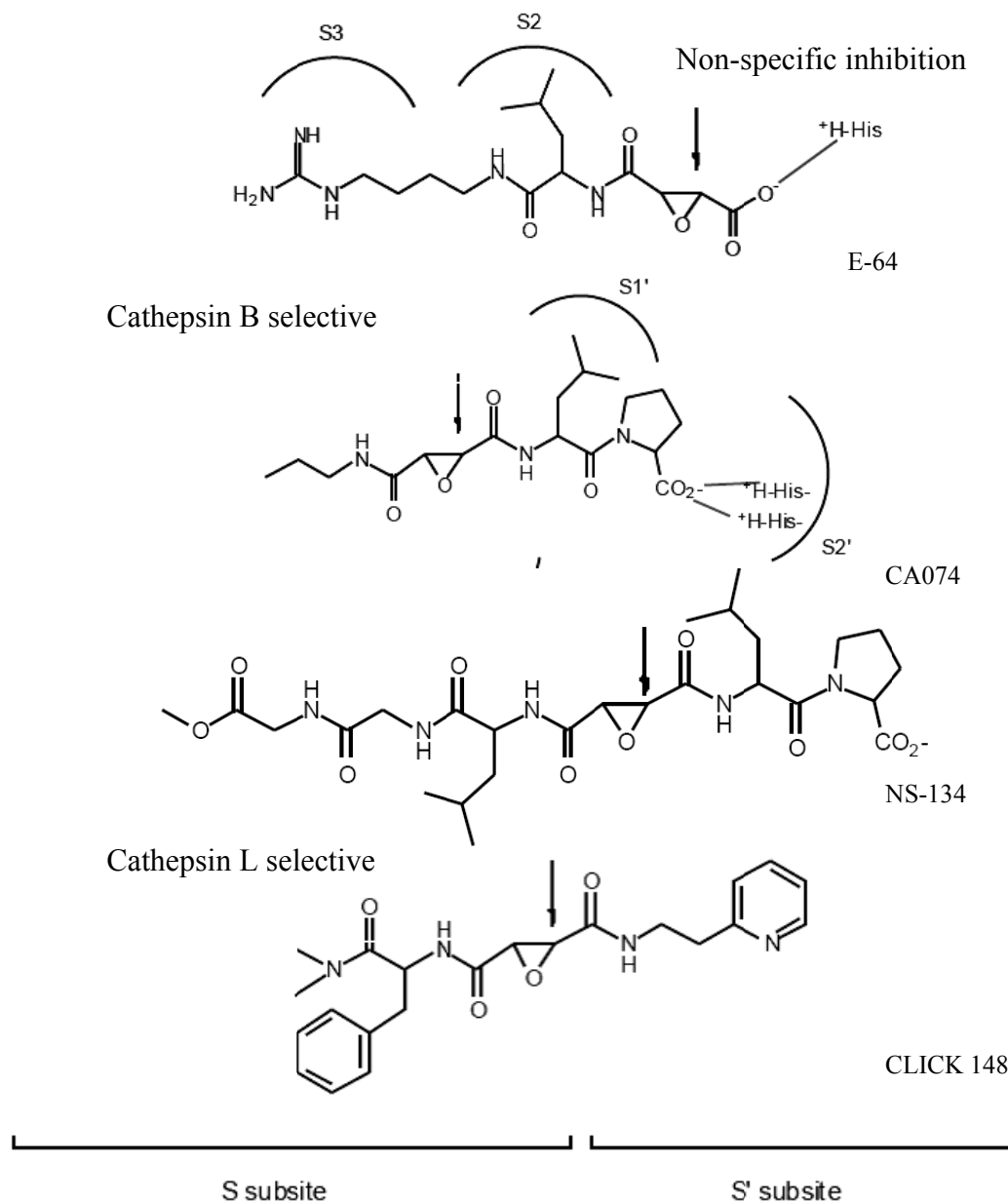


Figure 39. Binding modes of epoxysuccinyl peptide E-64 to cysteine proteases, CA074 to prime subsites of cathepsin B, and selective inhibitor CLICK 148 to cathepsin L. The arrow indicates the oxirane carbon attacked by the cysteine residue of the active site.

39, 110

Figure 40 shows four inhibitors of the CLIK series that showed strong selectivity for cathepsin L, while almost no inhibition of other cathepsin was observed.

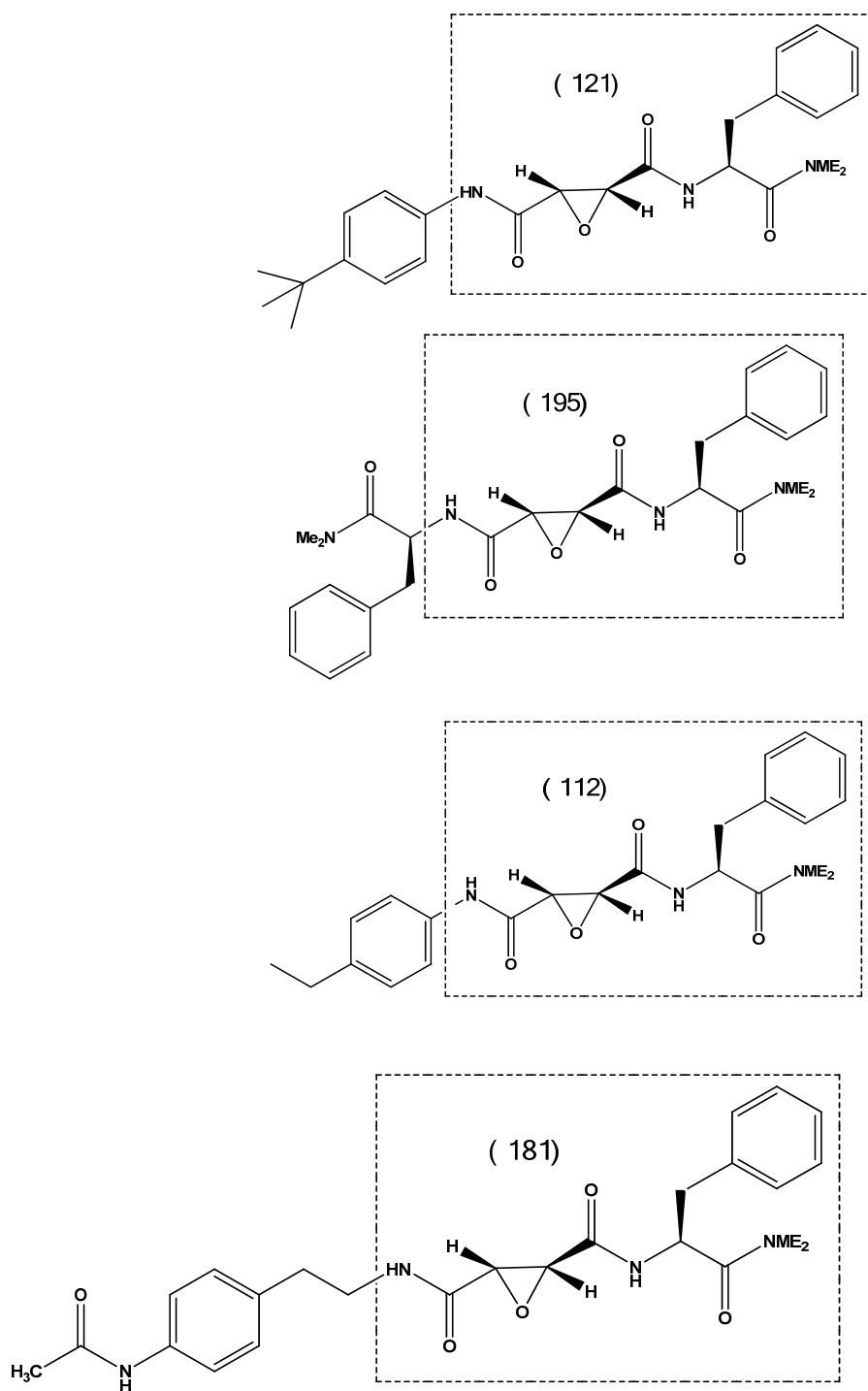


Figure 40. Four novel inhibitors of the cathepsin L inhibitor Katunuma (CLIK) specifically inhibited cathepsin L at a concentration of 10^{-7} M in vitro.¹⁰⁹

Aziridines

The inhibition mechanism of epoxysuccinyl peptides with the epoxide ring as a “quiescent” electrophilic trap led to the development of peptides containing the aza analogue aziridine ring.

Comparing the chemical reactivity of aziridines and epoxides to nucleophiles, aziridinyl peptides containing the same peptide sequence are the weaker inhibitors. Structural properties of aziridines vs. epoxides, which can partially explain the differences in inhibition behavior, are decreased ring strain, enhanced basicity and potential H-bond donation.³⁸

An advantage of replacement of oxygen with nitrogen in the three membered ring is the additional possibility of derivatization.

A second peptide chain cannot only be attached at the second carboxylic acid function but also at the aziridine nitrogen. Peptides and peptidomimetics of this type have been studied extensively and representative examples are aziridine-2,3-dicarboxylates containing either a Boc-Leu(Gly)-Caa (Caa = cyclic amino acid) or a Boc-Phe-Ala sequence attached to the aziridine nitrogen (Figure 41).

These compounds had activity against cathepsins L and B, but compounds containing a cyclic amino acid (Caa) displayed higher selectivities for cathepsin L over cathepsin B.^{39, 111}

β -Lactams

β -lactams are well-known as antibiotics with penicillin as the first and best known example. The development of β -lactams as cysteine protease inhibitors is very recent.¹²

Attack of the active site's cysteine leads to a covalently modified enzyme which in contrast to the acyl enzyme of the "normal" hydrolysis cannot further be hydrolyzed.

Molecular modeling studies with these inhibitors suggest that the N-1 atom of the oxapenam ring can be involved in hydrogen-bonding to a protonated imidazolium group in the active site.³⁹

Additionally, a substitution of the 6-position was found to possibly enhance the S₂ subsite interaction with papain. On the basis of these findings a series of 6-substituted oxapenams have been developed (Figure 42). Kinetic analyses suggested a reversible mode of inhibition with no covalent bond formation.

This inhibitor class was also tested for nonspecific reactivity towards thiol compounds such as glutathione and was found to be specific towards cathepsins. No reactivity with glutathione was observed.¹²

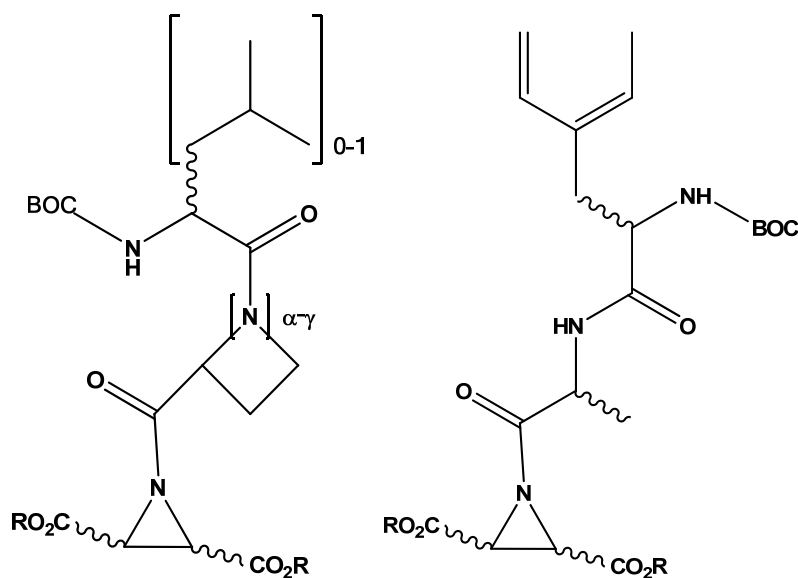


Figure 41. Schematic representation of the Boc-Gly-Caa-, Boc-Leu-Caa- (left) and Boc-Phe-Ala-containing (right) aziridinyl peptides; Caa, cyclic amino acid.^{39, 111}

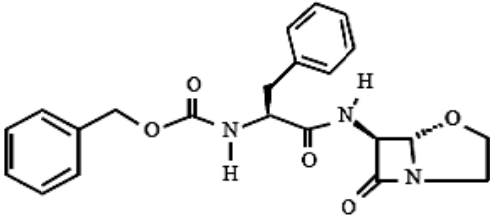
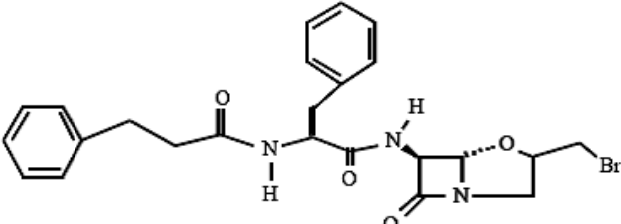
	IC ₅₀ (μM)	
	CatB	CatL
	12.2	0.0039
	1.91	0.016

Figure 42. Inhibition of cathepsin B and L by 6-substituted oxapenams.¹²

A series of potent inhibitors were generated within a penam series (Figure 43).

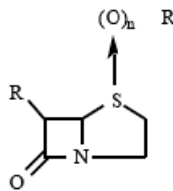
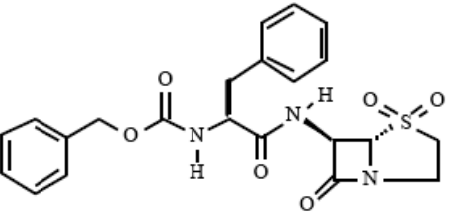
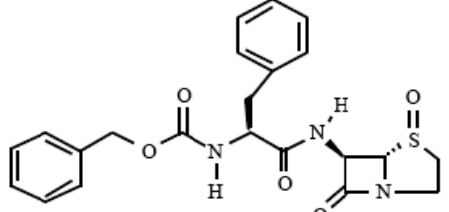
n	 R-Z / analogs - AA cycloalkyl heterocyclic	IC ₅₀ (μM)			
		Cat B	Cat L	Cat K	Cat S
2		0.35	0.00142	0.0005	0.0104
1		16.37	0.068	0.0352	0.07

Figure 43. Effect of the oxidation state of sulfur in 6-substituted penams on the inhibition of cathepsin.¹²

Structure-activity relationship (SAR) studies revealed two structural moieties to be important for the inhibitory potency of the compounds: i) the oxidation state of the sulfur in the penam structure (sulfones were more potent than sulfides) and ii) the stereochemistry at C5 (5 β were more active than the 5 α derivatives). The series produced very potent examples, but no selectivity could be achieved (Figure 43).¹²

Non-Peptidic Inhibitors of Cysteine Proteases

In comparison to the huge number of peptidic and peptidomimetic inhibitors of cysteine proteases which have been developed during the last twenty years the number of non-peptidic compounds with cysteine protease inhibiting properties is restricted to a few substance classes.

Furthermore, because peptidic compounds usually exhibit poor pharmacokinetics properties, such as low bioavailability and high clearance,^{112, 9} small non-peptidic inhibitors are desired.

In contrast to peptidic and peptidomimetic inhibitors the non-peptidic lead structures have mainly been discovered by computational or enzymatic industrial screenings and not by a rational approach.⁵⁸

Cyanamides

A screening of the Merck sample collection identified the 1-cyanopyrrolidine **1** (Figure 44) as a time dependent but fully reversible inhibitor of cathepsins K and L (IC₅₀ of 0.37 and 0.45 μ M respectively).

Removal of the quinoline moiety of **1** resulted in a moderate decrease in inhibition while acyclic cyanamides were totally inactive.

The most potent inhibitors of a series of 2,3-substituted 1-cyanopyrrolidines are benzenesulfonamide **2** (IC_{50} CK/CL= 0.05/0.08 μ M) and benzylcarbamate **3** (IC_{50} CK/CL = 0.04 / 0.054 μ M).

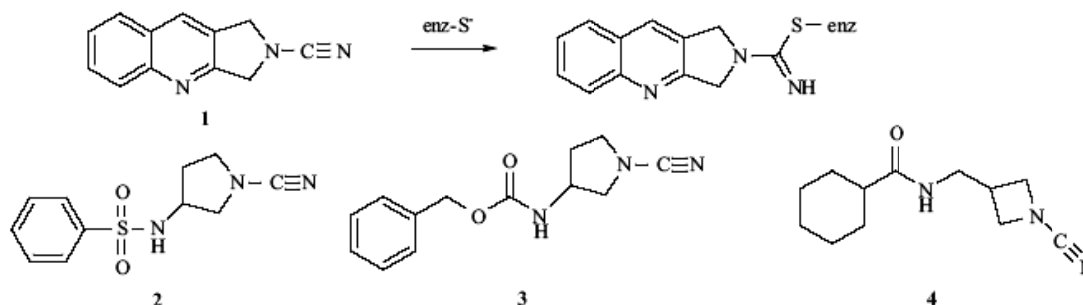


Figure 44. Cyanamides as inhibitors of cathepsin K and L.⁵⁸

Determination of association and dissociation rate constants showed that the inhibition fits an apparent single-step mechanism.

Replacement of the 1-cyanopyrrolidine moiety by 1-cyanoazetidine led to a 10-fold increase in inhibition with the cyclohexylamide **4** (IC_{50} Cathepsin K/Cathepsin L = 0.005/0.006 μ M) as the most potent inhibitor.

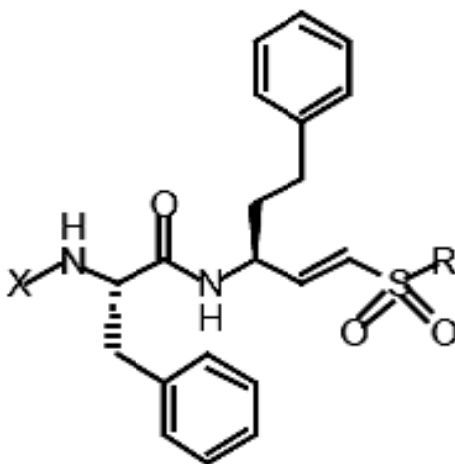
This increase in inhibition potency is probably a result of a higher chemical reactivity towards the cysteine of the enzyme's active site. Cyanamides are structurally related to peptidyl nitriles which are known to form thioimidate ester adducts with cysteine proteases. As could be expected, ¹³C-NMR experiments with papain showed the inhibition by cyanamides being due to reversible formation of a covalent isothiourethane adduct.^{58,64}

Vinyl Sulphones

Vinyl sulphones are highly potent cysteine protease irreversible inhibitors containing an activated double bond,^{110,57}

They are relatively novel inhibitors, and are considerably less toxic than aldehyde or diazomethylketones.¹¹³ This inhibitor class reacts as classical Michael acceptor as the active site cysteine undergoes 1,4-addition leading to an alkylated enzyme.³⁸

Prominent examples for vinyl sulfone based inhibitors are homophenylalanine containing vinyl sulfones (Figure 45). These compounds are highly potent on papain-like enzymes, but they do not react with serine proteases or low molecular weight thiols.¹¹⁰



R=Ph, OPh, NPh, CH₂Ph, NHOCH₂Ph, CH₂-CH₂Ph
X= Cbz, Mu (4-morpholinecarbonyl), Pip (piperazinyl)

Figure 45. Homophenylalanine containing vinyl sulfones are highly potent inhibitors of papain-like enzymes.¹¹⁰

Methylene Ketone Inhibitors

In contrast to vinyl sulfones, methylene ketone inhibition is reversible. Ethacrynic acid derivatives are a new interesting class of inhibitors. The compounds are derived from the well known diuretic drug. The key feature of ethacrynic acid derivatives is the α,β -unsaturated ketone moiety.

To investigate which structural features are necessary for inhibition, a prototype compound was modified on several positions and tested on various proteases (Figure 46).

It was concluded that, while serine proteases are not inhibited at all, either time-dependent or non-time dependent inhibition can be observed with cysteine proteases.

These studies showed that besides the activated double bond, the aromatic ring substituted with at least one chloro substituent is necessary for inhibition. Additional studies will be necessary to clarify the function of the chloro substituents: activation of the double bond or enhancement of lipophilicity.

In addition, esterification or amidation of the acid function improves inhibition. An ethyl group neighboring the double bond appears to be superior to a neighboring methyl group. This structure activity relationship is generally found for all tested cysteine proteases, meaning that selectivity is not yet reached.¹¹⁰

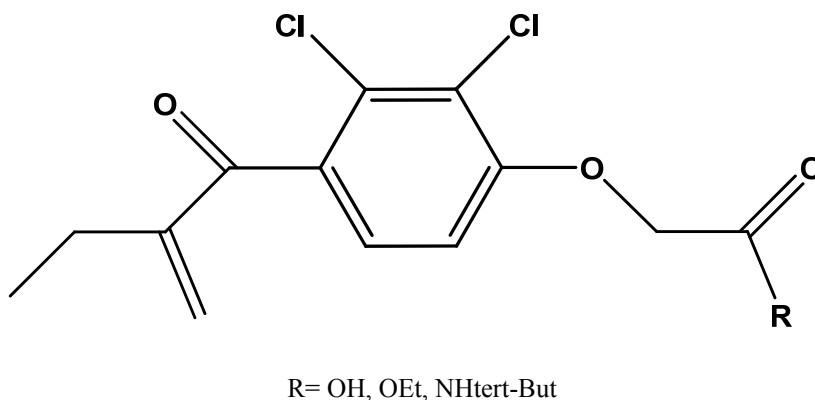


Figure 46. Ethacrynic acid derivatives have the potential to inhibit cysteine proteases.¹¹⁰

Thiosemicarbazones as Promising Lead Compounds

Du and coworkers¹¹⁷ were the first to prove the potential of the thiosemicarbazone warhead as an inhibitor to parasitic cysteine proteases (Figure 47). Substitutions on the aromatic phenyl ring at the meta position was proven to be essential for inhibitory activity.

Where a large group with high polarizability was preferred (trifluoromethyl > bromo > chloro moieties), while small and electronegative groups were preferred in the para position of the phenyl ring.

Several attempts on the modification of the thiosemicarbazone warhead were carried out ever since and it was reported that the incorporation of the thiosemicarbazone scaffold into other pharmacophores generated potent parasitic cysteine protease inhibitors.¹¹⁴⁻¹¹⁶

Siles and coworkers have reported two potent bromotetrahydronaphthalene thiosemicarbazone cruzain inhibitors with IC₅₀ values in the low nanomolar range (24 nM and 80 nM).¹¹⁷ Parasite localization provides a means for preferential inhibition of cruzain over the highly homologous human papain cysteine proteases cathepsins B, L, K, S, F, and V as the parasite resides in the host cell cytoplasm, whereas cathepsins are located in the less accessible lysosomes.¹¹⁸

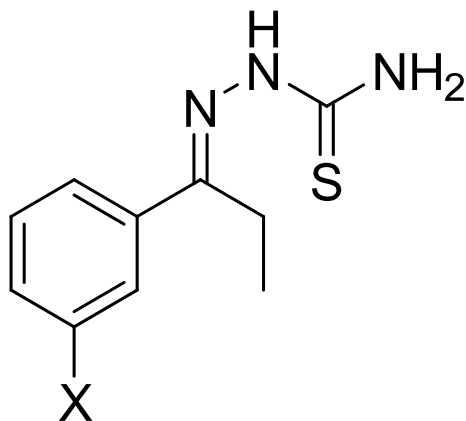


Figure 47. Thiosemicarbazone scaffold.

The proposed mechanism of action of inhibition of cysteine proteases by thiosemicarbazone analogues consisted of a reversible 1, 2-polar addition to the C=S bond instead of the C=N double bond.

As shown in Figure 48, the acidic hydrogen of the imidazole ring of His-159 protonates the negatively charged sulfur atom of the resulting thiolate group formed from Cys-25 attack on the electrophilic carbon of the thiosemicarbazone double bond.¹¹⁹

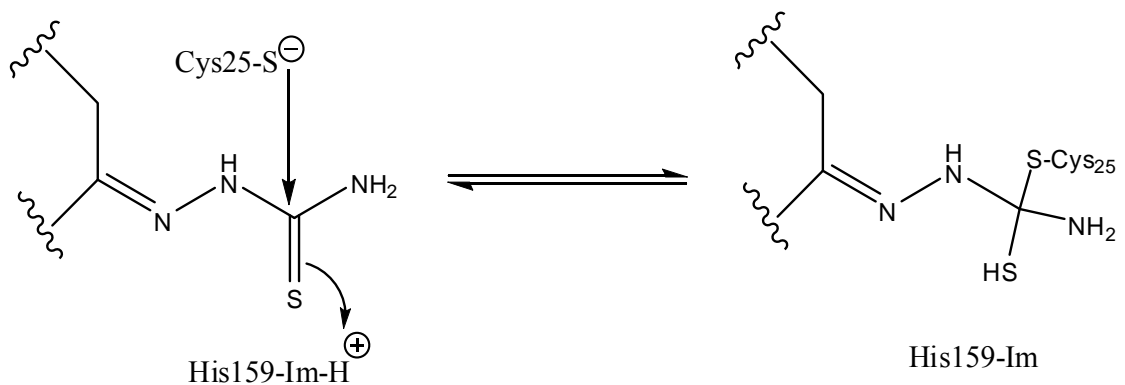


Figure 48. Mechanism of inhibition of a cysteine protease with a thiosemicarbazone by formation of a reversible covalent intermediate with the active site cysteine thiolate.³⁰

CHAPTER THREE

Experimental Procedures for the Biochemical and Biological Evaluation of Potential Cathepsin L Inhibitors

Experimental Procedures for the Biochemical Evaluation of Potential Cathepsin L Inhibitors

General Methods and Materials. Anhydrous sodium acetate (NaOAc), ethylenediaminetetraacetic acid (EDTA) and dithiothreitol (DTT) were purchased from EMD Biosciences. Dimethyl sulfoxide DMSO (99.9%), human liver cathepsin L and the substrate benzyloxycarbonyl-L-phenylalaninyl-L-argininyl-7-amido-4-methylcoumarin (Z-FR-AMC) were purchased from Sigma. All other chemicals were obtained from commercial companies such as Acros Chemicals, Alfa Aesar, EMD Biosciences, and Fisher Scientific. Water is always referred to the distilled ultrapure water obtained from the Barnstead Diamond™ purifier that has a resistance of 18 MΩ. A FluoroMax-2 fluorimeter was purchased from Horriba Jobin-Yvon and it was used for the evaluation of the majority of the cathepsin L inhibitors and their kinetic characterization with the exception of the last seven compounds of the library, which were evaluated in the Thermo Fluoroskan Ascent Fluorescence plate reader. Fluorescence quartz cuvettes were purchased from Starna Cells, Inc. and were always cleaned with water and dried with a jet of compressed nitrogen gas before and after use. Micropipettors were purchased from Eppendorf. The Büchi Heating Bath R-490 was purchased from Brinkmann Instruments, Inc. Analytical balances model numbers AX205 and AG204 were purchased from Mettler Toledo. A dry heater type 16500 was purchased from Thermolyne.

Preparation of sodium acetate buffer, 400 mM, pH 5.5. One liter of this buffer was prepared by dissolving 27.9 g (0.34 moles) of sodium acetate in 500 mL ultrapure water, then adding 3.7 mL acetic acid, and adjusting the pH to 5.5 with pure glacial acetic acid and 1 M NaOH. The total volume was adjusted to 1 L with supplementary water.

Preparation of assay/activation buffer. For each milliliter of solution required, 799 μ L sodium acetate buffer (400mM, pH 5.5), 100 μ L DTT (80 mM), 100 μ L EDTA (40 mM) and 1 μ L Brij 35 (30%) were mixed together in a 13 \times 100 mm glass test tube.

Preparation of baseline solution. The following reagents were pipetted into a fluorescence quartz cuvette and mixed well with gentle pipetting: 50 μ L assay/activation buffer, 20 μ L DMSO (7%) and 130 μ L water (185). Fluorescence readings were then taken for five minutes every five seconds at an excitation wavelength of 355 nm and emission wavelength of 460 nm.

Preparation of stock solution of 7-amino-4-methylcoumarin (AMC). Stock AMC solution (12.27 mM) was prepared by weighing 2.15 mg of AMC in a 1.6 mL microcentrifuge tube and dissolving in 1.0 mL DMSO.

Preparation of stock solution of benzyloxycarbonyl-L-phenylalaninyl-L-argininyl-7-amido-4-methylcoumarin (Z-FR-AMC). Z-FR-AMC stock solution (10 mM) was prepared by dissolving 6.49 mg (0.009 mmoles) of Z-FR-AMC in 1 mL DMSO in a 1.6-mL microcentrifuge tube.

Preparation of cathepsin L stock solution (10nM). A cathepsin L stock solution was prepared for daily use and it was stable up to 4 hours.

This solution (10nM) was prepared by diluting 1.5 μL of sigma stock solution (281 $\mu\text{g}/\text{ml}$) to 1200 μL with 1167.5 μL sodium acetate buffer (400 mM, pH 5.5), 30 μL EDTA (40 mM) and 1 μL Brij 35 (30%).

Preparation of inhibitors. The inhibitors to be tested were weighted using a Mettler Toledo AX microbalance with an accuracy of 0.01 mg and dissolved in pure DMSO (99.9%) giving 20 mM stock solutions from which at least eight serial dilutions were carried out to give final inhibitor concentrations ranging from 20 μM to 1 nM (Table 1).

Table 1. Inhibitor Serial Dilution Preparation.

Final Concentration in the assay [μM]	7% DMSO [μM]	Stock	DMSO [μl]	Water [μl]
2.0 E+01	4.0 E+02	10.0 μl 2.0 E+03 μM Stock	25.00	465
1.0 E+01	2.0 E+02	5.0 μl 2.0 E+03 μM Stock	30.00	465
7.0 E+00	1.4 E+02	3.5 μl 2.0 E+03 μM Stock	31.50	465
5.0 E+00	1.0 E+02	2.5 μl 2.0 E+03 μM Stock	32.50	465
4.0 E+00	8.0 E+01	2.0 μl 2.0 E+03 μM Stock	33.00	465
2.0 E+00	4.0 E+01	1.0 μl 2.0 E+03 μM Stock	34.00	465
1.0 E+00	2.0 E+01	0.5 μl 2.0 E+03 μM Stock	34.50	465
7.0 E-01	1.4 E+01	50.0 μl 7.0 E+00 μM Stock	32.00	418
5.0 E-01	1.0 E+01	50.0 μl 5.0 E+00 μM Stock	32.00	418
4.0 E-01	8.0 E+00	50.0 μl 4.0 E+00 μM Stock	32.00	418
2.0 E-01	4.0 E+00	50.0 μl 2.0 E+00 μM Stock	32.00	418
1.0 E-01	2.0 E+00	50.0 μl 1.0 E+00 μM Stock	32.00	418
7.0 E-02	1.4 E+00	50.0 μl 7.0 E-01 μM Stock	32.00	418
5.0 E-02	1.0 E+00	50.0 μl 5.0 E-01 μM Stock	32.00	418
4.0 E-02	8.0 E-01	50.0 μl 4.0 E-01 μM Stock	32.00	418
2.0 E-02	4.0 E-01	50.0 μl 2.0 E-01 μM Stock	32.00	418
1.0 E-02	2.0 E-01	50.0 μl 1.0 E-01 μM Stock	32.00	418
7.0 E-03	1.4 E-01	50.0 μl 7.0 E-02 μM Stock	32.00	418
5.0 E-03	1.0 E-01	50.0 μl 5.0 E-02 μM Stock	32.00	418
4.0 E-03	8.0 E-02	50.0 μl 4.0 E-02 μM Stock	32.00	418
2.0 E-03	4.0 E-02	50.0 μl 2.0 E-02 μM Stock	32.00	418
1.0 E-03	2.0 E-02	50.0 μl 1.0 E-02 μM Stock	32.00	418

Table 1 (Continued)

Final Concentration in the assay [μM]	7% DMSO [μM]	Stock	DMSO [μl]	Water [μl]
7.0 E-04	1.4 E-02	50.0 μl 7.0 E-03 μM Stock	32.00	418
5.0 E-04	1.0 E-02	50.0 μl 5.0 E-03 μM Stock	32.00	418
4.0 E-04	8.0 E-03	50.0 μl 4.0 E-03 μM Stock	32.00	418
2.0 E-04	4.0 E-03	50.0 μl 2.0 E-03 μM Stock	32.00	418
1.0 E-04	2.0 E-03	50.0 μl 1.0 E-03 μM Stock	32.00	418
7.0 E-05	1.4 E-03	50.0 μl 7.0 E-04 μM Stock	32.00	418
5.0 E-05	1.0 E-03	50.0 μl 5.0 E-04 μM Stock	32.00	418
4.0 E-05	8.0 E-04	50.0 μl 4.0 E-04 μM Stock	32.00	418
2.0 E-05	4.0 E-04	50.0 μl 2.0 E-04 μM Stock	32.00	418
1.0 E-05	2.0 E-04	50.0 μl 1.0 E-04 μM Stock	32.00	418
7.0 E-06	1.4 E-04	50.0 μl 7.0 E-05 μM Stock	32.00	418
5.0 E-06	1.0 E-04	50.0 μl 5.0 E-05 μM Stock	32.00	418
4.0 E-06	8.0 E-05	50.0 μl 4.0 E-05 μM Stock	32.00	418
1.0 E-06	2.0 E-05	50.0 μl 1.0 E-05 μM Stock	32.00	418

Aminomethylcoumarin (AMC) Standard Curve

A 7-Amino-4-methylcoumarin standard curve with eight concentrations ranged from 0.015 μM to 75 μM was prepared by serial dilution using the AMC stock (12.27 mM), DMSO and sodium acetate buffer (400 mM, pH 5.5).

The preparation table is shown in Table 2. Each AMC standard was then mixed with 75 μL of assay/activation buffer and 205 μL of water in fluorescence cuvettes to obtain concentrations from 1 nM to 5 μM .

The fluorescence readings were taken at 5 second intervals over 5 minutes for each concentration with excitation and emission wavelengths set to 355 and 460 nm and the generated data were analyzed with the software GraphPad Prism version 4.03.

Table 2. Preparation Table for AMC Standards.

Solution number	Concentration of AMC [μM]	Volume of Solution	Volume of DMSO [μL]	Volume of Sodium Acetate Buffer [μL]
1	75	6 μL of stock	94	900
2	22.5	300 μL of soln#1	70	630
3	15	200 μL of soln#1	80	720
4	4.5	300 μL of soln#3	70	630
5	1.5	100 μL of soln#3	90	810
6	0.15	100 μL of soln#5	90	810
7	0.075	50 μL of soln#5	95	855
8	0.015	200 μL of soln#7	80	720

Table is taken directly from Chen 2008.³⁰

K_M and V_{max} Determination of Cathepsin L

To test the accuracy of the assay conditions, the K_M value of cathepsin L was determined. Solutions of various concentrations of substrate (Z-FR-AMC) ranging from 0.3 μM to 150 μM were prepared by serial dilutions of 10 mM and 0.6 mM substrate (Z-FR-AMC) stock solutions as indicated in Table 3 and Table 4.

Activation buffer (60 μL), water (20 μL) and cathepsin L (20 μL) were mixed in fluorescence quartz cuvettes and incubated at 25°C for 5 minutes, followed by the addition of substrate (Z-FR-AMC) (100 μL) to initiate the reaction. Fluorescence intensity readings for each assay were taken at 10 second intervals for 15 minutes at 25°C. A linear trend line was fit to each data set. The slope of each trend line was derived as the velocity of each assay.

A Michaelis-Menten plot was constructed by plotting the velocities in the y-axis and substrate concentrations in the x-axis. V_{max} and K_M were derived by fitting the data to the Michaelis-Menten equation using the non-linear regression function with the software GraphPad Prism version 4.03.

Table 3. Preparation Table for 10 mM and 0.6 mM Z-FR-AMC Stock Solutions.

Solution Number	Z-FR-AMC Final concentrations in DMSO [μM]	Volume of [μL]	Z-FR-AMC Stock [mM]	Water [μL]
1	3000.0	300.0	10.0	700.0
2	2250.0	225.0	10.0	775.0
3	1500.0	150.0	10.0	850.0
4	600.0	60.0	10.0	940.0
5	300.0	30.0	10.0	970.0
6	250.0	25.0	10.0	975.0
7	200.0	20.0	10.0	980.0
8	100.0	10.0	10.0	990.0
9	30.0	50.0	.6	950.0
10	16.0	26.7	.6	973.3
11	6.0	10.0	.6	990.0

Table is taken directly from Chen 2008 with some modifications.³⁰

Table 4. Preparation Table for Substrate (Z-FR-AMC) Solutions in 7% DMSO.

Solution Number	Z-FR-AMC Concentration [μM]	Volume (μL)	Dilute from Z-FR-AMC [μM]	Volume of Water (μL)	Final Concentration in Assay
1	150.0	50	3000.0	950	10.00 μM
2	112.5	50	2250.0	950	7.50 μM
3	75.0	50	1500.0	950	5.00 μM
4	30.0	50	600.0	950	2.00 μM
5	15.0	50	300.0	950	1.00 μM
6	12.5	50	250.0	950	833.33 nM
7	10.0	50	200.0	950	666.67 nM
8	5.0	50	100.0	950	333.33 nM
9	1.5	50	30.0	950	100.00 nM
10	0.8	50	16.0	950	53.33 nM
11	0.3	50	6.0	950	20.00 nM

Table is taken directly from Chen 2008 with some modifications.³⁰

IC₅₀ Determination (Cuvette Assay Formate)

Fifty nine potential inhibitors of cathepsin L to be evaluated were synthesized by Rogelio Siles, Dr. Ming Zhou, Dr. Kishore Gaddale, Freeland Ackley, Jiangli Song, and Lindsay Jones from Dr. Kevin G. Pinney's laboratory at Baylor University.¹³⁷

First, the effect of a single inhibitor concentration (20 μ M) on cathepsin L was investigated for each inhibitor. No further analysis was done on compounds that did not inhibit cathepsin L at this concentration.

For those that did inhibit cathepsin L, at least eight serial dilutions (variable final inhibitor concentrations ranging from 20 μ M to 1 pM, depending on the inhibitor) were incubated separately with assay/activation buffer, water, and cathepsin L in fluorescence quartz cuvettes as described in Table 5 at 25 °C for 5 minutes, prior the initiation of the reaction with the addition of substrate Z-FR-AMC. The reaction mixtures were then monitored for 5 minutes at excitation and emission wavelengths of 355 and 460 nm, respectively.

The baseline control for each assay used the same conditions without the inhibitor. IC₅₀ values were determined by performing non-linear regression analysis fitting velocities and the logarithm of inhibitor concentrations to sigmoidal dose response model using the GraphPad Prism 4.03 software. K_I values of the best inhibitors were obtained by fitting the same data to the Williams-Morrison equation using the same software.

Table 5. Preparation Table for IC₅₀ Determination Experiment.

Item	Volume [μ L]
Assay/Activation Buffer	50
Water	20
Inhibitor/0.7% DMSO	10
Cathepsin L (10 nM)	20
Substrate (Z-FR-AMC) (10 μ M)	100

Microplate Assay for IC₅₀ Determination

Assays were performed in 96-wells plates with seven compounds synthesized by Dr. Kishore Gaddale, Jiangli Song and Lindsay Jones from Dr. Kevin G. Pinney's laboratory at Baylor University.

At least eight serial dilutions (10 μ l) (final inhibitor concentrations ranging from 20 μ M to 1 nM) were incubated separately and in triplicate with 50 μ l assay/activation buffer, 20 μ l water and 20 μ l cathepsin L (10 nM) in Constar NBS plates (non-binding surface) at 25°C for 5 minutes, prior to the initiation of the reaction with the addition of 100 μ l of substrate Z-FR-AMC (70 μ M). The reaction mixtures were then monitored for a maximum of 5 minutes at excitation and emission wavelengths of 355 and 460 nm, respectively.

The baseline control for each assay used the same conditions without the inhibitor.

IC₅₀ values were determined by performing non-linear regression analysis fitting velocities and the logarithm of inhibitor concentrations to sigmoidal dose response model using the GraphPad Prism 4.03 software.

Time Dependent Inhibition Study of the best Thiosemicarbazone Inhibitors against Cathepsin L

Time dependence inhibition studies were performed with compounds **2** and **22**, two of the most potent inhibitors of cathepsin L of the thiosemicarbazone library evaluated in this study.

Inhibition was evaluated using a single enzyme (1 nM) and substrate (5 μ M Z-FR-AMC) concentration, with analysis over a 2.5 hour time period.

Three inhibitor dilutions (final concentrations of 5 μM , 50 nM and 5 nM) were incubated separately with assay/activation buffer, water, and cathepsin L in fluorescence quartz cuvettes as described in Table 6 and incubated for 5 min, 15 min, 30 min, 60 min, 90 min, 120 min and 145 min at 25°C prior the initiation of the reaction with the addition of substrate Z-FR-AMC. Then reaction mixtures were then monitored for a maximum of 5 min at excitation and emission wavelengths of 355nm and 460 nm, respectively. The baseline control for each assay used the same conditions without the inhibitor. The GraphPad Prism 4.03 software was used for data analysis.

In separate experiments, compounds **2** and **22** were tested at concentrations of 5 μM , 50 nM and 5 nM using a 5 minute enzyme-inhibitor incubation time. The substrate Z-FR-AMC was then added at concentrations ranging from 0 to 100 μM and the reactions were monitored for a maximum of 5 minutes at excitation and emission wavelengths of 355nm and 460 nm, respectively. The baseline control for each assay used the same conditions without the inhibitor. The GraphPad Prism 4.03 software was used for data analysis.

Table 6. Preparation Table for Time Dependence Inhibition Studies.

Item	Volume (μL)
Assay/Activation Buffer	50
Water	20
Inhibitor/0.7% DMSO	10
Cathepsin L (10nM)	20
Substrate (Z-FR-AMC) (10 μM)	100

Reversibility Studies

An inhibitor concentration of approximately 5 times the IC_{50} value was used for this study.

Cathepsin L and each inhibitor were preincubated together (100-fold concentrated) over a 1 hour time period and then diluted into substrate-containing buffer prior the initiation of the enzymatic reaction. Buffer and enzyme concentrations and amounts are described in Table 7. Assays were performed in a Jobin-Yvon Fluoromax-2 using excitation and emission wavelengths of 355 and 460 nm respectively. The GraphPad Prism 4.03 software was used for data analysis.

Table 7. Preparation Table for Reversibility Studies.

Item	Volume (μ L)
Assay/Activation Buffer	50
Water	20
Inhibitor/0.7% DMSO (5nM)	10
Cathepsin L (10nM)	20
Substrate (Z-FR-AMC) (10 μ M)	100

Experimental Procedures for the Biological Evaluation of Cathepsin L Inhibitors

General Section for Reagents, Media and Materials Sources. A human prostate carcinoma cell line (DU-145) and a human epithelial kidney carcinoma cell line (HEK-293) were obtained from the American Type Culture Collection (ATCC). Cell culture media (DMEM) and supplements (fetal bovine serum, L-glutamine, sodium pyruvate and penicillin/streptomycin) were purchased from Sigma, and ATCC. Phosphate buffered saline (PBS) and 0.25% (w/v) porcine trypsin-0.53 mM EDTA solution were purchased from Sigma. Biocoat® Matrigel® invasion chambers and control inserts were purchased from BD Biosciences. The Diff-Quick stain kit was purchased from IMEB Inc. Precast 10% and 4-12% (w/v) bis-tris gels were purchased from Invitrogen. Agarose beads were purchased from Pierce.

The pre-stained protein molecular mass standard ranging from 10-250 kDa (Precision Plus; Kaleidoscope) and the DC protein assay kit with the gamma globulin standard and bovine serum albumin standard were purchased from Bio-Rad Laboratories. The mini-gel electrophoresis apparatus (X Cell Sure Lock™) was purchased from Invitrogen. Bradford reagent, the substrate benzyloxycarbonyl-L-phenylalaninyl-L-argininyl-7-amido-4-methylcoumarin (Z-FR-AMC), the standard 7-amino-4-methylcoumarin and cell culture grade DMSO were purchased from Sigma. Antibodies used for Western blotting included polyclonal rabbit anti-cathepsin L, polyclonal rabbit anti-cathepsin B and goat anti-rabbit IgG-HRP conjugate from Calbiochem. Polyclonal antibody to actin was purchased from Sigma. The horseradish peroxidase (HRP) enhanced chemiluminescence ECL kit was purchased from Amersham. This ECL Western blotting system uses HRP conjugated anti-rabbit antibodies for luminol-based detection of Western blots. The *QuickBlocker*™ blocking agent was purchased from Millipore. This reagent is a novel modified milk protein that does not inhibit peroxidase detection and has a high blocking efficiency with a clear background. All other reagents were purchased from Sigma or Fisher. Microcon YM-10, Centriprep and Amicon ultra-4 centrifugal filter units were from Millipore. The Trans-Blot semi-dry transfer apparatus, Immobilon-P transfer membrane and filter papers for transfer stacks were purchased from Bio-Rad Laboratories. Micropipettes were purchased from Mettler Toledo. The biosafety cabinet was purchased from The Baker Company. The CO₂ incubators were purchased from Thermo. The microcentrifuge 5415R and the centrifuge 5810R were purchased from Eppendorf. The inverted microscope Olympus IX 50 was purchased from Olympus. The hemocytometer was purchased from Hausser Scientific.

The Z-Coulter counter was purchased from Beckman Coulter. The RT 600D centrifuge and the 5810R centrifuge were purchased from Sorvall. Cryogenic vials and the Mr. Frosty freezing container were purchased from Nalgene.

The Sonicator 3000 was purchased from Misonix. The FluoroMax-2 fluorimeter was purchased from Horriba Jobin-Yvon Inc. Cell culture supplies for adherent cells (100 mm Cellstar™ cell culture dishes, 60 mm Cellstar™ cell culture dishes, 175 cm² Corning culture flasks, disposable pipettes, and 24-well plates) were purchased from Sigma and VWR. The DU 520 spectrophotometer was purchased from Beckman. Ultra Lum Discovery 12 imager and Omega 10 gel imager were purchased from Ultra Lum Inc. Water is always referred to the distilled water obtained from the Barnstead Diamond™ purifier that has resistance of 18 MΩ.

Cell Culture Media Supplementation

The human prostate carcinoma cell lines DU-145, established from a metastatic lesion in the central nervous system of a 69-year-old male⁶⁷ and HEK-293, established from human embryonic kidney cells were cultured in Dulbecco's modified Eagle's medium (DMEM). DMEM has optimized energy sources for protein production and nucleic acid metabolism while limiting toxic ammonia build-up. See appendix D for a detailed list of the components of this media. To make the complete growth medium, each bottle of 500 mL DMEM was supplemented with 50 mL fetal bovine serum (FBS), 5 mL L-glutamine (200 mM) and 5 mL penicillin/streptomycin (10,000 I.U./ml penicillin/ 10,000 µg/ml streptomycin).

DU-145 cells are used as an *in vitro* model for prostate cancer. They grow in continuous culture as adherent monolayers with an epithelial-like morphology.

The line is not detectably hormone sensitive.⁶⁷ HEK-293 cells were demonstrated to be a useful cell type to produce adenovirus, other viral vectors, and effectively glycosylated human recombinant proteins. They are therefore used for virology studies and transfected to express recombinant proteins for studies in a number of research fields.¹²⁰

Maintenance of Cell Culture in Dishes and Flasks

Skill in aseptic technique is important to maintain sterility during media preparation and cell culture procedures. The cells used in this study were grown as a monolayer attached to cell culture dishes or flasks. In order to keep adherent cells healthy and actively growing it was necessary to subculture regular intervals.

The general morphology, growth rate of a cell population and the presence of any microbial contaminants were checked regularly under an inverted microscope in phase contrast. Dishes or flasks with cells at about 80% confluence were treated with a trypsin-EDTA solution; the cells were then harvested and either frozen or divided for further proliferation.

For dishes with non-confluent cells the growth medium was discarded and replaced with fresh media. Media had to be changed two-three times a week and a careful record of all passages was kept.

Typically, cell viability was higher than 90%, and almost no debris resulting from ruptured cells was present. The cells were grown in 175 cm² culture flasks or 60/100 mm cell culture dishes depending on the application and the following conditions were maintained throughout this study: 37 °C, 90% humidity and 5% CO₂/air.

Cell Subculture Procedure

Culture medium was removed by aspiration and the cell monolayer was briefly rinsed with PBS to eliminate serum residues which contains traces of trypsin inhibitor (7-10 ml to 100 mm cell culture dish, 4 ml to 60 mm cell culture dish). Then, PBS was removed and 0.25% (w/v) trypsin - 0.53 mM EDTA solution was added (4 ml to 100 mm dishes, 2 ml to 60 mm dishes) and the cells were observed under an inverted microscope until the cell monolayer was dispersed (within approximately 5 to 15 minutes). Cells that were difficult to detach were placed in an incubator (37°C, 90% humidity and 5% CO₂/air) to facilitate dispersal for 3-5 minutes until the cells were rounded and detached. At this point, supplemented cell growth medium containing FBS had to be added in order to inhibit trypsin activity followed by mechanical detachment of cells from the surface of the dish with the help of a pipette tip to obtain a suspension of individual cells. After the cells had been dissociated into a suspension of mainly single cells, they were counted, diluted and transferred to new cell culture dishes containing fresh medium and incubated at 37 °C or aliquoted into cryogenic vials containing freezing medium for future use.

Cell Freezing Procedure

It is possible to maintain stocks of cells in a viable state for long periods at low temperatures. The essential features of the method are to add a cryoprotectant such as cell culture grade DMSO to the cell growth medium, to freeze the cells slowly and to keep them at a temperature below -70°C while frozen. The DMSO is used as a cryoprotectant in the freezing of cell cultures to avoid ice formation in the cells at cryogenic temperatures.

A harvested cell suspension was centrifuged in falcon tubes for 5 min at 1000 g, and the resulting supernatant was discarded. The cells were then counted and re-suspended at the appropriate dilution in cell freezing medium (Sigma) which consisted of growth culture medium (95%) and DMSO (5%). Typically, final cell concentration in each cryogenic vial was in the range of 1×10^6 to 5×10^6 cells/mL to ensure cell viability.

Aliquots of this suspension were transferred to cryogenic vials which were placed into the Nalgene freezing container and slow-cooled at a 1 °C/min cooling rate to -80°C overnight in a freezer before storing the vials the next day in liquid nitrogen vapor phase.

Cell Thawing Procedure

In order to revive cells from cryopreservation, the cryogenic vial was removed from the liquid nitrogen vapor phase and immediately transferred to a water bath or preferably a beaker with sterile water at 37°C. Once the contents were completely thawed, the outside of the vial was wiped with 70% ethanol to reduce bacterial contamination and the cell suspension was transferred to a cell culture dish with sufficient growth medium for the establishment of a cell monolayer and incubated overnight at 37°C. Then, the medium was removed to eliminate DMSO present and fresh growth medium was added.

Trypan Blue Exclusion Assay

Cell viability was determined by Trypan blue (0.4%) uptake where non-viable cells are able to take up the dye and are stained blue, whereas viable cells are not. The number of cells present in a cell suspension was calculated by counting the cells in a Neubauer hemocytometer chamber. First, 200 µl of the cell suspension was diluted in 200 µl of 0.4% trypan blue solution and mixed very well with gentle pipetting.

Then, both sides of the hemocytometer chamber were filled with 10 μl of this mixture and viable cells were counted in each of the four corner squares bordered by triple lines, omitting cells lying on these lines under the inverted microscope (Figure 49).

The viable cell concentration per mL was calculated using the following formula:

$$C_1 = t \times tb \times 1/4 \times 10^4$$

Here,

t = total viable cell count of four corner squares

tb = correction for the trypan blue dilution

1/4 = correction to give mean cells per corner square

10^4 = conversion factor for counting chamber

C_1 = initial cell concentration per mL

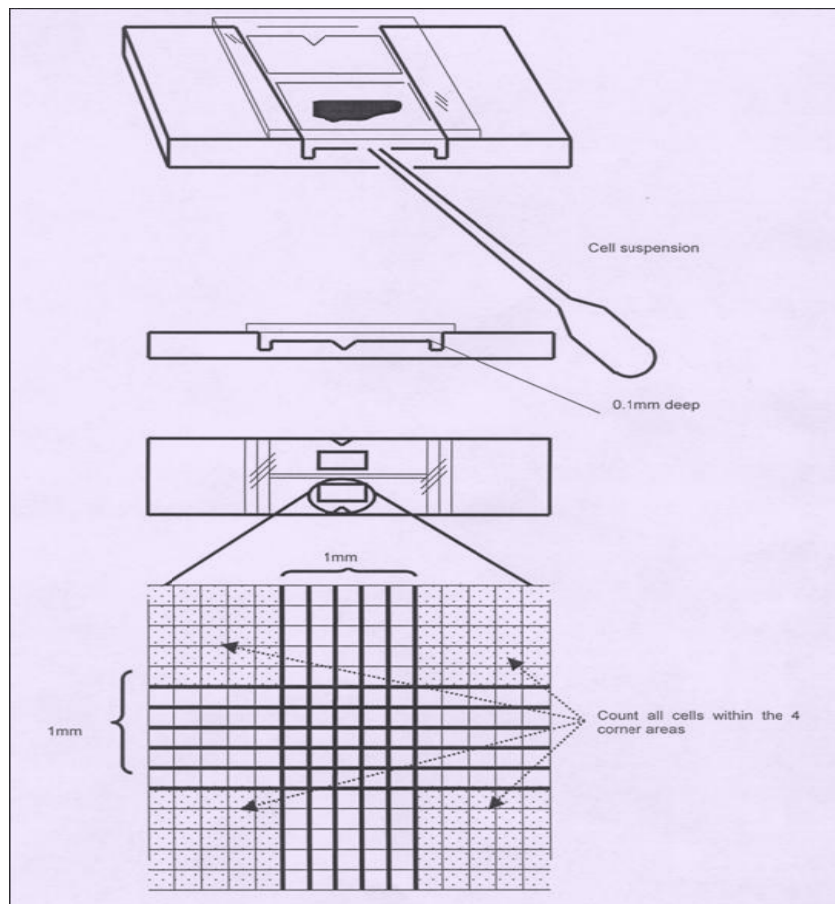


Figure 49. Scheme of cell number determination with the hemocytometer. Taken directly from <http://www.who.int/vaccines/en/poliolab/webhelp>.¹

Preliminary Cytotoxicity Studies

A suspension of HEK-293 cells was seeded in 24-well plates (4000 cells/well) in growth medium at 37 °C in an atmosphere containing 5% CO₂ in the air. After 12 hours the cells were transferred to serum free medium and incubated for 24 hours to allow the cells to adhere, the medium was then replaced with serum free medium containing the inhibitors previously dissolved in DMSO (**1**, **12**, **9**, **22**, **10**, **32**, **33**, **37** and **55**) at a final concentration of 20 µM and 0.1% DMSO (cell culture grade) as a solvent control to provide the reference for 100% cell growth in the test vessel.

After incubation for 24 hours, the media was removed from the cell culture dishes, the cell monolayer washed three times with PBS, and harvested to determine the cell population using the trypan blue exclusion assay to determine the percentage of viability, which was determined as a fraction of the loss of cell viability in the cultures.

Determination of Cathepsin L Inhibitors Activity on DU-145 Cell Culture

Cathepsin L activity in DU-145 cell lysate and cell conditioned media was determined as described by Colella and coworkers⁶² with some modifications. Briefly, DU-145 cells were incubated overnight in serum free medium containing the solvent control (0.1 % DMSO) and the inhibitors **2** and **22** at a final concentration of 20 µM to determine their inhibitory effects on intracellular active and latent secreted cathepsin L. The following day, the cell conditioned media was collected and the cells were rinsed and harvested in cold PBS. The cells were then lysed in falcon tubes containing cold PBS using a sonicator at medium setting for ten minutes with pauses at 0 °C for temperature equilibration.

The resulting homogenate was centrifuged at 13,000×g for 20 minutes and the supernatant incubated for 45 minutes in assay/activation buffer (pH 5.5). The assay/activation buffer consisted of 100 mM sodium acetate (pH 5.5), 4 mM EDTA, 8 mM DTT and 0.1% Brij 35. The cathepsin L activity of the supernatant was then measured using Z-FR-AMC (25 μM) as the substrate. The release of the fluorogenic AMC was measured in a Fluoro-Max-2 fluorometer at an excitation and emission wavelength of 355 nm and 460 nm, respectively.

Cathepsin L activity secreted in the medium (cell conditioned media) was measured as follows: cell conditioned media from three 100 mm cell culture dishes of the same group were pooled together and centrifuged at 27,000×g for 15 min, the pellet obtained was re-suspended and incubated with assay buffer (pH 5.5) for 90 minutes to activate the pro-forms of cathepsin L before measuring the activity.

Cell Invasion and Motility Studies

Briefly, Matrigel[®] coated 8 μm mesh inserts were rehydrated with serum free medium in 24 well plates for 2 hours at 37°C. Then, 0.5 mL of cell suspension (50×10⁴ cells/ml) in serum free medium containing the inhibitors to be tested at a final concentration of 20 μM was added to the upper section of the chamber and 750 μl of cell growth medium (containing 10% FBS as a chemoattractant) was added to the lower section of each chamber. The cells were then incubated for 24 hours at 37°C in an incubator containing 5% CO₂ in the air.

Since the stock solutions of the inhibitors were prepared in cell culture grade DMSO, a solution of 0.1% DMSO was used as a solvent control to provide the reference for 100% cell growth in the test vessel.

The commercially available general irreversible inhibitor of cysteine proteases, E-64 (*L-trans*-epoxysuccinyl-leucylamido (4-guanidino) butane) was used as a positive control due to its ability to block tumor cell invasion through Matrigel[®] and because of its lack of ability to readily penetrate the cell membrane, therefore inhibiting secreted cathepsin L.^{121, 70}

At the end of the incubation period, cells remaining above the insert membrane were removed by gentle scraping with a moist cotton swab and cells that had invaded through the Matrigel to the bottom of the insert, were stained with the Diff-Quick kit.

The Diff-Quik kit contains a fixative agent (1.8 mg/L triarylmethane in methyl-alcohol) and two stain solutions (1 g/L xanthene in sodium acide-preserved buffer and 0.625 g/L azure A with 0.625 g/L methylene blue in buffer).¹²² Staining was accomplished by sequentially transferring the inserts through the three solutions and two water rinses. The cell nuclei stain purple and the cytoplasm stains pink.

The inserts were allowed to air dry, the membrane removed from the insert, and then mounted on microscope cover slips for counting. The number of cells was counted in four progressive random fields on triplicate membranes under an inverted microscope (40 X).

The invasion fraction was determined by dividing the number of cells that invaded the Matrigel[®] matrix by the number of cells counted in the control inserts (i.e. number of migrating cells). Data are expressed as the percent invasion through the Matrigel[®] and membrane relative to the migration through the control insert membrane:

$$\% \text{ Invasion} = \frac{\text{Mean of number of cells invading through Matrigel insert membrane}}{\text{Mean of number of cell migration through control insert membrane}} \times 100$$

Control inserts were used for motility assays and contain only the 8 μm mesh without the Matrigel[®] coating. Migration was measured as described in the invasion assay.

DC Assay for Total Protein Concentration Determination

The determination of the total concentration of protein was done with the Bio-Rad DC Protein assay, which is a colorimetric assay for protein concentration following detergent solubilization. The reaction is analogous to the Lowry assay, but with a difference of reaction rate as it reaches 90% of its maximum color development within 15 minutes without significant color change after 2 hours of addition of reagents.

The principle of the assay is based on the reaction of a protein with an alkaline copper tartrate solution (reagent A) and folin reagent (reagent B) producing reduced species which have a characteristic blue color with maximum absorbance at 750 nm and minimum absorbance at 405 nm.¹²³ Folin reagent is the commercial name for 1, 2-naphthoquinone-4-sulfonate and is used to measure amine and amino acid levels.

For the assay, a working solution of reagent A' was prepared by adding 20 μL of reagent S to each mL of reagent A required for the run. Seven individual mixtures of 100 μL of blank (buffer alone), standard or samples (diluted to the appropriate concentration if needed), 500 μL reagent A' and 4.0 mL reagent B were incubated at room temperature for 15 minutes and the absorption measured in plastic disposable cuvettes at 750 nm.

A standard curve was prepared in the same buffer as the sample each time the assay was performed. Sigma BSA standards were prepared at the following concentrations: 0.1 mg/mL (5 μL stock BSA + 95 μL buffer), 0.5 mg/mL (25 μL stock BSA + 75 μL buffer), 1mg/mL (50 μL stock BSA + 50 μL buffer).

For data analysis, a calibration curve was obtained by plotting the absorption values against the concentration of standard in order to obtain a linear equation; the values of the sample absorption were introduced in the calibration equation, which was solved for the concentration of sample. The sample concentrations were corrected for dilution factors and multiplied by the total volume of sample to obtain the total milligrams of protein.

Western Blot Protocol for DU 145 Cell Lysate and Cell Conditioned Media

Sample Preparation Protocol

DU-145 cell monolayers were collected in PBS by scraping the culture plate with Corning cell scrapers and centrifugation in 15 mL falcon tubes at 5,000 g for 5 minutes. The cell pellet was then re-suspended in lysis buffer (20 mM Tris, pH 7.5, 150 mM NaCl, 1 mM MgCl₂, 2 mM EGTA, 10% glycerol, 0.15% SDS, 1% deoxycholate, 1% Triton X-100 and 1% sigma anti-protease cocktail (containing 4-(2-aminoethyl) benzenesulfonyl fluoride (AEBSF), pepstatinA, E-64, bestatin, leupeptin, and aprotinin)), sonicated at medium setting for ten minutes with pauses at 0°C for temperature equilibration.

Cell debris was then removed by centrifugation at 14000 rpm for 15 minutes at 4°C, the supernatant supplemented with SDS to a final concentration of 2%, and stored at -80°C.¹²⁴ For Western blot analysis of cathepsin L and B in cell conditioned media, an immunoprecipitation method was used to prepare the samples.¹⁰ The appropriate antibody (10 µl) was added to the collected cell conditioned media (amount equivalent to 100 µg protein in media previously concentrated 100-fold with a Centricon YM-10 filter unit (10000 NMWL) and incubated overnight at 4°C in a cold room with gentle rocking.

The immunocomplex was then captured with 20 μ l of protein G agarose beads with gentle rocking at 4 °C. After 2 hours, the agarose beads were concentrated by centrifugation (2 minutes at 14,000 g) and washed 3 times with lysis buffer. Finally, the beads were re-suspended in 30 μ l of sample buffer, boiled for 5 minutes, centrifuged and the supernatants loaded on SDS-PAGE gels as described below.

Final protein concentration for all the samples was determined using the DC protein assay from Bio-Rad Laboratories according to the manufacturer's instructions.

SDS-PAGE Protocol

A protocol described by Invitrogen was followed with slight modifications and electrophoretic characterization of DU145 cell lysates and cell conditioned media was performed under denaturing conditions using 4-12% (w/v) bis-tris gels and the mini-gel electrophoresis apparatus X Cell Sure Lock™.

The samples consisted of a positive control (commercially available cathepsins L and B), cell lysates, cell conditioned media and a multi-colored protein standard (Kaleidoscope) ranging from 10 to 250 kDa. To 10 μ g of sample, 2.5 μ L of NuPAGE® LDS sample buffer (4x), 1 μ L of NuPAGE® reducing agent (10x) and 6.5 μ L of ultrapure water was mixed in microcentrifuge tubes giving a total volume of 10 μ L. The mixture was centrifuged for 1 minute at 4°C, heated at 95°C for 10 minutes and then loaded to the 4-12% precast mini-gel.

The upper and lower® buffer chambers of the electrophoretic tank was filled with 200 mL (containing 500 μ L of NuPAGE®antioxidant) and 600 ml of 1x NuPAGE® LDS running buffer.

The gel was run at 200V for 35 minutes. The gels were stained using the SimplyBlue™ SafeStain microwave protocol for staining NuPAGE gels.

SimplyBlue™ SafeStain is a ready-to-use, fast, sensitive, and safe Coomassie® G-250 stain for visualizing protein bands on polyacrylamide gels. The gel was placed in 100 ml of ultrapure water and microwaved on high (950-1100 watts) for 1 minute.

After shaking the gel on an orbital shaker, the water was discarded and the process repeated twice.

SimplyBlue™ SafeStain (30 mL) was added and the gels were microwaved on high for 1 minute, shaken on an orbital shaker for 10 minutes and then washed in 100 ml ultrapure water for 10 minutes followed by shaking in 20 mL of 20% NaCl for 10 minutes.

Finally, the protein bands were visualized using the Omega 10 gel imager system. This system allows a multitude of fluorescent imaging applications using a high-resolution 10-bit CCD camera.

Western Blot Analysis for Cathepsin L and Cathepsin B in DU 145 Cells

Following electrophoresis, proteins were transferred to Immobilon-P membranes using a semi dry Trans-Blot apparatus.

The transfer sandwich consisted of blotting paper, a membrane, a gel and additional blotting paper (Figure 50). Briefly the gel was immersed in 100 ml of cathode buffer (25 mM tris base, 40 mM glycine, 10% methanol, pH 9.4) and allowed to equilibrate for 15 minutes.

Immobilon-P membranes were soaked in 100% methanol for 15 seconds, transferred into a container of ultrapure water for 2 minutes and then equilibrated in 100 mL anode buffer II (25 mM tris, 10% methanol, pH 10.4).

Filter papers used for the assembled transfer stack were soaked in cathode buffer, anode buffer II, and anode buffer I (0.3 M Tris, 10% methanol, pH 10.4).

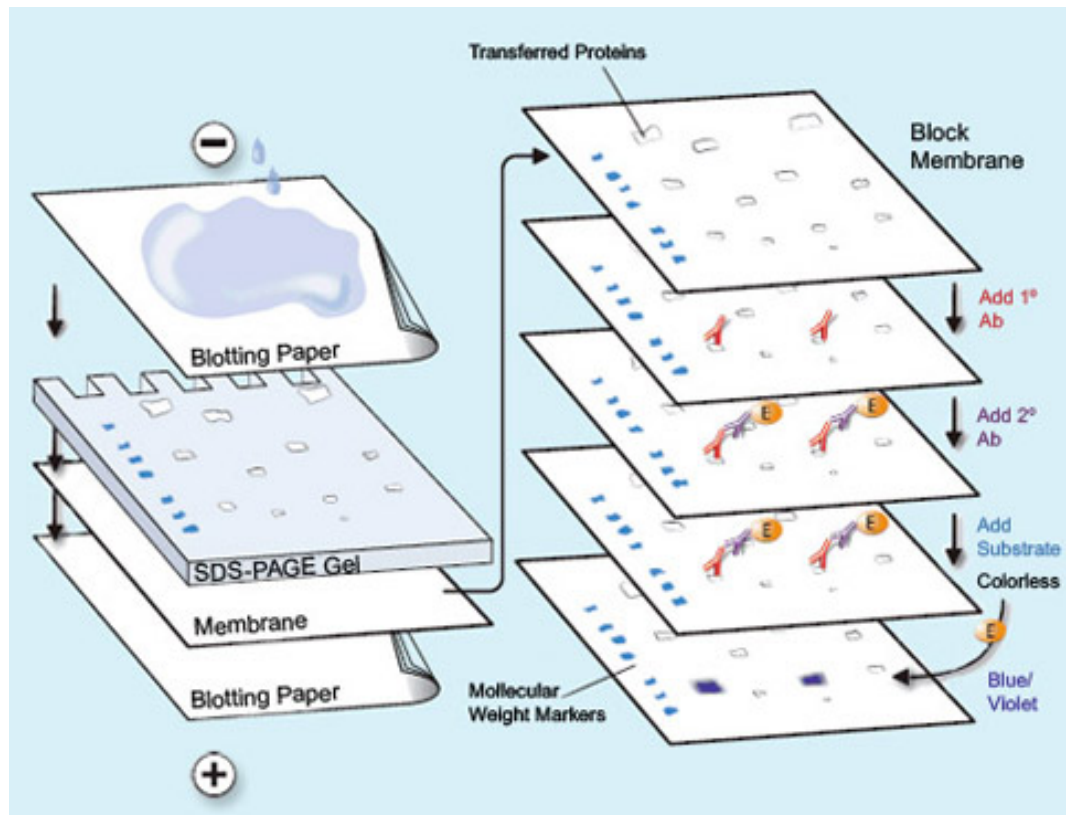


Figure 50. Assembled transfer stack for Western blot experiments. The transfer sandwich consisted of blotting paper, the membrane, the gel and additional blotting paper. Taken directly from www.millipore.com.¹²⁵

Following transfer, membranes were blocked for 45 minutes at room temperature in TBS containing 0.1% Tween-20 and 5% blocking agent (*QuickBlocker*TM) and incubated overnight with the primary antibody with gentle rocking at 4°C.

Following overnight incubation, membranes were washed three times for 5 minutes each in TBS-Tween and incubated for 1 hour at room temperature with a horse radish peroxidase (HRP) linked anti-rabbit secondary antibody.

The optimal antibody dilutions factors established were: rabbit anti-cathepsin L: 1:2000; rabbit anti-cathepsin B: 1:400 and goat anti-rabbit secondary antibody 1:20000. Membranes were then washed additional three times more for 5 minutes each in TBS-Tween and incubated for 5 minutes at room temperature with ECL HRP substrate.

Cathepsins B and L bands were detected using an UltraLum Discovery 12 chemiluminescence imager. The Discovery 12 system utilizes a powerful 12-bit high resolution (1.4 megapixel) cooled CCD camera to acquire clean, low-background images of western blots and other chemiluminescent assays in less time and with a more dynamic range than film.

CHAPTER FOUR

Results and Discussion

Biochemical Evaluation of Potential Cathepsin L Inhibitors

In this chapter, the results of the biochemical evaluation of a thiosemicarbazone library of fifty nine thiosemicarbazones derivatives of tetrahydronaphthalene, benzophenone, propiophenone, chromenone, thiochromenone, thiochromenone dioxide, indane, bromophenylcyclohexane, and bromophenylcyclopentane synthesized as potential cysteine proteases inhibitors in Dr. Kevin G. Pinney's laboratory at Baylor University will be presented.

The cathepsin L inhibitory potency of these compounds was evaluated by means of IC_{50} values, which represent the concentration of an inhibitor that is required for 50% percent inhibition of an enzyme *in vitro*. Also, the structure-activity relationship of these compounds and the results of the kinetic characterization of the most potent cathepsin L inhibitors from this library in terms of reversibility, time dependence and K_i values are discussed in this section.

In this study, three conditions were taken into account in order to work in the steady state region of the reaction according to the assumptions made by Michaelis-Menten and Briggs-Haldane to derive the following equation:

$$v_o = \frac{V_{\max}[S]}{\alpha K_M + [S]}$$

First, the initial velocity, v_o , was measured over a period of time so that the substrate concentration, $[S]$, remained constant.

Second, the concentration of substrate vastly exceeded the concentration of enzyme, so that in the chosen period of time, the substrate concentration is constant throughout the assay. Finally, the production of product was linear with time during the time interval used.¹²⁶

Cathepsin L Assay

Considering that cathepsin L hydrolyzes peptide bonds, benzyloxycarbonyl-L-phenylalaninyl-L-argininyl-7-amido-4-methylcoumarin, a fluorogenic synthetic peptide was utilized to monitor its activity.

Cathepsin L cleaves the amide bond between Arg and AMC and produces a non-fluorescent Z-FR peptide and a fluorescent AMC (Figure 51), whose rate can be obtained by monitoring the fluorescence intensity over time. The slope of the first linear portion of the curve equals the initial enzyme activity (Figure 52).

The sensitivity provided by the fluorogenic substrate used (Z-FR-AMC) and the high hydrolytic activity of cathepsin L allow for the use of low quantities of enzyme (nanomolar range) in the cathepsin L assay. Unfortunately, this leads to loss of enzymatic activity due to the problem of protein adhering to the inner walls of the cuvettes.¹²⁷ In order to overcome this issue; Brij 35 (a non-ionic detergent composed of polyoxyethylene lauryl ether and polyoxyethylene glycol dodecyl ether) was added to the activation/assay buffer.

The cathepsin L assay used for this project was developed on the basis of established procedures⁴⁵ and the final assay conditions throughout this study were 1 nM cathepsin L, 100 mM sodium acetate buffer (pH=5.55), 8 mM DTT, 4 mM EDTA and 0.01% Brij 35.

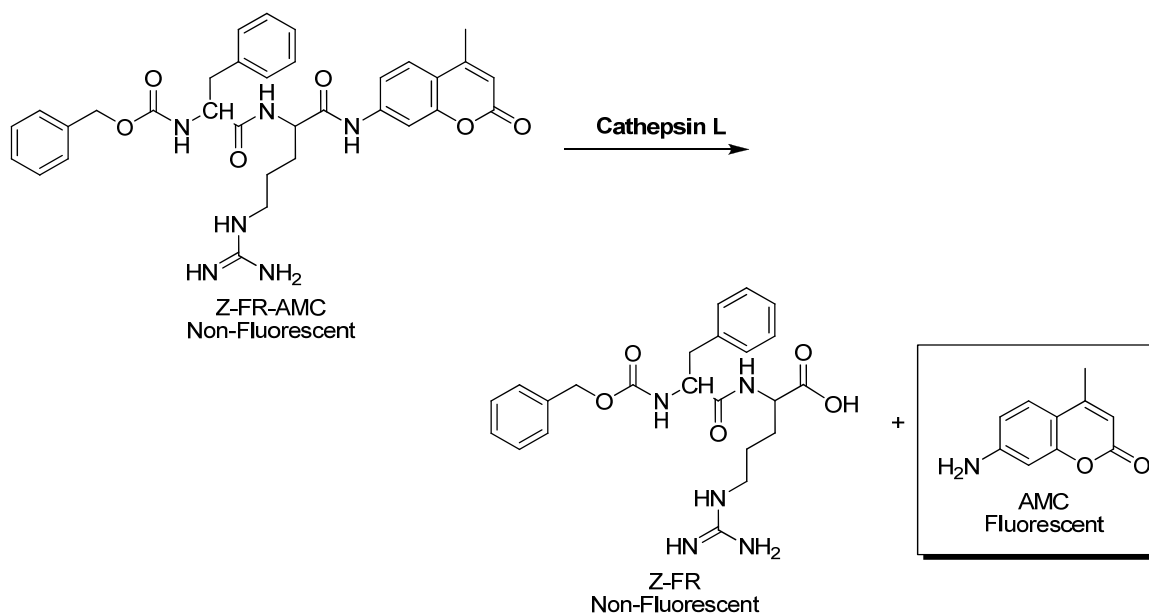


Figure 51. Non-fluorescent peptide substrate Z-FR-AMC is cleaved by cathepsin L and yields a non-fluorescent Z-FR and a fluorescent product 7-amino-4-methylcoumarin (AMC).

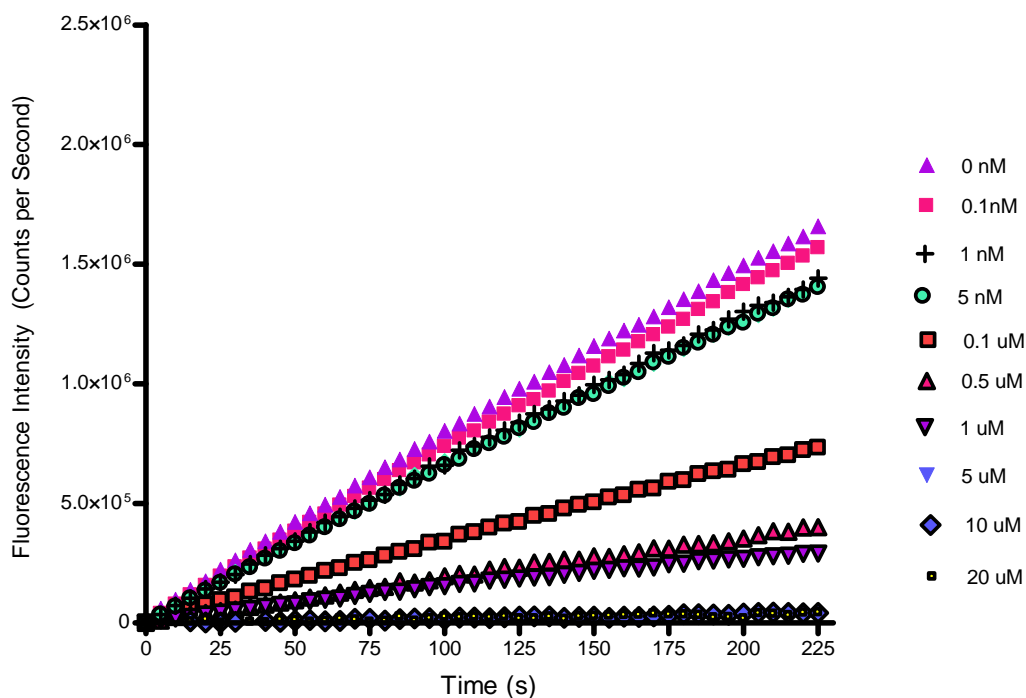


Figure 52. Monitoring of the Z-FR-AMC hydrolysis by cathepsin L in the presence of increasing concentrations of inhibitor. Ordinate values were corrected for background fluorescence.

V_{max} and K_M Determination of Cathepsin L

Cathepsin L velocity as a function of substrate concentration follows the Michaelis-Menten equation, therefore K_M is the concentration of substrate that leads to half-maximal velocity and V_{max} is the limiting velocity as substrate concentrations get very large.

The fluorogenic substrate benzyloxycarbonyl-L-phenylalaninyl-L-argininyl-7-amido-4-methylcoumarin (Z-FR-AMC) was used to monitor the production rate of 7-amino-4-methylcoumarin (AMC) by cathepsin L.

To obtain V_{max} and K_M , cathepsin L activity was measured with a fixed enzyme concentration while varying the substrate concentrations.

The final conditions of cathepsin L assays throughout this study were 1 nM cathepsin L, 100 mM sodium acetate buffer (pH=5.5), 4 mM DTT, 8mM EDTA and 0.01% Brij 35, and substrate (Z-FR-AMC) concentration ranging from 0.3 μ M to 150 μ M in a total volume of 200 μ L.

V_{max} and K_M were obtained by fitting the initial rates to the Michaelis-Menten equation $v_o = \frac{V_{max}[S]}{K_M+[S]}$ using non linear regression analysis with the Graphpad 4.03 software as shown in Figure 53.

The K_M value was found to be $1.3 \pm 0.2 \mu$ M, a value in agreement with the one previously reported in the literature (1.1 μ M).¹²⁸ The V_{max} was determined to be $592.8 \pm 27.8 \mu$ M/s.

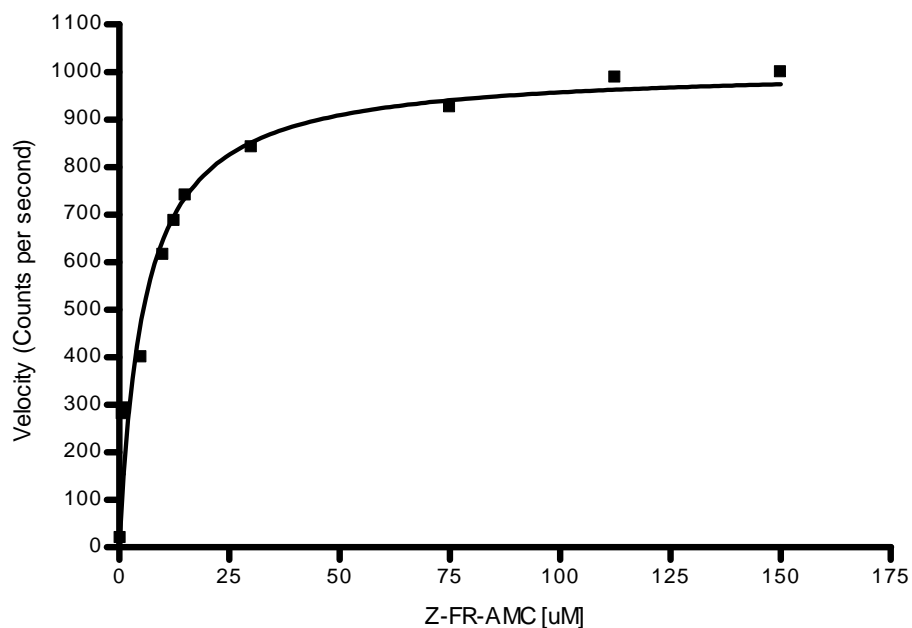


Figure 53. Dependence of cathepsin L activity on substrate concentration. (■) denote data points, and line (—) was fitted to the Michaelis-Menten equation with non-linear regression using the GraphPad software.

IC₅₀ Determination

A library of fifty nine thiosemicarbazones derivatives of tetrahydronaphthalene, benzophenone, propiophenone, chromenone, thiochromenone, thiochromenone dioxide, indane, bromophenylcyclohexane, and bromophenylcyclopentane synthesized by Rogelio Siles, Dr. Ming Zhou, Dr. Kishore Gaddale, Freeland Ackley, Jiangli Song, and Lindsay Jones from Dr. Kevin G. Pinney's laboratory at Baylor University¹³⁷ were evaluated for IC₅₀ values. Among the fifty nine compounds, fifty two were evaluated using a Fluoromax-2 fluorimeter and seven using the Thermo Fluoroskan Ascent Fluorescence plate reader.

Stock solutions (20 mM) of these inhibitors were prepared in DMSO (99.9%) and at least eight serial dilutions of inhibitors ranging from 1 nM to 20 μM were co-incubated with cathepsin L in the assay/activation buffer.

The mixtures were then assayed for activity by addition of 100 μL of 10 μM substrate Z-FR-AMC if using the Fluoromax-2 or 100 μL of 70 μM substrate Z-FR-AMC if using the Thermo Fluoroskan Ascent Fluorescence plate reader. The reactions were monitored for 5 minutes at an excitation of 355 nm and an emission wavelength of 460 nm at 25 $^{\circ}\text{C}$ for 5 minutes.

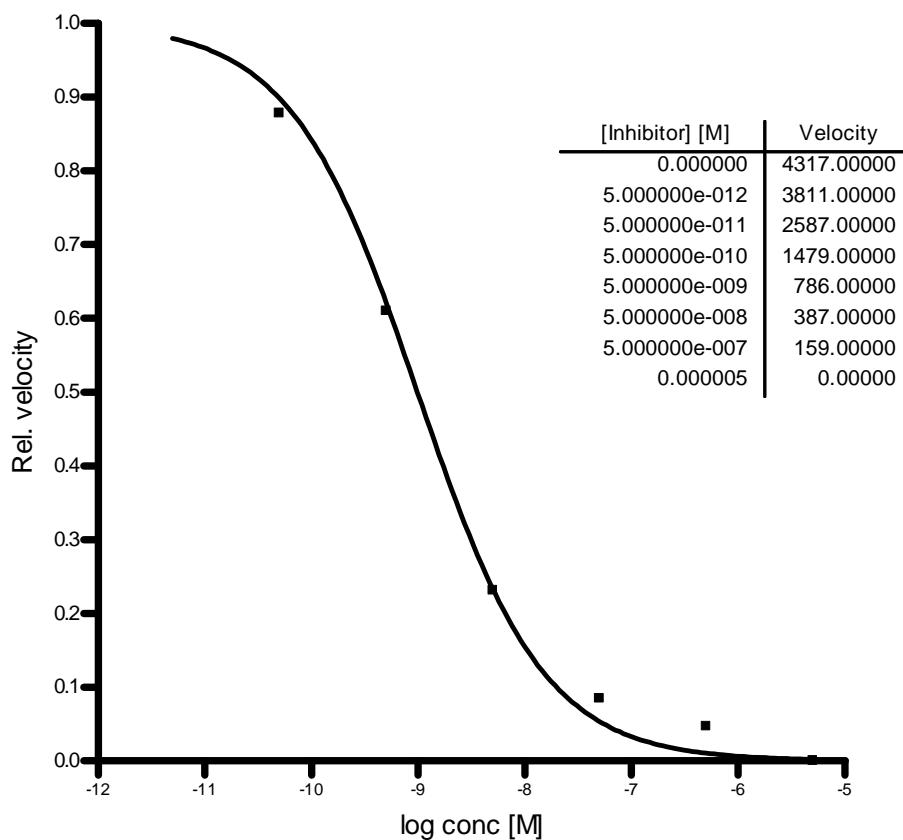
The final assay conditions were 1 nM cathepsin L, 100 mM sodium acetate buffer (pH 5.5), 4 mM DTT, 8 mM EDTA, and 0.01% Brij 35. Co-incubation of a constant enzyme concentration with increasing amounts of the same inhibitor results in a gradual loss of the enzyme activity, consequently, IC_{50} values were determined by performing non-linear regression analysis fitting velocities and the logarithm of inhibitor concentrations to a sigmoidal dose response with a variable slope model using the GraphPad Prism 4.03 software:

$$Y = v_o = v_{Min} + \frac{v_{Max} - v_{Min}}{1 + 10^{(\text{LogIC}_{50} - X) * \text{Hillslope}}}$$

Here, $Y = v_o$ is the initial enzyme velocity at various inhibitor concentrations. v_{Min} is the lowest enzyme activity when incubated with the highest concentration of the inhibitor. v_{Max} is the highest enzyme activity without inhibition. X is the logarithm of the inhibitor concentration at which the initial enzyme velocity is Y . Hillslope is the slope of the transition curve.

A representative data analysis is illustrated in Figure 54. LogIC_{50} , which is the logarithm of the IC_{50} value of the inhibitor, can be determined visually, but is more accurate to obtain this value from the non-linear regression fitting of the equation.

The IC_{50} values of these compounds are summarized in Table 8 and the detailed data analysis for each compound can be found in Appendix A.



Best-fit values	
BOTTOM	0.0
TOP	1.000
LOGEC50	-9.007
HILLSLOPE	-0.7322
EC50	9.835e-010
Std. Error	
LOGEC50	0.1286
HILLSLOPE	0.1396
95% Confidence Intervals	
LOGEC50	-9.338 to -8.677
HILLSLOPE	-1.091 to -0.3732
EC50	4.594e-010 to 2.106e-009
Goodness of Fit	
Degrees of Freedom	5
R ²	0.9807
Absolute Sum of Squares	0.02321
Sy.x	0.06813
Constraints	
BOTTOM	BOTTOM = 0.0
TOP	TOP = 1.000

Figure 54. Typical IC₅₀ determination using the dose-response sigmoid model from the GraphPad Prism 4.03 software.

Table 8. Inhibition of Cathepsin L by TSC Analogues and other Novel Cyclic Compounds.¹³⁷

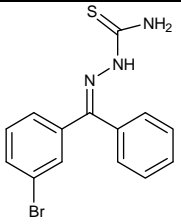
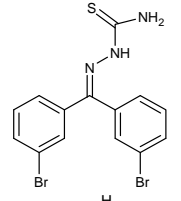
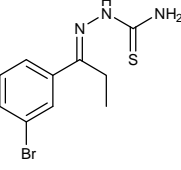
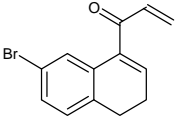
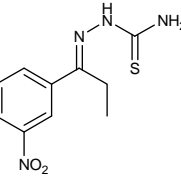
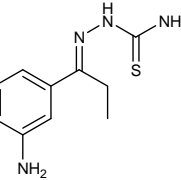
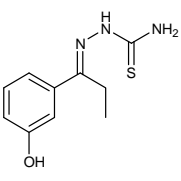
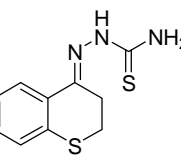
<i>Compound Number</i>	<i>Structure</i>	<i>IC₅₀ (nM)</i>
1		16200
2*		1.5
3		>10000
4		372
5		5790
6		1640
7		2570
8		983

Table 8 (Continued)

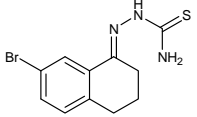
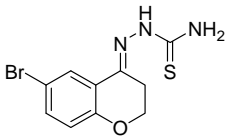
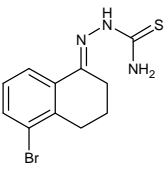
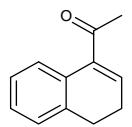
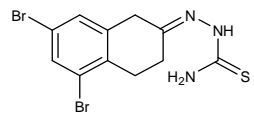
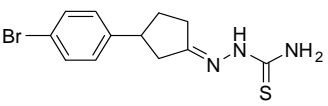
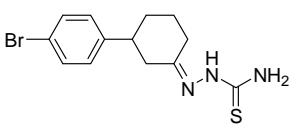
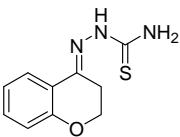
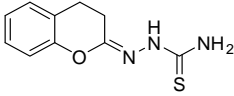
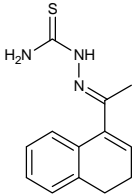
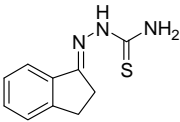
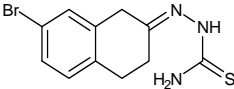
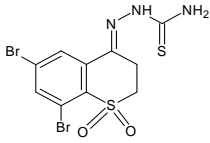
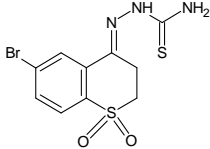
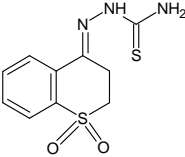
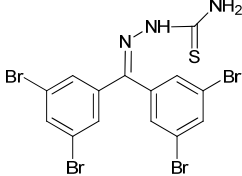
<i>Compound Number</i>	<i>Structure</i>	<i>IC₅₀ (nM)</i>
9		619
10		530
11		367
12		>10000
13		10900
14		>10000
15		2910
16		6380

Table 8. (Continued)

<i>Compound Number</i>	<i>Structure</i>	<i>IC₅₀ (nM)</i>
17		2450
18		>10000
19		>10000
20		4260
21		716
22		1
23		5050
24		ND*

*ND. This compound had solubility issues and therefore no IC₅₀ was determined.

Table 8. (Continued)

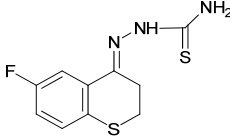
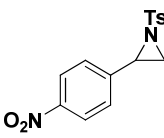
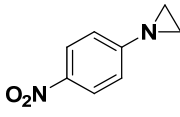
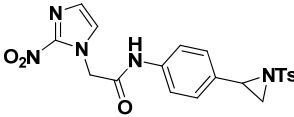
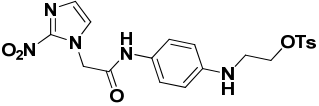
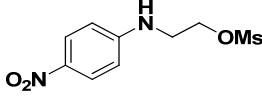
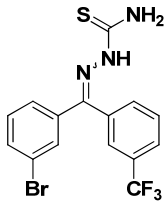
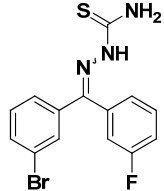
<i>Compound Number</i>	<i>Structure</i>	<i>IC₅₀ (nM)</i>
25		322
26		>20000
27		>20000
28		>20000
29		>20000
30		>20000
31		587
32		66.1

Table 8. (Continued)

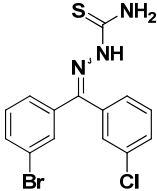
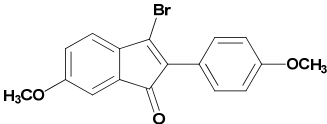
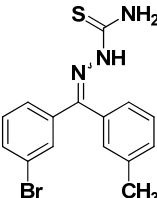
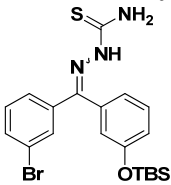
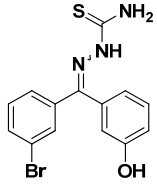
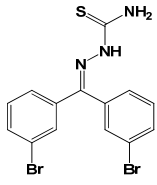
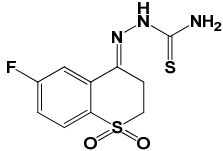
Compound Number	Structure	IC ₅₀ (nM)
33		997
34		>20000
35		980
36		>20000
37		140
38*		60.2
40		4500

Table 8. (Continued)

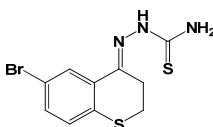
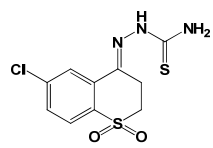
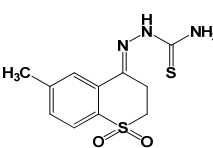
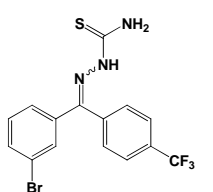
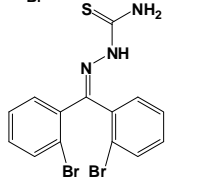
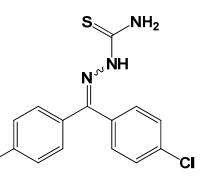
<i>Compound Number</i>	<i>Structure</i>	<i>IC₅₀ (nM)</i>
41		5400
42		17000
43		31000
44		7000
45		42000
46		>20000
47		>20000
48		16000

Table 8. (Continued)

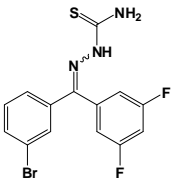
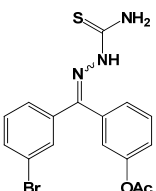
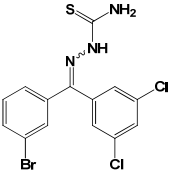
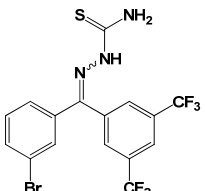
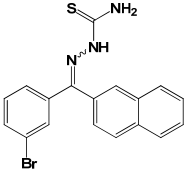
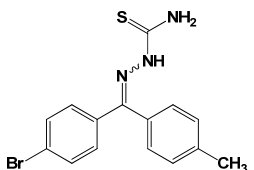
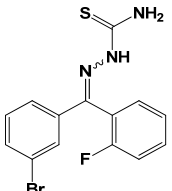
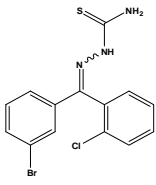
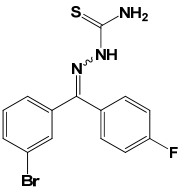
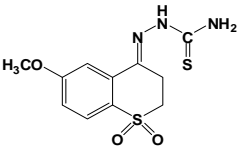
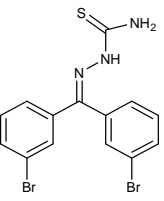
<i>Compound Number</i>	<i>Structure</i>	<i>IC₅₀ (nM)</i>
49		460
50		540
51		3500
52		4100
53		23000
54		6690
55		44.2

Table 8. (Continued)

<i>Compound Number</i>	<i>Structure</i>	<i>IC₅₀ (nM)</i>
56		16800
57		576
58		6360
59		20700
60*		63

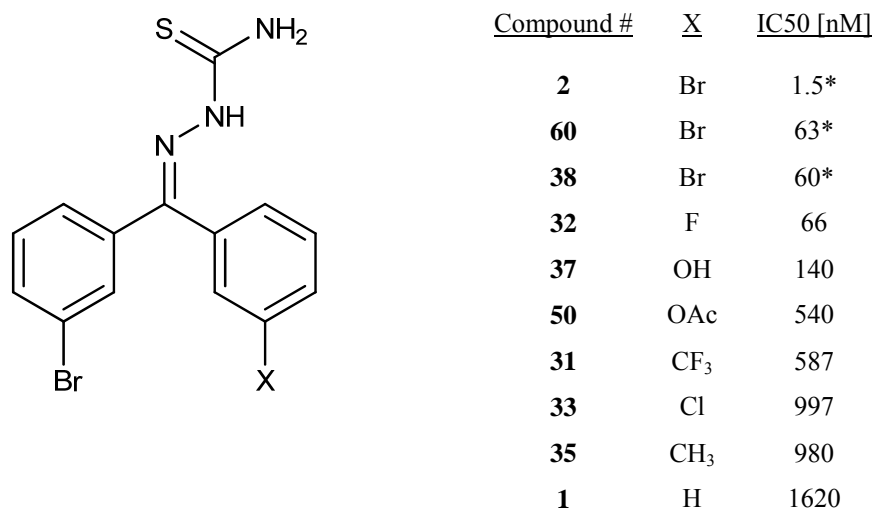
* Compounds **2**, **38** and **60** came from three different syntheses and although these compounds share the same chemical structure, **38** and **60** are purified in a higher degree than **2**. There is an unresolved discrepancy between their reported IC₅₀ values; additional experiments are currently ongoing in Dr. Pinney's laboratory to determine this difference. For the purpose of this discussion, the 63 nM value will be used.

Discussion of the Thiosemicarbazones (TSC) as Inhibitors of Cathepsin L

Inhibition of Cathepsin L by Benzophenone Thiosemicarbazone Derivatives

A set of benzophenone TSC were tested against cathepsin L (Scheme 1) and it can be observed that the potency trend in terms of IC₅₀ values is: X= Br* (1.5 nM, 63 nM) > F (66 nM) > OH (140 nM) > OAc (540 nM) > CF₃ (587 nM) > CH₃ (980 nM) > Cl (997 nM) > H (1620 nM).

Also, it must be noted that the substitution of the aromatic ring at the *meta* position with bromine or fluorine dramatically enhances the inhibitory potency against cathepsin L.



Scheme 1. Benzophenone thiosemicarbazone derivatives.

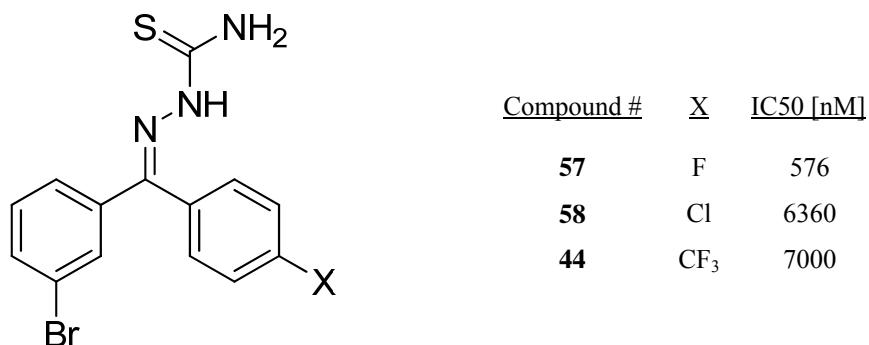
A comparison of the obtained IC₅₀ values for compound **1** (1620 nM) and compound **2** (63 nM) showed that the additional bromine substituted at the *meta* position of the second phenyl ring plays a key role in cathepsin L inhibition. Molecular modeling studies,³⁰ have suggested that the excellent inhibitory potency presented by compound **2** can be explained by three factors:

The thiosemicarbazone moiety is in close contact with the cathepsin L active site, one of the bromophenyl rings is in the S₂ pocket with the bromine constrained by the carbonyls of the S₂ pocket and the other bromophenyl ring is in the S₁ pocket

Encouraged by the results obtained for compound **2**, further structural variations (outlined in Schemes 2 to 5) were carried out maintaining the bromo benzophenone thiosemicarbazone scaffold. Substitution of the three positional isomers on the benzophenone groups with a variety of X substituents (Br, F, OH, OAc, CF₃, CH₃ and Cl) revealed interesting structure activity relationships.

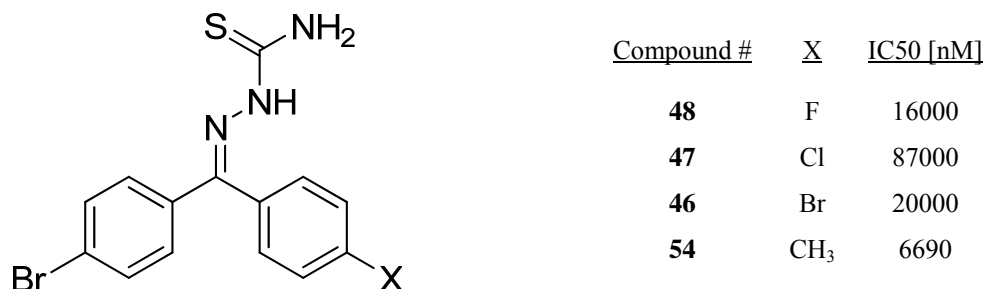
In general, a phenyl ring containing a bromine atom, chlorine atom, or a trifluoromethyl group was important for cathepsin L inhibition and it can be observed that the potency trend in decreasing order is fluorine > chlorine > trifluoromethyl group.

In the bromobenzophenone series, while retaining the bromination at the meta position, the substitution effect of moving the substituents to the para position on the aromatic ring (Scheme 2) dramatically decreased the inhibitory potency of these compounds (**31** versus **44**, **32** versus **57**; **33** versus **58**).



Scheme 2. *Para*-linked *m*-bromobenzophenone derivatives

The substitution effect of moving substituents on both aromatic rings to the para position proved to be even more detrimental to the cathepsin L inhibitory potency of these compounds as shown in Scheme 3.

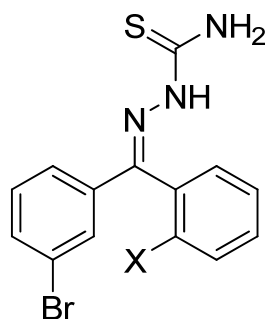


Scheme 3. *Para*-substitution in both aromatic rings of bromobenzophenone derivatives

It can be concluded that proper positioning of the X substituent is critical as the para-linked bromo benzophenone derivatives (Scheme 2) lost considerable activity against cathepsin L compared to their *meta* analogues (Scheme 1). While the *meta* benzophenone derivatives showed remarkable inhibitory potency toward cathepsin L, the para linkage led to a dramatic decrease in inhibitory activity (**2** versus **46**; **32** versus **48**; **33** versus **47**; **35** versus **54**).

The substitution effect of moving both bromine atoms from the *meta* to the ortho position proved to be also detrimental to the inhibitory potency of these compounds. Compound **2** was one of the most potent inhibitors of this library of compounds (IC₅₀= 1 nM), while **45** exhibited no inhibitory activity.

Phenyl ring substitution at the ortho position with a fluorine atom dramatically enhanced their inhibitory potency compared to a substitution with a chlorine atom or trifluoromethyl group as shown in Scheme 4.

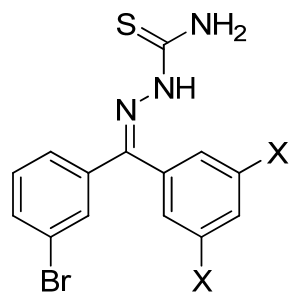


<u>Compound</u>	<u>X</u>	<u>IC50 [nM]</u>
55	F	44
56	Cl	16800

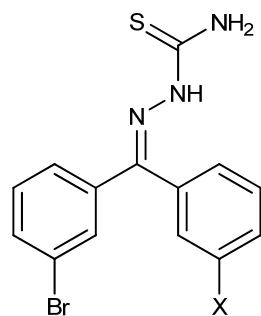
Scheme 4. Halogen monosubstitution in bromobenzophenone derivatives.

Bis-substitution with fluorine atoms at the meta positions of the phenyl ring, **49**, proved to be just slightly better compared to substitutions with a chlorine atom, **51**, or a trifluoromethyl group, **52**, which presented similar IC₅₀ values as shown in Scheme 5.

A comparison of IC₅₀ values between monosubstituted and disubstituted bromobenzophenone thiosemicarbazone derivatives proved the di-substitution effect to be detrimental to the cathepsin L inhibitory potency of these compounds (**32** and **55** versus **49**; **33** versus **51** and **56**; **31** versus **52**) as shown in Schemes 4 and 5.



<u>Compound #</u>	<u>X</u>	<u>IC50 [nM]</u>
49	F	460
51	Cl	3500
52	CF ₃	4100



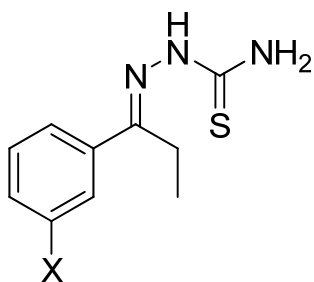
<u>Compound #</u>	<u>X</u>	<u>IC50 [nM]</u>
32	F	66
33	Cl	997
31	CF ₃	587

Scheme 5. Comparison between mono and di-substitution in bromobenzophenone TSC derivatives.

Inhibition of Cathepsin L by Propiophenone Thiosemicarbazone Derivatives

Compounds **3**, **5**, **6** and **7** share a propanone thiosemicarbazone moiety with the phenyl ring substituted at the meta position with an electron-withdrawing groups like nitro and bromine and two hydrogen bond donor-acceptor groups such as amino and hydroxyl (Scheme 6). The potency trend against cathepsin L in terms of IC₅₀ values is:

X= NH₂ (1640 nM) > OH (2570 nM) > NO₂ (5790 nM) > Br (10000 nM).



<u>Compound #</u>	<u>X</u>	<u>IC₅₀ [nM]</u>
3	Br	10000
5	NO ₂	5790
6	NH ₂	1640
7	OH	2570

Scheme 6. Propiophenone thiosemicarbazone derivatives

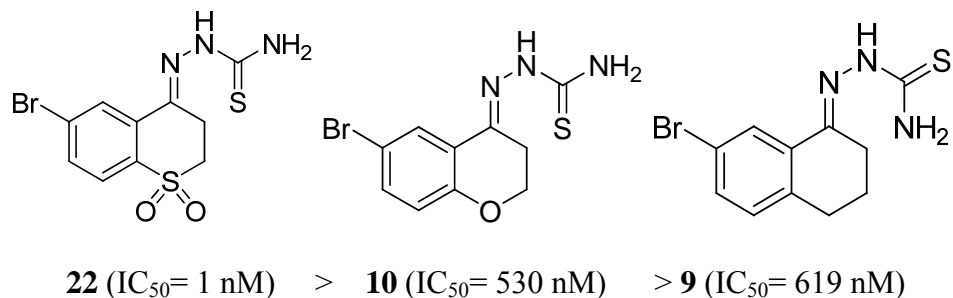
Inhibition of Cathepsin L by Tetrahydronaphthalene Derivatives

Therefore, it was of interest to incorporate the thiosemicarbazone moiety into tetrahydronaphthalenes skeletons as well as other functional groups that are shown in Schemes 7 to 11.

In the α -tetralone series, while retaining the bromination at the 7 position, the substitution effect of C4 with sulfone **22**, oxygen **10** and no substitution **9** are addressed (Scheme 7). A comparison of the IC₅₀ values for **22** (1 nM), **10** (530 nM), **9** (619 nM) showed that the substitution of C4 with sulfone considerably enhances the inhibitory potency against cathepsin L.

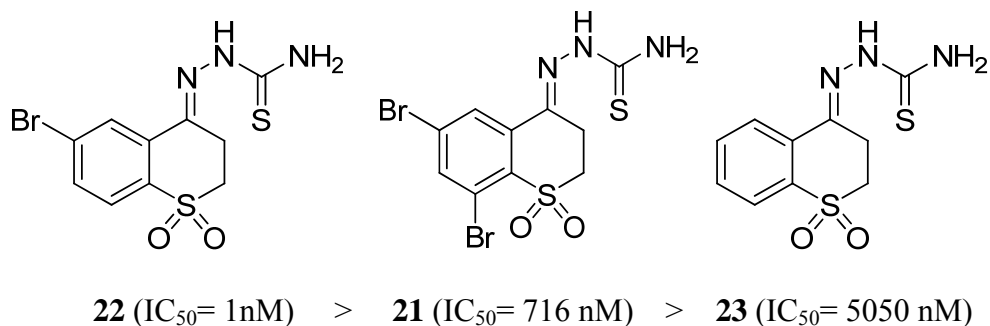
Comparing **10** and **22**, it can be hypothesized that the sulfone interaction is more favored because it is much bulkier than a single oxygen atom.

Other factors may also explain the exceptional inhibitory activity of **22** for example, the bromine is buried in the S_1' pocket, the sulfone is exposed to the water solvent, and the aromatic region is totally buried and encapsulated by the S_1' pocket. Also, the thiosemicarbazone moiety is in the active site in close contact with Cys-25 thiolate.³⁰



Scheme 7. Potency trend in α -tetralone monobromo derivatives

The degree of bromination on the α -tetralone scaffold was evaluated with the mono-bromo derivative **22**, the dibromo derivative **21**, and the unhalogenated derivative **23**. The potency trend in decreasing order is the mono-bromo derivative **22**, dibromo derivative **21**, and unhalogenated derivative **23** (Scheme 8). It can be concluded that substitution is essential for cathepsin L inhibition when a sulfone substitution is present at C4.



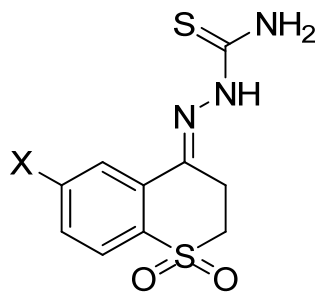
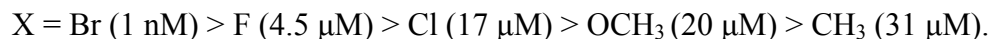
Scheme 8. Potency trend in α -tetralone derivatives

The series of unhalogenated and brominated derivatives of thiochromenone dioxide provided additional supporting evidence to demonstrate the importance of the bromine substitution in the thiochromenone scaffold.

A comparison of the IC₅₀ values for compound **9** (619 nM), compound **10** (530 nM), compound **11** (367 nM) and compound **21** (716 nM) showed similar potencies against cathepsin L in the nanomolar range while the unhalogenated compound **23** presented the weakest activity toward cathepsin L with an IC₅₀ value of 5 μM.

Encouraged by the low IC₅₀ obtained for **22**, it was decided to focus efforts on introducing other functional groups into the molecule (Scheme 9).

The potency trend of thiosemicarbazone derivatives of the sulfone analog of a substituted thiochroman-4-one against cathepsin L in terms of IC₅₀ values is:



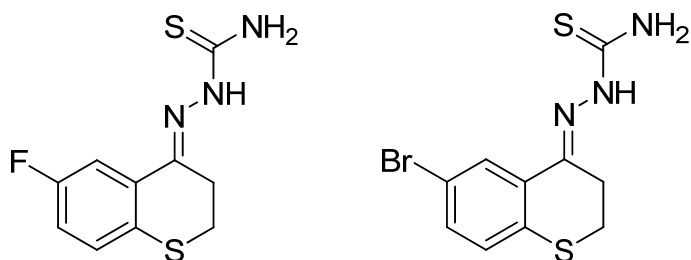
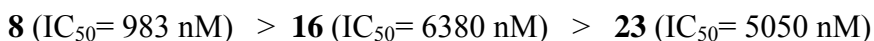
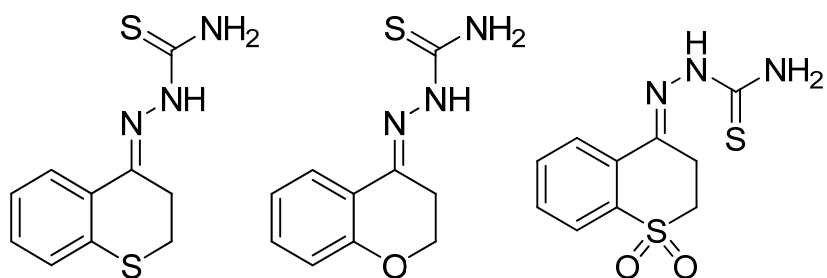
<u>Compound</u>	<u>X</u>	<u>IC50 [nM]</u>
22	Br	1
40	F	4500
42	Cl	17000
43	CH ₃	31000
59	OCH ₃	20000

Scheme 9. Thiosemicarbazone derivatives of the sulfone analog of a substituted thiochroman-4-one.

Another group of molecules to be discussed is the series containing tetrahydronaphthalene derivatives having a hetero-atom such as oxygen and sulfur replacing one benzylic carbon of the cyclohexane ring.

Substitutions at C4 position with sulfone **23**, sulfur **8**, and oxygen **16** in unhalogenated and halogenated **41** and **39** dihydronaphthalenyl thiosemicarbazone series are compared in Scheme 10.

A comparison of the IC₅₀ values for **8** (983 nM), **16** (6.4 μM) and **23** (5.0 μM), **39** (670 nM) and **41** (5.4 μM) showed that the substitution at the C4 position with sulfur increases the cathepsin L inhibitory potency compared to a sulfone or oxygen substitution and that the halogenation with a fluoride atom is slightly more efficient than one with a bromide.

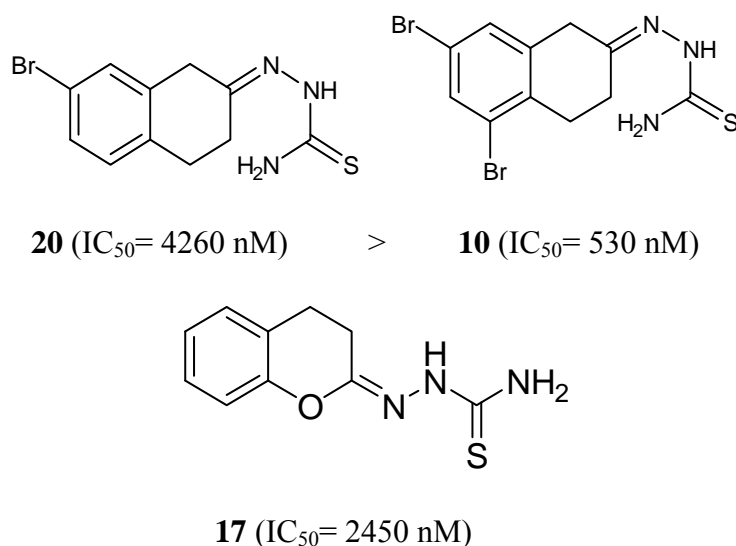


Scheme 10. Potency trend in halogenated and unhalogenated substituted α -tetralone series.

The bromination effect was also evaluated in the β -tetralone thiosemicarbazone derivatives (Scheme 11).

A comparison of the IC_{50} values for **20** (4.3 μ M) and **13** (10.9 μ M) showed that the mono-bromo β -tetralone derivative **20** is twice as effective than the di-bromo β -tetralone derivative **13**.

Replacement of a single carbon with an oxygen in an unhalogenated β -tetralone scaffold to afford chromen-2-one thiosemicarbazone **17** was carried out with slightly better inhibitory effects (IC_{50} =2.5 μ M).

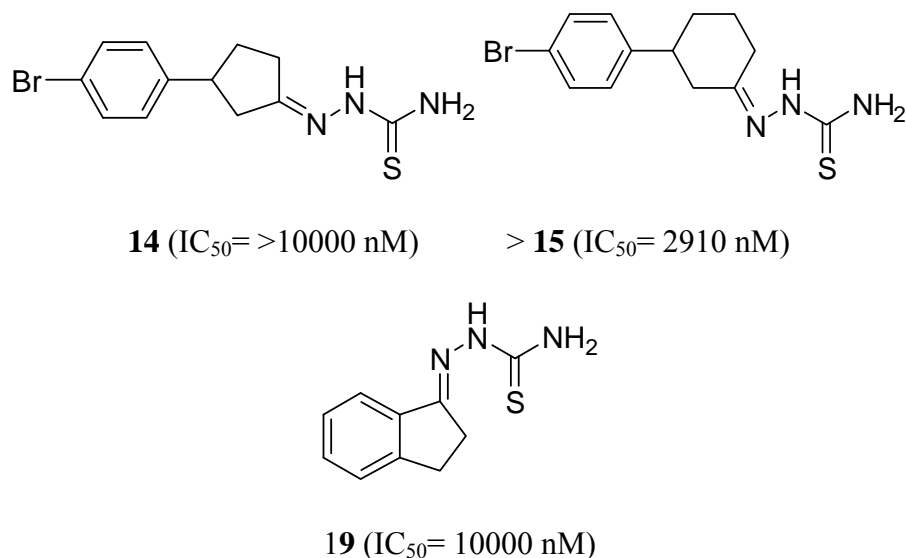


Scheme 11. Potency trends related to the bromination effect in β -tetralone thiosemicarbazone derivatives.

Inhibition of Cathepsin L by Naphthalene Derivatives

To investigate the effect of ring size on the non-aromatic region of the tetralone, an unhalogenated indanone thiosemicarbazone **19** was evaluated with no inhibitory effects toward cathepsin L. Two additional structures, **14** and **15**, explored other possible scaffolds of connected ring systems (Scheme 12).

It was concluded that connected ring systems do not show good inhibitory effects towards cathepsin L, which is not surprising considering that the solubility of these compounds is poor in aqueous solution.

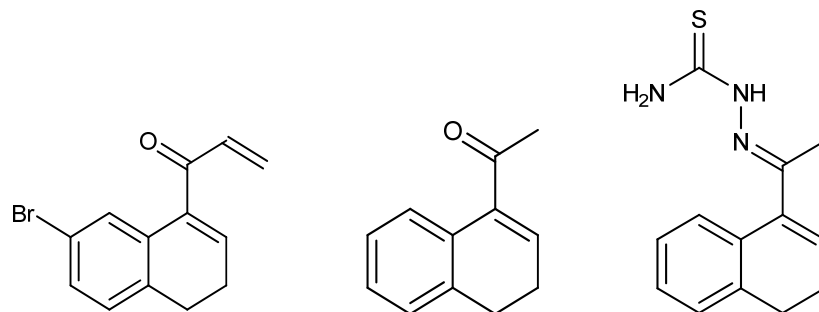


Scheme 12. Indaone and connected ring systems thiosemicarbazone derivatives evaluated.

Inhibition of Cathepsin L by naphthalene derivatives

Compounds **4** and **12**, two structures based on the naphthalene scaffold were evaluated to investigate the effect of the number of Michael acceptor presents in the molecule and the halogenations effect.

A comparison of the IC_{50} values for **4** (372 nM) and **12** (>10 μ M) showed that compound **4** with one bromine and two Michael acceptors is more potent than compound **12**, which only has one Michael acceptor. The extension of the thiosemicarbazone moiety with one additional carbon from the dihydronaphthalene scaffold was not advantageous as is demonstrated by the absence of inhibition by compound **18** (Scheme 13).

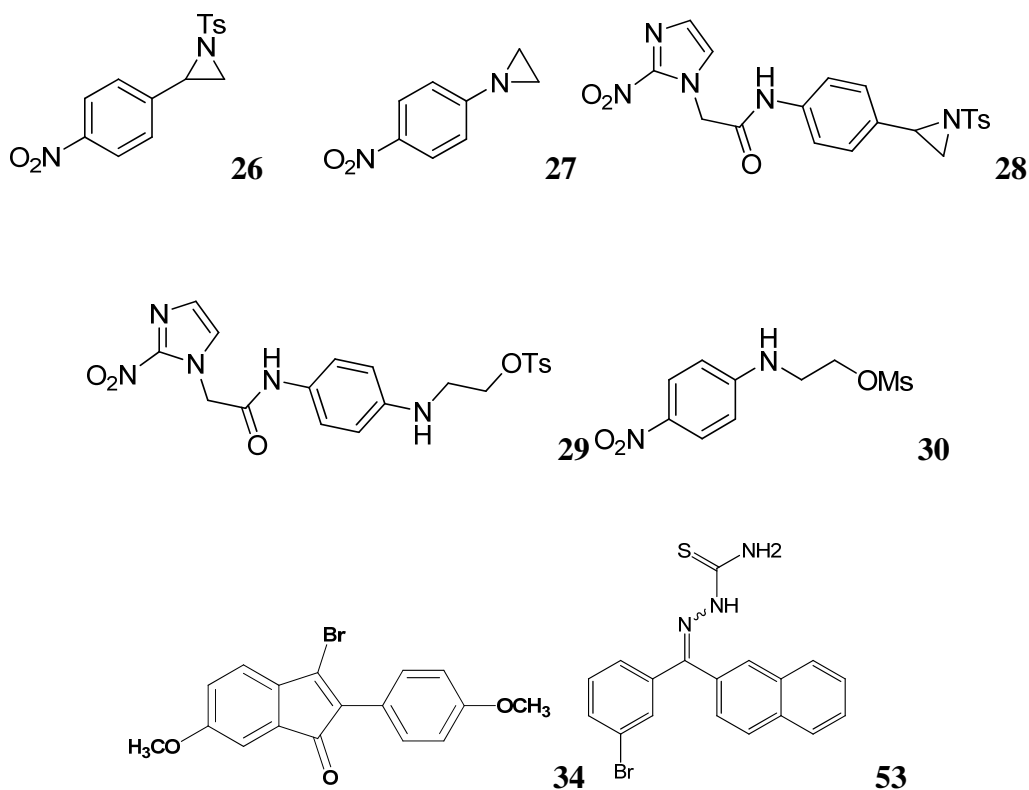


4 (IC_{50} = 372 nM) > **12** (IC_{50} = >10000 nM) and **18** (IC_{50} = >10000 nM)

Scheme 13. Potency trends in naphthalene derivatives.

Inhibition of Cathepsin L by aziridine derivatives and other cyclic compounds

Finally, it was determined that none of the aziridine derivatives (**26-30**) and compounds **34** and **35** showed inhibitory activity against cathepsin L, all with IC_{50} values higher than 20 μ M. Therefore no trends could be derived (Scheme 14).



Scheme 14. Evaluated aziridine derivatives and other cyclic compounds.

In summary, it has been shown that cathepsin L can be inhibited by thiosemicarbazone compounds. The SAR within this series indicated that one important structural requirement for cathepsin L inhibition is the need of the molecules to have hydrophobic moieties, particularly aliphatic and/or aromatic rings containing one bromine or fluorine atom.

Also, the presence of negatively charged oxygen-based functional groups such as sulfone increases the inhibitory potential of some compounds.

Advanced Kinetic Studies

A kinetic evaluation was carried out on the most potent cathepsin L inhibitors of the thiosemicarbazone library evaluated in this study: compounds **2** and **22**. Reversibility, time dependence and K_I value determination were used to characterize the enzyme-inhibitor interactions.

Compounds **2** and **22** were tested at concentrations of 5 μ M, 50 nM and 5 nM using a 5 minute enzyme-inhibitor incubation time. The substrate Z-FR-AMC was then added at concentrations ranging from 0 to 100 μ M and the reactions were monitored at excitation and emission wavelengths of 355 nm and 460 nm, respectively.

The baseline control for each assay used the same conditions without the inhibitor. GraphPad Prism 4.03 software was used for data analysis and the Michaelis-Menten plot obtained has shown that the V_{\max} decreased in the presence of the inhibitors and that the K_M value changed according to increasing concentrations of the inhibitor as shown in Figure 55.

Therefore, it was demonstrated that both compounds exhibited mixed type inhibition.

Considering the IC_{50} value in the low nanomolar range competitive inhibition kinetics was expected, but given that it was previously reported that mixed inhibition can lead to slow tight inhibition as well,¹⁰⁶ further experiments and more complex mathematical equations were needed to confirm this hypothesis and characterize the inhibitor-enzyme complex to determine K_I . In that context, time dependency and reversibility studies were performed next.

Time Dependence Inhibition Studies

Time dependence inhibition studies were performed for compounds **2** and **22** using a single enzyme (1 nM) and substrate Z-FR-ZMC (5 μ M) concentration and three inhibitor concentrations (5 μ M, 50 nM and 5 nM) with analysis over a 2.5 hour time period. Each inhibitor concentration was incubated separately with cathepsin L for 5 min, 15 min, 30 min, 60 min, 90 min, 120 min and 145 min at 25°C prior the initiation of the reaction with the addition of substrate Z-FR-AMC. The baseline control for each assay used the same conditions without the inhibitor.

GraphPad Prism 4.03 software was used for data analysis. This data was plotted as $\ln(v_t/v_i)$ versus time, where v_t is the remaining activity at time t and v_i is the activity in the absence of inhibitor.

Time-dependent inhibition kinetics were obtained for **2** and **22** as shown in Figure 56, this first order plots exhibit curvature as the inhibition approaches equilibrium, indicating reversibility. A completely linear plot would be expected for irreversible inhibition.¹⁰¹ Also, it should be noted that this behavior is consistent with slow-tight binding inhibition.

It has to be noticed that the the inhibitors **2** and **22** are extremely potent causing significant inhibition at very low concentrations comparable to the concentration of cathepsin L in the inhibition assay.

This situation is referred to as tight-binding inhibition. Partly as a result of their low concentrations, tight-binding inhibitors often show slow-binding characteristics that mean that unlike conventional inhibitors that act almost instantaneously, slow-binding inhibitors may take several seconds, minutes or even hours for their effect to be fully exhibited.

This association between slow-binding and tight-binding is relatively common and slow tight-binding inhibitors are extremely potent and specific.¹⁰⁶

Reversibility Studies

Reversibility studies were performed to confirm the reversible character of compounds **2** and **22**, two of the most potent cathepsin L inhibitors of the thiosemicarbazone library evaluated in this project.

The dilution method was employed to investigate the reversibility of the inhibitor interaction with cathepsins L.

Briefly, cathepsin L and each inhibitor were pre-incubated together (100-fold concentration) over a 1 hour time period and then diluted into substrate-containing buffer showing a complete recovery of the activity (Figure 57).

Enzyme activities were calculated from kinetic measurements performed by fluorometric detection of the product AMC at 25°C in fluorescence quartz cuvettes. Thus, the results were consistent with fully reversible inhibitor behavior.

Reversibility of cathepsins L inhibition is a desirable property for therapeutic applications since many enzymes contain cysteine active site and therefore a cross-reactivity possibility is strong. The *in vivo* consequences of irreversibly inactivating non-target enzymes lead to negative side effects.

K_I values of **2** and **22** were obtained by fitting the same progress curves for the onset of inhibition used to determine IC_{50} values to the Williams-Morrison equation describing slow tight binding inhibition using GraphPad Prism 4.03 software. (Figure 58).

Considering that for the given experimental conditions, the dissociation constant K_I , Michaelis-Menten constant K_m , and the amount of total enzyme E_t remain the same, a simplified version of the Williams-Morrison equation, described below, is used for non-linear regression analysis.

$$Y = \frac{v}{v_0} = \frac{E - X - K_I^{app} + \sqrt{\left((E - X - K_I^{app})^2 + 4 \times E \times K_I^{app}\right)}}{2 \times E}$$

Here, Y is the relative velocity of the enzyme, which is derived from the inhibited enzyme activity, v , divided by the uninhibited enzyme activity, v_0 . X is the inhibitor concentration used to inhibit the enzyme activity.

E is the total enzyme concentration, which is also fixed for a given experiment. K_I^{app} is the apparent dissociation constant, which is obtained from the non-linear regression fit of this model.

After the K_I^{app} is obtained from the model, the actual K_I can be obtained by solving the equation: $K_I^{app} = K_I \left(1 + \frac{S}{K_m}\right)$.

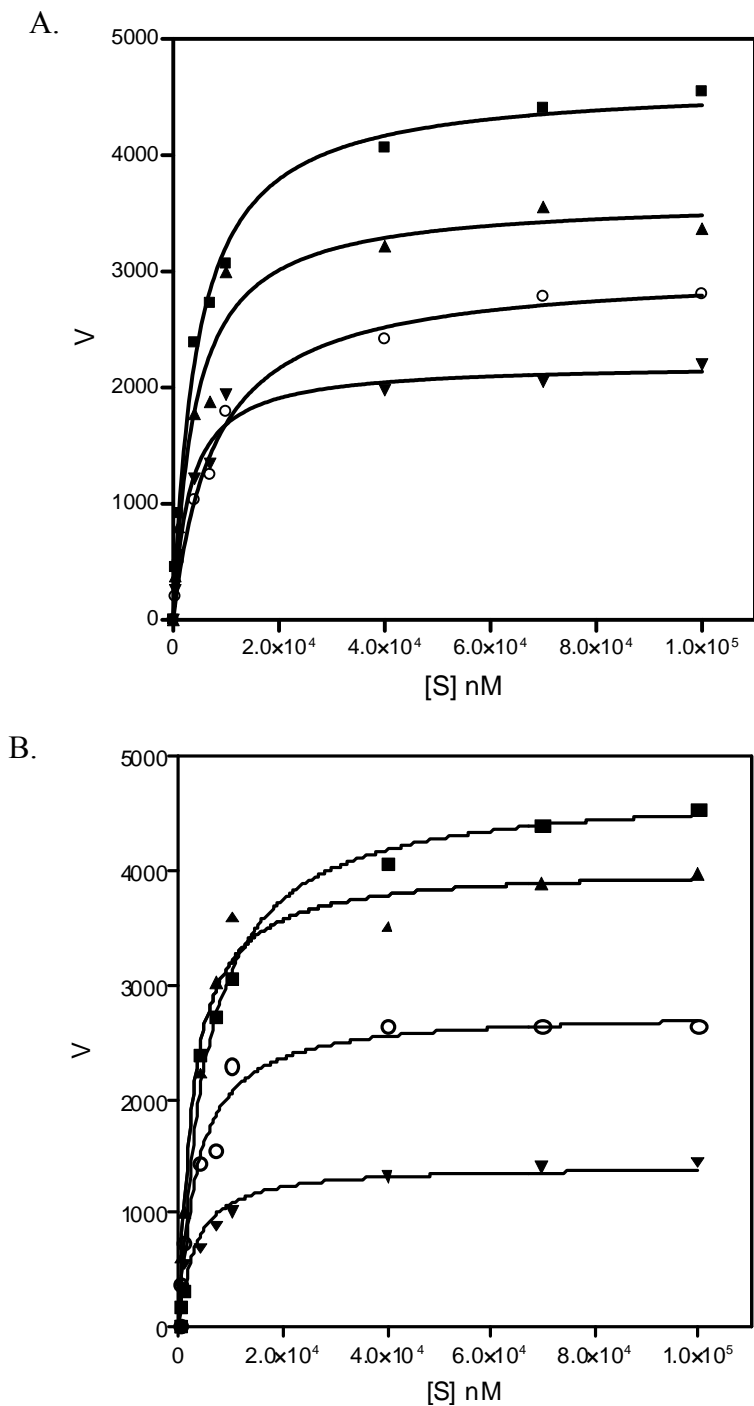


Figure 55. Plot of initial velocity of a simple Michaelis-Menten reaction versus the substrate concentration [S] in the presence of different concentrations of a inhibitor [I].
 A. Progress curves for the reaction of human liver cathepsin L in the presence of compound **2** as inhibitor [I] ○50nM ▲5nM ▼500nM ■ Control reaction without inhibitor.
 B. Progress curves for the reaction of human liver cathepsin L in the presence of compound **22** as inhibitor [I] ○50nM ▲5nM ▼500nM ■ Control reaction without inhibitor.

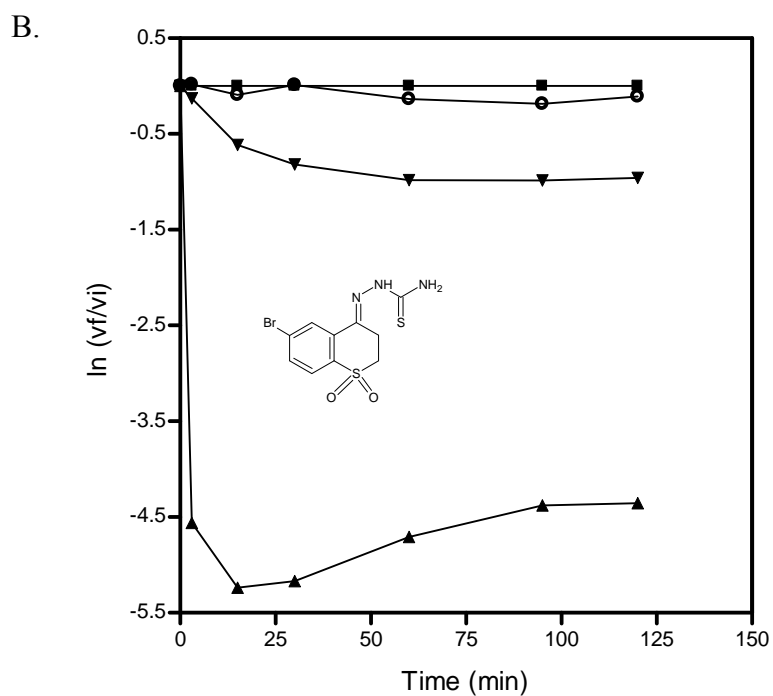
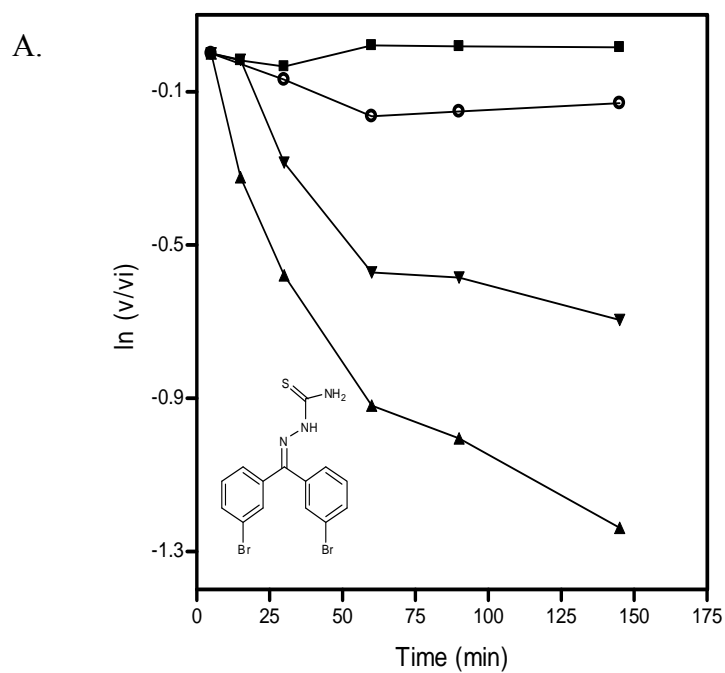


Figure 56. A. Time-dependent inhibition kinetics of compound **2** with cathepsin L. ■Control reaction without inhibitor [I], ○5nM [I], ▼50nM [I] and▲5µM [I]. B. Time-dependent inhibition kinetics of compound **22** with cathepsin L. ■Control reaction without inhibitor [I], ○5nM [I], ▼50nM [I] and▲5µM [I].

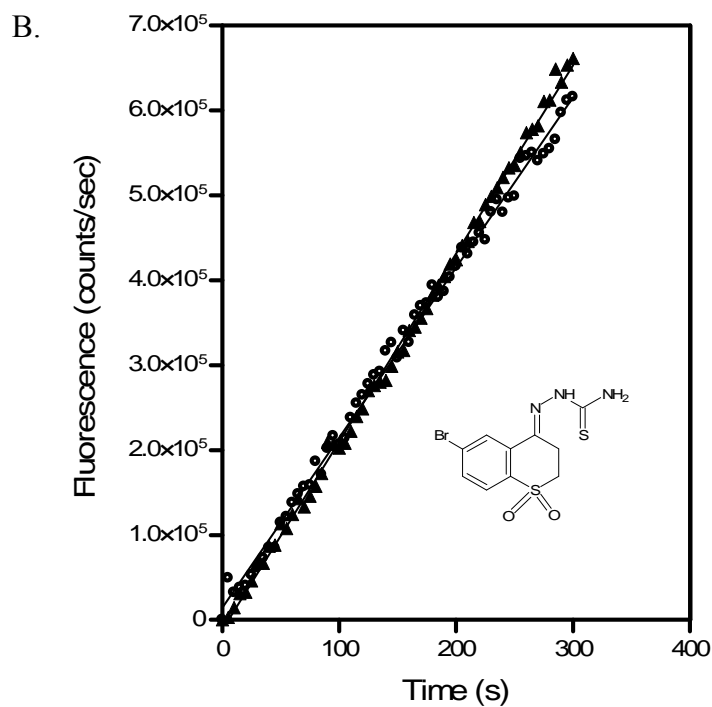
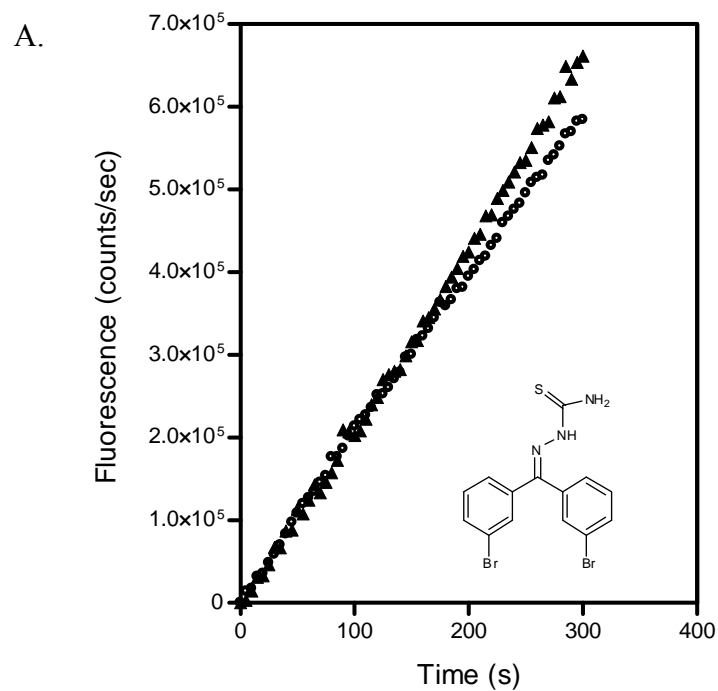


Figure 57. A. Progress curves for the reaction of human liver cathepsin L in the presence of compound **2**. (▲) Control reaction without inhibitor; (○) Reaction with compound **2**. B. Progress curves for the cathepsin L activity recovery in the presence of compound **22**. (▲) Control reaction without inhibitor; (○) Reaction with compound **22**.

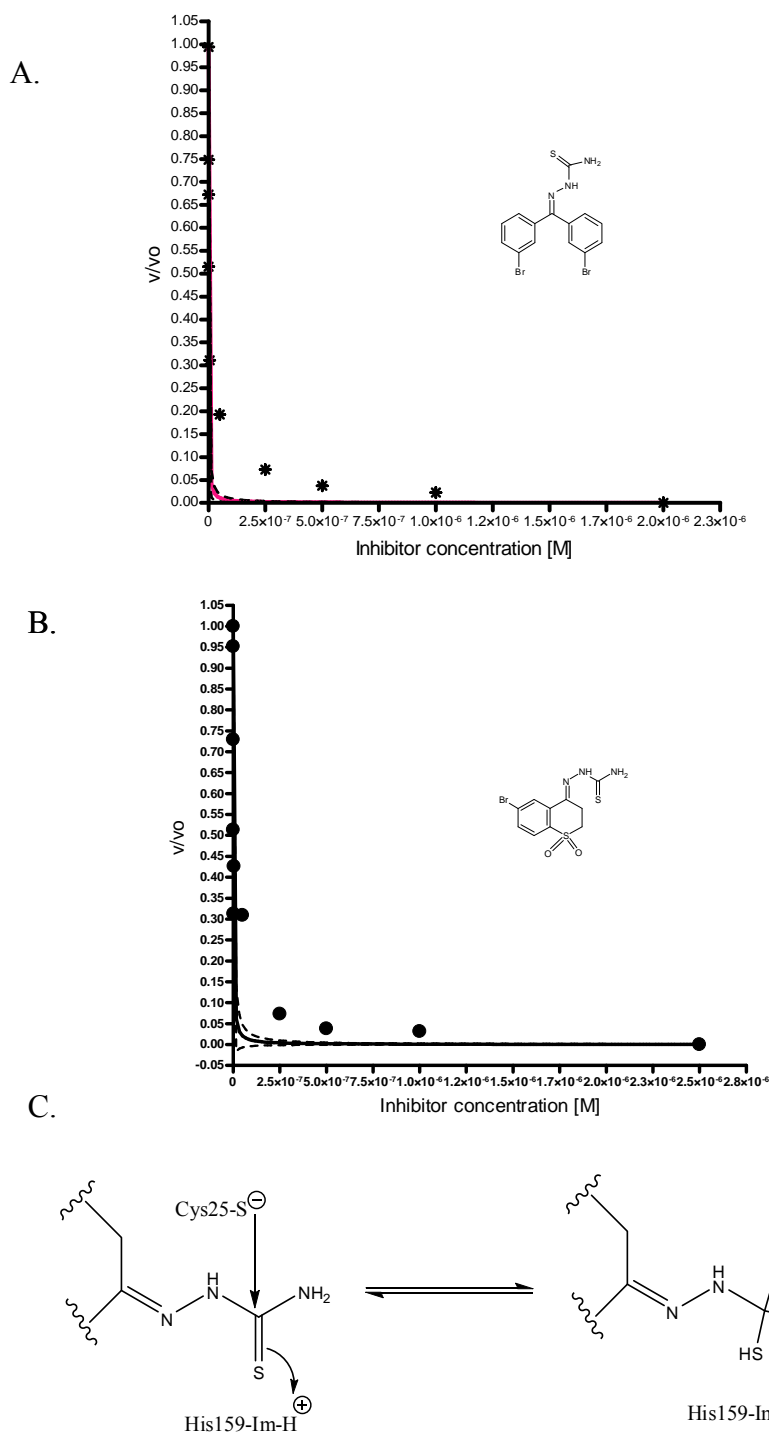


Figure 58. A. Williams-Morrison equation as the fitting model of compound **2** kinetic data. B. Williams and Morrison equation as the fitting model of compound **22** kinetic data. Relative velocities to inhibited cathepsin L reaction were plotted against inhibitor concentrations. The data points (—) were fitted to Williams and Morrison equation. C. Mechanism of inhibition of a cysteine protease with a thiosemicarbazone by formation of a reversible covalent intermediate with the active site cysteine thiolate.

Using the Williams-Morrison equation as the fitting model, which applies to reversible covalent inhibition as well as slow tight binding, we obtained a very satisfactory fit for compound **22**. The best-fit value for **22** was $K_i = 1.5 \pm 0.3$ nM for the tight-binding inhibition constant.

The good fit to the Williams-Morrison equation for **22** indicates this inhibitor is indeed a slow-tight inhibitor. The calculated K_i agrees well with the IC_{50} (1 nM). Compound **2** did not fit the Williams and Morrison model as well, but it converges giving a $K_i = 1.0 \pm 0.2$ nM

The kinetic behavior of slow, tight binding inhibitors is very similar to that of reversible mechanism-based inhibitors in which a transient, reversible, covalent bond is formed. Slow, tight and reversible covalent inhibitors bind to the enzyme slowly, and dissociate slowly (Figure 58 C).

Therefore, if **22** is a reversible covalent inhibitor, the kinetics of the inhibition should fit the same equation that describes slow, tight binding inhibitors.

If time dependency is observed, it is assumed that there is covalent modification at the active site during inhibition, although this is a contradiction in the case of inhibitor **22** as it is also assumed that small size inhibitors do not have sufficient non-bonding interactions to remain at the active site.³⁰

In summary, with standard determination of kinetic parameters, time dependency studies and reversibility studies, it was concluded that both **2** and **22** were active-site directed inhibitors of cathepsin L.

Mechanistically, both compounds behaved as time dependent, slow tight-binding reversible inhibitor.

Advanced Cell Culture Studies

Advanced cell culture studies were designed to determine if compounds **2** and **22**, the most potent cathepsin L inhibitors from the evaluated library, were able to retain their activity while in contact with the prostate cancer cell line DU-145. The biological evaluation studies included cytotoxicity, invasiveness and Western blot experiments.

The prostate cancer cell line DU-145 was used for this study because previous studies suggested that this cell line expressed high levels of cathepsins L.

General Considerations

The inhibitors to be tested were dissolved in cell culture grade DMSO and applied as a solution to a sub-confluent cell culture monolayer or cell suspension depending on the application. Blanks (culture vessels without cells) were included to detect any background interference when measuring the endpoint. Cell culture grade DMSO was used as a solvent control and provided the reference for 100% cell growth in the test vessel. The irreversible cysteine protease inhibitor E-64 was used as a positive control and it was tested concurrently with (and independent of) the test substance. The purpose of a positive control is to demonstrate that the cell culture system is responding with adequate sensitivity to a cytotoxic agent for which the magnitude of the cytotoxic response is well characterized.

Preliminary Cytotoxicity Studies

In recent years there has been a significant change in the way toxicity testing of test components is conducted. In general, the emphasis has changed from in vivo animal methods to in vitro toxicity methods. In this context, healthy mammalian cells such as HEK-293 cells, when maintained in culture, continuously divide and multiply over time.

The basis of this assay is that a cytotoxic chemical will interfere with this process and, thus, a reduction of the growth rate as reflected by cell number will provide an indication of toxicity. Ultimately, a compound with IC₅₀ values in the nanomolar range does not necessarily represent a good drug lead unless it also demonstrates low or no toxicity among other criteria.

Therefore, ten of the most potent cathepsin L inhibitors (Figure 59) were tested for cytotoxicity effects in HEK-293 cells using the trypan blue exclusion assay. Each of the assays was conducted in duplicate.

The enumeration and discrimination of living and dead cells were determined by counting cells using the cell viability dye trypan blue (0.1%) and a hemocytometer. Living cells have intact cell membranes and active cell metabolisms that exclude trypan blue, while nonviable cells are able to take up the dye and are stained blue cells because they have damaged membranes or impaired metabolisms.¹²⁷

The percentage viability was calculated using the following equation:

$$\% \text{ Viability} = \frac{\text{Unstained cell count}}{\text{Total cell count}} \times 100$$

As shown in Figure 60, the tested inhibitors did not show significant toxicity at a concentration of 20 μM after an incubation period of 24 hours at 37 °C, in an atmosphere containing 5% CO₂ in the air.

Determination of Cathepsin L Inhibitors Activity on Mammalian Cell Culture

In these series of experiments, the most potent cathepsin L inhibitors from the TSC library evaluated in this study were added to the cell culture in serum free medium at a final concentration of 20 μM to determine their inhibitory effects on intracellular active and latent secreted cathepsin L.

The effect of compounds **2** and **22** on the secretion of cathepsin L from DU-145 prostate cancer cells was determined using the fluorogenic substrate Z-FR-AMC. DU-145 cells were incubated with 20 μ M of each inhibitor for 24 hours at 37°C, in an atmosphere containing 5% CO₂ in the air.

Cathepsin L activity was only detected after the cell lysate and conditioned medium were incubated under acidic conditions for 30 minutes and 90 minutes, respectively, prior to assay suggesting that the proforms of the enzymes were released.

As shown in Figure 61, the secreted cathepsin L present in DU-145 cell conditioned media was completely inhibited in the presence of 20 μ M of compounds **2** and **22** compared to the control (0.1% DMSO-treated cells).

The same trend was followed in cell lysates (Figure 62) collected from DU 145 cells that were treated with 20 μ M of compounds **2** and **22**, which showed a significantly decreased amount of cathepsin L activity when compared with the control (0.1% DMSO-treated cells).

Cell Invasion and Motility Studies

Next, Biocoat[®] Matrigel[®] invasion chambers were used to determine the inhibitory effect of compounds **2** and **22** over DU-145 cells according to the manufacturer's protocol. Increased activities of cathepsin L and B are observed in some cancers⁵⁹ with both enzymes participating in the enzymatic cascade leading to the basement membrane degradation which is characteristic of metastasis.⁶⁷

Also, it has been reported that cathepsins L and B play an important role in the invasive ability of the prostate cancer cell line DU-145.⁶²

In this context, seven of the most potent cathepsin L inhibitors were tested for invasion of DU 145 cells through Matrigel[®] using Biocoat[®] Matrigel[®] invasion chambers. Matrigel[®] can be used *in vitro* as a reconstituted basement membrane and is constituted of laminin, collagen IV, heparin sulfate, proteoglycans, entactin, and nidogen.⁶⁷

The number of invaded cells for each experimental sample represents the average of triplicate experiments. The percentage of invasion represents the number of cells that penetrated an 8 μ m pore filter coated with Matrigel[®] divided by the number of migrating cells. The number of migrating cells was determined by counting the number of cells that crossed an 8 μ m pore BD control insert. To represent the results, the endpoint values obtained for each inhibitor were used to calculate the percentage of invasion or motility relative to the negative control (0.1% DMSO), which is arbitrarily set at 100%.

As shown in Figure 60, exposure of DU 145 cells to the compounds **2** and **22** at a final concentration of 20 μ M decreased their invasiveness through Matrigel[®] in a comparable degree to the irreversible general cysteine protease inhibitor E-64 at the same concentration, whereas **32**, **33** and **37** had no significant effect. Compounds **55** and **38** showed modest anti-invasive effect.

Also, it can be concluded that the anti-invasive effect observed cannot be accounted for through alteration of cell viability as the tested inhibitors are not cytotoxic, as previously determined (Figure 63).

If the invasion assay results are compared with the IC₅₀ values for each inhibitor, an inverse relationship can be found. The lower the IC₅₀ value, the higher the inhibition of DU 145 cell invasiveness (Table 9).

Together, these results indicate that compounds **2**, **22**, **38** and **55** not only have a low IC₅₀ value, but also reduce the capacity of the human prostate carcinoma cell line DU-145 to invade across Matrigel[®]

Compounds that can modify the invasive phenotype have obvious potential as anti-metastatic drugs.

Although the inhibitory mechanism of these compounds in DU-145 cells is not clear yet and needs further studies, the obtained results indicate that the anti-invasive effect of the inhibitors is associated with the inhibition of enzymatic degradative processes of tumor invasion.

In addition, other extracellular matrix degrading enzymes, including cysteine proteases and serine proteases could be potential targets of these inhibitors and involved in the mechanisms for the inhibition of cell invasiveness and motility.

Motility is also an important step in tumor invasion. To determine if these inhibitors had an effect on cell motility, cellular chemotaxis of DU 145 cells toward the chemoattractant (media with 10% FBS) in the presence of the inhibitors was tested using 8µm pore BD control inserts that were not coated with Matrigel[®].

As shown in Figure 64, the treatment with compounds **2**, **32**, **33**, **37**, **38** and **55**, decreased the ability of prostate tumor DU-145 cells to cross the filters by almost 50 % compared to the control.

It also can be noticed that all the tested inhibitors decreased the percentage of cell motility in a higher degree compared to E-64.

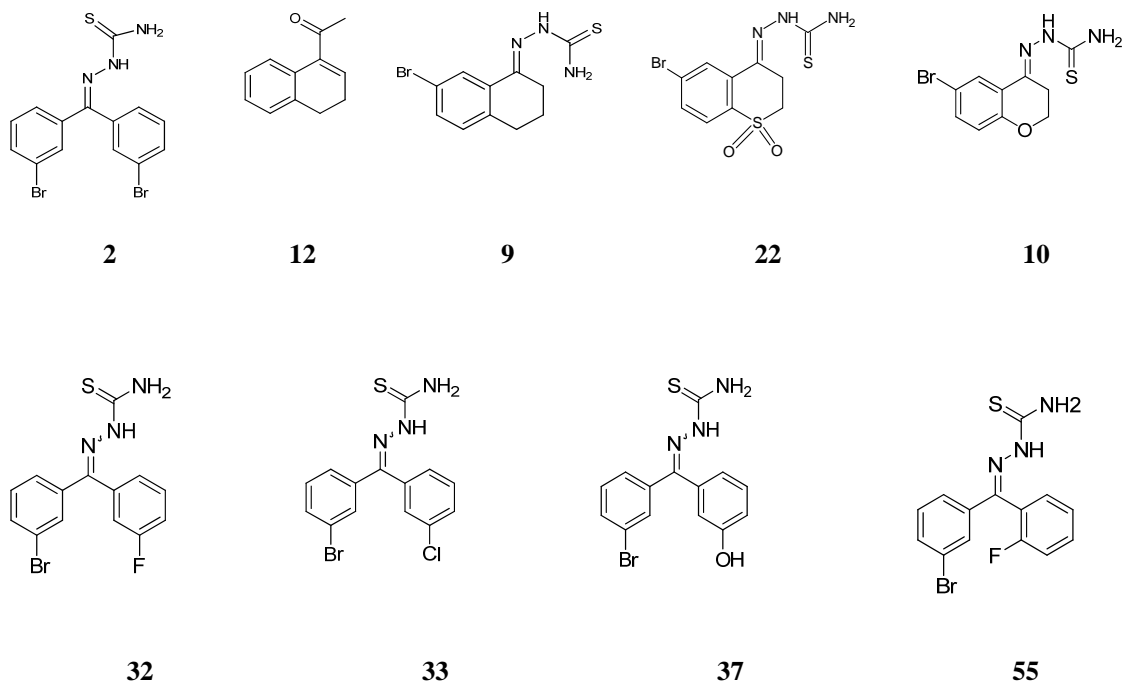


Figure 59. Cathepsin L inhibitors tested for cytotoxicity.

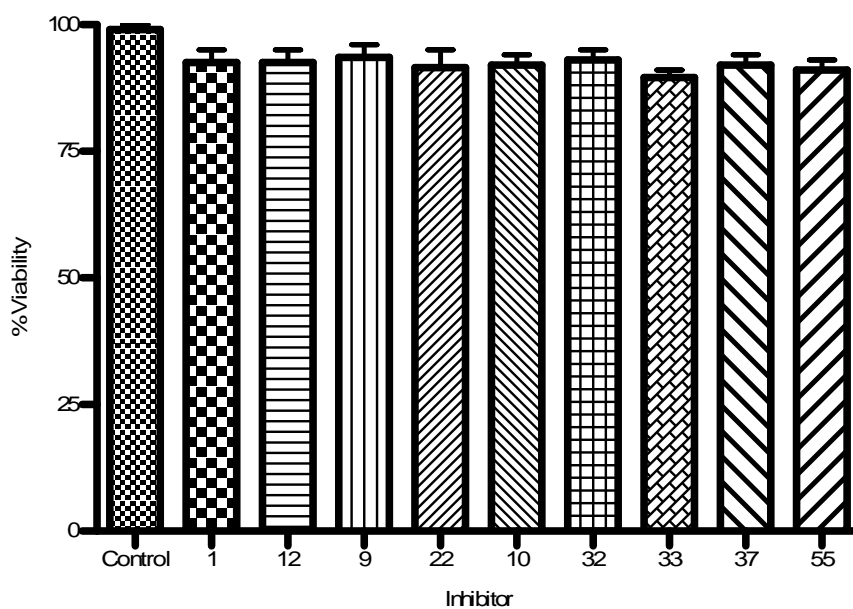


Figure 60. Cell viability expressed as percentage for ten of the best cathepsin L inhibitors using the trypan blue exclusion assay. DU-145 cells were treated with 0.1% DMSO (control) and 20 μ M inhibitor concentration for 24 hours. The endpoint values obtained for each inhibitor were used to calculate the percentage of cell viability or growth relative to the negative (DMSO) control, which was arbitrarily set at 100%.

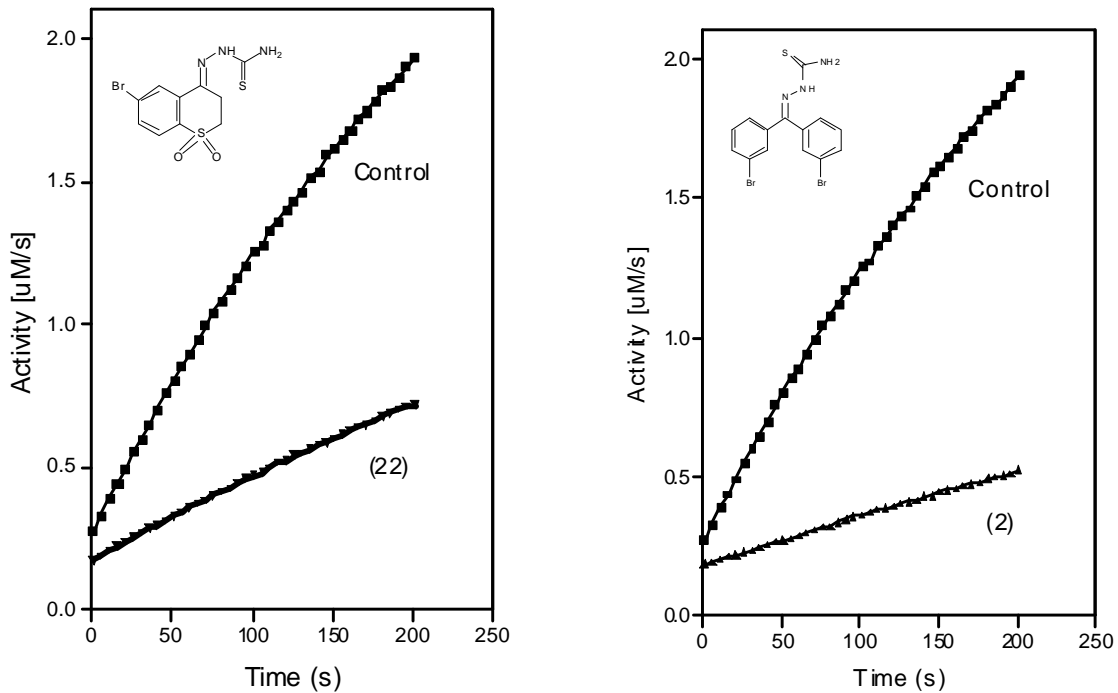


Figure 61. Inhibition of cathepsin L activity in DU-145 cell conditioned media by **2** and **22**.

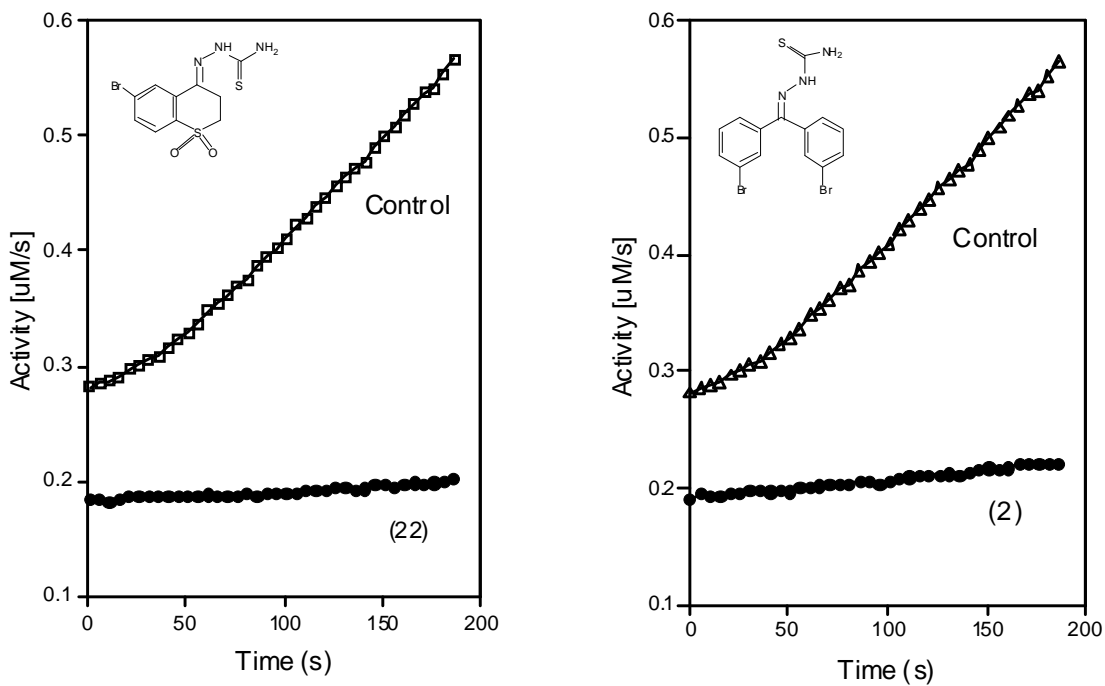
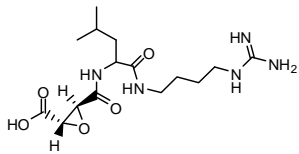
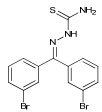
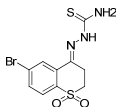
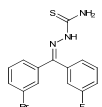
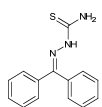
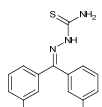
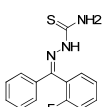
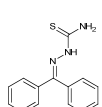
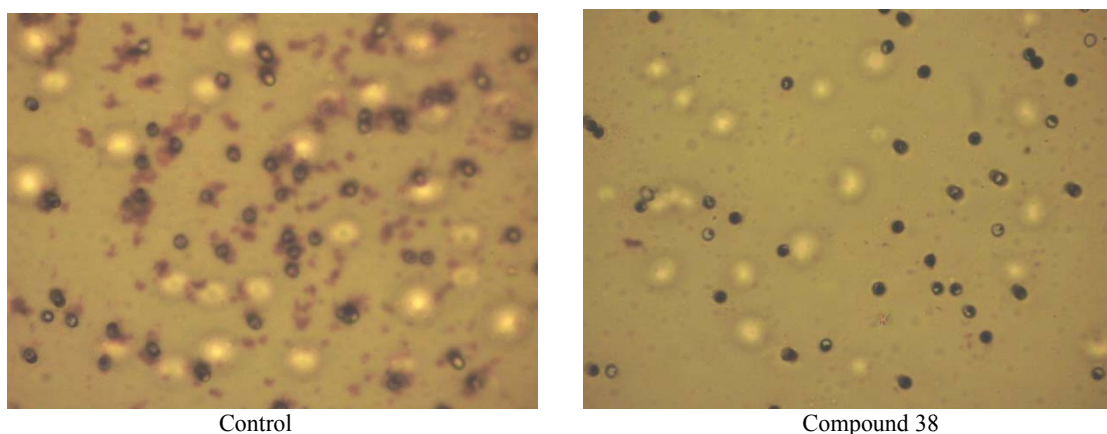


Figure 62. Inhibition of cathepsins L activity in DU-145 cell lysates by **2** and **22**.

Table 9. Comparison between IC₅₀ Values and % Cell Invasion and % Motility

Compound	Structure	IC ₅₀ [nM]	% Invasion	% Motility
E-64		15	45.3 ± 1.4	61.9 ± 4.9
2		1.5	47.1 ± 7.9	41.5 ± 7.1
22		1	46.0 ± 4.5	56.6 ± 11.8
32		66	70.5 ± 7.8	43.2 ± 1.13
33		997	86.0 ± 1.4	41.9 ± 1.6
37		140	78.0 ± 7.1	41.2 ± 7.9
55		44	61.5 ± 3.5	40.5 ± 3.5
38		60	53.0 ± 5.7	44.0 ± 1.4

A.



B.

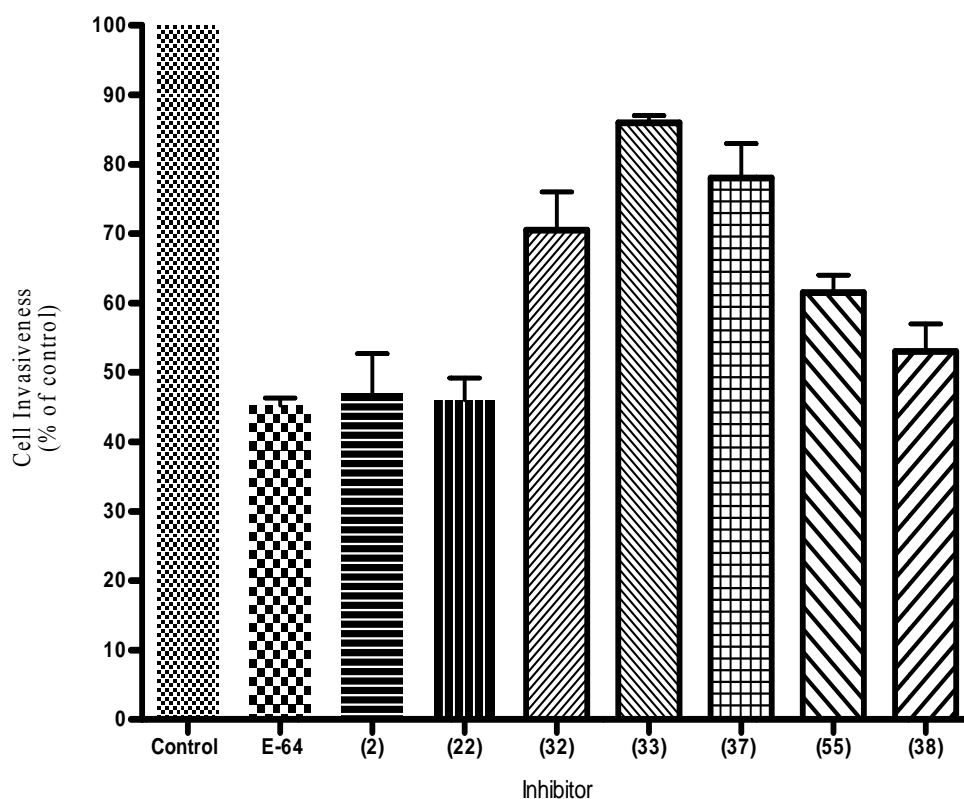


Figure 63. Invasiveness studies with DU-145 cells treated with seven of the most potent cathepsin L inhibitors and E64 at a final concentration of 20 μ M for 24 h. DU-145 cells were also treated with 0.1% DMSO (control). A. DU 145 cells that had invaded through Matrigel were stained with Diff Quick staining kit (cytoplasmic (pink) staining with nuclear (blue) staining) kit and counted. B. Invading cells were quantified and the control invasion of DU-145 was set as 100%. Data represent the mean \pm SD of at least three independent experiments. The standard deviation was calculated using the GraphPad Prism 4.03 software.

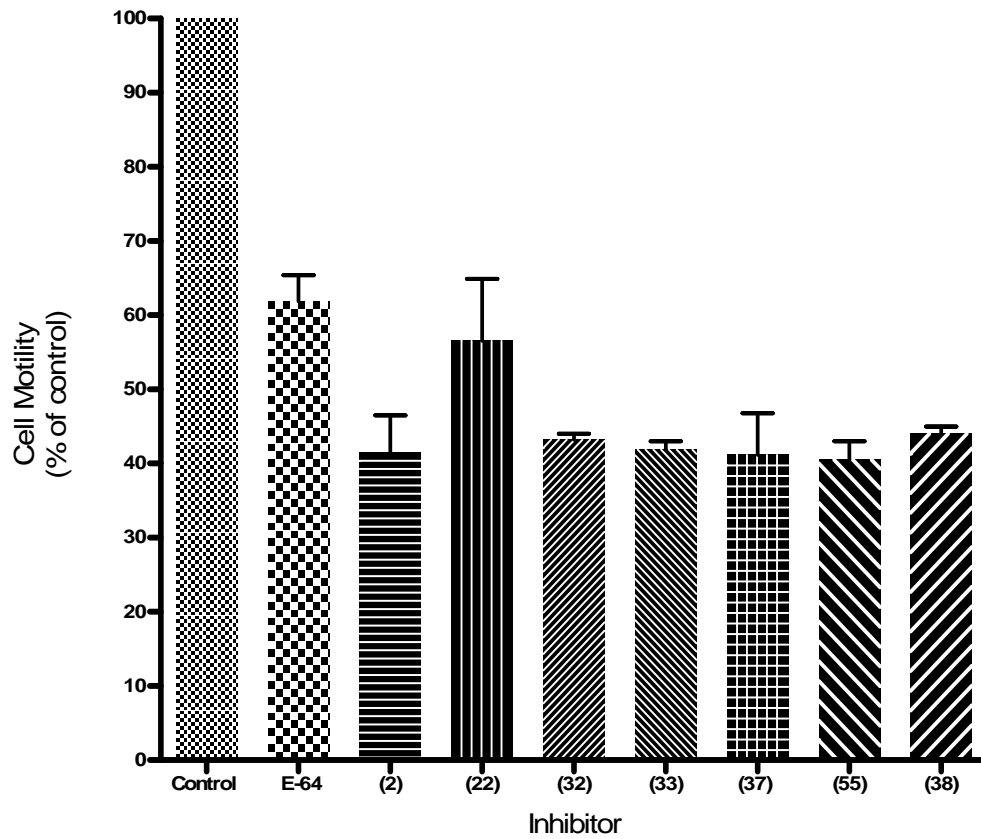


Figure 64. Motility assay results. DU-145 cells were treated with seven of the most potent cathepsin L inhibitors and E64 at a final concentration of 20 μ M for 24 h. DU-145 cells were also treated with 0.1% DMSO as a control. DU 145 cells were treated with different inhibitors in chambers with filters not coated with Matrigel for 24 h. Migration of DU-145 cells through the filters was measured as described in the invasion assay. Data represent the mean \pm SD of at least three independent experiments. The standard deviation was calculated using the GraphPad Prism 4.03 software.

Western Blot Analysis for Cathepsin L in DU 145 Cells

Cathepsins acquire mannose-6-phosphate (M6P) residues during their synthesis that target them to lysosomal vesicles via the M6P. However, in many cancer cells, these cysteine proteases escape from their processing pathways and they are either secreted or associate with the plasma membrane.^{67, 48, 129}

Secretion of latent proforms instead of the mature enzyme allows accumulation of cathepsins in the extracellular matrix at neutral pH without loss of activity.²⁹

Normal molecular weight of the proenzyme and mature forms of mammalian cathepsin L are 36 and 25 kDa, respectively. However, it has been reported that some cancer cell lines secrete latent cathepsins L precursors with a sizes of 42 and 70 kDa.¹³⁰

Most cathepsin-like proteases released by tumor cells have a higher molecular weight and unusual stability at neutral to alkaline pH, mainly due to their binding to the external cell surface proteins which increase their pH stability.⁷⁵ Since cathepsin L is implicated in tumor growth and invasion, it was of interest to investigate the prostate cancer cell line DU 145 for the secretion of cathepsin L.

The Western blot analysis of cathepsins L in DU 145 cell lysates and conditioned media is shown in Figure 65, and it can be noticed that three bands of 25, 37 and 50 kDa were detected in DU 145 cell lysates and a faint molecular weight form of 50 kDa was visible in DU 145 cell conditioned media samples, indicating the presence of high molecular weight forms of cathepsins L compared to the single band of 25 kDa that was detected for the commercially purified human liver cathepsin L (Figure 66).

It can be proposed that the 25 kDa form correspond to a single chain cathepsin L and the 37-50 kDa corresponds to pro-cathepsin L. The 37 kDa might display glycosylated single chain cathepsins L, which occurs as an intermediate form during procathepsin L processing.

However, incubation of pro-cathepsin L at acidic pH did not resulted in the activation of the precursors. These results demonstrate secretion of latent, non convertible, high molecular weight forms of cathepsins L indicating the presence of precursors or alternatively, complexed cathepsins L.

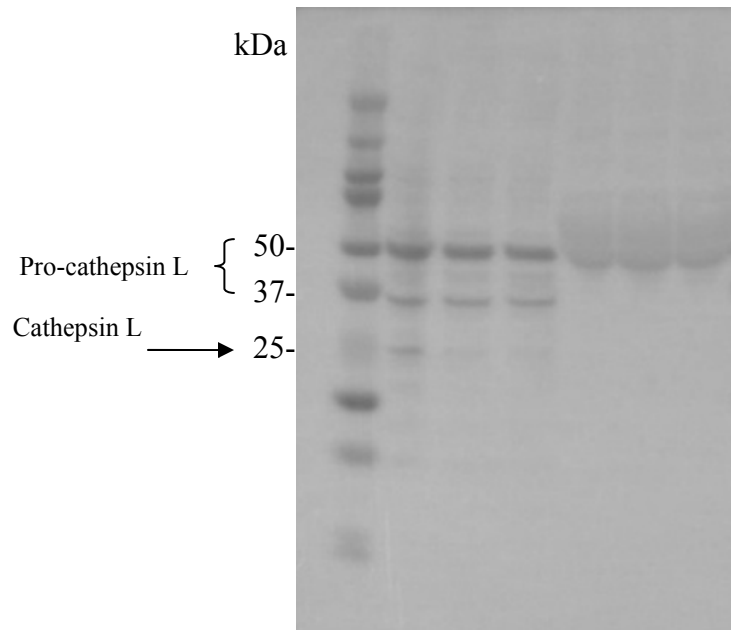


Figure 65. Immunodetection of cathepsin L in DU 145 cell lysates and cell conditioned media. Lane 1: standard; lanes 2, 3 and 4: Du 145 cell lysates; lanes 5, 6 and 7: DU 145 cell conditioned media.

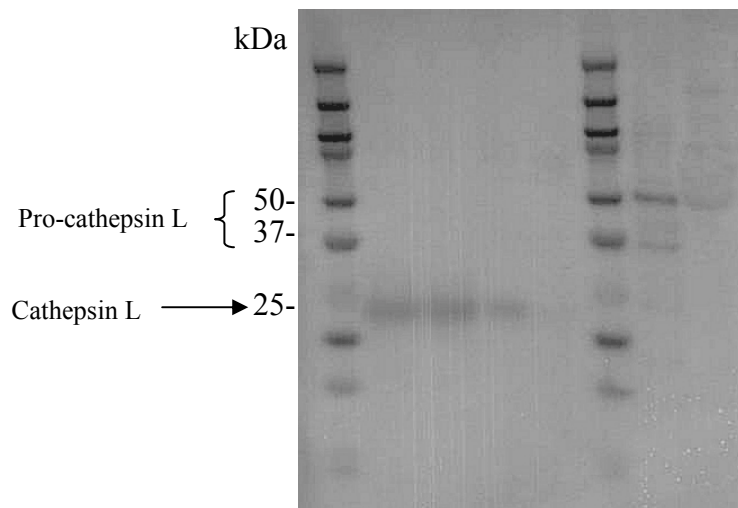


Figure 66. Immunodetection of cathepsin L in DU 145 cell lysates and cell conditioned media compared to commercial human liver cathepsin L. Each line had 10 μ g of sample loaded. Commercially purified human liver cathepsin L was used as reference. Lane 1: standard; lane 2: 36 ng purified human liver cathepsin L; lane 3: 18ng purified human liver cathepsin L; lane 4: 4ng purified human liver cathepsin L; lane 5: 1ng purified human liver cathepsin L; lane 6: standard; lane 7: DU145 cell lysate; lane 8: DU145 cell conditioned media.

The relationship of tumor proteases to the nonpathological forms is unclear. The question is whether tumor enzymes are incorrectly processed proenzymes or products of other genes.⁶⁹ In other series of experiments, when Microcon centrifugal filter devices and immunoprecipitation techniques were used with the same DU 145 cell lysates and cell conditioned media samples in order to concentrate the samples and improve the visibility of the bands, only one band of 50 kDa remained instead of the triple bands for the cell lysates, while faint bands were visible in the cell conditioned media sample (Figure 67).

More studies are necessary to validate the relevance of these observations and to improve the detection of secreted cathepsin L in cell conditioned media. Western blot detection of cathepsins L in cell conditioned media is not that simple because the target protein is present at a very low concentration and all other proteins are potential contaminants.

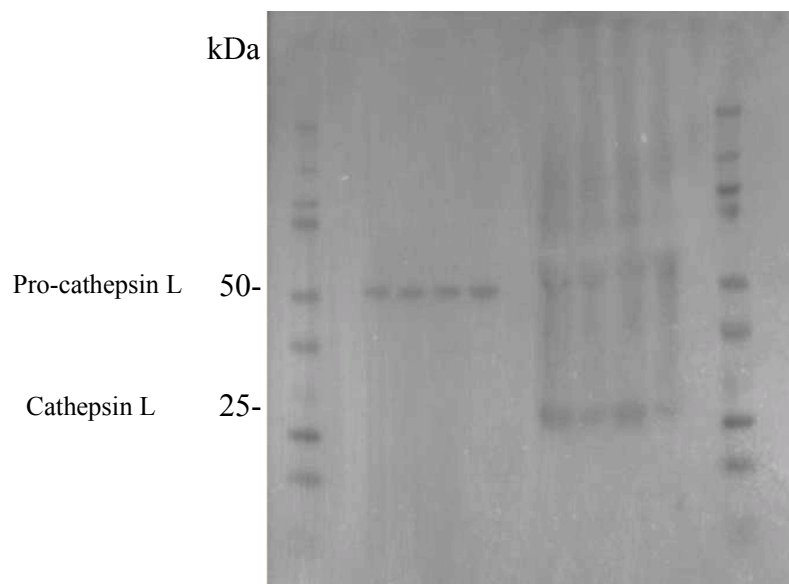


Figure 67. Immunodetection of cathepsin L in concentrated DU 145 cell lysates and cell conditioned media. Lane 1: standard; lanes 3, 4, 5 and 6: cell lysate samples; lanes 8, 9, 10, and 11: cell conditioned media samples; lane 13: standard.

CHAPTER FIVE

Experimental Procedure for the Recombinant Cruzain Purification and Evaluation of Potential Inhibitors of Cruzain for the Treatment of Chagas Disease

General Section for Chemical Sources and Materials

Ampicillin (Amp) and yeast extract were purchased from Research Organics. Tryptone was obtained from MO Bio Laboratories. Agar, glucose, and IPTG (Isopropyl β -D-1-thiogalactopyranoside) were purchased from OmniPur. Lysozyme, DNase (RNase free) and urea were purchased from Sigma. PMSF (phenylmethylsulphonyl fluoride) was purchased from G Biosciences. A Sepharose Q Fast Flow anion exchange column was purchased from Amersham Biosciences. The pre-stained protein molecular mass standard ranging from 10-250 kDa (Precision Plus; Kaleidoscope) and an anion-exchange column standardization kit were purchased from Bio-Rad Laboratories. Bradford reagent, bovine serum albumin standard, the substrate benzyloxycarbonyl-L-phenylalaninyl-L-argininyl-7-amido-4-methylcoumarin (Z-FR-AMC), and the standard 7-amino-4-methylcoumarin were purchased from Sigma. Other chemicals were obtained from commercial companies such as Acros Chemicals, Alfa Aesar, EMD Biosciences and Fisher Scientific. Petri dishes, a bunsen burner and an inoculation loop were purchased from VWR. A shaker incubator was purchased from Lab Line. Precast 4-12% (w/v) bis-tris gels, electrophoresis reagents and the mini-gel electrophoresis apparatus (X Cell Sure Lock™) were purchased from Invitrogen. Centricon YM-10 filter devices were purchased from Millipore. The microcentrifuge 5415R and micropipettors were purchased from Eppendorf.

The UV/VIS spectrophotometer DU 520 was purchased from Beckman. The centrifuge Sorvall RC 5B Plus and rotor SA-600 were purchased from Sorvall. The conductivity meter DUO-60 was purchased from Check-Mite. Cryogenic vials and Oakridge centrifuge tubes were purchased from Nalgene. The Sonicator 3000 was purchased from Misonix. The FluoroMax-2 fluorimeter was purchased from Horriba Jobin-Yvon Inc. UV micro quartz cuvettes and fluorescence micro quartz cuvettes were purchased from Starna Cells, Inc. and were subsequently cleaned with water and dried with a jet of compressed nitrogen gas before and after use. A heated plate stirrer was purchased from Corning. The centriprep centrifugal filter devices were purchased from Millipore. The fraction collector FC 203B was purchased from Gilson Inc. The peristaltic pump and the gradient maker were purchased from Amersham. The ultra Lum Discovery 12 imager and ultra Quant 6.0 gel imager were purchased from ultra Lum Inc. Laboratory grade ethylene glycol from Fisher Scientific was used to maintain constant temperature of the water baths. Water is always referred to the ultra pure distilled water obtained from the Barnstead Diamond™ purifier and has a resistance of 18 MΩ. All buffers were filtered through a Corning 0.22-0.45 micron vacuum filter (cellulose acetate or nylon) purchased from Millipore.

Preparation of buffers and other solutions

Preparation of Luria broth (LB) medium. 1.0 L of this solution was prepared by dissolving tryptone (10 g), yeast extract (5.0 g), and NaCl (10 g) in water adjusting the pH to 7.4 before the solution was autoclaved.

Preparation of LB amp medium. 500 mL of autoclaved LB medium was supplemented with ampicillin to a final concentration of 100 µg/ml.

Preparation of 2xYT (2 x yeast and tryptone) medium. 300 mL of this solution was prepared by dissolving tryptone (4.8 g), yeast extract (3.0 g) and NaCl (1.5 g) in water and adjusting the pH to 7.4 before the solution was autoclaved.

Preparation of 2xYT amp medium. 300 mL of autoclaved 2xYT medium was supplemented with ampicillin to a final concentration of 100 µg/ml.

Preparation of agar medium. Agar powder (75 g) was dissolved in 100 mL LB media, autoclaved and cooled to 55 °C before pouring the solution into petri dishes to cover the bottom of the dish. After the plate of agar was solidified, the dishes were inverted and allowed to dry for 24 hours at room temperature before use.

Preparation of buffer A 10X stock solution at pH 7.6, 8 or 10. Buffer A consisting of 50 mM Tris HCl, 1 mM EDTA and 50 mM NaCl was prepared by dissolving EDTA (3.72 g), NaCl (29.22 g) and Tris HCl (78.79 g) in 200 mL of water and then adjusting pH to 7.6, 8.0 or 10.0 with 1 M NaOH dropwise while stirring and taking pH readings on a Corning pH meter which had previously been calibrated with calibration buffers. Finally, each solution's volume was adjusted to 1.0 L.

Preparation of sodium acetate buffer, 400 mM, pH 5.5, 0.1% Brij 35. 1.0 L of this buffer was prepared by dissolving (27.9 g) sodium acetate in 500 mL 0.1% Brij 35 solution, adding 3.7 mL acetic acid, and adjusting the pH to 5.5. The total volume was adjusted to 1.0 L with additional 0.1% Brij 35 solution.

Preparation of assay/activation buffer. 1.0 mL DTT (120 mM) and 5.0 mL sodium acetate buffer (400 mM, pH 5.5, 0.1% Brij 35) were mixed together in a 13×100 mm glass.

Preparation of a baseline solution. The following reagents were pipetted into a fluorescence quartz cuvette and mixed well with gentle pipetting: 50 μ L assay/activation buffer, 20 μ L DMSO (7%) and 130 μ L water. Fluorescence readings were then taken for five minutes every five seconds at an excitation wavelength of 355 nm and emission wavelength of 460 nm in a FluoroMax- 2 fluorometer.

Preparation of stock solution of 7-amino-4-methylcoumarin (AMC). A 12.27 mM stock AMC solution was prepared by dissolving AMC 2.15 mg in 1.0 mL DMSO.

Preparation of stock solution of benzyloxycarbonyl-L-phenylalaninyl-L-argininyl-7-amido-4-methylcoumarin (Z-FR-AMC). Z-FR-AMC stock solution (10 mM) was prepared by dissolving 6.49 mg of Z-FR-AMC in 1 mL DMSO.

Preparation of 20 μ M solution of benzyloxycarbonyl-L-phenylalaninyl-L-Argininyl-7-amido-4-methylcoumarin (Z-FR-AMC). 2.0 mL of 20 μ M Z-FR-AMC was prepared by diluting 4 μ L Z-FR-AMC stock solution (10 mM) with 1996 μ L of 0.1% Brij- 35 solution.

Preparation of inhibitor dilutions. The 28 synthetic inhibitors evaluated in this study were obtained from collaboration with the Pinney Research group at Baylor University. The inhibitors were weighted using a Mettler Toledo AX microbalance with an accuracy of 0.01 mg.

The compounds were then dissolved in pure DMSO (99.9%) giving 20 mM stock solutions followed by serial dilutions giving final inhibitor concentrations of 20 μ M to 1 nM in a total volume of 500 μ l (as shown in Table 10).

Table 10. Inhibitor Serial Dilution Preparation.

Final Concentration in the assay μ M	7% DMSO μ M	Stock	DMSO μ l	Water μ l
2.0 E+01	4.0 E+02	10.0 μ l 2.0 E+03 μ M Stock	25.0	465
1.0 E+01	2.0 E+02	5.0 μ l 2.0 E+03 μ M Stock	30.0	465
7.0 E+00	1.4 E+02	3.5 μ l 2.0 E+03 μ M Stock	31.5	465
5.0 E+00	1.0 E+02	2.5 μ l 2.0 E+03 μ M Stock	32.5	465
4.0 E+00	8.0 E+01	2.0 μ l 2.0 E+03 μ M Stock	33.0	465
2.0 E+00	4.0 E+01	1.0 μ l 2.0 E+03 μ M Stock	34.0	465
1.0 E+00	2.0 E+01	0.5 μ l 2.0 E+03 μ M Stock	34.5	465
5.0 E-01	1.0 E+01	50 μ l 5.0 E+00 μ M Stock	32.0	418
1.0 E-01	2.0 E+00	50 μ l 1.0 E+00 μ M Stock	32.0	418
5.0 E-02	1.0 E+00	50 μ l 5.0 E-01 μ M Stock	32.0	418
1.0 E-02	2.0 E-01	50 μ l 1.0 E-01 μ M Stock	32.0	418
5.0 E-03	1.0 E-01	50 μ l 5.0 E-02 μ M Stock	32.0	418
1.0 E-03	2.0 E-02	50 μ l 1.0 E-02 μ M Stock	32.0	418

Recombinant Cruzain Purification Procedure

The main objective of this purification was to obtain electrophoretically pure recombinant cruzain visualized by a single band observed in SDS-PAGE. The purification protocol was generously provided by Dr. James McKerrow and Mrs. Elizabeth Hansell from the University of California at San Francisco and is described in this section.¹³¹ Briefly, a culture of *E. coli* bacteria (strain DH5 α) containing the expression plasmid CheY15LOX, was grown overnight at 37 °C, diluted 10-fold into LB medium containing ampicillin (100 μ g/ml), and incubated at 37 °C for 1 h before adding IPTG (1 mM) to induce the cells followed by shaking incubation for 8 hours at 37 °C.

Next, cells were lysed by sonication, insoluble proteins were solubilized with urea (8M) and the fusion protein refolded. The proteins were then fractionated by ion exchange chromatography on a Sepharose Q Fast Flow column using a 0-1.0 M gradient of NaCl.

The purified fusion protein was made to 100 mM Na Acetate pH 5.5 (using a 10x stock buffer), 0.9 M NaCl, 5 mM DTT, 10 mM EDTA and incubated at 37 °C for 4 to 72 hours until the solution cleared and the protein present was determined to be 27 kDa in size by gel electrophoresis.

Protein Expression

A glycerol stock of *E. coli* bacteria (strain DH5 α) previously transformed with the expression plasmid CheY15LOX in Dr. Trawick's laboratory was used to grow the clone used for cruzain purification. First, the transformed *E. coli* bacteria (strain DH5 α) were streaked on agar plates to obtain isolated colonies and incubated overnight at 37 °C. Then, a single colony was transferred into a sterile test tube containing 3 ml LB, 3 μ l of ampicillin (100 μ g/ml) and 100 μ l glucose (50%), and incubated for 8 hours at 37 °C in a shaker incubator.

Next, this solution was transferred to 300 mL of 2xYT amp solution and incubated overnight at 37 °C in a shaker incubator. Following incubation, the cells were rinsed by centrifugation in Oakridge centrifuge tubes at 2000 rcf for 15 minutes, the pellet re-suspend in 12 mL LB and then diluted into 1.0 Liter LB amp media. After 1 hour (or A₆₀₀ of 0.5), the cells were induced with 1 mM IPTG (from 1 M stock) for 8 hours and then pelleted at 3000-5000 rcf for 10 minutes in a GS-3 rotor.

Cell Lysis and Isolation of Inclusion Bodies

The cell pellet isolated from the protein previously explain was re-suspended in 25 ml of 1X Buffer A (pH 8) with 100 μ M PMSF and 25 ml of 1X Buffer A (pH 8) containing 100 μ M PMSF, 2% TX-100, lysozyme (0.4 mg/ml), and DNase (200 units/ml) and was placed on ice for 30-60 minutes with occasional mixing. The cells were, then lysed by sonication (sapphire tipped horn at a power setting of 1 for approximately 5 minutes at 4°C to release the inclusion bodies, which were then pelleted by centrifugation at 5000 rcf for 20 minutes, re-suspended in 25 ml of buffer A (pH 8) supplemented with 100 μ M PMSF and TX-100 at a final concentration of 1%. The solution was then re-spon three times at 5000 rcf for 10 minutes to remove completely the lysozyme and DNase.

Protein Refolding

The obtained inclusion body pellet was re-suspended in a solution containing 30 mL of urea (8 M), 5 ml 10X buffer A (pH 8) and 15 mL of water. The solution was stirred for 4 hours on ice and centrifuged in Oakridge centrifuge tubes at 8000 rcf for 15 minutes to remove any insoluble material. Next, the supernatant was slowly added to 10 volumes (300 ml) of buffer A (pH 10.7) and was stirred at 25 °C for 1 hour. Subsequently the pH was dropped to 8.0 with 1N HCl and the supernatant was allowed to continue to stir for 1 hour at 25°C.

Cruzain Purification and Analysis of Column Fractions

Then, the supernatant was filtered twice, first through a 0.45 micron cellulose acetate filter and then through a 0.2 micron cellulose acetate filter and it was loaded slowly (2.0 ml/min) onto the equilibrated and standardized Sepharose Q Fast Flow column.

The column was washed with 100 mL of buffer A (pH 7.6) and, the fraction collector (with an 80 tube rack) and the gradient maker were initiated to capture the elution of bound proteins with 300 mL of a 1 M NaCl gradient ranging from 0 to 100 % as shown in Figure 68.

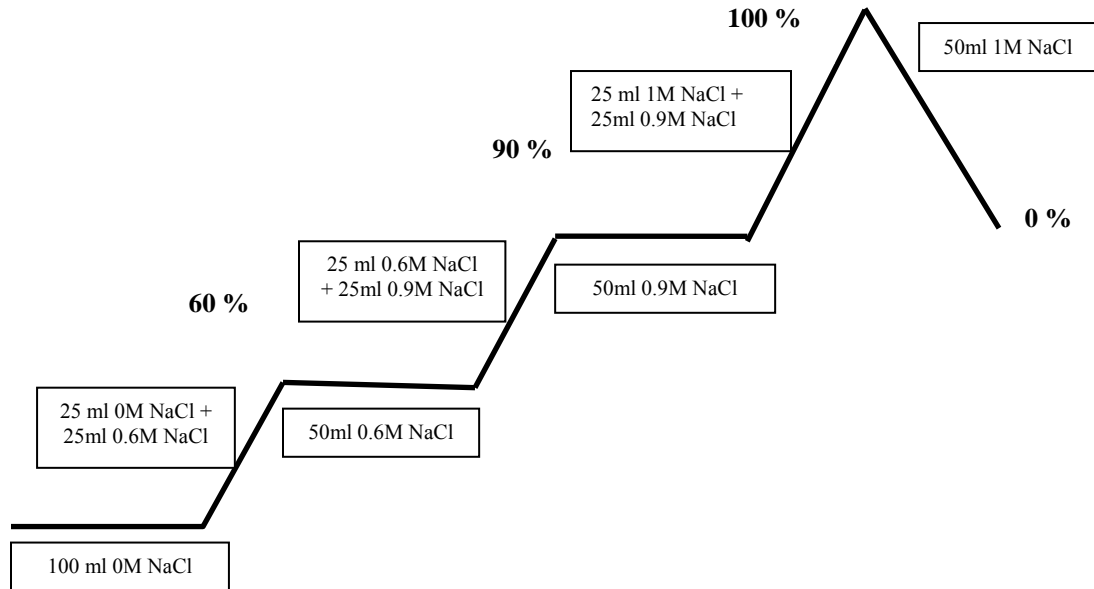


Figure 68. Elution gradient used for cruzain purification

Finally, the column was cleaned by reversing the phase, washing for 15 minutes in 2 M NaCl (75 mL), water (375 mL) and 0.5 M NaOH for 1-2 hours followed by equilibration in water and 20% ethanol for storage.

Analysis of column fractions

Approximately 70 fractions of 6 mL/tube were collected at 1 min/tube; these fractions were kept on ice while measuring protein concentration (UV-VIS, Bradford), and activity.

Activity Determination

Since cruzain hydrolyzes peptide bonds, a fluorogenic synthetic substrate, benzyloxycarbonyl-L-phenylalaninyl-L-argininyl-7-amido-4-methylcoumarin (Z-FR-AMC), was utilized to monitor its activity. Cruzain cleaves the amide bond between Arg and AMC and produces a non-fluorescent Z-FR peptide and a fluorescent AMC molecule in a similar reaction to the one catalyzed by cathepsin L.

A sample of 25 μL of each column fraction was incubated in 75 μL of an assay/activation buffer (100 mM sodium acetate, pH 5.5, 10 mM DTT) at 25°C for 5 minutes before adding 100 μL of substrate (Z-FR-AMC) at a concentration of 20 μM to initiate the reaction. Excitation and emission wavelength, were 355 nm and 460 nm, respectively. Velocity of enzyme reaction was measured as the rate of release of 7-amino-4-methylcoumarin (AMC) per unit time.

The amount of AMC released by the reaction of cruzain on Z-FR-AMC was used to define the activity of the enzyme; one unit of cruzain is defined as the amount of enzyme that hydrolyzes one micromole of Z-FR-AMC per minute at 25°C at pH 5.5.

Total Protein Concentration

Total protein concentration was determined by using the Bradford assay. Bradford reagent is Brilliant Blue G dye that shifts its absorption from 465 to 595 nm when bound to proteins where the absorption at 595nm is proportional to the concentration of protein.¹³²

A BSA standard curve was prepared with the following concentrations: 0.1 mg/mL (2.5 μL stock BSA + 47.5 μL buffer), 0.5 mg/mL (12.5 μL stock BSA + 37.5 μL buffer), 1mg/mL (25 μL stock BSA + 25 μL buffer).

A solution of 50 μL of fraction, blank (buffer alone), or standard were each incubated 1.5 mL with Bradford reagent at 25°C for 15 minutes before the visible absorption was measured at 595 nm in polyacrylamide disposable cuvettes.

Samples were diluted to the appropriate concentration when needed. To analyze the results: a calibration curve was obtained by graphing absorption vs. concentration of the standard to create a linear equation; the values of sample absorption were introduced in the calibration equation where the concentration of each fraction was determined mathematically.

SDS-PAGE

Fractions of interest were TCA precipitated and separated on 4-12% (w/v) bis-tris reducing SDS-PAGE gel electrophoresis following a protocol described by Invitrogen. Expected bands associated with cruzain delta C are around 60 kDa, 45 kDa and 27 kDa. Briefly, 1 volume of cold TCA (50%) was added to 4 volumes of protein sample in a microcentrifuge tube and incubated for 10 minutes at 4°C.

The mixture was then centrifuged at 14000 rpm for 5 minutes and the supernatant removed, leaving the protein pellet intact, which was washed twice with 200 μL of cold acetone twice. Finally, the pellet was dried by placing the microcentrifuge tube in a 95°C heat block for 5-10 minutes to evaporate the acetone.¹³³

A mixture of 10 μg of sample, 2.5 μL of NuPAGE® LDS sample buffer (4x), 1 μL of NuPAGE® reducing agent (10x) and 6.5 μL of ultrapure water were combined giving a total volume of 10 μL .

This mixture was then centrifuged for 1 minute at 4 °C, heated at 95 °C for 10 minutes and loaded on to a 4-12% (w/v) bis-tris precasted mini-gel.

The multi-colored protein mixture (Kaleidoscope) ranging from 10 to 250 kDa was used as a standard. The upper and lower buffer chambers of the electrophoretic tank were filled with 200 mL (containing 500 μ L of NuPAGE®antioxidant) and 600 ml of 1x NuPAGE® LDS running buffer. The gel was run at 200V constant for 35 minutes.

The gels were stained using the SimplyBlue™ SafeStain microwave protocol for staining NuPAGE gels. The gel was placed in 100 ml of ultrapure water and microwaved on high (950-1100 watts) for 1 minute. After shaking the gel on an orbital shaker, the water was discarded and the process repeated twice. Then, SimplyBlue™ SafeStain (30.0 ml) was added and the gels were microwaved on high for 1 minute, shaken on an orbital shaker for 10 minutes, washed in 100 ml ultrapure water for 10 minutes, and then shaken again in 20 ml of 20% NaCl for 10 minutes. Finally, the protein bands were visualized using the ultra Quant 6.0 gel imager.

Activation of rCruzain

The pooled active fractions were made to 100 mM Na Acetate (pH 5.5) (using a 10x stock buffer), 0.9 M NaCl, 5 mM DTT, 10 mM EDTA and incubated at 37 °C with occasional mixing.

Initially the solution became cloudy and the protein precipitated and incubation was continued for 28 hours until the solution cleared and the protein was all at the 27 kDa size by gel electrophoresis (monitored every 2-4 hours of incubation).

Finally, the purified cruzain was concentrated using Centricon YM-10 filter devices and stored in 100 μ L aliquots at -70 °C. At this point, the enzyme is ready to be used in cruzain inhibition assays for inhibitor screening.

K_M and V_{max} Determination of Cruzain

In order to determine the kinetic parameters K_M and V_{max} , solutions of various concentrations of substrate (Z-FR-AMC) ranging from 0.3 μM to 150 μM were prepared by serial dilutions of 10 mM and 0.6 mM substrate (Z-FR-AMC) stock solutions as indicated in Table 11 and Table 12.

Activation buffer (50 μL), water (36.7 μL) and cruzain (100 μL) were mixed in fluorescence quartz cuvettes and incubated at 25°C for 5 minutes followed by addition of substrate (Z-FR-AMC) (13.3 μL) to initiate the reaction.

Fluorescence intensity readings for each assay were taken at 10 second intervals for 15 minutes at 25 °C. A trend line was fit to each data set and the slope of each trend line was derived as the velocity of each assay. K_M and V_{max} were derived by fitting the data to the Michaelis-Menten equation using the non-linear regression function with GraphPad Prism software version 4.03.

Table 11. Preparation Table for 10 mM and 0.6 mM Z-FR-AMC Stock Solutions.

Solution Number	Z-FR-AMC Final concentrations in DMSO [μM]	Volume of [μL]	Z-FR-AMC Stock [mM]	Water [μL]
1	3000.0	300.0	10.0	700.0
2	2250.0	225.0	10.0	775.0
3	1500.0	150.0	10.0	850.0
4	600.0	60.0	10.0	940.0
5	300.0	30.0	10.0	970.0
6	250.0	25.0	10.0	975.0
7	200.0	20.0	10.0	980.0
8	100.0	10.0	10.0	990.0
9	30.0	50.0	0.6	950.0
10	16.0	26.7	0.6	973.3
11	6.0	10.0	0.6	990.0

Table is taken directly from Chen 2008 with some modifications.³⁰

Table 12. Preparation Table for Substrate (Z-FR-AMC) Solutions in 7% DMSO.

Solution Number	Z-FR-AMC Concentration [μM]	Volume (μL)	Dilute from Z-FR-AMC [μM]	Volume of Water (μL)	Final Concentration in Assay
1	150.0	50	3000.0	950	10.00 μM
2	112.5	50	2250.0	950	7.50 μM
3	75.0	50	1500.0	950	5.00 μM
4	30.0	50	600.0	950	2.00 μM
5	15.0	50	300.0	950	1.00 μM
6	12.5	50	250.0	950	833.33 nM
7	10.0	50	200.0	950	666.67 nM
8	5.0	50	100.0	950	333.33 nM
9	1.5	50	30.0	950	100.00 nM
10	0.8	50	16.0	950	53.33 nM
11	0.3	50	6.0	950	20.00 nM

Table is taken directly from Chen 2008 with some modifications.³⁰

IC₅₀ Determination of Potential Cruzain Inhibitors

Out of the sixty compounds evaluated against cathepsin L, twenty five of them were evaluated for Cruzain inhibitory activity. The effect of a single inhibitor concentration (20 μM) on cruzain inhibition was first investigated for each compound and no further analysis was done on compounds that did not inhibit cruzain at this concentration.

For those that did inhibit cruzain, at least eight serial dilutions (ranging from 20 μM to 1 nM) were incubated separately with assay/activation buffer, water, and cruzain in fluorescence quartz cuvettes as described in Table 13 for 5 minutes at 25°C prior the initiation of the reaction with the addition of substrate Z-FR-AMC.

The reaction mixtures were then monitored for 10 minutes at excitation and emission wavelengths of 355 and 460 nm, respectively. The final condition for this assay was 100 mM sodium acetate buffer (pH 5.5), 5 mM DTT and 0.1% Brij 35.

The baseline control for each assay used the same conditions without the inhibitor. IC₅₀ values were determined by performing non-linear regression analysis fitting velocities and the logarithm of inhibitor concentrations to a sigmoidal dose response model using GraphPad Prism software version 4.03.

Table 13. Preparation Table for IC₅₀ Determination Experiment

Item	Volume (μL)
Assay/Activation Buffer	50.0
Water	33.3
Inhibitor/20% DMSO	3.3
Cruzain (0.5 nM)	100
Substrate (Z-FR-AMC) (150 μM)	13.3

CHAPTER SIX

Results and Discussion for the Recombinant Cruzain Purification and Evaluation of Potential Inhibitors of Cruzain for the Treatment of Chagas Disease

Recombinant Cruzain Purification

Genomic DNA from epimastigotes of *T. cruzi* was generously provided by Dr. James McKerrow from University of California at San Francisco in San Francisco, CA. Cruzain, the major cysteine protease of *Trypanosoma cruzi*, was initially expressed in *Escherichia coli* bacteria as an insoluble fusion polypeptide with the first 40 amino acids of the *E. coli* protein, CheY.

Then, it was isolated from the bacterial lysate, refolded, purified and recovered from the fusion peptide by incubation in sodium acetate activation buffer (pH 5.5) for 28 hours at 37 °C. This incubation period activated the proteolytic processing events that removed the CheY fusion, the prodomain, and the COOH-terminal domain of the cruzain.⁸⁹

Since it has been reported that the pI of activated cruzain is 3.5, inactivated cruzain was purified using an anion exchange chromatography column (Q Sepharose Fast Flow) at pH 7.6, with a 1 M NaCl elution gradient.

In order to test the column efficiency, 2 mL of a mixture of commercial standard proteins with known pI's (equine myoglobin (pI 6.9), conalbumin (pI 4.9), chicken ovalbumin (pI 4.6) and soybean trypsin inhibitor (pI 4.5) were run on the equilibrated Q Sepharose Fast Flow column.

The protein with the highest pI, the equine myoglobin, eluted first at fraction 25, the next protein, conalbumin, with a pI of 4.9 eluted at fraction 36 and finally, the last two proteins, chicken ovalbumin and soybean trypsin inhibitor, both eluted at about the same time as their pI, 4.6, and 4.5, are similar (Figure 69).

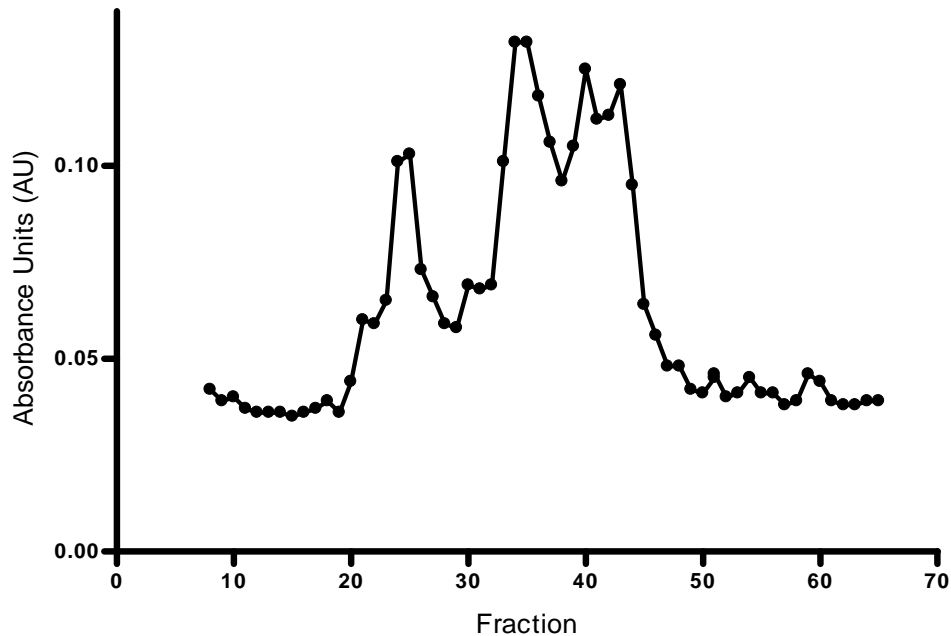


Figure 69. Elution profile of four proteins from a Bio-Rad column standard kit containing equine myoglobin (pI 6.9), conalbumin (pI 4.9), chicken ovalbumin (pI 4.6) and soybean trypsin inhibitor (pI 4.5).

This standardization process demonstrated the Q Sepharose Fast Flow column was set up and packed effectively as the protein elution predicted was obtained experimentally.

Cruzain Purification and Analysis of Column Fractions

The proteins contained in the supernatant from the previous cruzain purification step were fractionated by ion exchange chromatography on a 2.5 x 30 cm Sepharose Q Fast Flow column using a 0-1 M gradient of NaCl.

See Appendix B for detailed characteristics of this column. In order to be able to use this column, the matrix was previously activated with 1 CV of buffer A (pH 7.6) containing 1M NaCl at maximum flow rate, equilibrated overnight with 10 CV of buffer A (pH 8) at a flow rate of 1mL/min collecting fractions of 8 mL/tube to monitor conductivity and pH.

Then, a sample containing the cruzain fusion peptide was loaded on to the column and the resulting elution profile and the quantitative assays of this chromatography run are shown in Figure 70. It can be observed that the eluting of the peak was greater than 1.5 absorbance unit (AU) under elution conditions during the 60-90% ramp and it occurred at the same fraction as the main Bradford peak. Also, when the activity was measured directly from 25 ul of each column fraction during the wash, four peaks of activity were initially detected at 225 through 288 mL and at 360 mL during the wash.

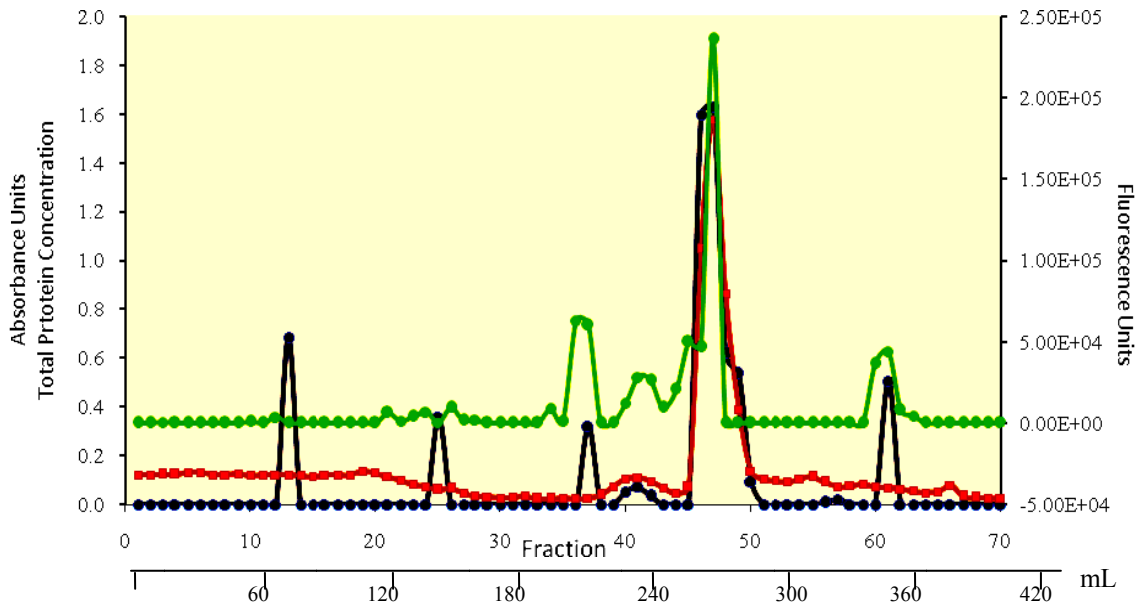


Figure 70. Elution profile of sample run in Q Sepharose Fast Flow column with buffer A (pH 7.6). --■--absorption of the sample at 280 nm,---●--- activity, --●--- total protein concentration determined by Bradford.

Next, the active fractions were pooled together with 100 mM sodium acetate buffer (pH 5.5) containing 0.9 M NaCl, 5 mM DTT and 10 mM EDTA and incubated at 37 °C resulting in auto-proteolysis and subsequent increase in activity that was monitored by the release of the fluorogenic AMC from the peptide substrate Z-FR-AMC.

Initially the solution became cloudy as the protein precipitated, but after 20 hours the maximal activity was attained and incubation was continued for a total of 28 hours until the solution cleared (Figure 71). This purified material was then concentrated with a Centriprep centrifugal filter device to 1.11 μ M and 3.7 μ M final concentrations and stored at -70 °C to be used for inhibitor screening procedures.

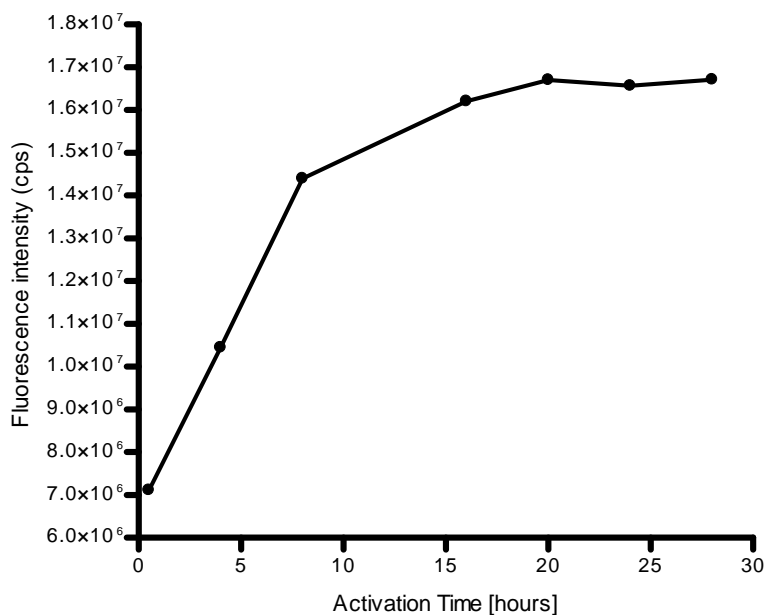


Figure 71. Cruzain auto-activation monitoring profile

The purity of these two batches of concentrated cruzain was determined using polyacrylamide gel electrophoresis. As shown in Figure 72, the samples exhibited a single band with an approximate molecular weight of 25 kDa in good agreement with the already reported 27 kDa.⁸⁹

The estimated yield of the fusion protein produced in DH5α *E. coli* cells is 24 mg/liter of bacterial culture (6.9 g wet weight of cell pellet.) After refolding, purification and activation, the final concentration of two solutions of mature cruzain was determined to be 3.7 μM and 1.1 μM, respectively. The final cruzain yield was determined to be 3.3 mg.

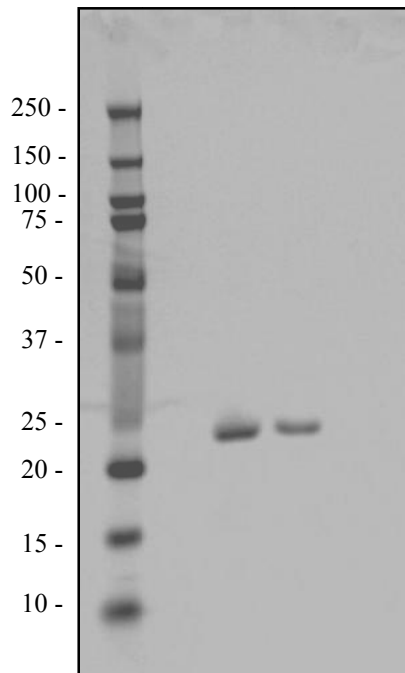


Figure 72. SDS-PAGE analysis of two purified and concentrated recombinant cruzain samples. Molecular masses (kDa) of the bands are marked. The two cruzain samples were loaded on the gel in lanes 3 (3.7 μM) and 4 (1.1 μM). The only bands present were the purified cruzain and no other bands suggesting contamination were present. Precision Plus Protein Kaleidoscope standards are marked.

The molecular mass of the protein was calculated with the equation obtained from the calibration curve of standard molecular masses and their migration distances in the gel (Figure 73).

$$MW_{\text{SDS-PAGE}} = 10^{(-3.3518 \cdot \text{cm} + 8.3177)}$$

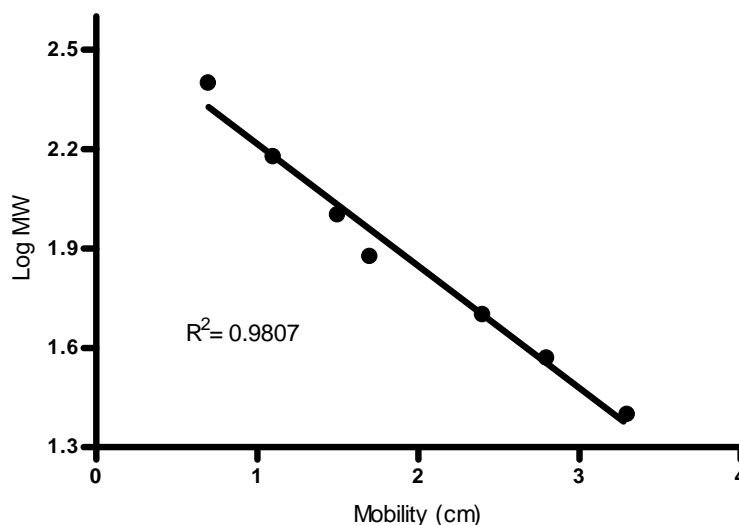


Figure 73. Calibration curve generated by plotting log molecular weight (MW) versus mobility [cm] of each band in Precision Plus Protein Kaleidoscope standards through an SDS-PAGE gel.

V_{max} and K_M Determination of Cruzain

Kinetic parameters of the recombinant cruzain with the fluorogenic synthetic peptide benzyloxycarbonyl-L-phenylalaninyl-L-argininyl-7-amido-4-methylcoumarin (Z-FR-AMC), indicates that cruzain velocity as a function of substrate concentration follows the Michaelis-Menten equation, therefore K_M is the concentration of substrate that leads to half-maximal velocity and V_{max} is the limiting velocity as the substrate concentrations increase.

To obtain V_{max} and K_M , cruzain activity was measured with a fixed enzyme concentration while varying the substrate concentrations. V_{max} and K_M were obtained by fitting the initial rates to the Michaelis-Menten equation using non-linear regression analysis with Graphpad 4.03 software as shown in Figure 74. The K_M value was found to be $1.3 \pm 0.3 \mu\text{M}$, similar to the one previously reported in literature ($0.96 \mu\text{M}$).³⁰ The V_{max} was determined to be $13625 \pm 1128 \mu\text{M/s}$. R^2 of the fit was 0.96.

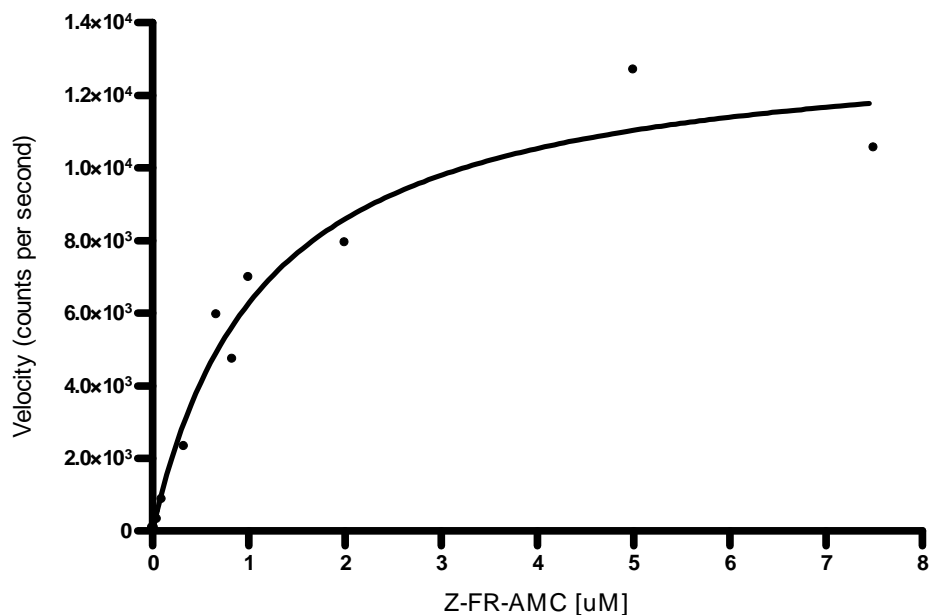


Figure 74. Dependence of cathepsin L activity on substrate concentration. (■) denote data points, and line (—) was fitted to the Michaelis-Menten equation with non-linear regression using the GraphPad software.

IC₅₀ Determination

A library of 25 thiosemicarbazones derivatives of tetrahydronaphthalene, benzophenone, propiophenone, chromenone, thiochromenone, thiochromenone dioxide, indane, bromophenylcyclohexane, and bromophenylcyclopentane synthesized by Dr. Kishore Gaddale, Freeland Ackley, Jiangli Song, and Lindsay Jones from Dr. Kevin G. Pinney's laboratory at Baylor University¹³⁷ were evaluated for IC₅₀ values.

Stock solutions (20 mM) of these inhibitors were prepared in DMSO (99.9%) and serial dilutions were subsequently made with DMSO and ultrapure water. At least eight concentrations of inhibitors ranging from 1 nM to 20 μM were then co-incubated with cruzain for 5 minutes in the assay/activation buffer. These mixtures were assayed for activity upon addition of 13.3 μL of the 150 μM substrate Z-FR-AMC.

The reactions were monitored for 10 minutes at an excitation of 355 nm and an emission wavelength of 460 nm at 25 °C for 10 minutes. Co-incubation of a constant enzyme concentration with increasing amounts of the same inhibitor results in a gradual loss of the enzyme activity, consequently, IC₅₀ values were determined by performing non-linear regression analysis fitting velocities and the logarithm of inhibitor concentrations to a sigmoidal dose response model using the GraphPad Prism 4.03 software. The average of duplicate IC₅₀ values of these compounds is summarized in Table 14.

Discussion of the Thiosemicarbazones as Inhibitors of Cruzain

Inhibition of Cruzain by Benzophenone Thiosemicarbazone Derivatives

The benzophenone thiosemicarbazones **1** and **2** from the thiosemicarbazone library evaluated in this study were previously reported as potent cruzain inhibitors with IC₅₀ values of 80 nM and 24 nM, respectively and are included here for comparison purposes.

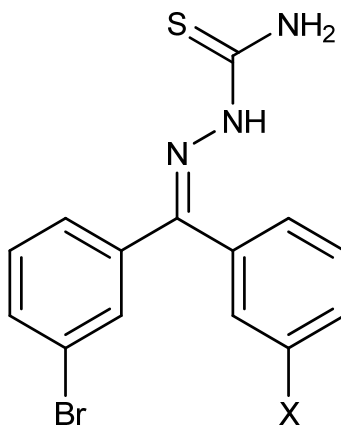
Compound **1** presents a poor inhibitory activity against cathepsins L, which makes this potent cruzain inhibitor a very promising starting point for the development of selective cruzain inhibitors.

As shown in Scheme 15, the following potency trend in terms of IC₅₀ values was observed in the bromo benzophenone series: X= Br (24 nM) > H (80 nM) > CH₃ (355 nM) > F (366 nM) > CF₃ (587 nM) > OAc (418 nM).

It can be noticed that the substitution of the aromatic ring at the *meta* position with bromine in compound **2** dramatically enhances its inhibitory potency.

It was also observed that compound **2** is significantly active against cathepsin L by a factor of 16-fold compared to its activity for cruzain.

Compound **32** proved to inhibit both cruzain and cathepsin L exhibiting a moderate activity against cruzain, with an IC₅₀ value of 366 nM, and a more pronounced active against cathepsin L by a factor of 5-fold.



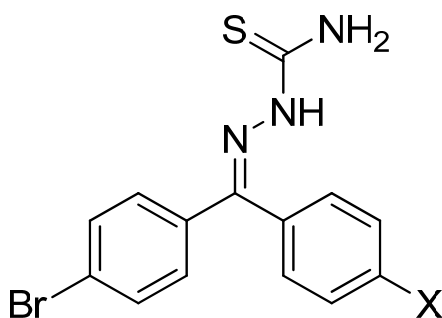
<u>Compound#</u>	<u>X</u>	<u>Cruzain inhibition IC50 [nM]</u>	<u>Cathepsin L Inhibition IC50 [nM]</u>
1	H	80	16200
2	Br	24	1.5
32	F	366	66
31	CF ₃	622	587
35	CH ₃	355	980
50	OAc	418	540

Scheme 15. Benzophenone thiosemicarbazone derivatives. Compound **1** and **2** have been previously reported in the literature. It is included here for the purpose of comparison (see reference 117).

The substitution effect of moving the CF₃ substituent to the para position on the aromatic ring (compound **44**) decreased the inhibitory potency of this compound by a factor of 10-fold (**31** versus **44**). A similar potency trend was observed for cathepsin L.

The substitution effect of moving substituents on both aromatic rings to the para position proved to be even more detrimental to the cruzain inhibitory potency of these compounds as shown in Scheme 16.

It must be noted that these compounds also exhibit a nearly identical inhibitory potency trend as on cathepsin L.

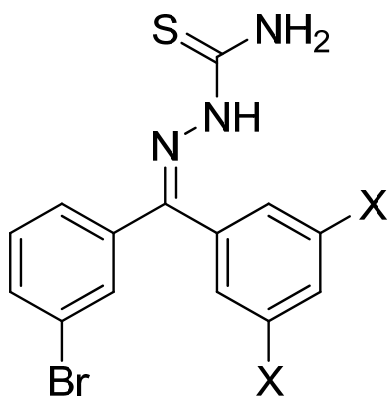


<u>Compound#</u>	<u>X</u>	<u>Cruzain inhibition IC50 [nM]</u>	<u>Cathepsin L Inhibition IC50 [nM]</u>
48	F	17000	16000
47	Cl	> 20000	> 20000
46	Br	> 20000	> 20000

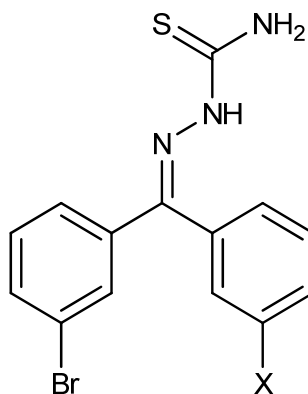
Scheme 16. Para-substitution in both aromatic rings of bromobenzophenone derivatives

Bis-substitution with fluorine atoms at the meta positions of the phenyl ring **49** proved to increase the inhibitory potency by a factor of 10-fold compared to substitutions with a chlorine atom **51** or a trifluoromethyl group **52**, which presented similar IC₅₀ values as shown in Scheme 17.

A comparison of IC₅₀ values between monosubstituted and disubstituted bromobenzophenone thiosemicarbazone derivatives proved the disubstitution effect to be detrimental to the cruzain inhibitory potency of these compounds (**32** versus **49**; **31** versus **52**) (Scheme 17).



<u>Compound #</u>	<u>X</u>	<u>Cruzain inhibition IC50 [nM]</u>	<u>Cathepsin L Inhibition IC50 [nM]</u>
49	F	170	460
51	Cl	1825	3500
52	CF ₃	1066	4100



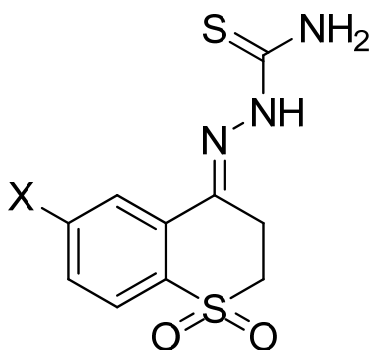
<u>Compound #</u>	<u>X</u>	<u>Cruzain inhibition IC50 [nM]</u>	<u>Cathepsin L Inhibition IC50 [nM]</u>
32	F	366	66
31	CF ₃	622	587

Scheme 17. Comparison between mono and disubstitution in bromobenzophenone TSC derivatives.

Inhibition of Cathepsin L by Tetrahydronaphthalene Derivatives

Thiosemicarbazone derivatives of the sulfone analog of a substituted thiochroman-4-one revealed interesting insights into the structure-activity relationship parameters.

The substitution with a chlorine atom at the meta positions of the phenyl ring **42** resulted in a potent inhibitor compared to substitutions with a fluorine atom **40** or a trifluoromethyl group **43**, which presented no inhibitory activity against cruzain (Scheme (scheme 18)). Compound **42** does not present any inhibitory activity against cathepsins L, which makes this compound a very promising starting point for the development of selective cruzain inhibitors.

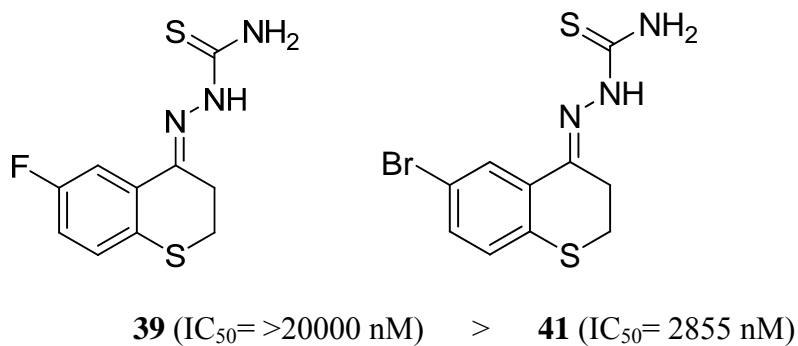


<u>Compound#</u>	<u>X</u>	<u>Cruzain inhibition IC50 [nM]</u>	<u>Cathepsin L Inhibition IC50 [nM]</u>
40	F	>20000	4500
42	Cl	202	17000
43	CF ₃	>20000	31000

Scheme 18. Thiosemicarbazone derivatives of the sulfone analog of a substituted thiochroman-4-one.

Two additional molecules discussed here are series containing tetrahydronaphthalene derivatives having a sulfur replacement of one benzylic carbon of the cyclohexane ring at the C4 position in halogenated dihydronaphthalenyl thiosemicarbazone scaffolds (Scheme 19).

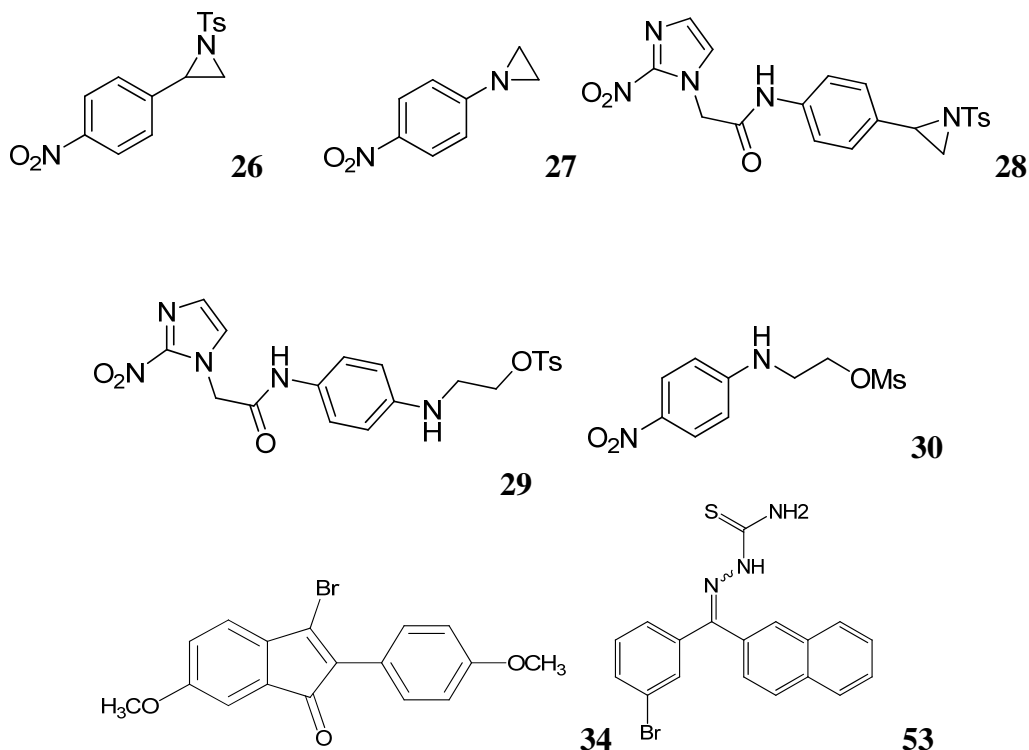
A comparison of the IC₅₀ values for **39** (> 20000 nM) and **41** (2855 nM) showed that halogenation with a fluoride has detrimental effects in cruzain inhibitory potency and that **41** presents weak activity toward cruzain.



Scheme 19. Potency trend in halogenated sulfur substituted α -tetralone compounds.

Inhibition of cruzain by aziridine derivatives and other cyclic compounds

Finally, it was determined that none of the aziridine derivatives (**26-30**) and compounds **34** and **35** showed inhibitory activity against cruzain. Therefore no trend could be derived (Scheme 20).



Scheme 20. Evaluated aziridine derivatives and other cyclic compounds.

Table 14. Inhibition of Cruzain by TSC Analogues and other Novel Cyclic Compounds.¹³⁷

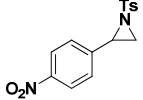
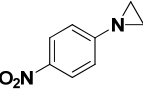
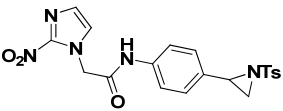
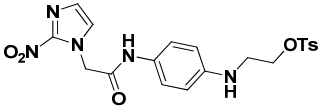
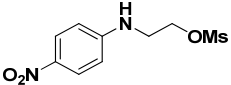
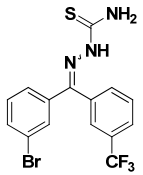
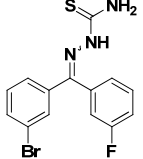
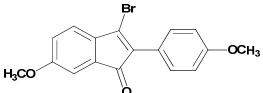
<i>Compound Number</i>	<i>Structure</i>	<i>IC₅₀ (nM)</i>
26		>20000
27		>20000
28		>20000
29		>20000
30		>20000
31		622
32		366
34		>20000

Table 14 (Continued)

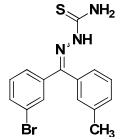
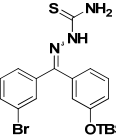
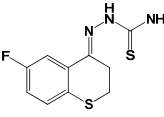
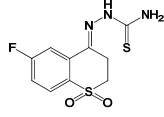
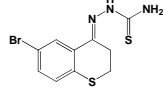
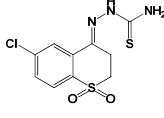
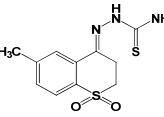
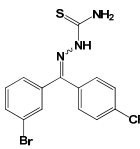
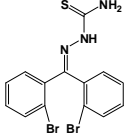
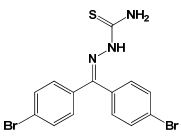
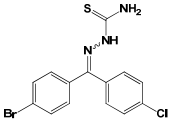
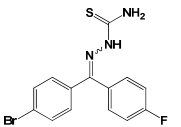
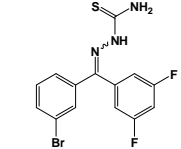
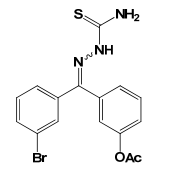
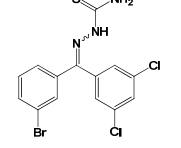
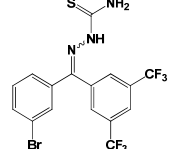
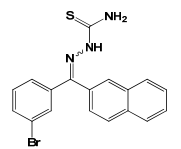
<i>Compound Number</i>	<i>Structure</i>	<i>IC₅₀ (nM)</i>
35		355
36		>20000
39		23295
40		>20000
41		2855
42		202
43		>20000
44		3777
45		>20000

Table 14. (Continued)

<i>Compound Number</i>	<i>Structure</i>	<i>IC₅₀ (nM)</i>
46		>20000
47		>20000
48		>17000
49		170
50		418
51		1825
52		1066
53		1572

CHAPTER SEVEN

Conclusions and Future Directions

A new library of compounds bearing α -tetralone, benzophenone, propiophenone and related rigid molecular skeletons functionalized with thiosemicarbazone or α,β -unsaturated carbonyl moieties were evaluated for their ability to inhibit human cathepsin L and the parasitic cysteine protease cruzain. In the present study, a novel series of small non-peptidic thiosemicarbazone compounds were identified as potent inhibitors of cathepsin L.

Out of fifty nine newly synthesized compounds, two were determined to be very effective inhibitors of cathepsin L: a dibromobenzophenone (**2**) and a sulfone analog of the bromo substituted thiochroman-4-one (**22**) with IC_{50} values of 60 nM and 1.0 nM, respectively, which are among the best reported in literature for non-peptidyl inhibitors.

The structures of other cathepsins L inhibitors in the nanomolar range included the benzophenone thiosemicarbazones **32** (IC_{50} = 66 nM), **37** (IC_{50} = 140 nM), **50** (IC_{50} = 540 nM), **55** (IC_{50} = 44 nM), **57** (IC_{50} = 576 nM), the bromothiochromenone dioxide **21** (IC_{50} = 716 nM), the α -tetralone **9** (IC_{50} = 619 nM), **10** (IC_{50} = 530 nM), **11** (IC_{50} = 367 nM), and **25** (IC_{50} = 322 nM).

Kinetic analysis proved that compounds **2** and **22** inhibited cathepsins L in a time-dependent fashion. They were also found to be reversible, time dependent, slow, tight binding inhibitors of cathepsin L.

The mechanism of inhibition was also studied for both compounds and it was concluded that both **2** and **22** are active-site directed inhibitors of cathepsin L.

Mechanistically, however, they were different as compound **22** was found to be a tight-binding reversible inhibitor while compound **2** appeared to be a time-dependent inhibitor. Moreover, these inhibitors proved to be active in mammalian cell culture as demonstrated by the reduction in invasiveness and motility properties of the prostate cancer cell line, DU-145.

However, further studies must be performed to determine the selectivity of these compounds as the design of therapeutically effective cathepsin L inhibitors requires a high degree of selectivity over cathepsin K and S, cysteine proteases from the same family with active site similarities.

Further studies are also necessary to determine the mechanisms by which both compounds inhibit the invasive and motility properties of DU-145 prostate carcinoma cells. Immunoblotting analyses in cancer cell lines are proposed to determine whether procathepsins B and L or their mature forms are being inhibited, to specify which form is secreted or alternatively if it is a product processed from the procathepsins after secretion into the medium.

From the same library of thiosemicarbazone derivatives evaluated against cathepsin L, 25 compounds were evaluated against cruzain from which six compounds were in the nano-molar range with IC_{50} values ranging from 170 nM to 622 nM.

Compound **42** does not present any inhibitory activity against cathepsins L, which makes this compound a very promising starting point for the development of selective cruzain inhibitors.

The structures of the most potent cruzain inhibitors included the benzophenone thiosemicarbazones **49** (IC₅₀= 170 nM), **35** (IC₅₀= 355 nM), **32** (IC₅₀= 366 nM), **50** (IC₅₀= 418 nM), **31** (IC₅₀= 622 nM) and the 6-bromothiochromenone dioxide **42** (IC₅₀= 202 nM).

The structure-activity relationships of this novel library of compounds contributed conclusions about the following structural requirements for the development of more selective cathepsins L and cruzain inhibitors:

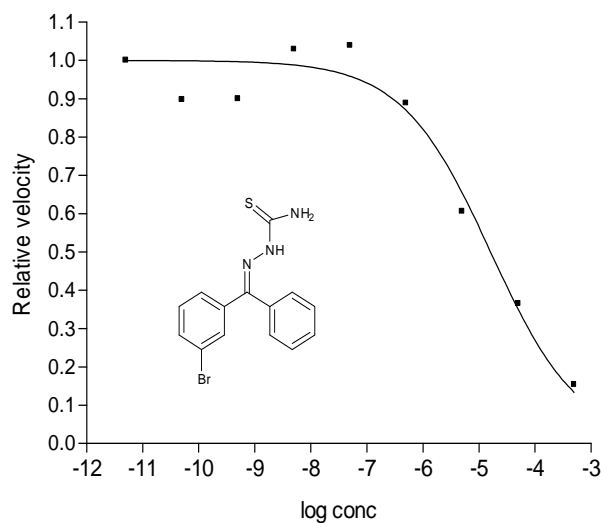
- 1) The presence of a benzene ring containing a bromine atom attached at the *meta* position is essential for inhibitory activity in cathepsins L and cruzain.
- 2) A comparison of IC₅₀ values between mono-substituted and di-substituted bromobenzophenone thiosemicarbazone derivatives proved the disubstitution effect to be detrimental to the cathepsin L inhibitory potency of these compounds
- 3) Substitution of the three positional isomers on the benzophenone groups with a variety of X substituents (Br, F, OH, OAc, CF₃, CH₃ and Cl) revealed that a phenyl ring containing a bromine atom or a fluorine atom was more effective for cathepsin L inhibition.
- 4) The isosteric replacement of the benzylic methylene group in the tetrahydronaphthalene derivative by oxygen, a sulfur atom or a sulfone group resulted in a reduction in cruzain inhibition, but a sulfur substitution increased the cathepsin L inhibitory potency compared to a sulfone or oxygen substitution.
- 5) Connected ring systems, aziridine derivatives, and other cyclic compounds did not show good inhibitory effects towards cruzain and cathepsin L

In summary, the SAR within this series indicated that the main important structural requirement for cathepsin L inhibition is the need of inhibitors to possess hydrophobic moieties, particularly aromatic rings containing one bromine or fluorine atom. Also, the presence of negatively charged oxygen-based functional groups, such as sulfones increases the inhibitory potential of some compounds.

APPENDICES

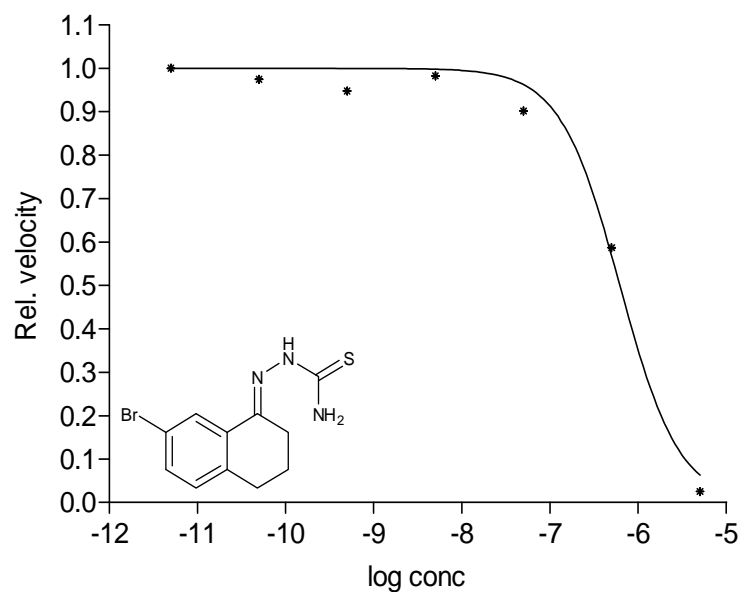
APPENDIX A

Cathepsin L IC50 Determination Data and Plots



Goodness of Fit		[M]	vel.
Degrees of Freedom	5	0.00	4500.00
R ²	0.9679	5.00e-012	4578.00
Absolute Sum of Squares	0.02603	5.00e-011	4113.00
Sy.x	0.07215	5.00e-010	4122.00
		5.00e-009	4713.00
Equation 2		5.00e-008	4758.00
Best-fit values		5.00e-007	4068.00
BOTTOM	0.0	5.00e-006	2773.80
TOP	1.000	5.00e-005	1671.90
LOGEC50	-4.792	5.00e-004	703.50
HILLSLOPE	-0.5461		
EC50	1.616e-005		
Std. Error			
LOGEC50	0.1463		
HILLSLOPE	0.09312		
95% Confidence Intervals			
LOGEC50	-5.138 to -4.446		
HILLSLOPE	-0.7663 to -0.3259		

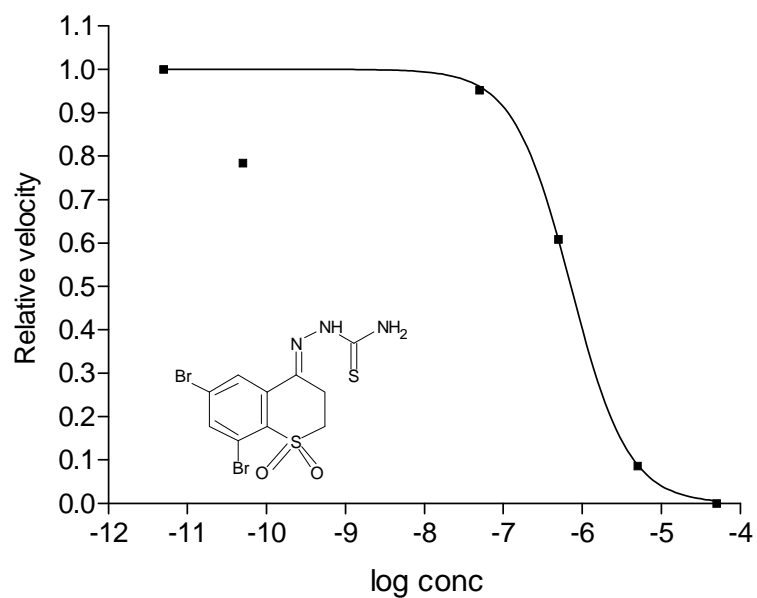
Figure A1. IC50 Determination of Compound 1.



Goodness of Fit			
Degrees of Freedom	3		
R ²	0.9980		
Absolute Sum of Squares	0.001545		
Sy.x	0.02269		
Equation 2			
Best-fit values			
BOTTOM	0.0		
TOP	1.000		
LOGEC50	-6.208		
HILLSLOPE	-1.289		
EC50	6.192e-007		
Std. Error			
LOGEC50	0.05734		
HILLSLOPE	0.2668		
95% Confidence Intervals			
LOGEC50	-6.356 to -6.061		
HILLSLOPE	-1.976 to -0.6035		

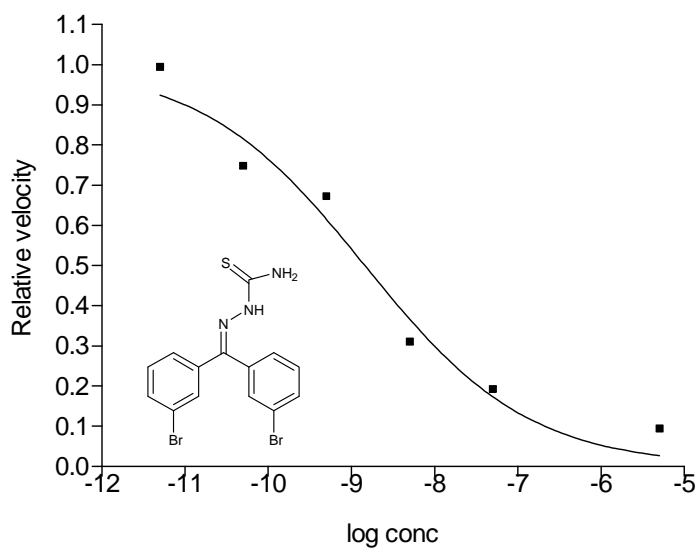
Conc [M]	Vel.
5.0e-012	3920.0
5.0e-011	3822.0
5.0e-010	3716.0
5.0e-009	3852.0
5.0e-008	3536.0
5.0e-007	2300.0
5.0e-006	99.1

Figure A2. IC50 Determination of Compound 9.



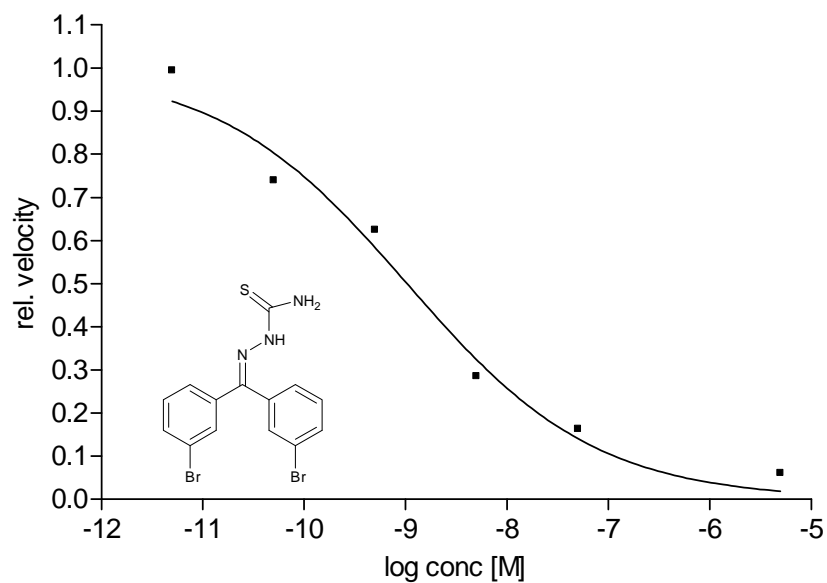
Goodness of Fit		conc [M]	velocity
Degrees of Freedom	2	5.0e-012	4397.40
R ²	0.9706	5.0e-011	3447.00
Absolute Sum of Squares	0.02755	5.0e-010	1382.60
Sy.x	0.1174	5.0e-009	622.80
		5.0e-008	4183.20
Equation 2		5.0e-007	2675.40
Best-fit values		0.0	377.52
BOTTOM	0.0	0.0	0.00
TOP	1.000		
LOGEC50	-6.145		
HILLSLOPE	-1.196		
EC50	7.161e-007		
Std. Error			
LOGEC50	0.1576		
HILLSLOPE	0.5322		
95% Confidence Intervals			
LOGEC50	-6.583 to -5.707		
HILLSLOPE	-2.673 to 0.2816		

Figure A3. IC50 Determination of Compound 21.



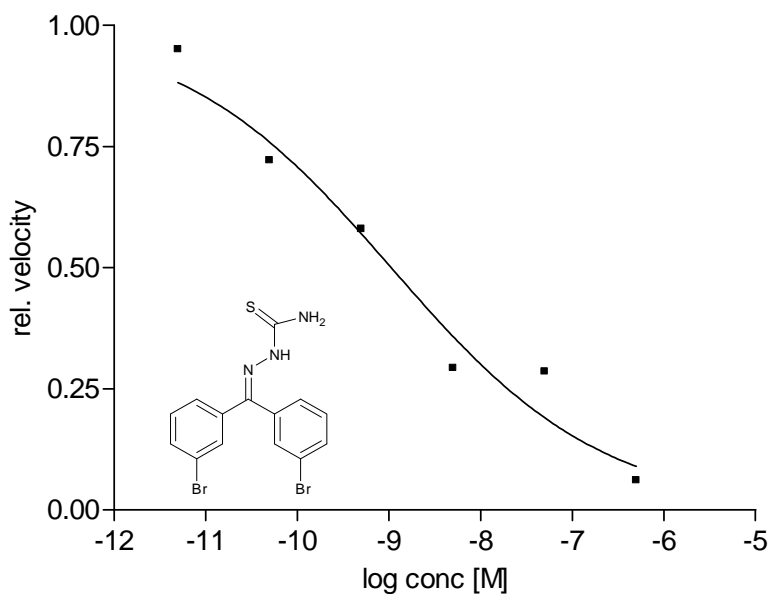
Points above curve	3	conc [m]	velocity
Points below curve	3	0.00	4399.50
Number of runs	5	5.00e-012	4375.00
P value (runs test)	0.9000	5.00e-011	3292.80
Deviation from Model	Not Significant	5.00e-010	2958.20
		5.00e-009	1368.15
Equation 2		5.00e-008	848.75
Best-fit values		5.00e-006	416.85
BOTTOM	0.0		
TOP	1.000		
LOGEC50	-8.839		
HILLSLOPE	-0.4413		
EC50	1.450e-009		
Std. Error			
LOGEC50	0.1784		
HILLSLOPE	0.07772		
95% Confidence Intervals			
LOGEC50	-9.334 to -8.343		
HILLSLOPE	-0.6570 to -0.2255		

Figure A4. IC50 Determination of Compound 2.



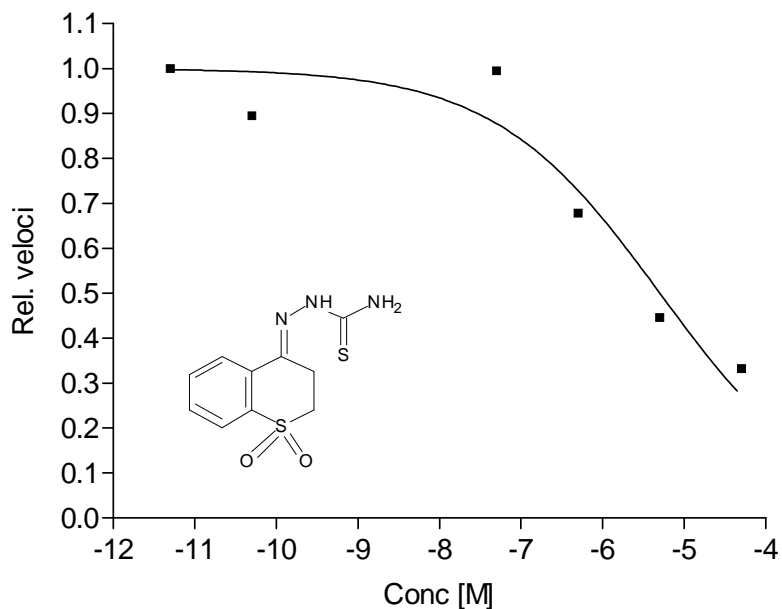
	velocity	conc [m]	velocity
Sigmoidal dose-response (variable slope)			4242.500
Best-fit values		-11.30103	4218.000
BOTTOM	0.0	-10.30103	3135.800
TOP	1.000	-9.30103	2651.200
LOGEC50	-8.987	-8.30103	1211.150
HILLSLOPE	-0.4655	-7.30103	691.750
EC50	1.031e-009	-5.30103	259.850
Std. Error			
LOGEC50	0.1453		
HILLSLOPE	0.06928		
95% Confidence Intervals			
LOGEC50	-9.390 to -8.583	-11.301	0.994
HILLSLOPE	-0.6578 to -0.2732	-10.301	0.739
EC50	4.072e-010 to 2.610e-009	-9.301	0.625
		-8.301	0.285
		-7.301	0.163
		-5.301	0.061
Goodness of Fit			
Degrees of Freedom	4		
R ²	0.9779		
Absolute Sum of Squares	0.01475		
Sy.x	0.06072		
Constraints			
BOTTOM	BOTTOM = 0.0		
TOP	TOP = 1.000		

Figure A5. IC50 Determination of Compound 2.



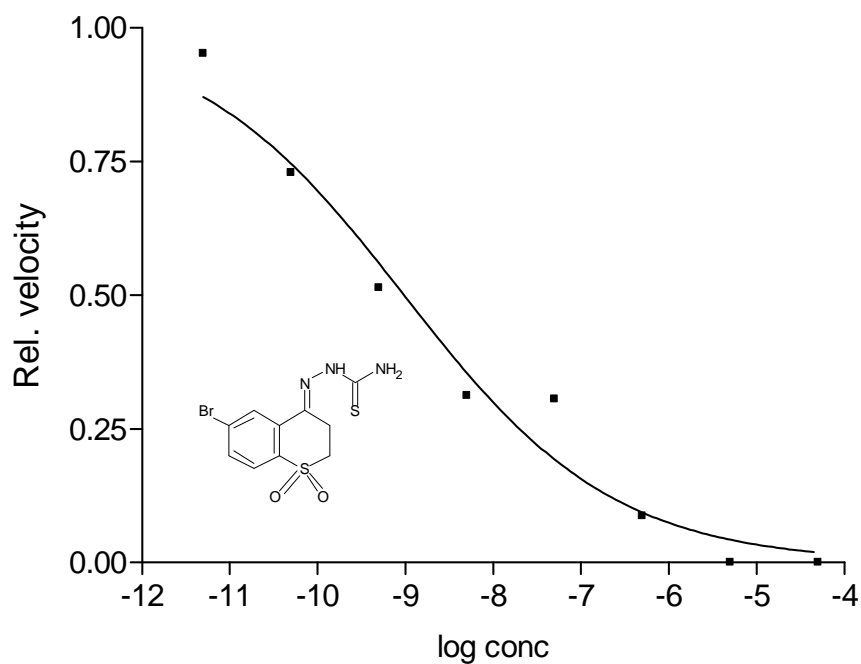
Sigmoidal dose-response (variable slope)		conc [M]	velocity
Best-fit values		0.000000	4000.000
BOTTOM	0.0	5.000000e-012	3802.000
TOP	1.000	5.000000e-011	2885.800
LOGEC50	-8.975	5.000000e-010	2319.400
HILLSLOPE	-0.3756	5.000000e-009	1171.480
EC50	1.060e-009	5.000000e-008	1144.840
Std. Error		5.000000e-007	244.840
LOGEC50	0.1910		
HILLSLOPE	0.06069		
95% Confidence Intervals			
LOGEC50	-9.505 to -8.444	conc [M]	velocity
HILLSLOPE	-0.5441 to -0.2071	-11.301	1.000
EC50	3.126e-010 to 3.595e-009	-10.301	0.951
Goodness of Fit		-9.301	0.580
Degrees of Freedom	4	-8.301	0.293
R ²	0.9619	-7.301	0.286
Absolute Sum of Squares	0.02049	-6.301	0.061
Sy.x	0.07157		
Constraints			
BOTTOM	BOTTOM = 0.0		
TOP	TOP = 1.000		

Figure A6. IC50 Determination of Compound 2.



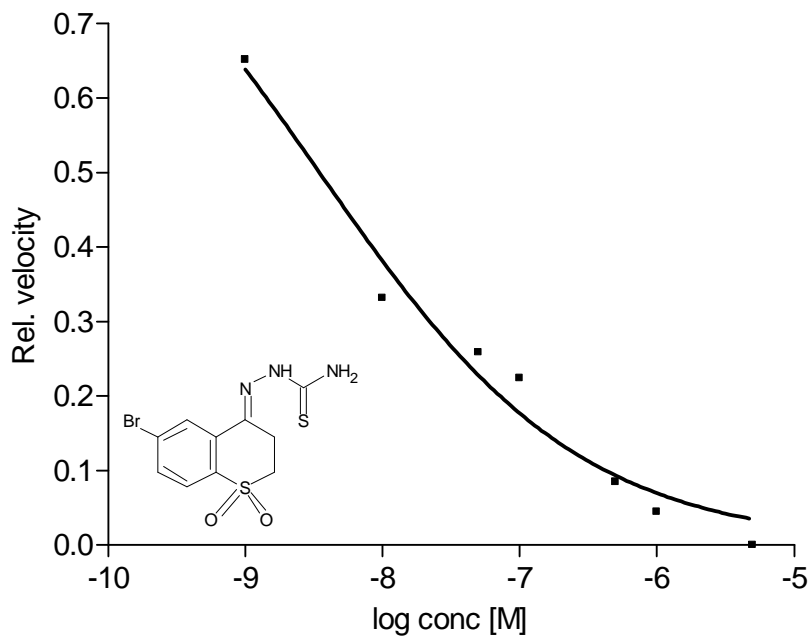
Goodness of Fit		Conc [M]	velocity
Degrees of Freedom	2	0.00	4421.330
R ²	0.9697	5.00e-012	4480.000
Absolute Sum of Squares	0.01248	5.00e-011	4010.670
Sy.x	0.07900	5.00e-008	4456.000
		5.00e-010	2870.000
Equation 2		5.00e-007	3038.670
Best-fit values		5.00e-009	2545.330
BOTTOM	0.0	5.00e-006	1998.670
TOP	1.000	5.00e-005	1489.330
LOGEC50	-5.297		
HILLSLOPE	-0.4268		
EC50	5.049e-006		
Std. Error			
LOGEC50	0.2374		
HILLSLOPE	0.1113		
95% Confidence Intervals			
LOGEC50	-5.956 to -4.638		
HILLSLOPE	-0.7358 to -0.1178		

Figure A7. IC50 Determination of Compound 23.



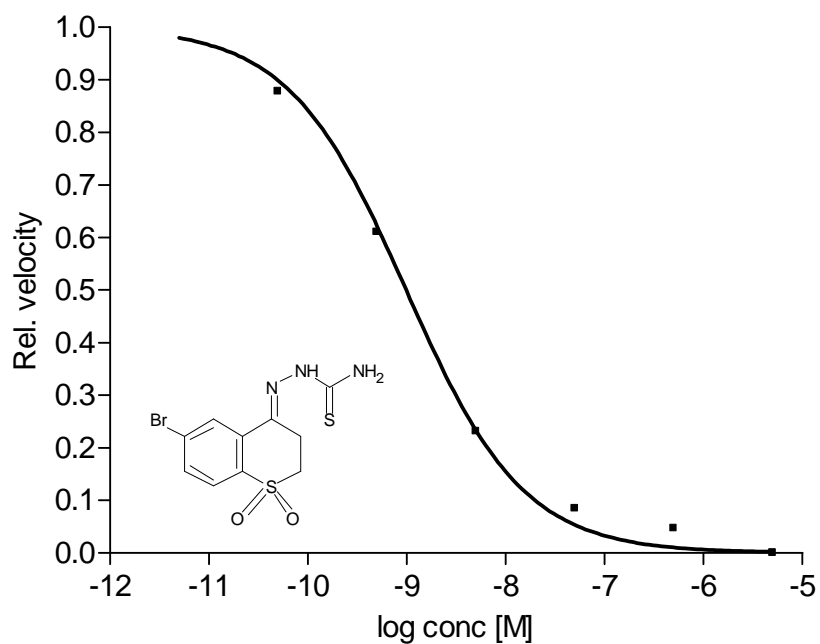
		conc [M]	velocity
Goodness of Fit		0.00	4114.80
Degrees of Freedom	6	5.00e-012	3916.80
R ²	0.5609	5.00e-011	3000.60
Absolute Sum of Squares	0.3729	5.00e-010	2113.20
Sy.x	0.2493	5.00e-009	1286.28
Sigmoidal dose-response (variable slope)		5.00e-008	1259.64
Best-fit values		5.00e-007	359.64
BOTTOM	0.0	5.00e-006	0.00
TOP	1.000	5.00e-005	0.00
LOGEC50	-9.015		
HILLSLOPE	-0.3630		
EC50	9.662e-010		
Std. Error			
LOGEC50	0.1780		
HILLSLOPE	0.05107		
95% Confidence Intervals			
LOGEC50	-9.450 to -8.579		
HILLSLOPE	-0.4879 to -0.2380		

Figure A8. IC50 Determination of Compound 22.



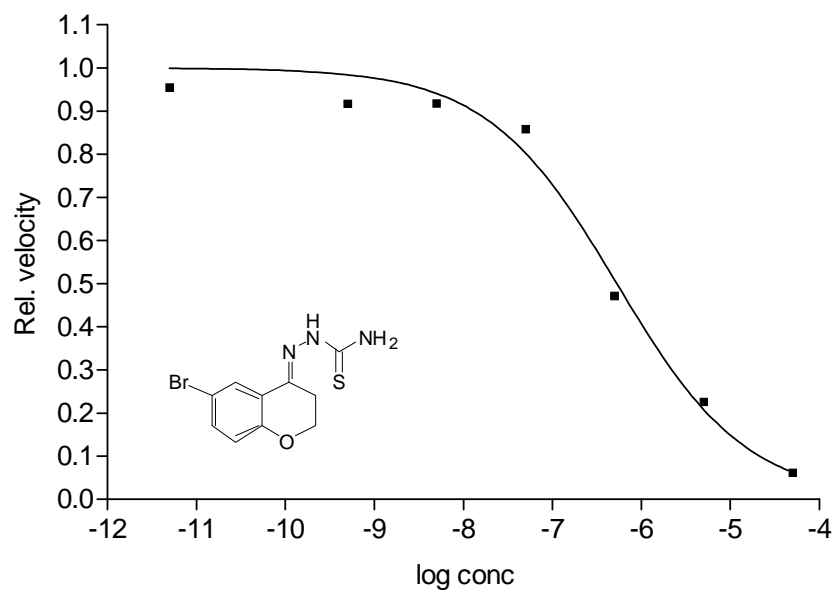
		conc [M]	cps
Best-fit values		0.000000	4912.0
BOTTOM	0.0	1.000000e-009	2484.0
TOP	1.000	1.000000e-008	1264.0
LOGEC50	-8.459	5.000000e-008	987.0
HILLSLOPE	-0.4572	1.000000e-007	854.0
EC50	3.474e-009	5.000000e-007	324.0
Std. Error		0.000001	170.0
LOGEC50	0.1049	0.000005	0.0
HILLSLOPE	0.04657		
95% Confidence Intervals			
LOGEC50	-8.729 to -8.190		
HILLSLOPE	-0.5770 to -0.3375		
EC50	1.867e-009 to 6.463e-009		
Goodness of Fit			
Degrees of Freedom	5		
R ²	0.9740		
Absolute Sum of Squares	0.007727		
Sy.x	0.03931		
Constraints			
BOTTOM	BOTTOM = 0.0		
TOP	TOP = 1.000		

Figure A9. IC50 Determination of Compound 22.



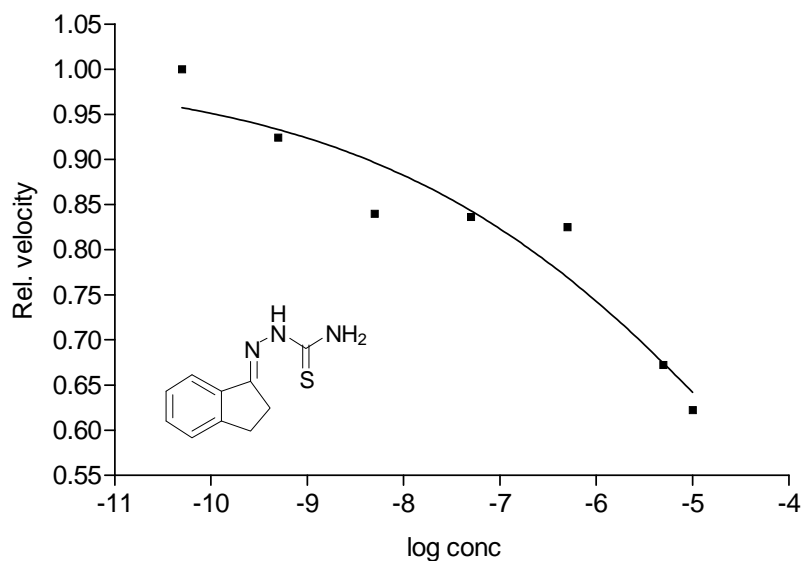
Best-fit values		conc [M]	velocity
BOTTOM	0.0	0.000000	4317.00000
TOP	1.000	5.000000e-012	3811.00000
LOGEC50	-9.007	5.000000e-011	2587.00000
HILLSLOPE	-0.7322	5.000000e-010	1479.00000
EC50	9.835e-010	5.000000e-009	786.00000
Std. Error		5.000000e-008	387.00000
LOGEC50	0.1286	5.000000e-007	159.00000
HILLSLOPE	0.1396	0.000005	0.00000
95% Confidence Intervals			
LOGEC50	-9.338 to -8.677		
HILLSLOPE	-1.091 to -0.3732		
EC50	4.594e-010 to 2.106e-009		
Goodness of Fit			
Degrees of Freedom	5		
R ²	0.9807		
Absolute Sum of Squares	0.02321		
Sy.x	0.06813		
Constraints			
BOTTOM	BOTTOM = 0.0		
TOP	TOP = 1.000		

Figure A10. IC50 Determination of Compound 22.



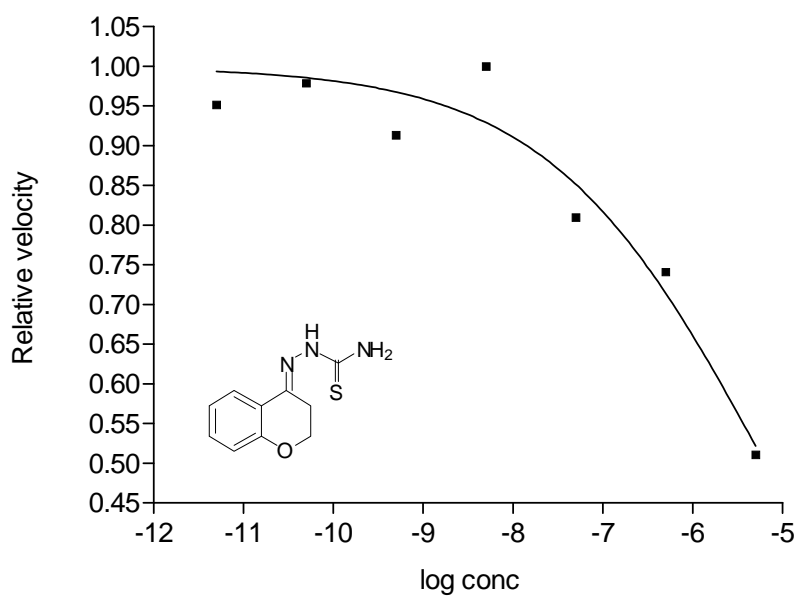
Sigmoidal dose-response (variable slope)		conc [M]	velocity
Best-fit values		0.0	3600.0
BOTTOM	0.0	5.0e-012	3437.0
TOP	1.000	5.0e-008	3089.0
LOGEC50	-6.276	5.0e-011	1868.0
HILLSLOPE	-0.5942	5.0e-007	1698.0
EC50	5.302e-007	5.0e-010	3301.0
Std. Error		5.0e-006	815.4
LOGEC50	0.1019	5.0e-009	3303.2
HILLSLOPE	0.07434	5.0e-005	222.0
95% Confidence Intervals			
LOGEC50	-6.537 to -6.014		
HILLSLOPE	-0.7853 to -0.4031		
EC50	2.901e-007 to 9.692e-007		
Goodness of Fit			
Degrees of Freedom	5		
R ²	0.9858		
Absolute Sum of Squares	0.01181		
Sy.x	0.04861		

Figure A11. IC50 Determination of Compound 10.



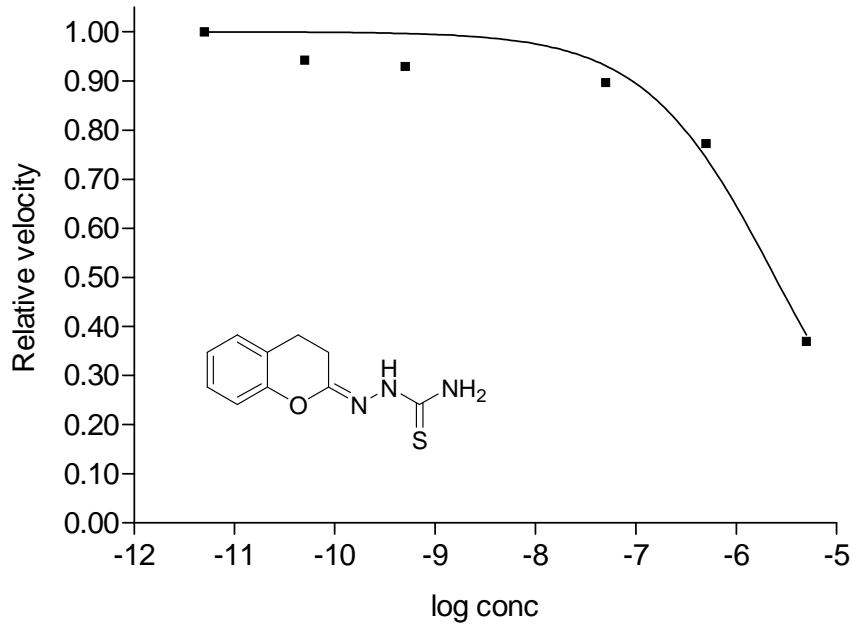
Sigmoidal dose-response (variable slope)		X Title	velocity
Best-fit values		0.00	4213.0
BOTTOM	0.0	5.00e-011	4900.0
TOP	1.000	5.00e-010	4529.0
LOGEC50	-3.778	5.00e-009	4115.0
HILLSLOPE	-0.2074	5.00e-008	4098.0
EC50	0.0001668	5.00e-007	4043.0
Std. Error		5.00e-006	3295.0
LOGEC50	0.4459	1.00e-005	3050.0
HILLSLOPE	0.03799		
95% Confidence Intervals			
LOGEC50	-4.924 to -2.632		
HILLSLOPE	-0.3051 to -0.1097		
EC50	1.191e-005 to 0.002336		
Goodness of Fit			
Degrees of Freedom	5		
R ²	0.9174		
Absolute Sum of Squares	0.008644		
Sy.x	0.04158		

Figure A12. IC50 Determination of Compound 19.



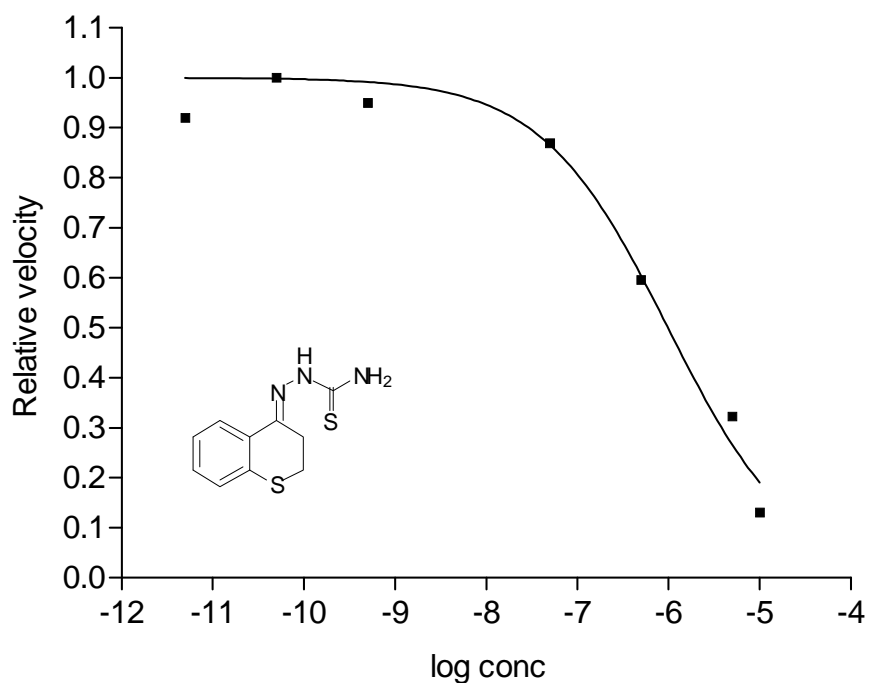
Sigmoidal dose-response (variable slope)		conc [M]	velocity
Best-fit values		0.00	4449.0
BOTTOM	0.0	5.00e-012	4363.0
TOP	1.000	5.00e-011	4487.0
LOGEC50	-5.195	5.00e-010	4188.0
HILLSLOPE	-0.3601	5.00e-009	4583.0
EC50	6.376e-006	5.00e-008	3711.0
Std. Error		5.00e-007	3396.0
LOGEC50	0.2320	5.00e-006	2342.0
HILLSLOPE	0.06838		
95% Confidence Intervals			
LOGEC50	-5.792 to -4.599		
HILLSLOPE	-0.5359 to -0.1843		
EC50	1.615e-006 to 2.518e-005		
Goodness of Fit			
Degrees of Freedom	5		
R ²	0.9322		
Absolute Sum of Squares	0.01232		
Sy.x	0.04963		

Figure A13. IC50 Determination of Compound 16.



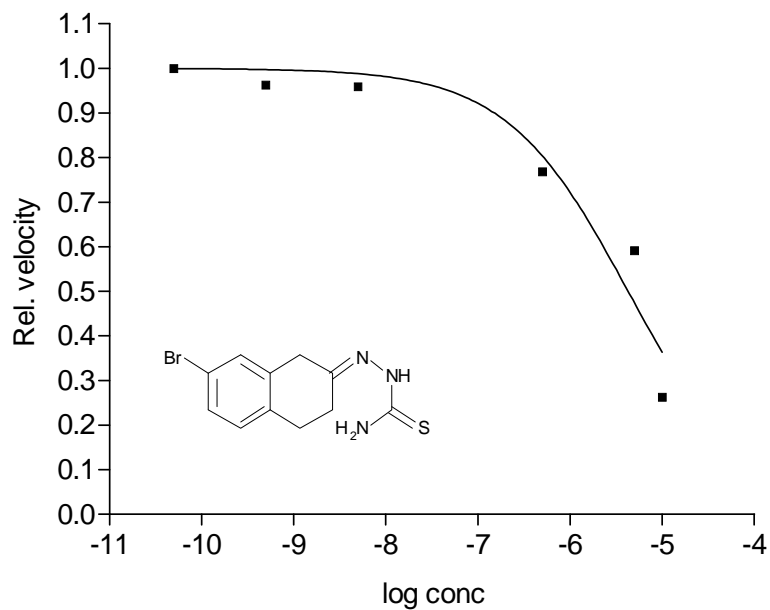
Sigmoidal dose-response (variable slope)		conc [M]	velocity
Best-fit values		0.00	4248.0
BOTTOM	0.0	5.00e-012	4554.0
TOP	1.000	5.00e-011	4292.0
LOGEC50	-5.610	5.00e-008	4084.0
HILLSLOPE	-0.6696	5.00e-010	4234.0
EC50	2.452e-006	5.00e-007	3518.0
Std. Error		5.00e-009	2352.0
LOGEC50	0.1076	5.00e-006	1685.2
HILLSLOPE	0.1202		
95% Confidence Intervals			
LOGEC50	-5.909 to -5.312		
HILLSLOPE	-1.003 to -0.3359		
EC50	1.233e-006 to 4.876e-006		
Goodness of Fit			
Degrees of Freedom	4		
R ²	0.9634		
Absolute Sum of Squares	0.009895		
Sy.x	0.04974		

Figure A14. IC50 Determination of Compound 17.



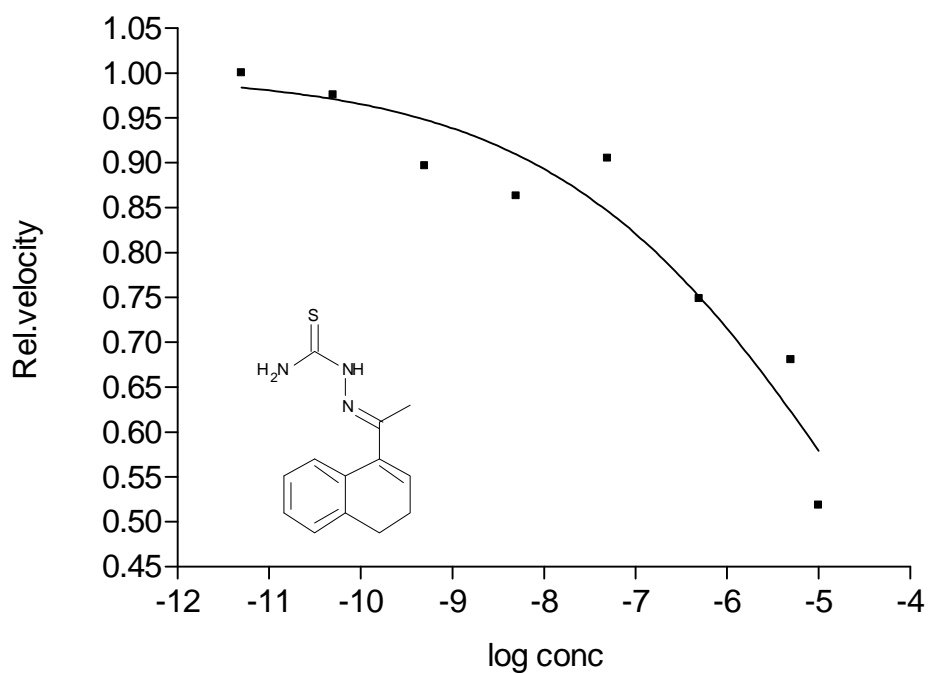
Sigmoidal dose-response (variable slope)		conc [M]	velocity
Best-fit values		0.000	3828.0
BOTTOM	0.0	5.000e-012	3242.0
TOP	1.000	5.000e-011	3525.0
LOGEC50	-6.007	5.000e-010	3347.0
HILLSLOPE	-0.6246	5.000e-009	4466.0
EC50	9.833e-007	5.000e-008	3064.0
Std. Error		5.000e-007	2100.0
LOGEC50	0.1058	5.000e-006	1137.0
HILLSLOPE	0.08993	1.000e-005	461.5
95% Confidence Intervals			
LOGEC50	-6.279 to -5.735		
HILLSLOPE	-0.8558 to -0.3934		
EC50	5.257e-007 to 1.839e-006		
Goodness of Fit			
Degrees of Freedom	5		
R ²	0.9788		
Absolute Sum of Squares	0.01493		
Sy.x	0.05465		

Figure A15. IC50 Determination of Compound 8



Sigmoidal dose-response (variable slope)		conc [M]	velocity
Best-fit values		0.0	4327.0
BOTTOM	0.0	5.0e-011	3790.0
TOP	1.000	5.0e-010	3650.0
LOGEC50	-5.370	5.0e-009	3634.0
HILLSLOPE	-0.6578	5.0e-008	1162.0
EC50	4.263e-006	5.0e-007	2911.0
Std. Error		5.0e-006	2241.0
LOGEC50	0.1452	1.0e-005	996.4
HILLSLOPE	0.2053		
95% Confidence Intervals			
LOGEC50	-5.773 to -4.967		
HILLSLOPE	-1.228 to -0.08783		
EC50	1.685e-006 to 1.078e-005		
Goodness of Fit			
Degrees of Freedom	4		
R ²	0.9343		
Absolute Sum of Squares	0.02722		
Sy.x	0.08249		

Figure A16. IC50 Determination of Compound 20.



Sigmoidal dose-response (variable slope)

Best-fit values

BOTTOM

0.0

TOP

1.000

LOGEC50

-4.469

HILLSLOPE

-0.2611

EC50

3.399e-005

Std. Error

LOGEC50

0.3243

HILLSLOPE

0.05014

95% Confidence Intervals

LOGEC50

-5.262 to -3.675

HILLSLOPE

-0.3838 to -0.1384

EC50

5.466e-006 to 0.0002113

Goodness of Fit

Degrees of Freedom

6

R²

0.9166

Absolute Sum of Squares

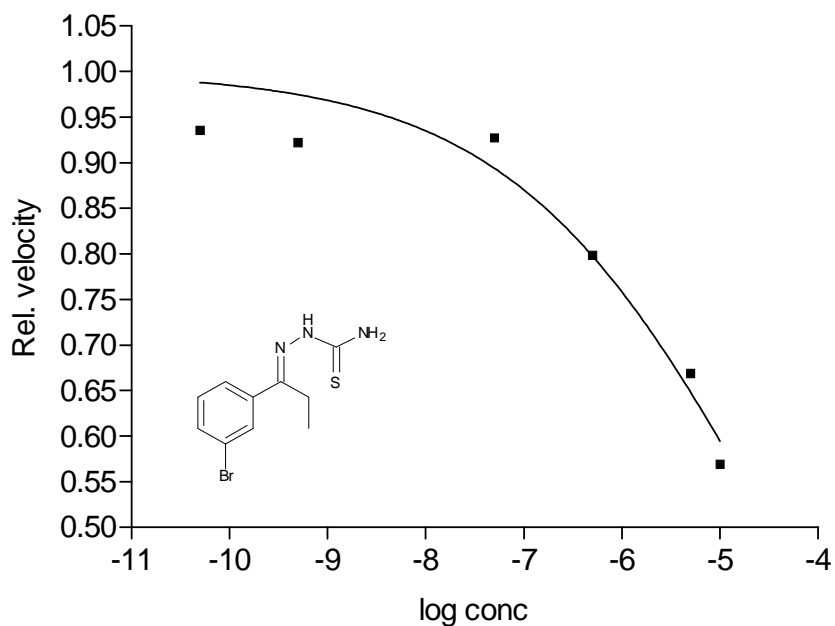
0.01560

Sy.x

0.05099

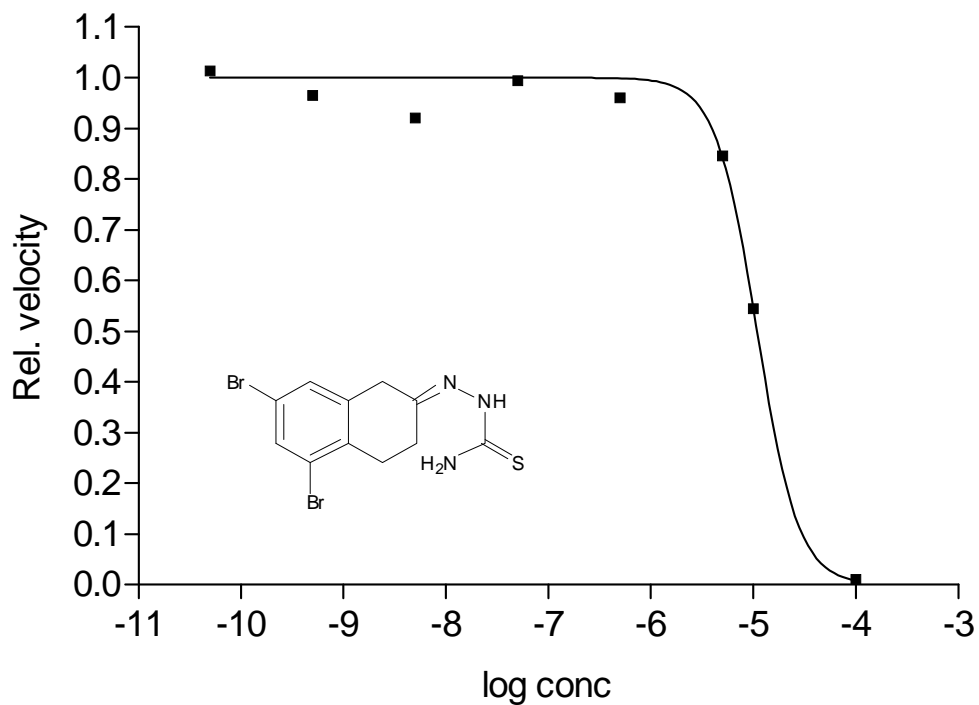
conc [M]	velocity
0.000	4416.0
5.000e-012	5086.0
5.000e-011	4961.0
5.000e-010	4560.0
5.000e-009	4389.0
5.000e-008	4601.0
5.000e-007	3806.0
5.000e-006	3460.0
1.000e-005	2635.0

Figure A17. IC50 Determination of Compound 18.



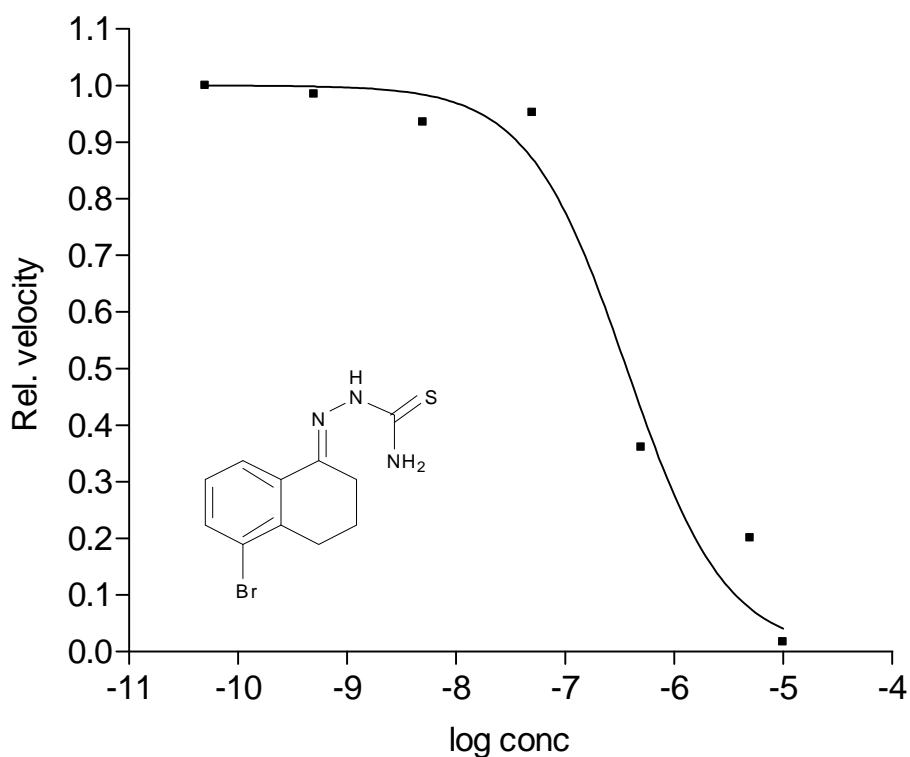
Sigmoidal dose-response (variable slope)		conc M	velocity
Best-fit values		0.00	4537.0
BOTTOM	0.0	5.00e-011	4243.0
TOP	1.000	5.00e-010	4183.0
LOGEC50	-4.496	5.00e-009	3493.0
HILLSLOPE	-0.3301	5.00e-008	4207.0
EC50	3.188e-005	5.00e-007	3623.0
Std. Error		5.00e-006	3034.0
LOGEC50	0.2614	1.00e-005	2583.0
HILLSLOPE	0.06985		
95% Confidence Intervals			
LOGEC50	-5.222 to -3.771		
HILLSLOPE	-0.5240 to -0.1362		
EC50	5.995e-006 to 0.0001695		
Goodness of Fit			
Degrees of Freedom	4		
R ²	0.9357		
Absolute Sum of Squares	0.007705		
Sy.x	0.04389		

Figure A18. IC50 Determination of Compound 3.



Sigmoidal dose-response (variable slope)		conc [M]	velocity
Best-fit values		0.000	4512.0
BOTTOM	0.0	5.000e-011	4573.0
TOP	1.000	5.000e-010	4355.0
LOGEC50	-4.963	5.000e-009	4154.0
HILLSLOPE	-2.167	5.000e-008	4488.0
EC50	1.089e-005	5.000e-007	4335.0
Std. Error		5.000e-006	3816.0
LOGEC50	0.03565	1.000e-005	2459.0
HILLSLOPE	0.4697	1.000e-004	48.0
95% Confidence Intervals			
LOGEC50	-5.050 to -4.876		
HILLSLOPE	-3.316 to -1.017		
EC50	8.907e-006 to 1.331e-005		
Goodness of Fit			
Degrees of Freedom	6		
R ²	0.9891		
Absolute Sum of Squares	0.009153		
Sy.x	0.03906		

Figure A19. IC50 Determination of Compound 13.



Sigmoidal dose-response (variable slope)

Best-fit values

BOTTOM

0.0

TOP

1.000

LOGEC50

-6.435

HILLSLOPE

-0.9575

EC50

3.675e-007

Std. Error

LOGEC50

0.1254

HILLSLOPE

0.2337

95% Confidence Intervals

LOGEC50

-6.757 to -6.112

HILLSLOPE

-1.558 to -0.3566

EC50

1.750e-007 to 7.719e-007

Goodness of Fit

Degrees of Freedom

5

R²

0.9726

Absolute Sum of Squares

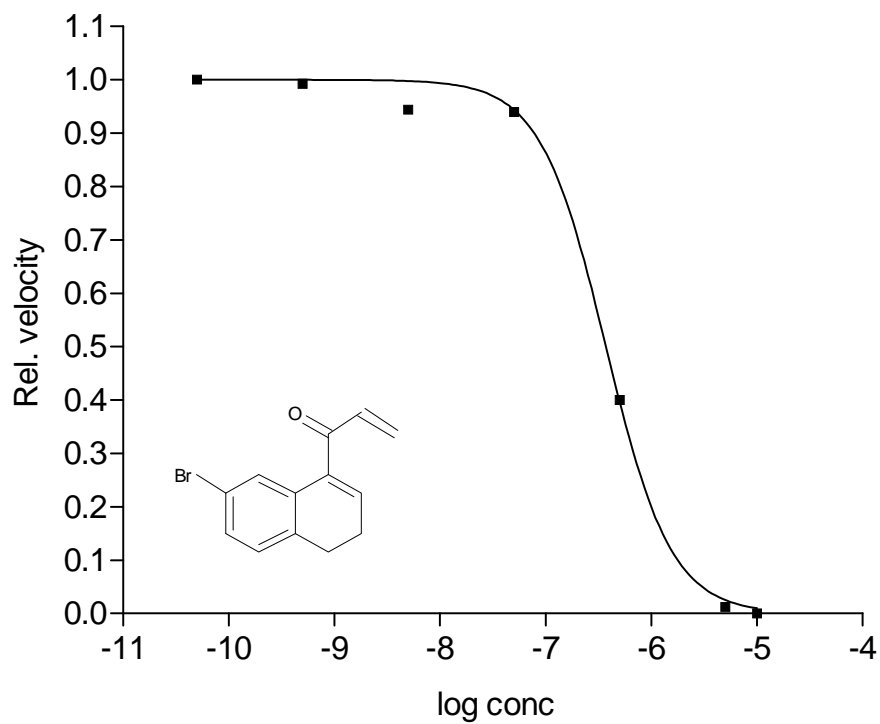
0.02989

Sy.x

0.07732

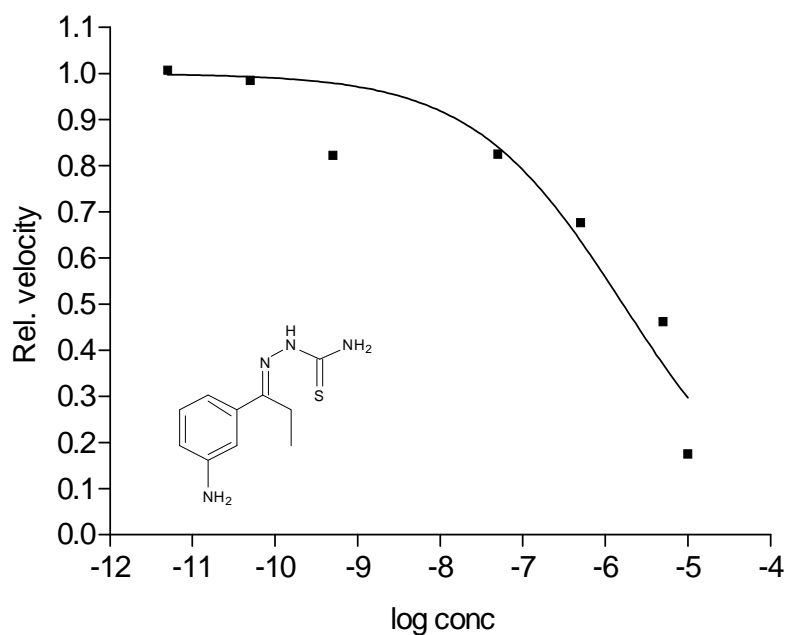
conc [M]	velocity
0.0	3753.0
5.0e-011	3828.0
5.0e-008	3647.0
5.0e-010	3769.0
5.0e-007	1380.0
5.0e-009	3579.5
5.0e-006	769.7
1.0e-005	63.4

Figure A20. IC50 Determination of Compound 11.



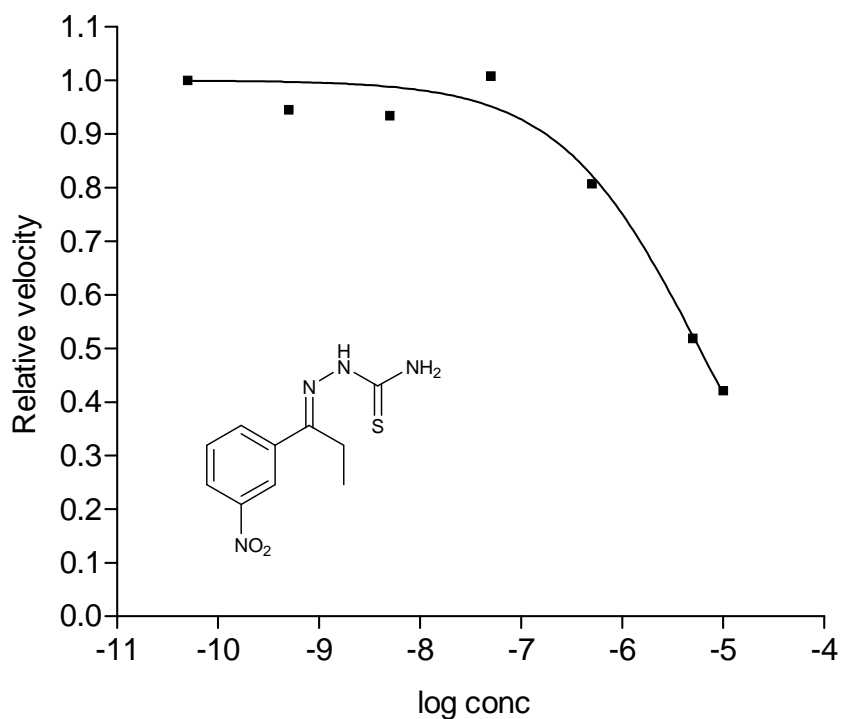
Sigmoidal dose-response (variable slope)		conc [M]	velocity
Best-fit values		0.00	4583.0
BOTTOM	0.0	5.00e-011	4445.0
TOP	1.000	5.00e-008	4179.0
LOGEC50	-6.430	5.00e-010	4413.0
HILLSLOPE	-1.406	5.00e-007	1780.0
EC50	3.718e-007	5.00e-009	4197.0
Std. Error		5.00e-006	54.0
LOGEC50	0.03402	1.00e-005	0.0
HILLSLOPE	0.1851		
95% Confidence Intervals			
LOGEC50	-6.517 to -6.342		
HILLSLOPE	-1.882 to -0.9300		
EC50	3.040e-007 to 4.548e-007		
Goodness of Fit			
Degrees of Freedom	5		
R ²	0.9975		
Absolute Sum of Squares	0.003201		
Sy.x	0.02530		

Figure A21. IC50 Determination of Compound 4.



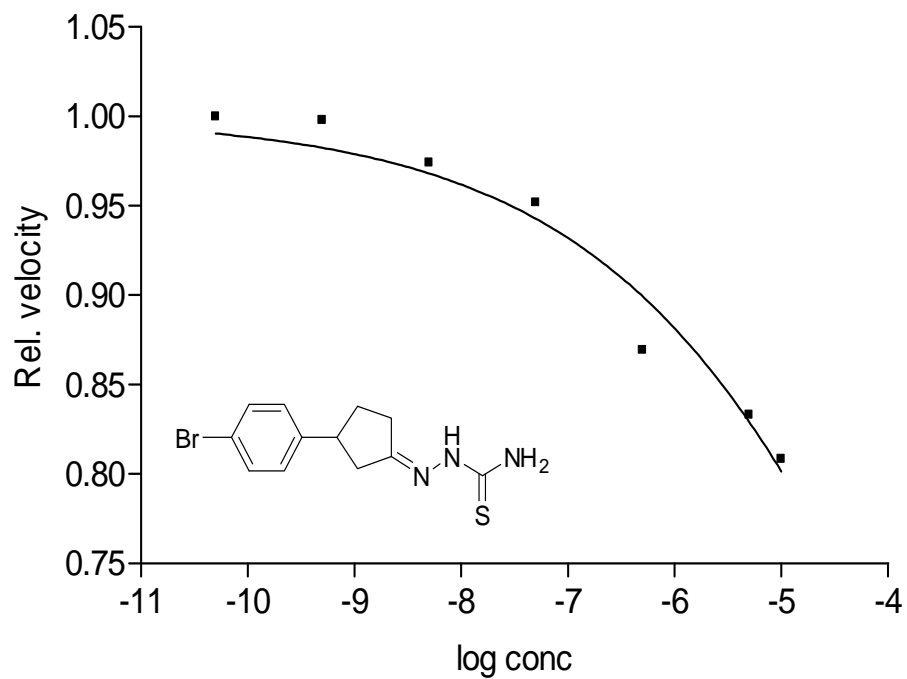
Sigmoidal dose-response (variable slope)		0.00	4546.0
Best-fit values		5.00e-012	4581.0
BOTTOM	0.0	5.00e-011	4482.0
TOP	1.000	5.00e-008	3755.0
LOGEC50	-5.786	5.00e-010	3742.0
HILLSLOPE	-0.4766	5.00e-007	3078.0
EC50	1.638e-006	5.00e-009	2710.0
Std. Error		5.00e-006	2102.0
LOGEC50	0.2206	1.00e-005	796.0
HILLSLOPE	0.1361		
95% Confidence Intervals			
LOGEC50	-6.353 to -5.219		
HILLSLOPE	-0.8265 to -0.1267		
EC50	4.436e-007 to 6.046e-006		
Goodness of Fit			
Degrees of Freedom	5		
R ²	0.9079		
Absolute Sum of Squares	0.04969		
Sy.x	0.09968		

Figure A22. IC50 Determination of Compound 6.



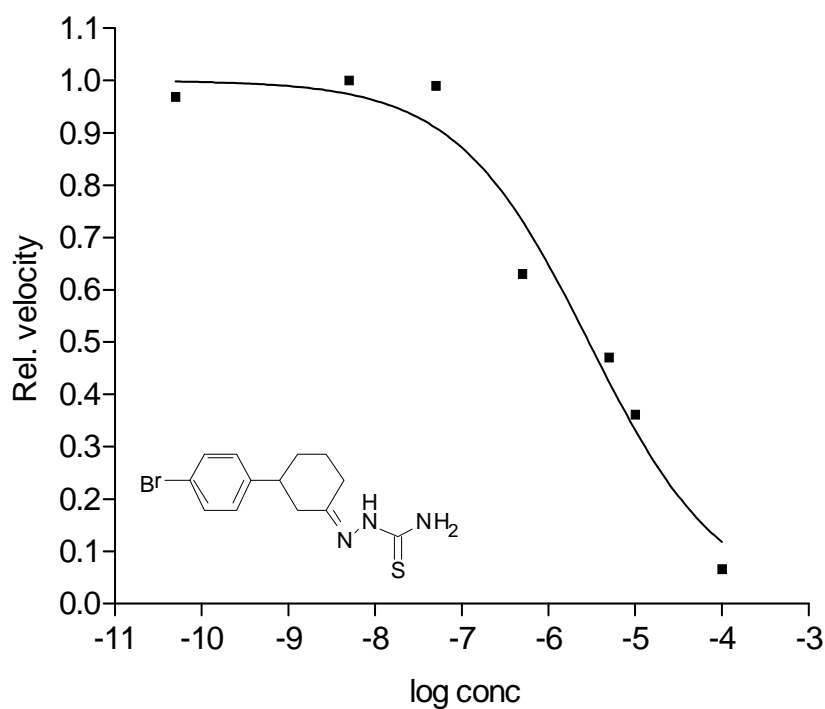
Sigmoidal dose-response (variable slope)		conc [M]	velocity
Best-fit values		0.00	4426.0
BOTTOM	0.0	5.00e-011	4123.0
TOP	1.000	5.00e-010	3899.0
LOGEC50	-5.237	5.00e-009	3853.0
HILLSLOPE	-0.6271	5.00e-008	4157.0
EC50	5.793e-006	5.00e-007	3329.0
Std. Error		5.00e-006	2140.0
LOGEC50	0.07972	1.00e-005	1737.0
HILLSLOPE	0.09751		
95% Confidence Intervals			
LOGEC50	-5.442 to -5.032		
HILLSLOPE	-0.8778 to -0.3765		
EC50	3.614e-006 to 9.287e-006		
Goodness of Fit			
Degrees of Freedom	5		
R ²	0.9737		
Absolute Sum of Squares	0.009059		
Sy.x	0.04256		

Figure A23. IC50 Determination of Compound 5.



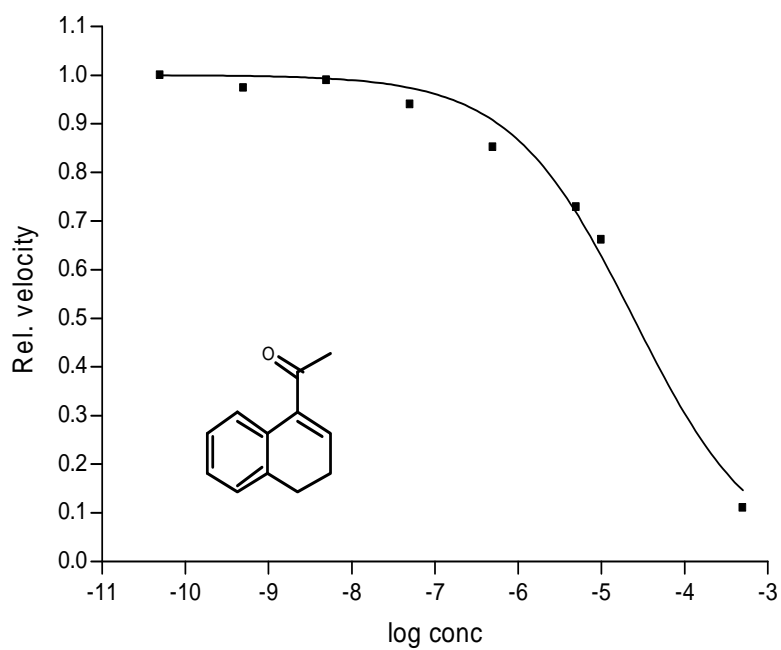
Goodness of Fit			
Degrees of Freedom	3		
R ²	0.9919	conc [M]	velocity
Absolute Sum of Squares	0.0003159	0.000	4433.0
Sy.x	0.01026	5.000e-011	3993.0
		5.000e-010	3985.0
		5.000e-009	3890.0
Equation 2		5.000e-008	3801.0
Best-fit values		5.000e-007	3471.0
BOTTOM	0.0	5.000e-006	3327.0
TOP	1.000	1.000e-005	3229.0
LOGEC50	-2.717		
HILLSLOPE	-0.2654		
EC50	0.001919		
Std. Error			
LOGEC50	0.4211		
HILLSLOPE	0.03878		
95% Confidence Intervals			
LOGEC50	-3.800 to -1.634		
HILLSLOPE	-0.3651 to -0.1657		

Figure A24. IC50 Determination of Compound 14.



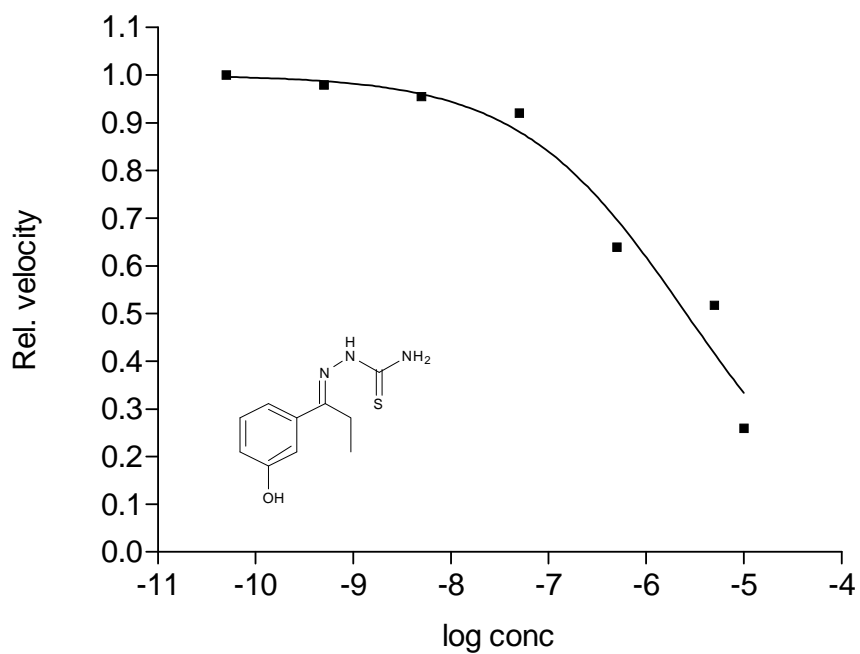
Sigmoidal dose-response (variable slope)		conc [M]	velocity
Best-fit values		0.000	3902.0
BOTTOM	0.0	5.000e-011	3723.0
TOP	1.000	5.000e-010	3272.0
LOGEC50	-5.536	5.000e-009	3843.0
HILLSLOPE	-0.5684	5.000e-008	3804.0
EC50	2.912e-006	5.000e-007	2421.0
Std. Error		5.000e-006	1809.0
LOGEC50	0.1311	1.000e-005	1390.0
HILLSLOPE	0.1001	1.000e-004	254.0
95% Confidence Intervals			
LOGEC50	-5.873 to -5.199		
HILLSLOPE	-0.8258 to -0.3109		
EC50	1.340e-006 to 6.326e-006		
Goodness of Fit			
Degrees of Freedom	5		
R ²	0.9698		
Absolute Sum of Squares	0.02406		
Sy.x	0.06937		

Figure A25. IC50 Determination of Compound 15.



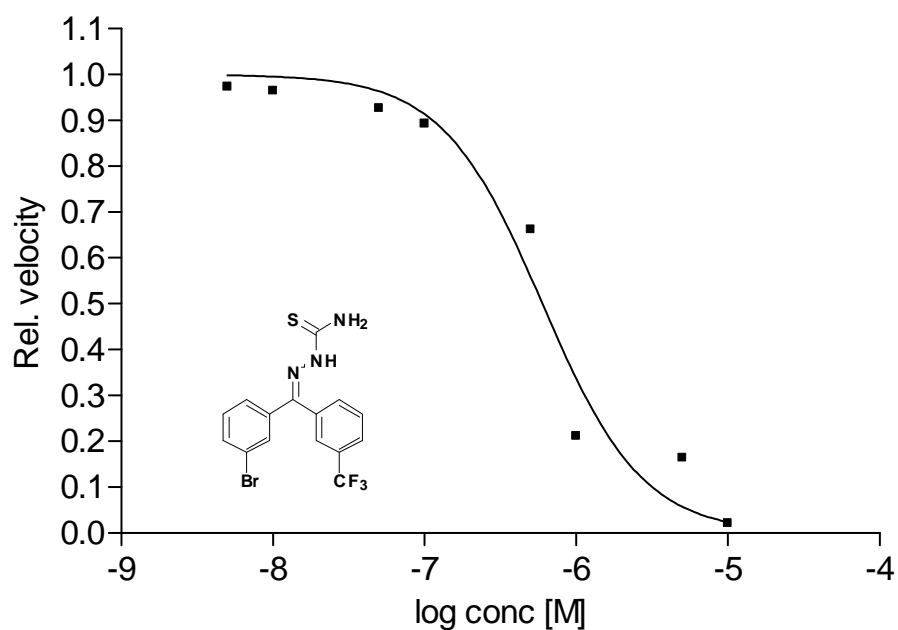
Sigmoidal dose-response (variable slope)		conc [M]	velocity
Best-fit values		0.00	4483.0
BOTTOM	0.0	5.00e-011	4148.0
TOP	1.000	5.00e-010	4037.0
LOGEC50	-4.612	5.00e-009	4104.0
HILLSLOPE	-0.5844	5.00e-008	3896.0
EC50	2.444e-005	5.00e-007	3532.0
Std. Error		5.00e-006	3020.0
LOGEC50	0.08432	1.00e-005	2742.0
HILLSLOPE	0.06000	5.00e-004	457.0
95% Confidence Intervals			
LOGEC50	-4.818 to -4.405		
HILLSLOPE	-0.7312 to -0.4376		
EC50	1.520e-005 to 3.931e-005		
Goodness of Fit			
Degrees of Freedom	6		
R ²	0.9881		
Absolute Sum of Squares	0.007425		
Sy.x	0.03518		

Figure A26. IC50 Determination of Compound 12.



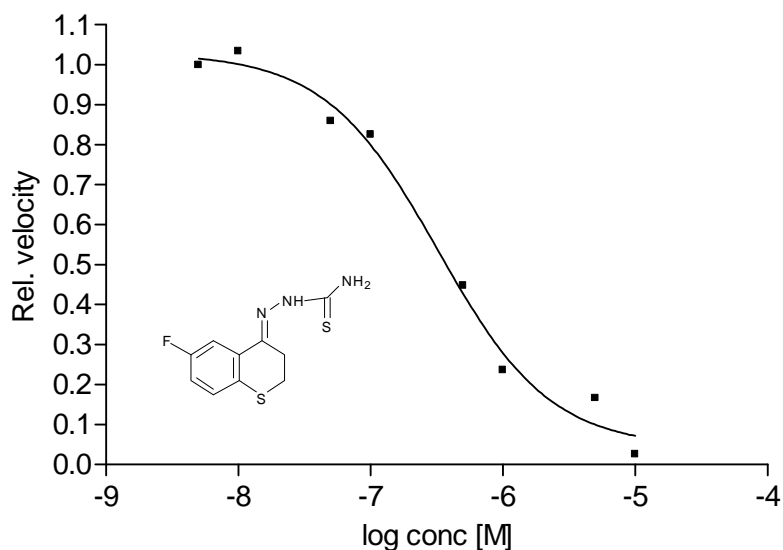
Sigmoidal dose-response (variable slope)		conc [M]	velocity
Best-fit values		0.0	4551.0
BOTTOM	0.0	5.0e-011	3662.0
TOP	1.000	5.0e-010	3586.0
LOGEC50	-5.591	5.0e-009	3497.0
HILLSLOPE	-0.5096	5.0e-008	3372.0
EC50	2.567e-006	5.0e-007	2341.0
Std. Error		5.0e-006	1896.0
LOGEC50	0.1354	1.0e-005	951.0
HILLSLOPE	0.09363		
95% Confidence Intervals			
LOGEC50	-5.939 to -5.242		
HILLSLOPE	-0.7503 to -0.2689		
EC50	1.152e-006 to 5.723e-006		
Goodness of Fit			
Degrees of Freedom	5		
R ²	0.9578		
Absolute Sum of Squares	0.02078		
Sy.x	0.06447		

Figure A27. IC50 Determination of Compound 7.



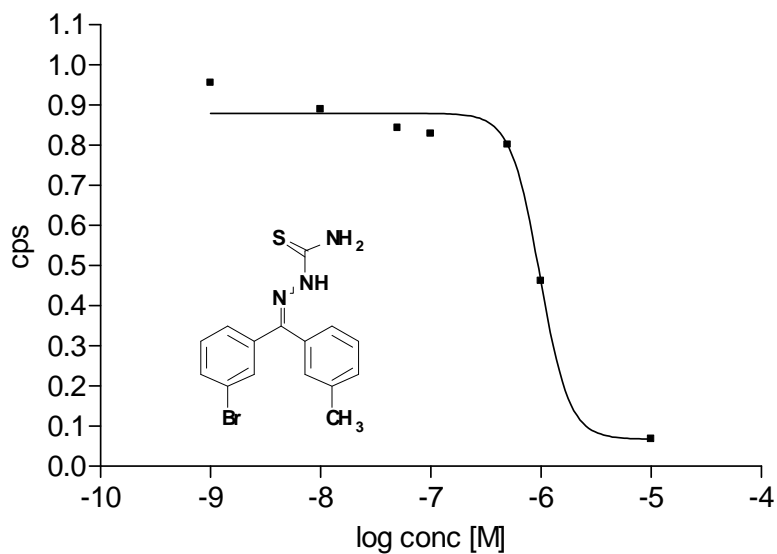
Data Set-A	
Sigmoidal dose-response (variable slope)	
Best-fit values	
BOTTOM	0.0
TOP	1.000
LOGEC50	-6.223
HILLSLOPE	-1.318
EC50	5.988e-007
Std. Error	
LOGEC50	0.07853
HILLSLOPE	0.3358
95% Confidence Intervals	
LOGEC50	-6.415 to -6.031
HILLSLOPE	-2.139 to -0.4959
EC50	3.847e-007 to 9.320e-007
Goodness of Fit	
Degrees of Freedom	6
R ²	0.9642
Absolute Sum of Squares	0.04099
Sy.x	0.08265
Constraints	
BOTTOM	BOTTOM = 0.0
TOP	TOP = 1.000
Data	
Number of X values	9
Number of Y replicates	1
Total number of values	8
Number of missing values	1

Figure A28. IC50 Determination of Compound 31.



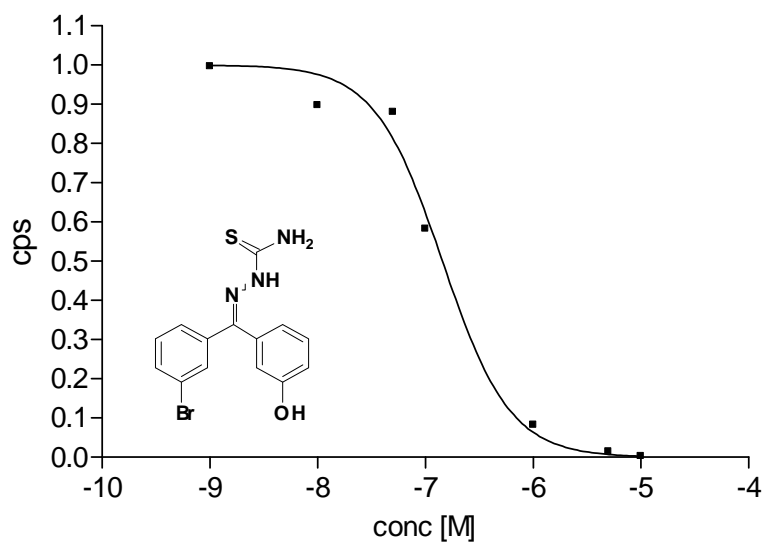
	velocity	conc [M]	velocity
Sigmoidal dose-response (variable slope)		0.0	6996.0
Best-fit values		5.0e-009	6992.0
BOTTOM	0.04307	1.0e-008	7238.0
TOP	1.029	5.0e-008	6013.0
LOGEC50	-6.492	1.0e-007	5775.0
HILLSLOPE	-1.019	5.0e-007	3135.0
EC50	3.220e-007	1.0e-006	1655.0
Std. Error		5.0e-006	1165.0
BOTTOM	0.06170	1.0e-005	184.8
TOP	0.05236		
LOGEC50	0.1071		
HILLSLOPE	0.2350		
95% Confidence Intervals		conc [M]	velocity
BOTTOM	-0.1282 to 0.2144		1.000
TOP	0.8841 to 1.175	-8.301	0.999
LOGEC50	-6.789 to -6.195	-8.000	1.035
HILLSLOPE	-1.672 to -0.3672	-7.301	0.859
EC50	1.624e-007 to 6.386e-007	-7.000	0.825
Goodness of Fit		-6.301	0.448
Degrees of Freedom	4	-6.000	0.237
R ²	0.9890	-5.301	0.167
Absolute Sum of Squares	0.01250	-5.000	0.026
Sy.x	0.05591		
Data			
Number of X values	9		
Number of Y replicates	1		
Total number of values	8		
Number of missing values	1		

Figure A29. IC50 Determination of Compound 25.



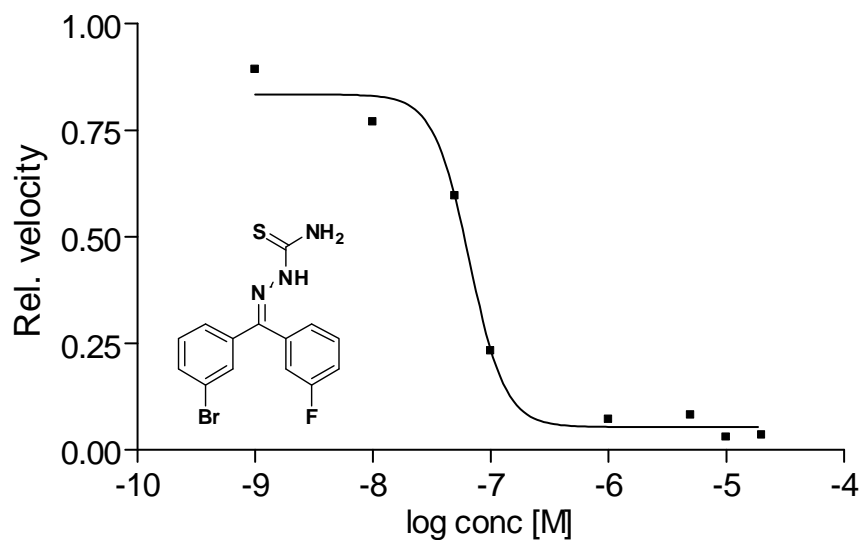
	Velocity	conc [M]	Velocity
Sigmoidal dose-response (variable slope)		0.000000	4807.0
Best-fit values		1.000000e-009	4593.0
BOTTOM	0.06770	1.000000e-008	4273.0
TOP	0.8794	5.000000e-008	4053.0
LOGEC50	-6.008	1.000000e-007	3983.0
HILLSLOPE	-3.299	5.000000e-007	3853.0
EC50	9.824e-007	0.000001	2218.0
Std. Error		0.000010	327.6
BOTTOM	0.05713		
TOP	0.02861		
LOGEC50	0.04205		
HILLSLOPE	1.303		
95% Confidence Intervals			
BOTTOM	0.0 to 0.2495	-9.000	0.955
TOP	0.7883 to 0.9704	-8.000	0.889
LOGEC50	-6.142 to -5.874	-7.301	0.843
HILLSLOPE	-7.444 to 0.8471	-7.000	0.829
EC50	7.219e-007 to 1.337e-006	-6.301	0.802
EC50		-6.000	0.461
EC50		-5.000	0.068
Goodness of Fit			
Degrees of Freedom	3		
R ²	0.9839		
Absolute Sum of Squares	0.009730		
Sy.x	0.05695		
Constraints			
BOTTOM	BOTTOM > 0.0		
TOP	TOP < 1.000		
Data			

Figure A30. IC50 Determination of Compound 35.



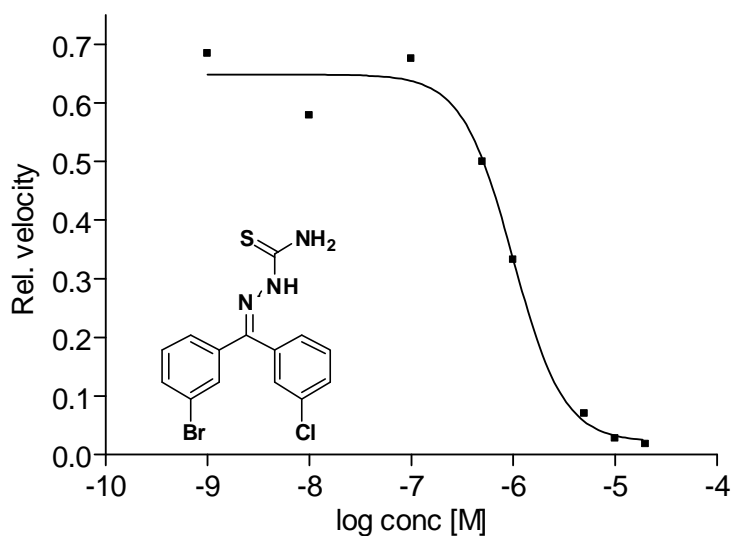
Sigmoidal dose-response (variable slope)		conc [M]	Velocity
Best-fit values		0.000000	8596.00
BOTTOM	0.0	1.000000e-009	8564.00
TOP	1.000	1.000000e-008	7709.00
LOGEC50	-6.842	5.000000e-008	7564.00
HILLSLOPE	-1.386	1.000000e-007	5010.00
EC50	1.440e-007	0.000001	710.30
Std. Error		0.000005	127.50
LOGEC50	0.06913	0.000010	24.28
HILLSLOPE	0.2788		
95% Confidence Intervals			
LOGEC50	-7.019 to -6.664		
HILLSLOPE	-2.103 to -0.6693		
EC50	9.563e-008 to 2.168e-007		
Goodness of Fit			
Degrees of Freedom	5		
R ²	0.9894		
Absolute Sum of Squares	0.01288		
Sy.x	0.05076		
Constraints			
BOTTOM	BOTTOM = 0.0		
TOP	TOP = 1.000		
Data			
Number of X values	8		
Number of Y replicates	1		
Total number of values	7		
Number of missing values	1		

Figure A31. IC50 Determination of Compound 37.



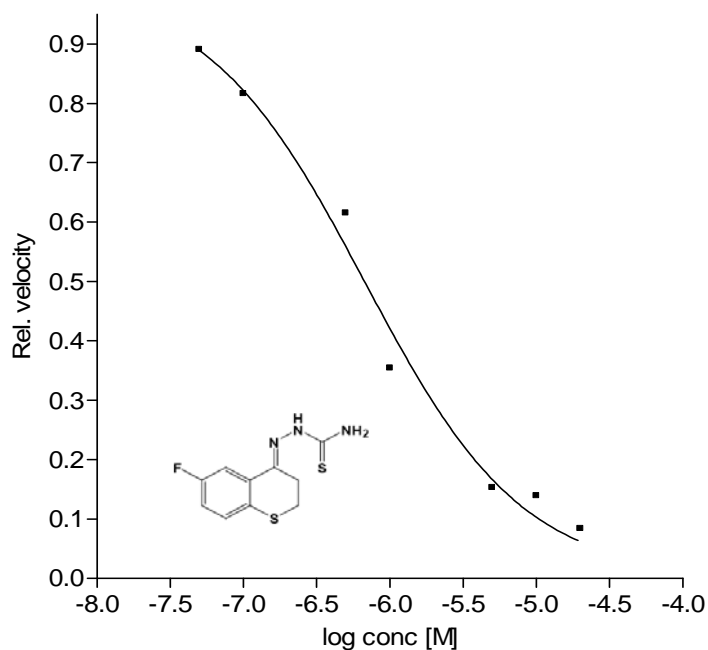
	velocity	conc [M]	velocity
Sigmoidal dose-response (variable slope)		0.000000	1.000000
Best-fit values		1.000000e-009	0.893059
BOTTOM	0.05382	1.000000e-008	0.769069
TOP	0.8340	5.000000e-008	0.596369
LOGEC50	-7.180	1.000000e-007	0.232149
HILLSLOPE	-2.870	0.000001	0.071117
EC50	6.607e-008	0.000005	0.081368
Std. Error		0.000010	0.029824
BOTTOM	0.02412	0.000020	0.035049
TOP	0.03478		
LOGEC50	0.03940		
HILLSLOPE	0.6794		
95% Confidence Intervals			
BOTTOM	-0.01312 to 0.1208		1.000
TOP	0.7374 to 0.9305	-9.000	0.893
LOGEC50	-7.289 to -7.071	-8.000	0.769
HILLSLOPE	-4.756 to -0.9845	-7.301	0.596
EC50	5.136e-008 to 8.499e-008	-7.000	0.232
Goodness of Fit		-6.000	0.071
Degrees of Freedom	4	-5.301	0.081
R ²	0.9896	-5.000	0.030
Absolute Sum of Squares	0.009277	-4.699	0.035
Sy.x	0.04816		
Data			
Number of X values	9		
Number of Y replicates	1		
Total number of values	8		

Figure A32. IC50 Determination of Compound 32.



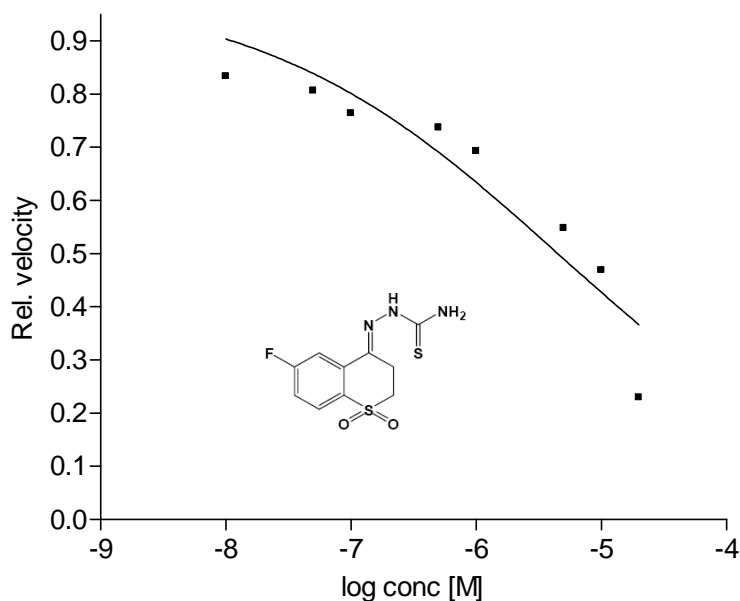
	velocity	conc [M]	velocity
Sigmoidal dose-response (variable slope)		0.000000	1.000000
Best-fit values		1.000000e-009	0.684432
BOTTOM	0.02139	1.000000e-008	0.578947
TOP	0.6486	1.000000e-007	0.675679
LOGEC50	-6.001	5.000000e-007	0.499501
HILLSLOPE	-1.748	0.000001	0.332632
EC50	9.971e-007	0.000005	0.070006
Std. Error		0.000010	0.027490
BOTTOM	0.03547	0.000020	0.018094
TOP	0.02725		
LOGEC50	0.07923	conc [M]	velocity
HILLSLOPE	0.6290		1.000
95% Confidence Intervals		-9.000	0.684
BOTTOM	-0.07707 to 0.1199	-8.000	0.579
TOP	0.5730 to 0.7243	-7.000	0.676
LOGEC50	-6.221 to -5.781	-6.301	0.500
HILLSLOPE	-3.494 to -0.002136	-6.000	0.333
EC50	6.009e-007 to 1.655e-006	-5.301	0.070
Goodness of Fit		-5.000	0.027
Degrees of Freedom	4	-4.699	0.018
R ²	0.9866		
Absolute Sum of Squares	0.007830		
Sy.x	0.04424		
Data			
Number of X values	9		
Number of Y replicates	1		
Total number of values	8		

Figure A33. IC50 Determination of Compound 33.



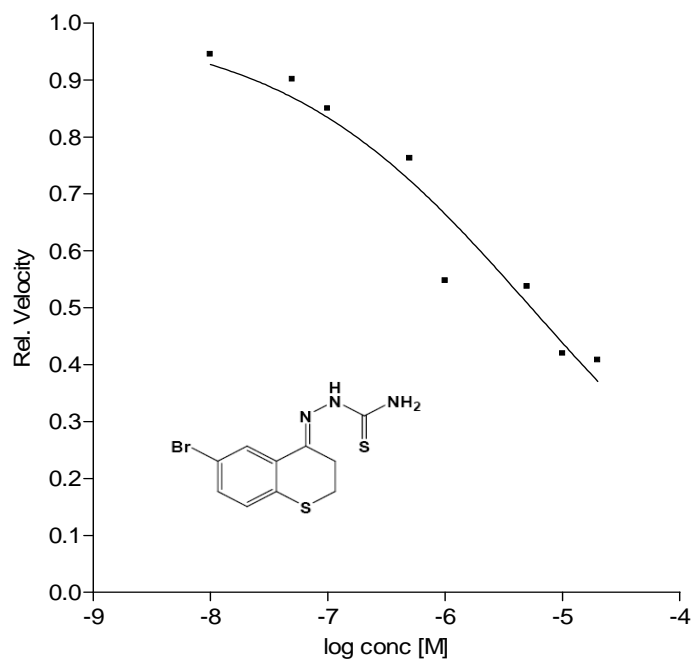
	Velocity	conc [M]	Velocity
Sigmoidal dose-response (variable slope)		0.000000	6131.0
Best-fit values		5.000000e-008	5461.0
BOTTOM	0.0	1.000000e-007	5004.0
TOP	1.000	5.000000e-007	3773.0
LOGEC50	-6.174	0.000001	2171.0
HILLSLOPE	-0.8018	0.000005	937.7
EC50	6.703e-007	0.000010	851.3
Std. Error		0.000020	513.0
LOGEC50	0.05576		
HILLSLOPE	0.07579		
95% Confidence Intervals		conc [M]	Velocity
LOGEC50	-6.317 to -6.030		1.000
HILLSLOPE	-0.9967 to -0.6069	-7.301030	0.891
EC50	4.818e-007 to 9.324e-007	-7.000000	0.816
Goodness of Fit		-6.301030	0.615
Degrees of Freedom	5	-6.000000	0.354
R ²	0.9859	-5.301030	0.153
Absolute Sum of Squares	0.009646	-5.000000	0.139
Sy.x	0.04392	-4.698970	0.084
Constraints			
BOTTOM	BOTTOM = 0.0		
TOP	TOP = 1.000		
Data			
Number of X values	8		
Number of Y replicates	1		
Total number of values	7		
Number of missing values	1		

Figure A34. IC50 Determination of Compound 39.



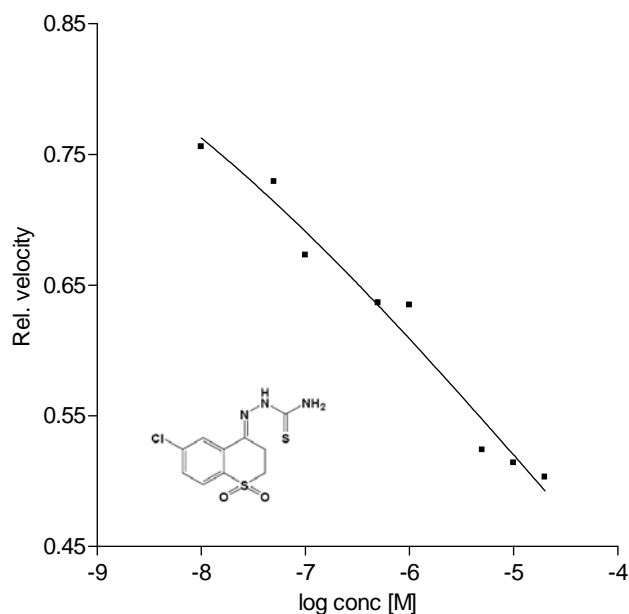
Sigmoidal dose-response (variable slope)		conc [M]	Velocity
Best-fit values		0.000000	6285.0
BOTTOM	0.0	1.000000e-008	5240.0
TOP	1.000	5.000000e-008	5070.0
LOGEC50	-5.348	1.000000e-007	4799.0
HILLSLOPE	-0.3665	5.000000e-007	4631.0
EC50	4.487e-006	0.000001	4353.0
Std. Error		0.000005	3444.0
LOGEC50	0.1753	0.000010	2948.0
HILLSLOPE	0.06857	0.000020	1445.0
95% Confidence Intervals			
LOGEC50	-5.777 to -4.919		
HILLSLOPE	-0.5343 to -0.1987		
EC50	1.671e-006 to 1.205e-005		
Goodness of Fit			
Degrees of Freedom	6		
R ²	0.8774		
Absolute Sum of Squares	0.03659		
Sy.x	0.07809		
Constraints			
BOTTOM	BOTTOM = 0.0		
TOP	TOP = 1.000		
Data			
Number of X values	9		
Number of Y replicates	1		
Total number of values	8		
Number of missing values	1		

Figure A35. IC50 Determination of Compound 40.



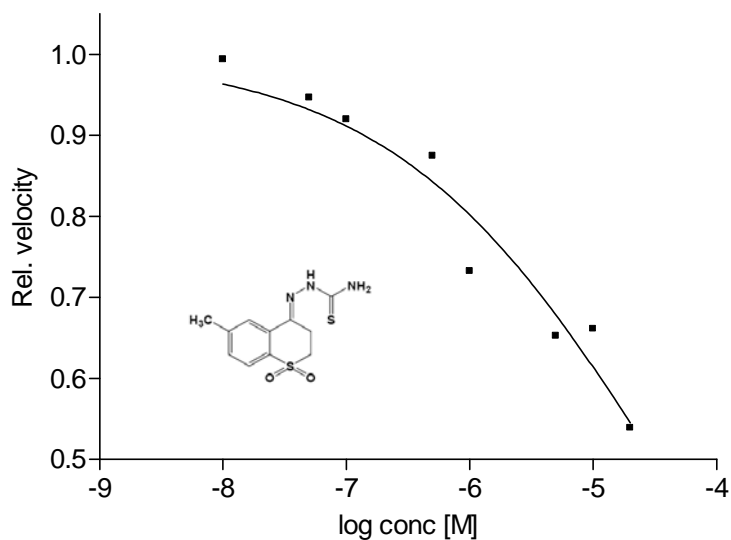
Sigmoidal dose-response (variable slope)		conc [M]	Velocity
Best-fit values		0.000000	6062
BOTTOM	0.0	1.000000e-008	5731
TOP	1.000	5.000000e-008	5465
LOGEC50	-5.267	1.000000e-007	5153
HILLSLOPE	-0.4045	5.000000e-007	4620
EC50	5.408e-006	0.000001	3317
Std. Error		0.000005	3257
LOGEC50	0.1204	0.000010	2542
HILLSLOPE	0.05521	0.000020	2472
95% Confidence Intervals			
LOGEC50	-5.562 to -4.972		
HILLSLOPE	-0.5396 to -0.2694		
EC50	2.745e-006 to 1.066e-005		
Goodness of Fit		conc [M]	Velocity
Degrees of Freedom	6	-8.000	1.000
R ²	0.9420	-7.301	0.902
Absolute Sum of Squares	0.01942	-7.000	0.850
Sy.x	0.05689	-6.301	0.762
Constraints		-6.000	0.547
BOTTOM	BOTTOM = 0.0	-5.301	0.537
TOP	TOP = 1.000	-5.000	0.419
Data		-4.699	0.408
Number of X values	9		
Number of Y replicates	1		
Total number of values	8		
Number of missing values	1		

Figure A36. IC50 Determination of Compound 41.



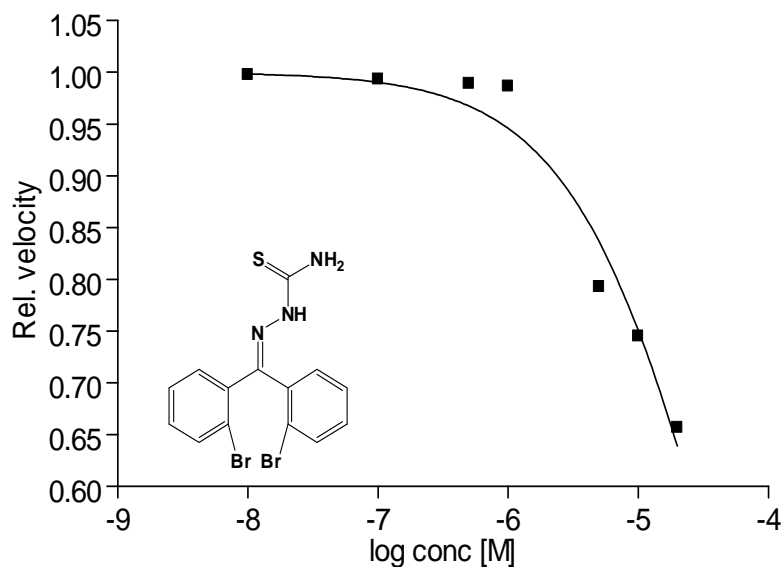
		conc [M]	Velocity
Sigmoidal dose-response (variable slope)		0.000000	5849
Best-fit values			
BOTTOM	0.0	1.000000e-008	4421
TOP	1.000	5.000000e-008	4265
LOGEC50	-4.779	1.000000e-007	3936
HILLSLOPE	-0.1574	5.000000e-007	3722
EC50	1.663e-005	0.000001	3713
Std. Error		0.000005	3065
LOGEC50	0.1185	0.000010	3007
HILLSLOPE	0.01170	0.000020	2942
95% Confidence Intervals			
LOGEC50	-5.069 to -4.489		
HILLSLOPE	-0.1861 to -0.1288		
EC50	8.525e-006 to 3.242e-005		
Goodness of Fit			
Degrees of Freedom	6		
R ²	0.9711		
Absolute Sum of Squares	0.001962		
Sy.x	0.01808		
Constraints			
BOTTOM	BOTTOM = 0.0		
TOP	TOP = 1.000		
Data			
Number of X values	9		
Number of Y replicates	1		
Total number of values	8		
Number of missing values	1		

Figure A37. IC50 Determination of Compound 42.



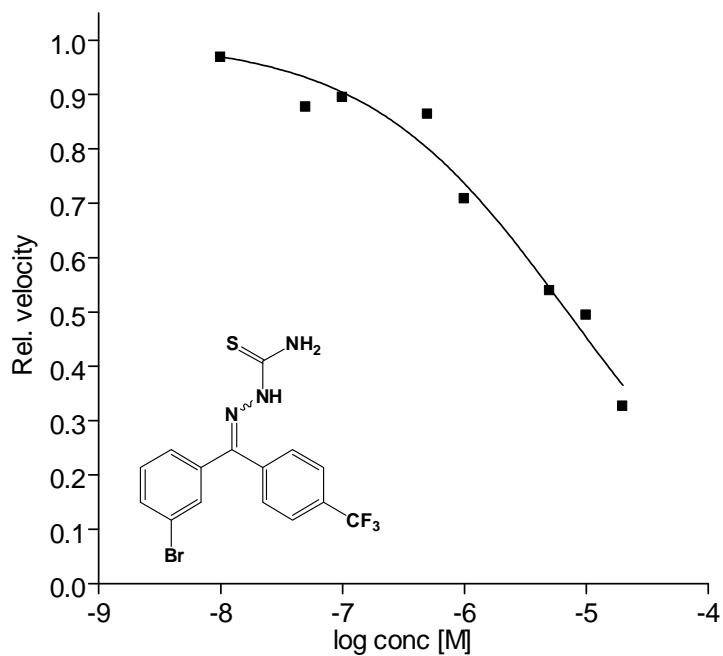
Sigmoidal dose-response (variable slope)		conc [M]	Velocity
Best-fit values		0.000000	5579.0
BOTTOM	0.0	1.000000e-008	5544.0
TOP	1.000	5.000000e-008	5282.0
LOGEC50	-4.504	1.000000e-007	5131.0
HILLSLOPE	-0.4057	5.000000e-007	4879.0
EC50	3.133e-005	0.000001	4085.0
Std. Error		0.000005	3640.0
LOGEC50	0.1457	0.000010	3689.0
HILLSLOPE	0.05572	0.000020	3008.0
95% Confidence Intervals			
LOGEC50	-4.861 to -4.148		
HILLSLOPE	-0.5421 to -0.2693		
EC50	1.378e-005 to 7.120e-005		
Goodness of Fit		conc [M]	Velocity
Degrees of Freedom	6		1.000
R ²	0.9478	-8.000	0.994
Absolute Sum of Squares	0.01002	-7.301	0.947
Sy.x	0.04086	-7.000	0.920
Constraints		-6.301	0.875
BOTTOM	BOTTOM = 0.0	-6.000	0.732
TOP	TOP = 1.000	-5.301	0.652
Data		-5.000	0.661
Number of X values	9	-4.699	0.539
Number of Y replicates	1		
Total number of values	8		
Number of missing values	1		

Figure A38. IC50 Determination of Compound 43.



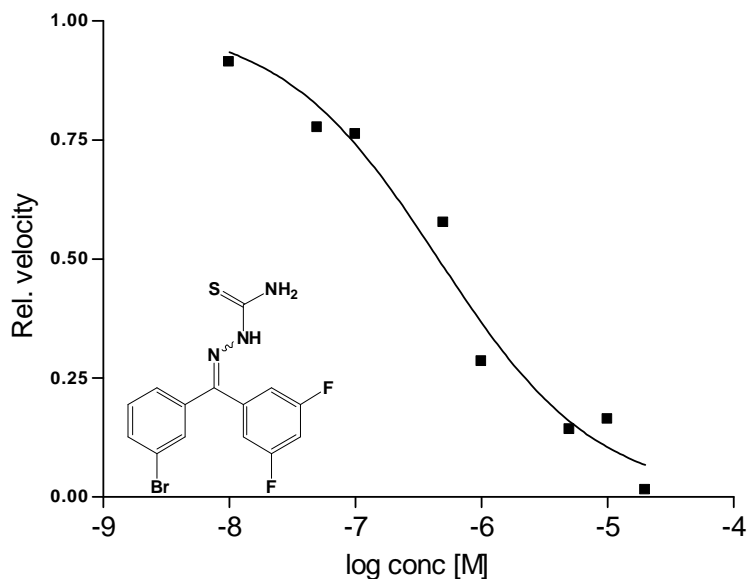
Best-fit values		conc [M]	vel
BOTTOM	0.0		1.000
TOP	1.000	-8.000	0.998
LOGEC50	-4.374	-7.000	0.993
HILLSLOPE	-0.7643	-6.301	0.989
EC50	4.223e-005	-6.000	0.986
Std. Error		-5.301	0.793
LOGEC50	0.1046	-5.000	0.745
HILLSLOPE	0.1229	-4.699	0.657
95% Confidence Intervals			
LOGEC50	-4.643 to -4.106		
HILLSLOPE	-1.080 to -0.4483		
EC50	2.274e-005 to 7.842e-005		
Goodness of Fit		conc [M]	vel
Degrees of Freedom	5	0.000000	5481.0
R ²	0.9653	1.000000e-008	5469.3
Absolute Sum of Squares	0.004356	1.000000e-007	5445.0
Sy.x	0.02952	5.000000e-007	5421.6
Constraints		0.000001	5406.3
BOTTOM	BOTTOM = 0.0	0.000005	4345.2
TOP	TOP = 1.000	0.000010	4086.0
		0.000020	3600.0

Figure A39. IC50 Determination of Compound 45.



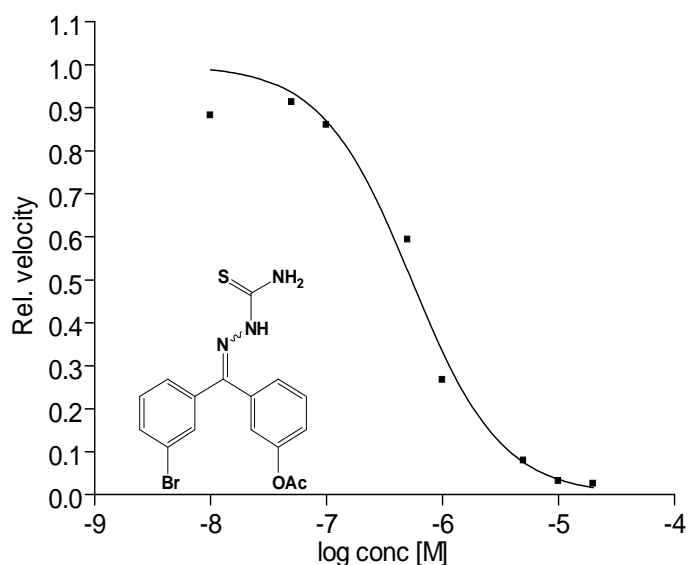
Best-fit values		conc [M]	vel
BOTTOM	0.0		1.000
TOP	1.000	-8.000	0.968
LOGEC50	-5.154	-7.301	0.877
HILLSLOPE	-0.5280	-7.000	0.895
EC50	7.011e-006	-6.301	0.864
Std. Error		-6.000	0.708
LOGEC50	0.07443	-5.301	0.539
HILLSLOPE	0.05566	-5.000	0.494
95% Confidence Intervals		-4.699	0.327
LOGEC50	-5.336 to -4.972		
HILLSLOPE	-0.6642 to -0.3918	conc [M]	vel
EC50	4.609e-006 to 1.066e-005	0.000000	5673.6
Goodness of Fit		1.000000e-008	5494.5
Degrees of Freedom	6	5.000000e-008	4975.2
R ²	0.9709	1.000000e-007	5076.9
Absolute Sum of Squares	0.01092	5.000000e-007	4900.5
Sy.x	0.04267	0.000001	4018.5
Constraints		0.000005	3058.2
BOTTOM	BOTTOM = 0.0	0.000010	2802.6
TOP	TOP = 1.000	0.000020	1854.0

Figure A40. IC50 Determination of Compound 44.



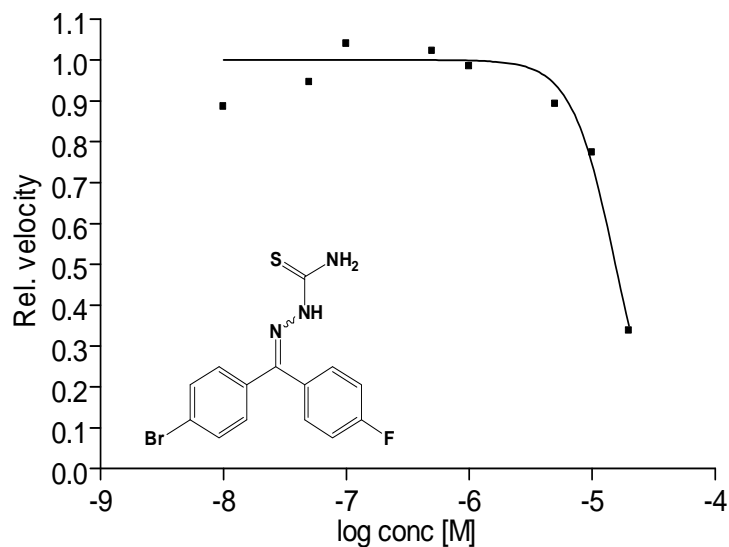
Best-fit values		conc [M]	vel
BOTTOM	0.0		1.000
TOP	1.000	-8.000	0.914
LOGEC50	-6.341	-7.301	0.777
HILLSLOPE	-0.6947	-7.000	0.762
EC50	4.563e-007	-6.301	0.577
Std. Error		-6.000	0.285
LOGEC50	0.08790	-5.301	0.142
HILLSLOPE	0.08904	-5.000	0.164
95% Confidence Intervals		-4.699	0.015
LOGEC50	-6.556 to -6.126		
HILLSLOPE	-0.9126 to -0.4768	conc [M]	vel
EC50	2.781e-007 to 7.488e-007	0.000000	4889.7
Goodness of Fit		1.000000e-008	4470.3
Degrees of Freedom	6	5.000000e-008	3798.0
R ²	0.9702	1.000000e-007	3726.9
Absolute Sum of Squares	0.02470	5.000000e-007	2819.7
Sy.x	0.06417	0.000001	1393.2
Constraints		0.000005	696.4
BOTTOM	BOTTOM = 0.0	0.000010	800.1
TOP	TOP = 1.000	0.000020	75.6

Figure A41. IC50 Determination of Compound 49.



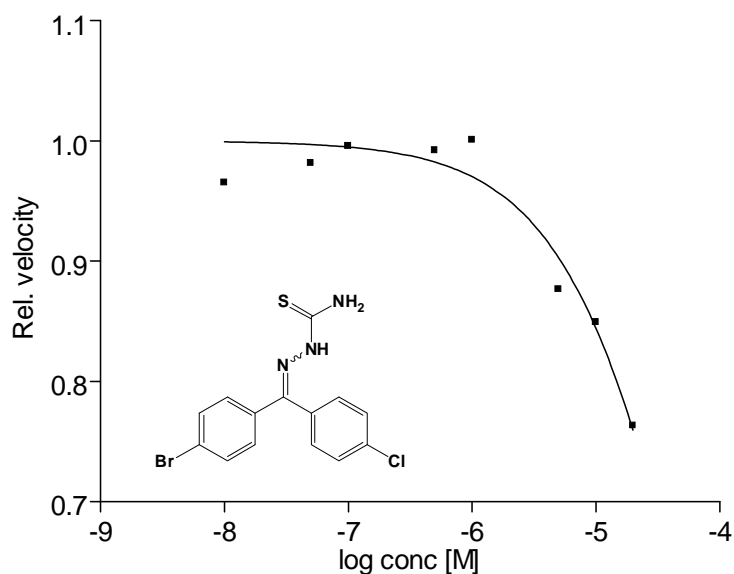
Best-fit values		conc [M]	vel
BOTTOM	0.0		1.000
TOP	1.000	-8.000	0.882
LOGEC50	-6.268	-7.301	0.913
HILLSLOPE	-1.123	-7.000	0.860
EC50	5.393e-007	-6.301	0.593
Std. Error		-6.000	0.267
LOGEC50	0.06359	-5.301	0.080
HILLSLOPE	0.1761	-5.000	0.032
95% Confidence Intervals		-4.699	0.026
LOGEC50	-6.424 to -6.113		
HILLSLOPE	-1.554 to -0.6917		
EC50	3.769e-007 to 7.717e-007		
Goodness of Fit		0.000000	5344.20
Degrees of Freedom	6	1.000000e-008	4712.40
R ²	0.9805	5.000000e-008	4877.10
Absolute Sum of Squares	0.02170	1.000000e-007	4596.30
Sy.x	0.06014	5.000000e-007	3170.70
Constraints		0.000001	1428.30
BOTTOM	BOTTOM = 0.0	0.000005	426.78
TOP	TOP = 1.000	0.000010	170.19
		0.000020	136.98

Figure A42. IC₅₀ Determination of Compound 50.



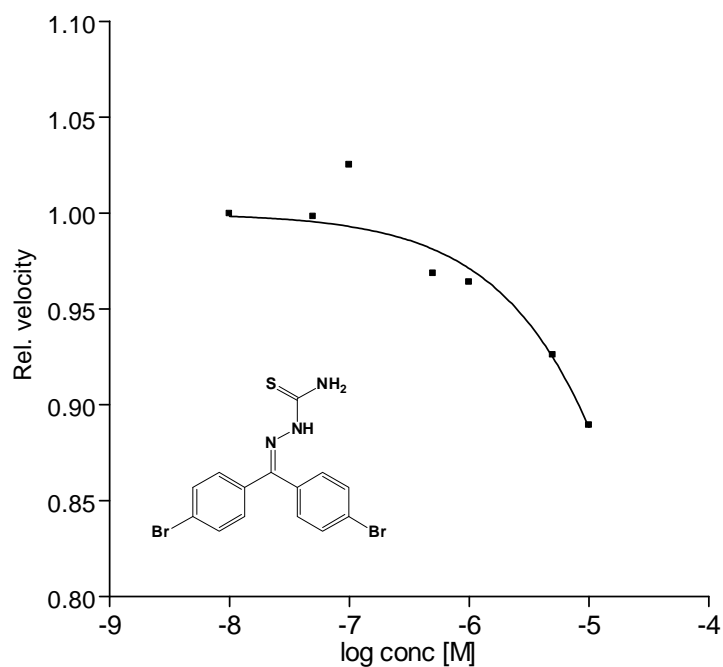
Best-fit values		conc [M]	vel
BOTTOM	0.0		1.000
TOP	1.000	-8.000	0.886
LOGEC50	-4.809	-7.301	0.946
HILLSLOPE	-2.438	-7.000	1.040
EC50	1.551e-005	-6.301	1.022
Std. Error		-6.000	0.984
LOGEC50	0.03592	-5.301	0.892
HILLSLOPE	0.5080	-5.000	0.773
95% Confidence Intervals		-4.699	0.338
LOGEC50	-4.897 to -4.721		
HILLSLOPE	-3.682 to -1.195		
EC50	1.267e-005 to 1.899e-005	conc [M]	vel
Goodness of Fit		0.000000	4171.2
Degrees of Freedom	6	1.000000e-008	3696.0
R ²	0.9407	5.000000e-008	3944.6
Absolute Sum of Squares	0.02153	1.000000e-007	4338.4
Sy.x	0.05991	5.000000e-007	4261.4
Constraints		0.000001	4106.3
BOTTOM	BOTTOM = 0.0	0.000005	3721.3
TOP	TOP = 1.000	0.000010	3226.3
		0.000020	1409.1

Figure A43. IC50 Determination of Compound 48.



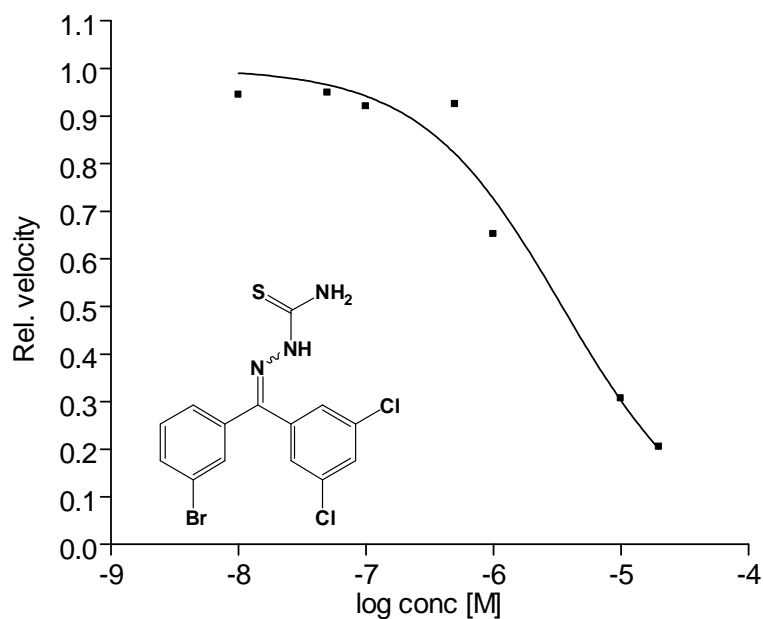
Best-fit values		conc [M]	vel
BOTTOM	0.0		1.000
TOP	1.000	-8.000	0.965
LOGEC50	-4.059	-7.301	0.982
HILLSLOPE	-0.7804	-7.000	0.996
EC50	8.725e-005	-6.301	0.992
Std. Error		-6.000	1.001
LOGEC50	0.1665	-5.301	0.877
HILLSLOPE	0.1482	-5.000	0.849
95% Confidence Intervals		-4.699	0.763
LOGEC50	-4.467 to -3.652		
HILLSLOPE	-1.143 to -0.4178	conc [M]	vel
EC50	3.414e-005 to 0.0002230	0.000000	4224.0
Goodness of Fit		1.000000e-008	4077.7
Degrees of Freedom	6	5.000000e-008	4145.9
R ²	0.9420	1.000000e-007	4205.3
Absolute Sum of Squares	0.003145	5.000000e-007	4191.0
Sy.x	0.02290	0.000001	4227.3
Constraints		0.000005	3702.6
BOTTOM	BOTTOM = 0.0	0.000010	3587.1
TOP	TOP = 1.000	0.000020	3224.1

Figure A44. IC50 Determination of Compound 47.



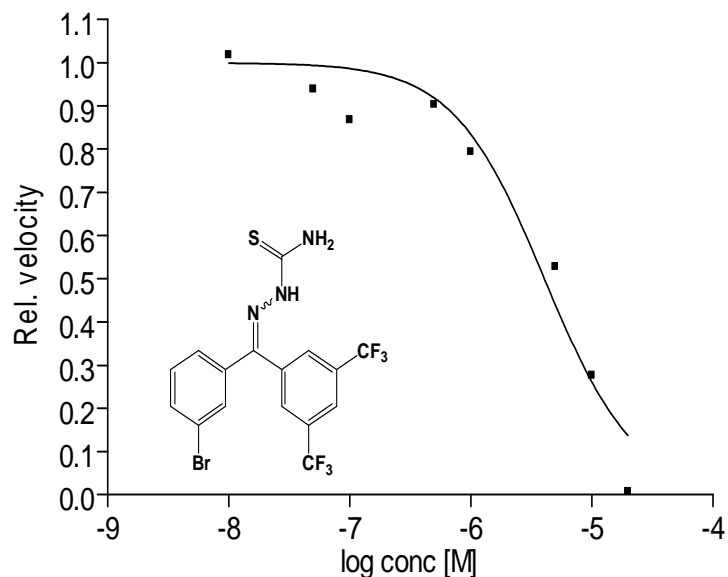
BOTTOM	0.0	conc [M]	Data Set-A
TOP	1.000	0.000000	4047.0
LOGEC50	-3.567	1.000000e-008	4046.0
HILLSLOPE	-0.6281	5.000000e-008	4040.0
EC50	0.0002712	1.000000e-007	4149.0
Std. Error		5.000000e-007	3920.0
LOGEC50	0.4485	0.000001	3901.0
HILLSLOPE	0.1716	0.000005	3748.0
95% Confidence Intervals		0.000010	3599.0
LOGEC50	-4.720 to -2.414	conc [M]	vel
HILLSLOPE	-1.069 to -0.1869		1.000
EC50	1.907e-005 to 0.003858		0.998
Goodness of Fit			1.025
Degrees of Freedom	5		0.969
R ²	0.9045		0.964
Absolute Sum of Squares	0.001256		0.926
Sy.x	0.01585		0.889
Constraints			
BOTTOM	BOTTOM = 0.0		
TOP	TOP = 1.000		

Figure A45. IC50 Determination of Compound 46.



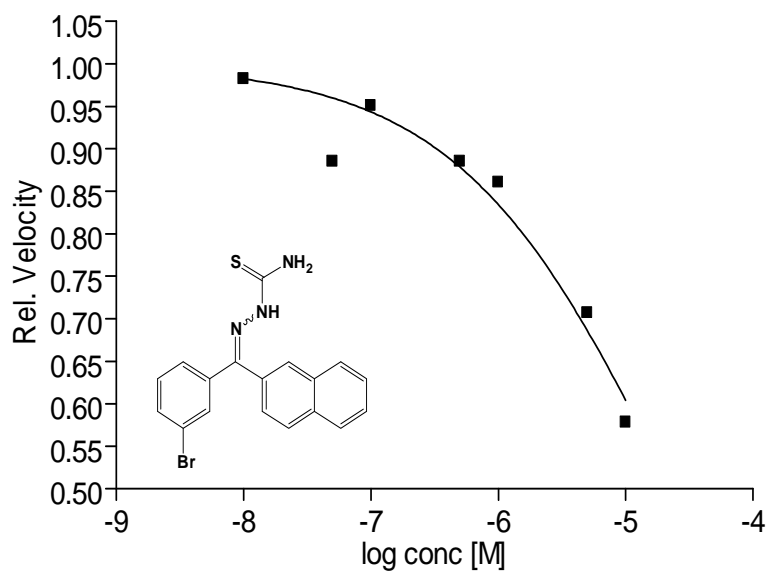
Best-fit values		Conc [M]	Vel
BOTTOM	0.0	0.000000	4140.00
TOP	1.000	1.000000e-008	3910.00
LOGEC50	-5.461	5.000000e-008	3930.00
HILLSLOPE	-0.7868	1.000000e-007	3810.00
EC50	3.458e-006	5.000000e-007	3829.00
Std. Error		0.000001	2700.00
LOGEC50	0.09308	0.000010	1270.00
HILLSLOPE	0.1078	0.000020	850.00
95% Confidence Intervals		Conc [M]	Vel
LOGEC50	-5.700 to -5.222	-8.000	0.944
HILLSLOPE	-1.064 to -0.5097	-7.301	0.949
EC50	1.993e-006 to 6.001e-006	-7.000	0.920
Goodness of Fit		-6.301	0.925
Degrees of Freedom	5	-6.000	0.652
R ²	0.9692	-5.000	0.307
Absolute Sum of Squares	0.01920	-4.699	0.205
Sy.x	0.06196		
Constraints			
BOTTOM	BOTTOM = 0.0		
TOP	TOP = 1.000		

Figure A46. IC50 Determination of Compound 51.



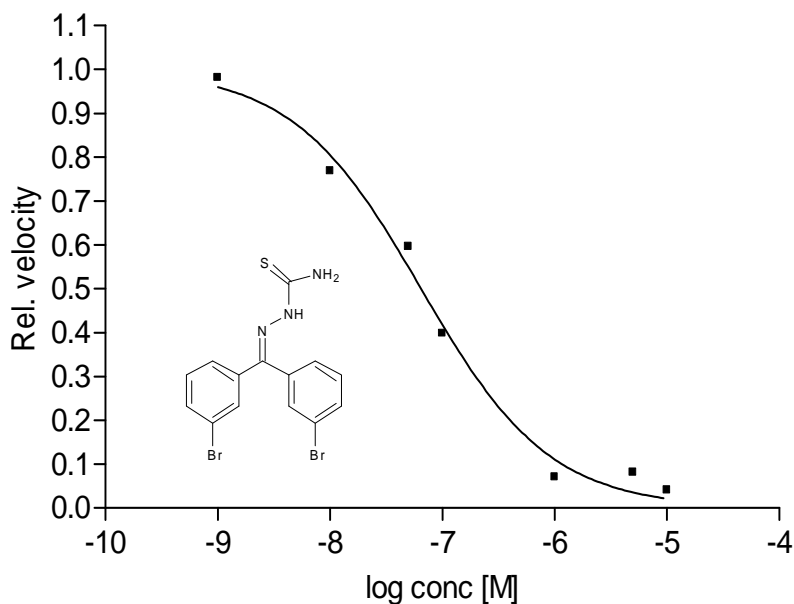
Best-fit values		Conc [M]	Vel
BOTTOM	0.0	0.000000	4215.00
TOP	1.000	1.000000e-008	4289.00
LOGEC50	-5.390	5.000000e-008	3957.00
HILLSLOPE	-1.154	1.000000e-007	3655.00
EC50	4.070e-006	5.000000e-007	3807.00
Std. Error		0.000001	3346.00
LOGEC50	0.08949	0.000005	2224.00
HILLSLOPE	0.2404	0.000010	1165.00
95% Confidence Intervals		0.000020	27.64
LOGEC50	-5.609 to -5.171		
HILLSLOPE	-1.743 to -0.5662		
EC50	2.458e-006 to 6.739e-006		
Goodness of Fit		Conc [M]	Vel
Degrees of Freedom	6	-8.000	1.000
R ²	0.9517	-7.301	0.939
Absolute Sum of Squares	0.04433	-7.000	0.867
Sy.x	0.08595	-6.301	0.903
Constraints		-6.000	0.794
BOTTOM	BOTTOM = 0.0	-5.301	0.528
TOP	TOP = 1.000	-5.000	0.276
		-4.699	0.007

Figure A47. IC50 Determination of Compound 52.



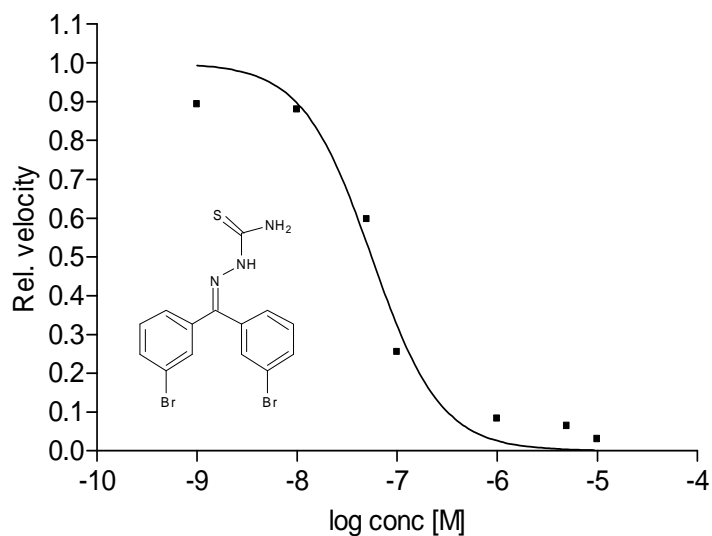
Best-fit values		Conc [M]	Vel
BOTTOM	0.0	0.000000	4522.0
TOP	1.000	1.000000e-008	4441.0
LOGEC50	-4.646	5.000000e-008	4003.0
HILLSLOPE	-0.5191	1.000000e-007	4300.0
EC50	2.261e-005	5.000000e-007	4003.0
Std. Error		0.000001	3891.0
LOGEC50	0.1512	0.000005	3197.0
HILLSLOPE	0.08332	0.000010	2615.0
95% Confidence Intervals		Conc [M]	Vel
LOGEC50	-5.034 to -4.257		1.000
HILLSLOPE	-0.7333 to -0.3049		
EC50	9.237e-006 to 5.536e-005		
Goodness of Fit		-8.000	0.982
Degrees of Freedom	5	-7.301	0.885
R ²	0.9396	-7.000	0.951
Absolute Sum of Squares	0.007437	-6.301	0.885
Sy.x	0.03857	-6.000	0.860
Constraints		-5.301	0.707
BOTTOM	BOTTOM = 0.0	-5.000	0.578
TOP	TOP = 1.000		

Figure A48. IC50 Determination of Compound 53.



Sigmoidal dose-response (variable slope)		conc [M]	velocity
Best-fit values		0.000	4516.500
BOTTOM	0.0	1.000e-009	4433.500
TOP	1.000	1.000e-008	3473.500
LOGEC50	-7.188	5.000e-008	2693.500
HILLSLOPE	-0.7599	1.000e-007	1798.500
EC50	6.480e-008	1.000e-006	321.200
Std. Error		5.000e-006	367.500
LOGEC50	0.05944	1.000e-005	184.700
HILLSLOPE	0.08557		
95% Confidence Intervals		conc [M]	velocity
LOGEC50	-7.341 to -7.036		1.000
HILLSLOPE	-0.9799 to -0.5399	-9.000	0.982
EC50	4.558e-008 to 9.213e-008	-8.000	0.769
Goodness of Fit		-7.301	0.596
Degrees of Freedom	5	-7.000	0.398
R ²	0.9900	-6.000	0.071
Absolute Sum of Squares	0.008526	-5.301	0.081
Sy.x	0.04129	-5.000	0.041
Constraints			
BOTTOM	BOTTOM = 0.0		
TOP	TOP = 1.000		

Figure A49. IC50 Determination of Compound 38.



Sigmoidal dose-response (variable slope)

Best-fit values

BOTTOM 0.0
 TOP 1.000
 LOGEC50 -7.255
 HILLSLOPE -1.260
 EC50 5.563e-008

Std. Error

LOGEC50 0.07360
 HILLSLOPE 0.3332

95% Confidence Intervals

LOGEC50 -7.444 to -7.065
 HILLSLOPE -2.117 to -0.4034
 EC50 3.598e-008 to 8.600e-008

Goodness of Fit

Degrees of Freedom 5
 R² 0.9698
 Absolute Sum of Squares 0.02673
 Sy.x 0.07312

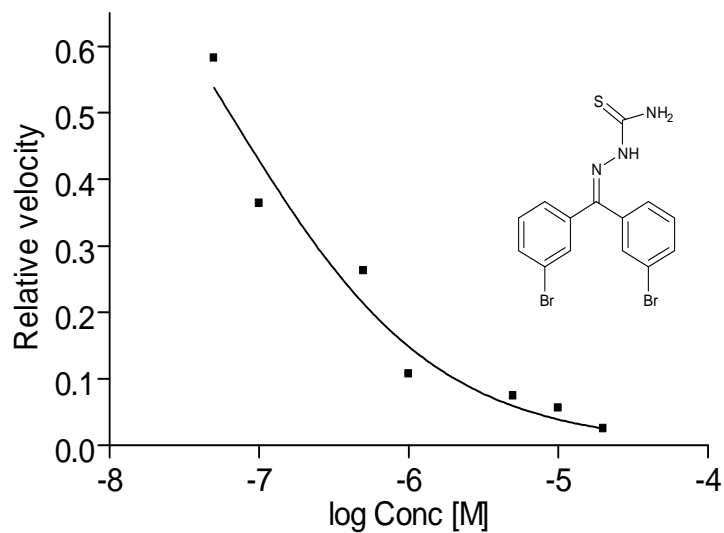
Constraints

BOTTOM BOTTOM = 0.0
 TOP TOP = 1.000

conc [M]	velocity
0.000	4754.210
1.000e-009	4245.790
1.000e-008	4182.632
5.000e-008	2835.263
1.000e-007	1208.947
1.000e-006	390.737
5.000e-006	301.579
1.000e-005	141.789

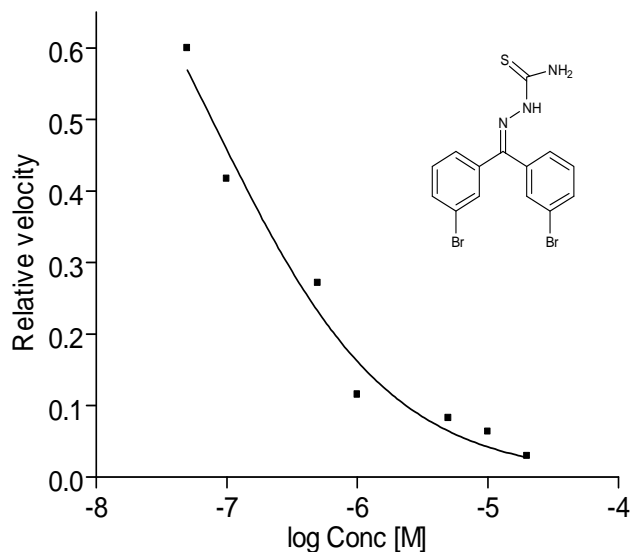
log conc [M]	velocity
	1.000
-9.000	0.893
-8.000	0.880
-7.301	0.596
-7.000	0.254
-6.000	0.082
-5.301	0.063
-5.000	0.030

Figure A50. IC50 Determination of Compound 38.



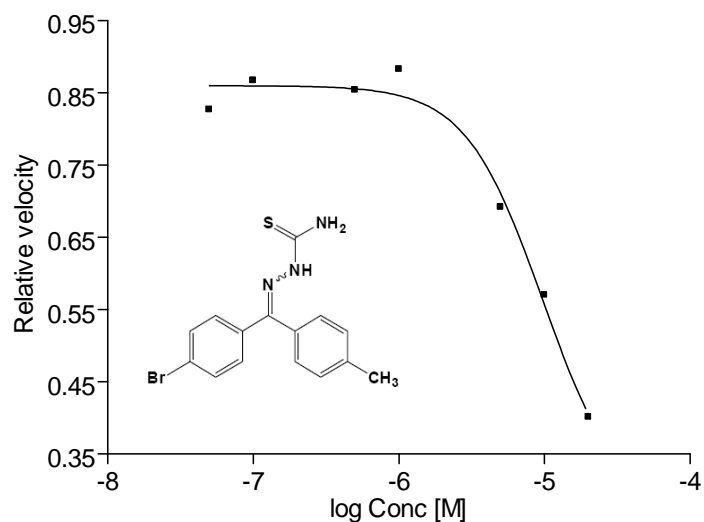
Sigmoidal dose-response (variable slope)		Conc [M]	vel
Best-fit values		0.000000	0.206090
BOTTOM	0.0	5.000000e-008	0.120002
TOP	1.000	1.000000e-007	0.075000
LOGEC50	-7.198	5.000000e-007	0.054110
HILLSLOPE	-0.6328	0.000001	0.022210
EC50	6.338e-008	0.000005	0.015368
Std. Error		0.000010	0.011540
LOGEC50	0.09243	0.000020	0.005230
HILLSLOPE	0.09111		
95% Confidence Intervals			
LOGEC50	-7.436 to -6.960		
HILLSLOPE	-0.8671 to -0.3986		
EC50	3.667e-008 to 1.095e-007		
Goodness of Fit			
Degrees of Freedom	5	-7.301	0.582
R ²	0.9571	-7.000	0.364
Absolute Sum of Squares	0.01081	-6.301	0.263
Sy.x	0.04649	-6.000	0.108
Constraints			
BOTTOM	BOTTOM = 0.0	-5.301	0.075
TOP	TOP = 1.000	-5.000	0.056
		-4.699	0.025

Figure A51. IC50 Determination of Compound 38.



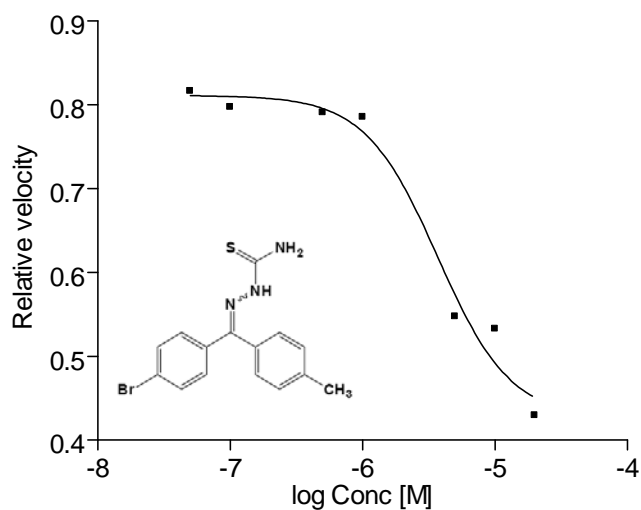
Sigmoidal dose-response (variable slope)		Conc [M]	vel
Best-fit values		0.000000	0.216090
BOTTOM	0.0	5.000000e-008	0.129540
TOP	1.000	1.000000e-007	0.090090
LOGEC50	-7.113	5.000000e-007	0.058630
HILLSLOPE	-0.6412	0.000001	0.024909
EC50	7.700e-008	0.000005	0.017773
Std. Error		0.000010	0.013682
LOGEC50	0.06938	0.000020	0.006363
HILLSLOPE	0.07087		
95% Confidence Intervals		Conc [M]	vel
LOGEC50	-7.292 to -6.935		1.000
HILLSLOPE	-0.8234 to -0.4590	-7.301	0.599
EC50	5.106e-008 to 1.161e-007	-7.000	0.417
Goodness of Fit		-6.301	0.271
Degrees of Freedom	5	-6.000	0.115
R ²	0.9740	-5.301	0.082
Absolute Sum of Squares	0.007170	-5.000	0.063
Sy.x	0.03787	-4.699	0.029
Constraints			
BOTTOM	BOTTOM = 0.0		
TOP	TOP = 1.000		

Figure A52. IC50 Determination of Compound 38.



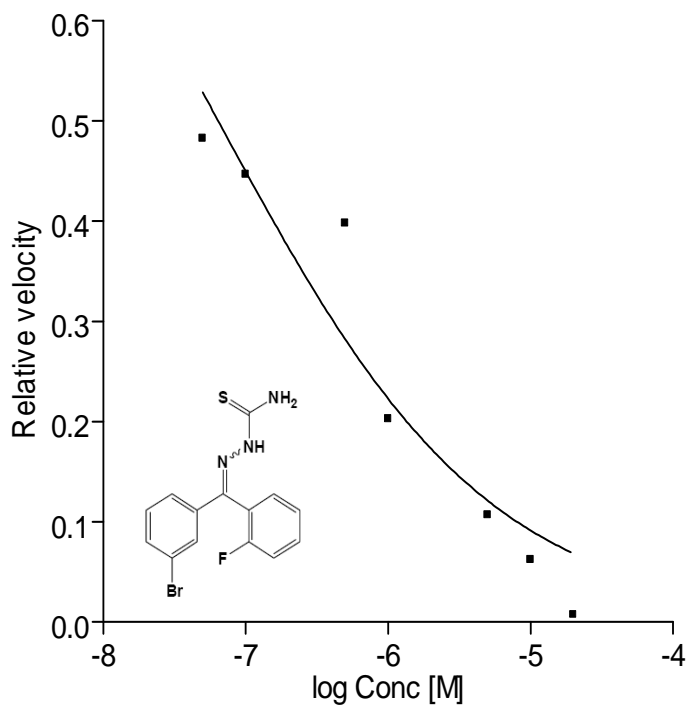
Sigmoidal dose-response (variable slope)		Conc [M]	vel
Best-fit values		0.000000	0.16050
BOTTOM	0.2685	5.000000e-008	0.13270
TOP	0.8601	1.000000e-007	0.13920
LOGEC50	-5.014	5.000000e-007	0.13710
HILLSLOPE	-1.647	0.000001	0.14170
EC50	9.681e-006	0.000005	0.11110
Std. Error		0.000010	0.09153
BOTTOM	0.2277	0.000020	0.06447
TOP	0.01887		
LOGEC50	0.2390		
HILLSLOPE	0.8155		
95% Confidence Intervals		Conc [M]	vel
BOTTOM	-0.4561 to 0.9930	-7.301	1.000
TOP	0.8001 to 0.9202	-7.000	0.827
LOGEC50	-5.775 to -4.254	-6.301	0.867
HILLSLOPE	-4.242 to 0.9476	-6.000	0.854
EC50	1.680e-006 to 5.578e-005	-6.000	0.883
Goodness of Fit		-5.301	0.692
Degrees of Freedom	3	-5.000	0.570
R ²	0.9848	-4.699	0.402
Absolute Sum of Squares	0.003059		
Sy.x	0.03193		

Figure A53. IC50 Determination of Compound 54.



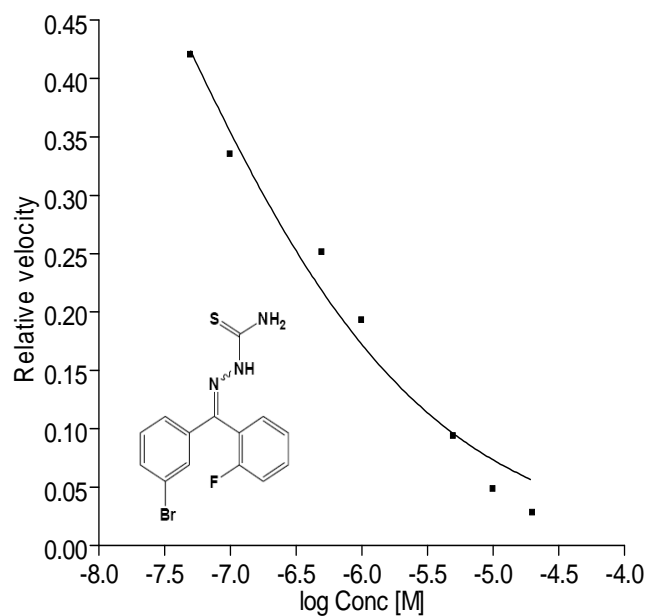
Sigmoidal dose-response (variable slope)		Conc [M]	vel
Best-fit values			1.000
BOTTOM	0.4259	-7.301	0.816
TOP	0.8113	-7.000	0.798
LOGEC50	-5.432	-6.301	0.791
HILLSLOPE	-1.583	-6.000	0.786
EC50	3.699e-006	-5.301	0.548
Std. Error			0.533
BOTTOM	0.05908	-4.699	0.430
TOP	0.02352		
LOGEC50	0.1435		
HILLSLOPE	0.6859		
95% Confidence Intervals			
BOTTOM	0.2379 to 0.6139	0.000000	0.168900
TOP	0.7365 to 0.8861	5.000000e-008	0.137900
LOGEC50	-5.889 to -4.975	1.000000e-007	0.134700
HILLSLOPE	-3.766 to 0.5998	5.000000e-007	0.133600
EC50	1.292e-006 to 1.059e-005	0.000001	0.132700
Goodness of Fit			0.092520
Degrees of Freedom	3	0.000010	0.090010
R ²	0.9790	0.000020	0.072570
Absolute Sum of Squares	0.003298		
Sy.x	0.03316		

Figure A54. IC50 Determination of Compound 54.



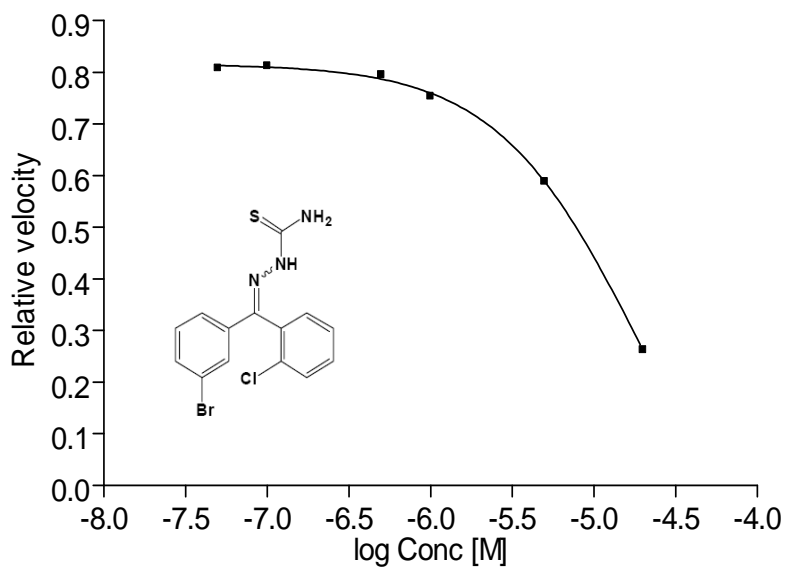
Best-fit values		Conc [M]	Vel
BOTTOM	0.0	0.000000	0.157800
TOP	1.000	5.000000e-008	0.076200
LOGEC50	-7.192	1.000000e-007	0.070520
HILLSLOPE	-0.4548	5.000000e-007	0.062810
EC50	6.431e-008	0.000001	0.032010
Std. Error		0.000005	0.016920
LOGEC50	0.1702	0.000010	0.009850
HILLSLOPE	0.08560	0.000020	0.001195
95% Confidence Intervals		Conc [M]	Vel
LOGEC50	-7.629 to -6.754		1.000
HILLSLOPE	-0.6749 to -0.2348		-7.301
EC50	2.349e-008 to 1.761e-007		0.483
Goodness of Fit			-7.000
Degrees of Freedom	5		0.447
R ²	0.9107		-6.301
Absolute Sum of Squares	0.02064		0.398
Sy.x	0.06425		-6.000
Constraints			0.203
BOTTOM	BOTTOM = 0.0		-5.301
TOP	TOP = 1.000		0.107
			-5.000
			0.062
			-4.699
			0.008

Figure A55. IC50 Determination of Compound 55.



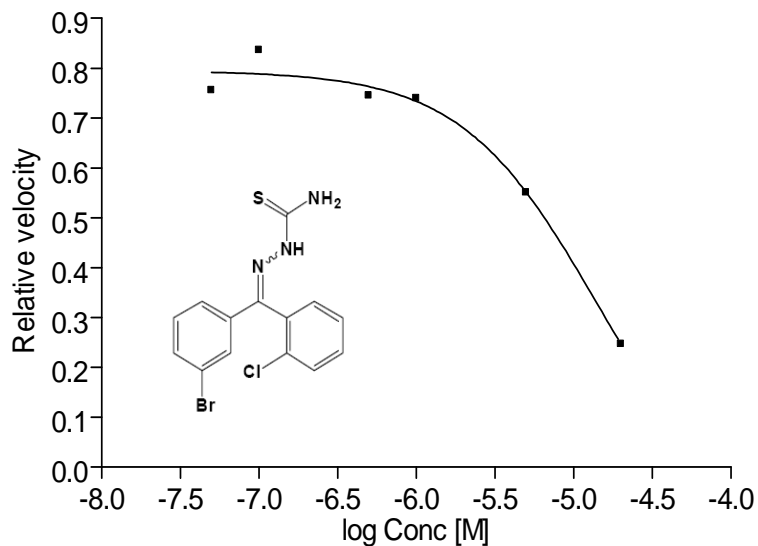
Sigmoidal dose-response (variable slope)		Conc [M]	Vel
Best-fit values		0.000000	0.144100
BOTTOM	0.0	5.000000e-008	0.060550
TOP	1.000	1.000000e-007	0.048280
LOGEC50	-7.620	5.000000e-007	0.036200
HILLSLOPE	-0.4207	0.000001	0.027750
EC50	2.401e-008	0.000005	0.013480
Std. Error		0.000010	0.006945
LOGEC50	0.1061	0.000020	0.004045
HILLSLOPE	0.03942		
95% Confidence Intervals		Conc [M]	Vel
LOGEC50	-7.892 to -7.347		1.000
HILLSLOPE	-0.5220 to -0.3193	-7.301	0.420
EC50	1.281e-008 to 4.498e-008	-7.000	0.335
Goodness of Fit		-6.301	0.251
Degrees of Freedom	5	-6.000	0.193
R ²	0.9753	-5.301	0.094
Absolute Sum of Squares	0.003292	-5.000	0.048
Sy.x	0.02566	-4.699	0.028
Constraints			
BOTTOM	BOTTOM = 0.0		
TOP	TOP = 1.000		

Figure A56. IC50 Determination of Compound 55.



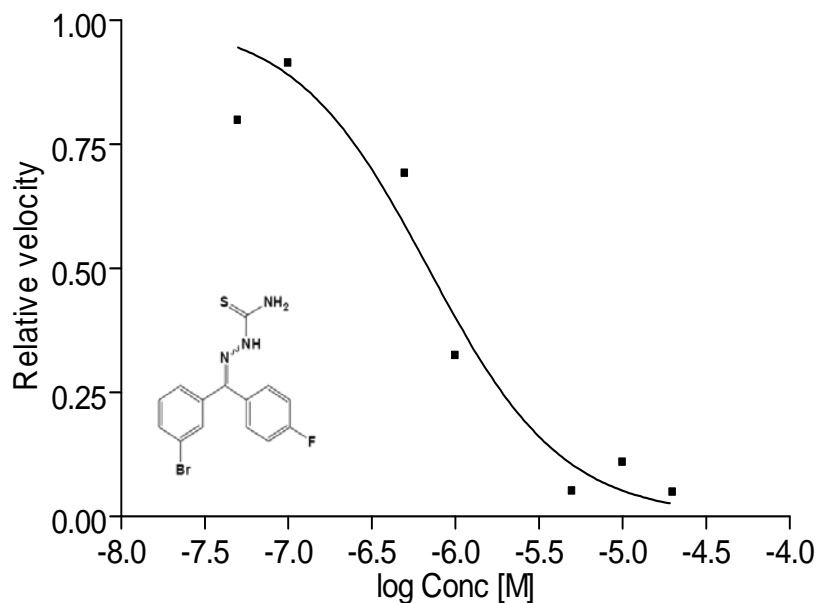
		Conc [M]	Vel
Sigmoidal dose-response (variable slope)		0.000000	0.16290
Best-fit values		5.000000e-008	0.13170
BOTTOM	-0.2782	1.000000e-007	0.13230
TOP	0.8162	5.000000e-007	0.12950
LOGEC50	-4.710	0.000001	0.12270
HILLSLOPE	-0.9795	0.000005	0.09591
EC50	1.952e-005	0.000020	0.04274
Std. Error			
BOTTOM	0.3285		
TOP	0.007763		
LOGEC50	0.2615		
HILLSLOPE	0.1599		
95% Confidence Intervals			
BOTTOM	-1.692 to 1.136	-7.301	0.808
TOP	0.7828 to 0.8496	-7.000	0.812
LOGEC50	-5.835 to -3.584	-6.301	0.795
HILLSLOPE	-1.667 to -0.2917	-6.000	0.753
EC50	1.462e-006 to 0.0002605	-5.301	0.589
		-4.699	0.262
Goodness of Fit			
Degrees of Freedom	2		
R ²	0.9994		
Absolute Sum of Squares	0.0001348		
Sy.x	0.008209		

Figure A57. IC50 Determination of Compound 56.



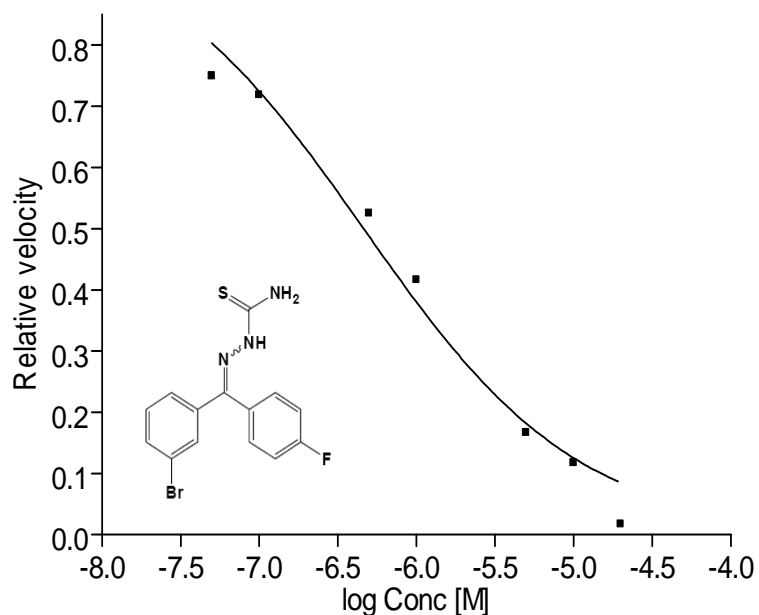
BOTTOM	-0.1381	Conc [M]	Vel
TOP	0.7948	0.000000	0.15760
LOGEC50	-4.851	5.000000e-008	0.11900
HILLSLOPE	-1.005	1.000000e-007	0.13180
EC50	1.409e-005	5.000000e-007	0.11750
Std. Error		0.000001	0.11660
BOTTOM	1.022	0.000005	0.08687
TOP	0.04149	0.000020	0.03893
LOGEC50	0.9941		
HILLSLOPE	0.7994		
95% Confidence Intervals		Conc [M]	Vel
BOTTOM	-4.538 to 4.261		1.000
TOP	0.6162 to 0.9733	-7.301	0.755
LOGEC50	-9.129 to -0.5737	-7.000	0.836
HILLSLOPE	-4.444 to 2.435	-6.301	0.746
EC50	7.434e-010 to 0.2669	-6.000	0.740
Goodness of Fit		-5.301	0.551
Degrees of Freedom	2	-4.699	0.247
R ²	0.9831		
Absolute Sum of Squares	0.003982		
Sy.x	0.04462		

Figure A58. IC50 Determination of Compound 56.



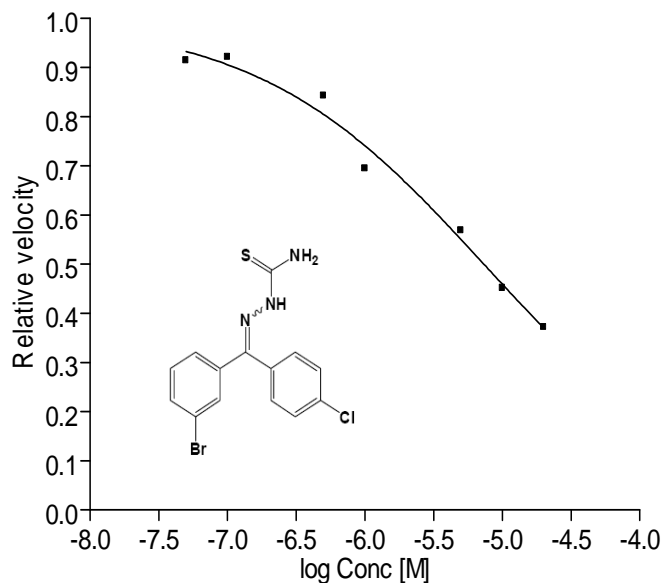
		Conc [M]	vel.
Best-fit values			
BOTTOM	0.0	0.000000	0.107900
TOP	1.000	5.000000e-008	0.086110
LOGEC50	-6.161	1.000000e-007	0.098610
HILLSLOPE	-1.083	5.000000e-007	0.074640
EC50	6.903e-007	0.000001	0.034930
Std. Error		0.000005	0.005513
LOGEC50	0.1025	0.000010	0.011780
HILLSLOPE	0.2677	0.000020	0.005255
95% Confidence Intervals			
LOGEC50	-6.424 to -5.897		
HILLSLOPE	-1.771 to -0.3946		
EC50	3.763e-007 to 1.266e-006		
Goodness of Fit			
Degrees of Freedom	5	-7.301	0.798
R ²	0.9454	-7.000	0.914
Absolute Sum of Squares	0.04586	-6.301	0.692
Sy.x	0.09577	-6.000	0.324
Constraints		-5.301	0.051
BOTTOM	BOTTOM = 0.0	-5.000	0.109
TOP	TOP = 1.000	-4.699	0.049

Figure A59. IC50 Determination of Compound 57.



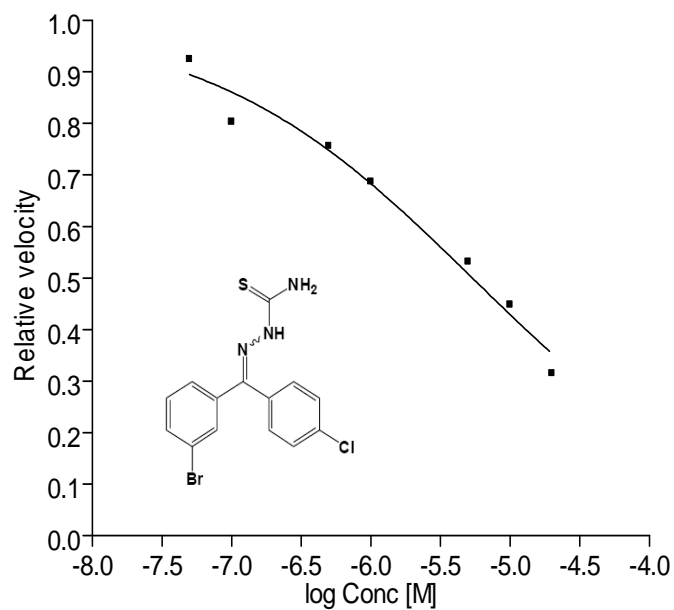
Sigmoidal dose-response (variable slope)		Conc [M]	vel.
Best-fit values		0.000000	0.107900
BOTTOM	0.0	5.000000e-008	0.087510
TOP	1.000	1.000000e-007	0.083870
LOGEC50	-6.335	5.000000e-007	0.061300
HILLSLOPE	-0.6317	0.000001	0.048610
EC50	4.622e-007	0.000005	0.019470
Std. Error		0.000010	0.013700
LOGEC50	0.06702	0.000020	0.001989
HILLSLOPE	0.06070		
95% Confidence Intervals		Conc [M]	vel.
LOGEC50	-6.507 to -6.163		0.925
HILLSLOPE	-0.7878 to -0.4756	-7.301	0.750
EC50	3.108e-007 to 6.873e-007	-7.000	0.719
Goodness of Fit		-6.301	0.525
Degrees of Freedom	5	-6.000	0.417
R ²	0.9799	-5.301	0.167
Absolute Sum of Squares	0.01044	-5.000	0.117
Sy.x	0.04570	-4.699	0.017
Constraints			
BOTTOM	BOTTOM = 0.0		
TOP	TOP = 1.000		

Figure A60. IC50 Determination of Compound 57.



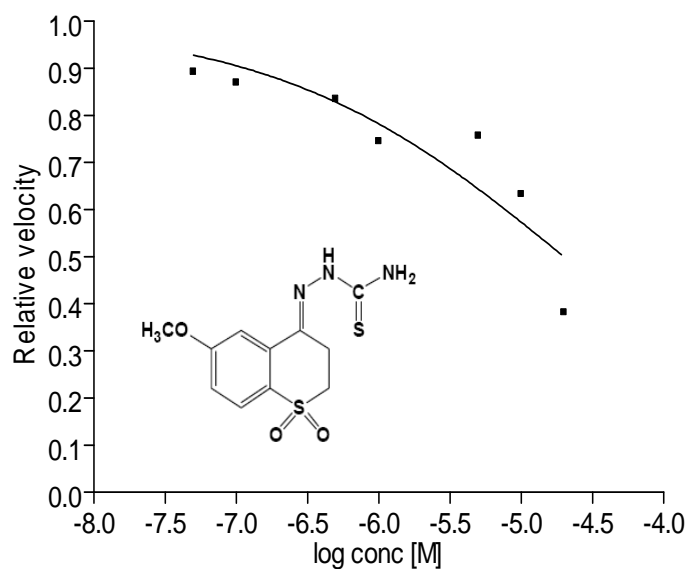
Sigmoidal dose-response (variable slope)		Conc [M]	Vel.
Best-fit values		0.000000	0.21120
BOTTOM	0.0	5.000000e-008	0.19310
TOP	1.000	1.000000e-007	0.19460
LOGEC50	-5.134	5.000000e-007	0.17790
HILLSLOPE	-0.5274	0.000001	0.14670
EC50	7.340e-006	0.000005	0.12010
Std. Error		0.000010	0.09541
LOGEC50	0.05303	0.000020	0.07853
HILLSLOPE	0.04071		
95% Confidence Intervals		Conc [M]	Vel.
LOGEC50	-5.271 to -4.998		1.000
HILLSLOPE	-0.6320 to -0.4227	-7.301	0.914
EC50	5.362e-006 to 1.005e-005	-7.000	0.921
Goodness of Fit		-6.301	0.842
Degrees of Freedom	5	-6.000	0.695
R ²	0.9849	-5.301	0.569
Absolute Sum of Squares	0.004531	-5.000	0.452
Sy.x	0.03010	-4.699	0.372
Constraints			
BOTTOM	BOTTOM = 0.0		
TOP	TOP = 1.000		

Figure A61. .IC50 Determination of Compound 58.



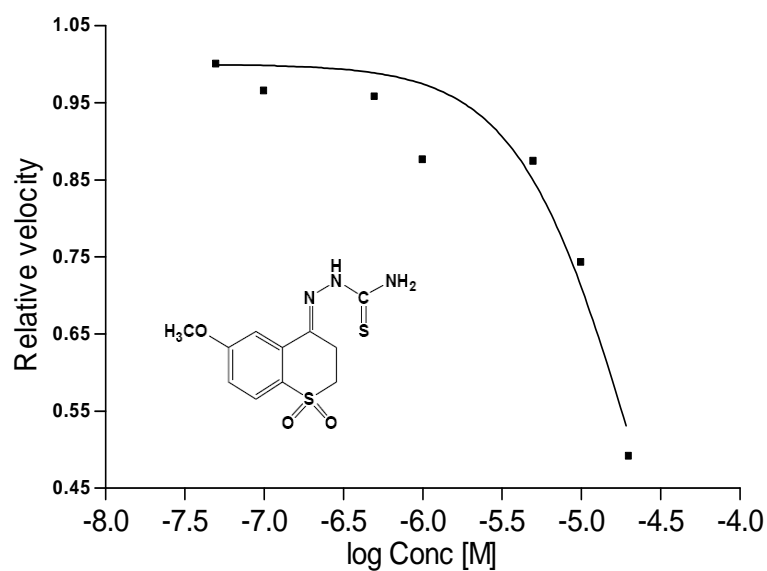
Sigmoidal dose-response (variable slope)		Conc [M]	Vel.
Best-fit values		0.000000	0.21430
BOTTOM	0.0	5.000000e-008	0.19810
TOP	1.000	1.000000e-007	0.17220
LOGEC50	-5.269	5.000000e-007	0.16210
HILLSLOPE	-0.4577	0.000001	0.14730
EC50	5.379e-006	0.000005	0.11400
Std. Error		0.000010	0.09607
LOGEC50	0.06922	0.000020	0.06760
HILLSLOPE	0.04146		
95% Confidence Intervals		Conc [M]	Vel.
LOGEC50	-5.447 to -5.091		1.000
HILLSLOPE	-0.5643 to -0.3511	-7.301	0.924
EC50	3.571e-006 to 8.103e-006	-7.000	0.804
Goodness of Fit		-6.301	0.756
Degrees of Freedom	5	-6.000	0.687
R ²	0.9759	-5.301	0.532
Absolute Sum of Squares	0.006671	-5.000	0.448
Sy.x	0.03653	-4.699	0.315
Constraints			
BOTTOM	BOTTOM = 0.0		
TOP	TOP = 1.000		

Figure A62. IC50 Determination of Compound 58.



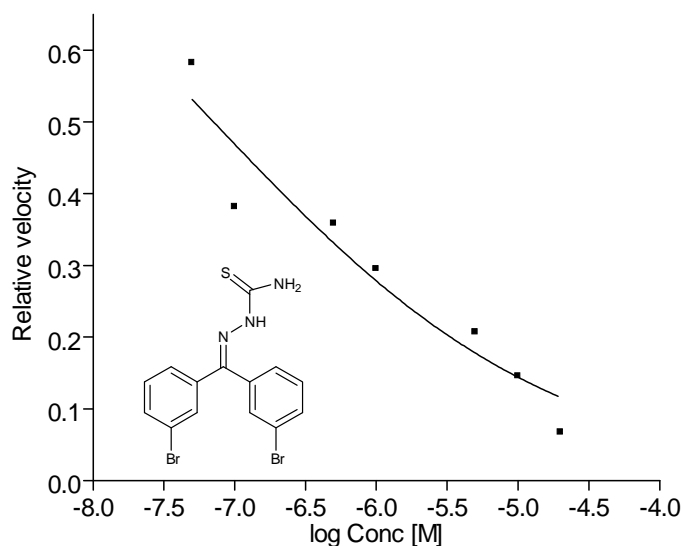
Sigmoidal dose-response (variable slope)		Conc [M]	Vel.
Best-fit values		0.000000	0.18810
BOTTOM	0.0	5.000000e-008	0.16790
TOP	1.000	1.000000e-007	0.16360
LOGEC50	-4.698	5.000000e-007	0.15710
HILLSLOPE	-0.4268	0.000001	0.14020
EC50	2.004e-005	0.000005	0.14230
Std. Error		0.000010	0.11910
LOGEC50	0.2403	0.000020	0.07185
HILLSLOPE	0.1128		
95% Confidence Intervals		Conc [M]	Vel.
LOGEC50	-5.316 to -4.080		1.000
HILLSLOPE	-0.7169 to -0.1366	-7.301	0.893
EC50	4.834e-006 to 8.313e-005	-7.000	0.870
Goodness of Fit		-6.301	0.835
Degrees of Freedom	5	-6.000	0.745
R ²	0.8187	-5.301	0.757
Absolute Sum of Squares	0.03416	-5.000	0.633
Sy.x	0.08266	-4.699	0.382
Constraints			
BOTTOM	BOTTOM = 0.0		
TOP	TOP = 1.000		

Figure A63. IC50 Determination of Compound 59.



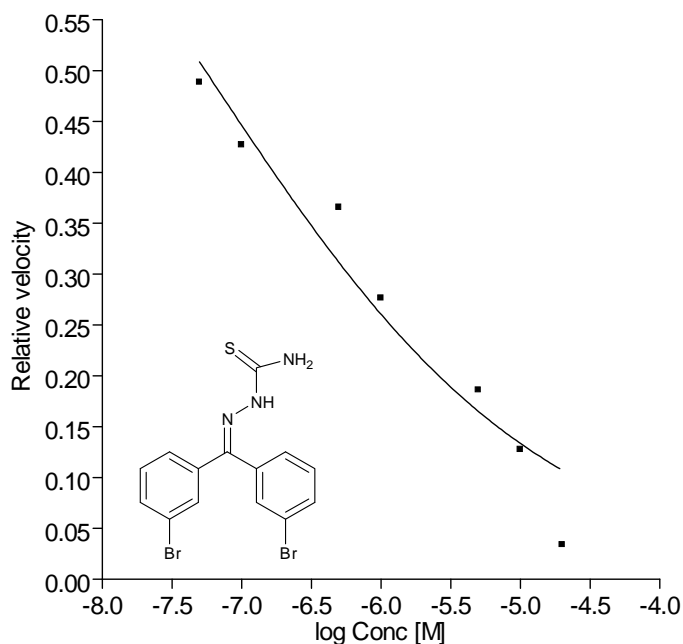
Sigmoidal dose-response (variable slope)		Conc [M]	Vel.
Best-fit values		0.000000	0.18150
BOTTOM	0.0	5.000000e-008	0.17990
TOP	1.000	1.000000e-007	0.17360
LOGEC50	-4.671	5.000000e-007	0.17230
HILLSLOPE	-1.190	0.000001	0.15760
EC50	2.131e-005	0.000005	0.15720
Std. Error		0.000010	0.13360
LOGEC50	0.07690	0.000020	0.08841
HILLSLOPE	0.2838		
95% Confidence Intervals		Conc [M]	Vel.
LOGEC50	-4.869 to -4.474		1.009
HILLSLOPE	-1.920 to -0.4605	-7.301	1.000
EC50	1.352e-005 to 3.360e-005	-7.000	0.965
Goodness of Fit		-6.301	0.958
Degrees of Freedom	5	-6.000	0.876
R ²	0.9250	-5.301	0.874
Absolute Sum of Squares	0.01412	-5.000	0.743
Sy.x	0.05315	-4.699	0.491
Constraints			
BOTTOM	BOTTOM = 0.0		
TOP	TOP = 1.000		

Figure A64. IC50 Determination of Compound 59.



Sigmoidal dose-response (variable slope)		Conc [M]	Vel.
Best-fit values			
BOTTOM	0.0	0.000000	0.18420
TOP	1.000	5.000000e-008	0.10730
LOGEC50	-7.150	1.000000e-007	0.07032
HILLSLOPE	-0.3597	5.000000e-007	0.06608
EC50	7.086e-008	0.000001	0.05441
Std. Error		0.000005	0.03815
LOGEC50	0.1710	0.000010	0.02683
HILLSLOPE	0.05752	0.000020	0.01244
95% Confidence Intervals			
LOGEC50	-7.589 to -6.710		
HILLSLOPE	-0.5076 to -0.2118	Conc [M]	Vel.
EC50	2.575e-008 to 1.950e-007	-7.301	0.583
Goodness of Fit		-7.000	0.382
Degrees of Freedom	5	-6.301	0.359
R ²	0.9175	-6.000	0.295
Absolute Sum of Squares	0.01451	-5.301	0.207
Sy.x	0.05387	-5.000	0.146
Constraints		-4.699	0.068
BOTTOM	BOTTOM = 0.0		
TOP	TOP = 1.000		

Figure A65. IC50 Determination of Compound 60.



Sigmoidal dose-response (variable slope)		Conc [M]	Vel.
Best-fit values		0.000000	0.189600
BOTTOM	0.0	5.000000e-008	0.092600
TOP	1.000	1.000000e-007	0.080950
LOGEC50	-7.260	5.000000e-007	0.069300
HILLSLOPE	-0.3594	0.000001	0.052350
EC50	5.491e-008	0.000005	0.035240
Std. Error		0.000010	0.024170
LOGEC50	0.1518	0.000020	0.006430
HILLSLOPE	0.04909		
95% Confidence Intervals		Conc [M]	Vel.
LOGEC50	-7.651 to -6.870		1.000
HILLSLOPE	-0.4856 to -0.2332	-7.301	0.488
EC50	2.235e-008 to 1.349e-007	-7.000	0.427
Goodness of Fit		-6.301	0.366
Degrees of Freedom	5	-6.000	0.276
R ²	0.9405	-5.301	0.186
Absolute Sum of Squares	0.009795	-5.000	0.127
Sy.x	0.04426	-4.699	0.034
Constraints			
BOTTOM	BOTTOM = 0.0		
TOP	TOP = 1.000		

Figure A66. IC50 Determination of Compound 60.

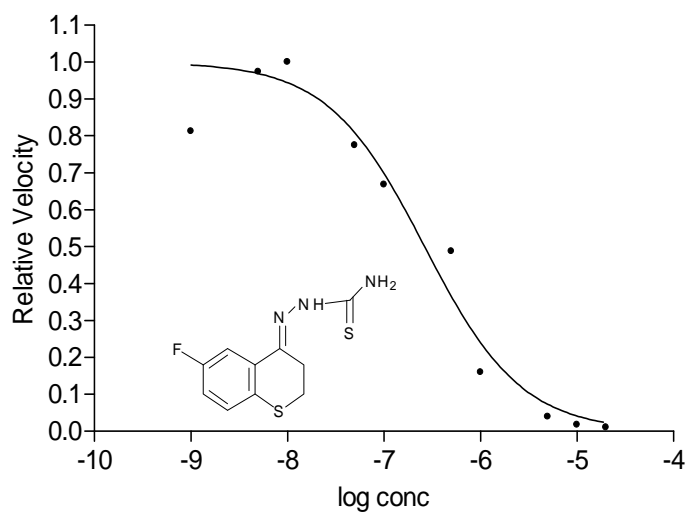
APPENDIX B

Table B1. Q Sepharose Fast Flow Anion Exchange Column Characteristics

Type of ion exchanger:	Strong anion	
Total ionic capacity:	0.18-0.25 mmole/ml gel	
Available capacity:	Thyroglobulin (M _t 669,000)	3 mg/ml
	HAS (M _t 68,000)	120 mg/ml
	α-lactalbumin (M _t 14,300)	110 mg/ml
Bead structure:	6% highly cross-linked agarose	
Bead size range:	45-165 μm	
Mean particle size:	90 μm	
Linear flow rate:	400-700 cm/h at 25°C, 0.1 MPa, XK, 50/30 column, 15 cm bed height, mobile phase 0.1 M NaCl	
Max. operating pressure:	0.3 MPa	
pH stability working range	2-12	
long term	2-12	
short term	1-14	
Chemical stability	All commonly used aqueous buffers, 1.0 M NaOH, 8M urea, 8M guanidine hydrochloride, 24% ethanol (tested at 40 °C for 7 days)	
Physical stability	Negligible volume variation due to changes in pH or ionic strength	
Autoclavable	In 0.1 M NaCl at 121 °C for 30 min.	

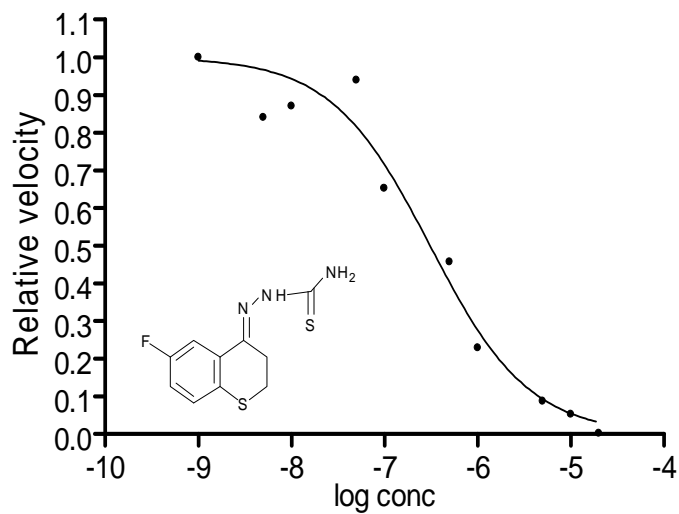
APPENDIX C

Cruzain IC50 Determination Data and Plots



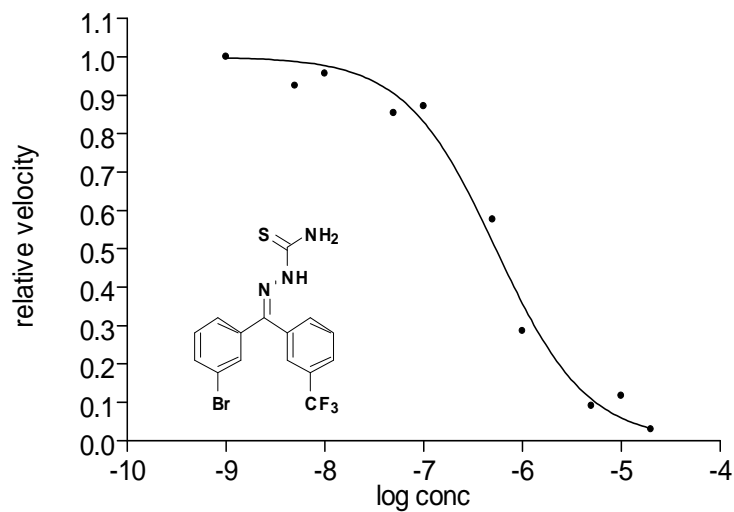
	Vel	Con [M]	Vel
Sigmoidal dose-response (variable slope)		0.000000	18560.0
Best-fit values		1.000000e-009	11460.0
BOTTOM	0.0	5.000000e-009	13720.0
TOP	1.000	1.000000e-008	14100.0
LOGEC50	-6.578	5.000000e-008	10920.0
HILLSLOPE	-0.8651	1.000000e-007	9415.0
EC50	2.641e-007	5.000000e-007	6867.0
Std. Error		0.000001	2257.0
LOGEC50	0.1072	0.000005	553.7
HILLSLOPE	0.1574	0.000010	245.8
95% Confidence Intervals		0.000020	138.6
LOGEC50	-6.825 to -6.331		
HILLSLOPE	-1.228 to -0.5021		
EC50	1.495e-007 to 4.665e-007		
Goodness of Fit			
Degrees of Freedom	8		
R ²	0.9591		
Absolute Sum of Squares	0.06044		
Sy.x	0.08692		
Constraints			
BOTTOM	BOTTOM = 0.0		
TOP	TOP = 1.000		
Data			
Number of X values	11		
Number of Y replicates	1		
Total number of values	10		
Number of missing values	1		

Figure C1. IC50 Determination of Compound 25.



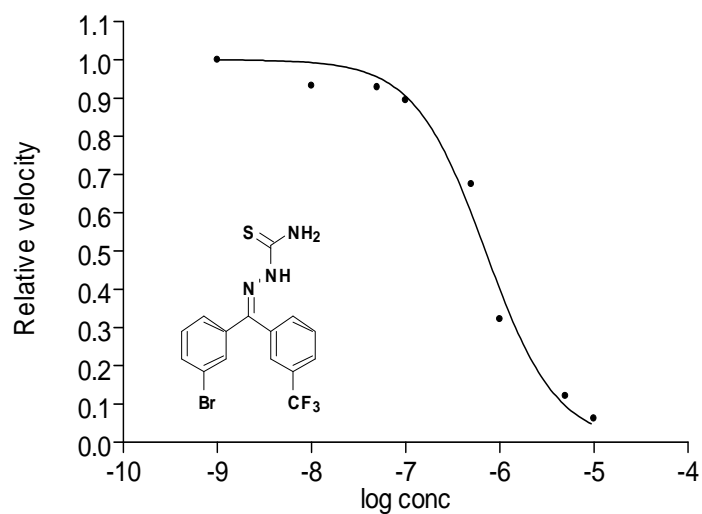
	Vel	Con [M]	Vel
Sigmoidal dose-response (variable slope)		0.000000	8479.00
Best-fit values		1.000000e-009	9668.00
BOTTOM	0.0	5.000000e-009	8121.00
TOP	1.000	1.000000e-008	8417.00
LOGEC50	-6.511	5.000000e-008	9077.00
HILLSLOPE	-0.8175	1.000000e-007	6308.00
EC50	3.082e-007	5.000000e-007	4415.00
Std. Error		0.000001	2214.00
LOGEC50	0.09643	0.000005	849.70
HILLSLOPE	0.1280	0.000010	505.60
95% Confidence Intervals		0.000020	26.11
LOGEC50	-6.734 to -6.289		
HILLSLOPE	-1.113 to -0.5223		
EC50	1.847e-007 to 5.142e-007	Con [M]	Vel
Goodness of Fit			0.877
Degrees of Freedom	8	-9.000	1.000
R ²	0.9670	-8.301	0.840
Absolute Sum of Squares	0.04656	-8.000	0.871
Sy.x	0.07629	-7.301	0.939
Constraints		-7.000	0.652
BOTTOM	BOTTOM = 0.0	-6.301	0.457
TOP	TOP = 1.000	-6.000	0.229
		-5.301	0.088
Data		-5.000	0.052
Number of X values	11	-4.699	0.003
Number of Y replicates	1		
Total number of values	10		
Number of missing values	1		

Figure C2. IC₅₀ Determination of Compound 25.



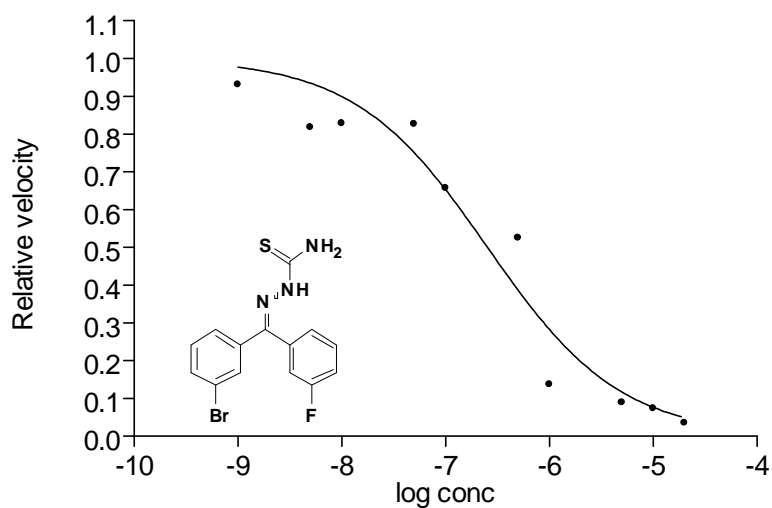
	Vel	Con [M]	Vel
Sigmoidal dose-response (variable slope)		0.000000	13850.0
Best-fit values		1.000000e-009	14040.0
BOTTOM	0.0	5.000000e-009	12990.0
TOP	1.000	1.000000e-008	13430.0
LOGEC50	-6.269	5.000000e-008	11990.0
HILLSLOPE	-0.9450	1.000000e-007	12240.0
EC50	5.381e-007	5.000000e-007	8096.0
Std. Error		0.000001	4011.0
LOGEC50	0.05948	0.000005	1281.0
HILLSLOPE	0.1103	0.000010	1643.0
95% Confidence Intervals		0.000020	419.5
LOGEC50	-6.406 to -6.132		
HILLSLOPE	-1.199 to -0.6907	Con [M]	Vel
EC50	3.924e-007 to 7.380e-007		0.986
Goodness of Fit		-9.000	1.000
Degrees of Freedom	8	-8.301	0.925
R ²	0.9855	-8.000	0.957
Absolute Sum of Squares	0.02093	-7.301	0.854
Sy.x	0.05115	-7.000	0.872
Constraints		-6.301	0.577
BOTTOM	BOTTOM = 0.0	-6.000	0.286
TOP	TOP = 1.000	-5.301	0.091
		-5.000	0.117
Data		-4.699	0.030
Number of X values	11		
Number of Y replicates	1		
Total number of values	10		
Number of missing values	1		

Figure C3. IC50 Determination of Compound 31.



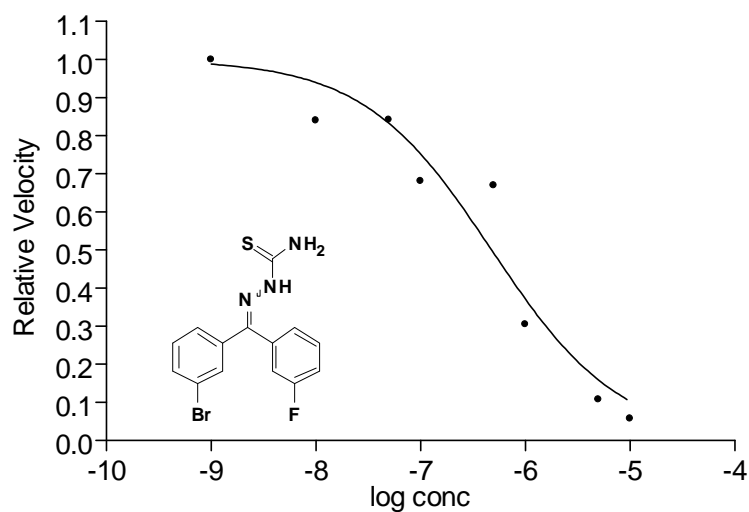
	Vel	Con [M]	Vel
Sigmoidal dose-response (variable slope)		0.000000	11090.0
Best-fit values		1.000000e-009	11640.0
BOTTOM	0.0	5.000000e-009	8934.0
TOP	1.000	1.000000e-008	10850.0
LOGEC50	-6.152	5.000000e-008	10800.0
HILLSLOPE	-1.152	1.000000e-007	10410.0
EC50	7.052e-007	5.000000e-007	7853.0
Std. Error		0.000001	3746.0
LOGEC50	0.05577	0.000005	1408.0
HILLSLOPE	0.1733	0.000010	718.6
95% Confidence Intervals		0.000020	4441.0
LOGEC50	-6.288 to -6.015		
HILLSLOPE	-1.576 to -0.7276		
EC50	5.150e-007 to 9.656e-007	Con [M]	Vel
Goodness of Fit			0.953
Degrees of Freedom	6	-9.000	1.000
R ²	0.9835	-8.000	0.932
Absolute Sum of Squares	0.01760	-7.301	0.928
Sy.x	0.05416	-7.000	0.894
Constraints		-6.301	0.675
BOTTOM	BOTTOM = 0.0	-6.000	0.322
TOP	TOP = 1.000	-5.301	0.121
Data		-5.000	0.062
Number of X values	11		
Number of Y replicates	1		
Total number of values	8		
Number of missing values	3		

Figure C4. IC50 Determination of Compound 31.



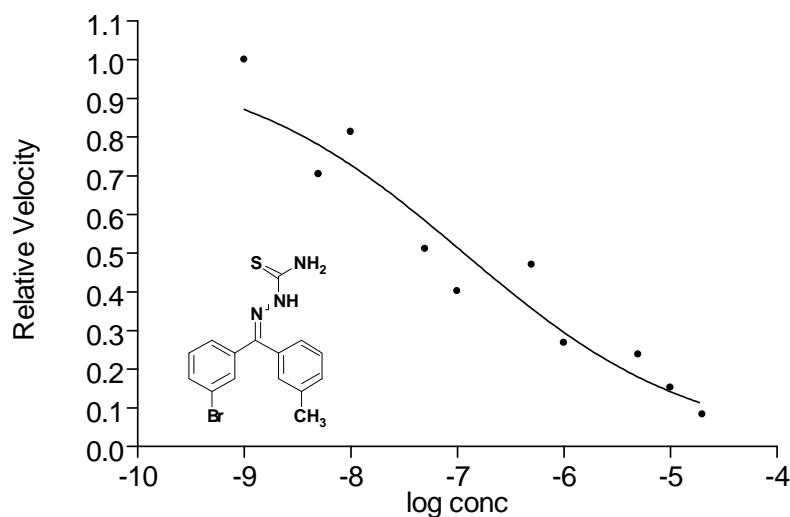
	Vel	Con [M]	Vel
Sigmoidal dose-response (variable slope)		0.000000	12120.0
Best-fit values		1.000000e-009	11290.0
BOTTOM	0.0	5.000000e-009	9914.0
TOP	1.000	1.000000e-008	10040.0
LOGEC50	-6.595	5.000000e-008	10020.0
HILLSLOPE	-0.6785	1.000000e-007	7964.0
EC50	2.540e-007	5.000000e-007	6366.0
Std. Error		0.000001	1659.0
LOGEC50	0.1276	0.000005	1080.0
HILLSLOPE	0.1190	0.000010	900.9
95% Confidence Intervals		0.000020	422.5
LOGEC50	-6.890 to -6.301		
HILLSLOPE	-0.9528 to -0.4041		
EC50	1.290e-007 to 5.003e-007		
Goodness of Fit			
Degrees of Freedom	8	-9.000	0.932
R ²	0.9444	-8.301	0.818
Absolute Sum of Squares	0.06805	-8.000	0.828
Sy.x	0.09223	-7.301	0.827
Sy.x		-7.000	0.657
Constraints		-6.301	0.525
BOTTOM	BOTTOM = 0.0	-6.000	0.137
TOP	TOP = 1.000	-5.301	0.089
Data		-5.000	0.074
Number of X values	11	-4.699	0.035
Number of Y replicates	1		
Total number of values	10		
Number of missing values	1		

Figure C5. IC50 Determination of Compound 32.



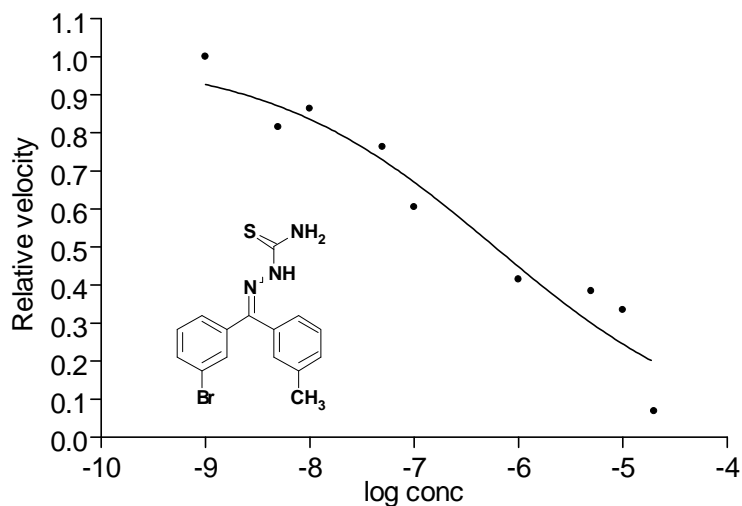
	Vel	Con [M]	Vel
Sigmoidal dose-response (variable slope)		0.000000	3824.0
Best-fit values		1.000000e-009	8699.0
BOTTOM	0.0	5.000000e-009	14090.0
TOP	1.000	1.000000e-008	7307.0
LOGEC50	-6.321	5.000000e-008	7323.0
HILLSLOPE	-0.7104	1.000000e-007	5923.0
EC50	4.774e-007	5.000000e-007	5821.0
Std. Error		0.000001	2648.0
LOGEC50	0.1318	0.000005	934.1
HILLSLOPE	0.1449	0.000010	493.4
95% Confidence Intervals		0.000020	1146.0
LOGEC50	-6.644 to -5.999		
HILLSLOPE	-1.065 to -0.3559		
EC50	2.272e-007 to 1.003e-006	Con [M]	Vel
Goodness of Fit		-9.000	1.000
Degrees of Freedom	6	-8.000	0.840
R ²	0.9378	-7.301	0.842
Absolute Sum of Squares	0.05605	-7.000	0.681
Sy.x	0.09665	-6.301	0.669
Constraints		-6.000	0.304
BOTTOM	BOTTOM = 0.0	-5.301	0.107
TOP	TOP = 1.000	-5.000	0.057
Data			
Number of X values	11		
Number of Y replicates	1		
Total number of values	8		
Number of missing values	3		

Figure C6. IC50 Determination of Compound 32.



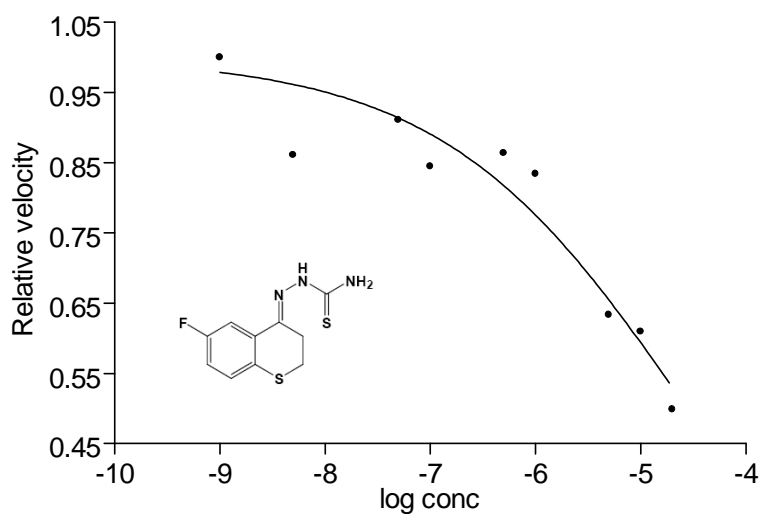
	Vel	Con [M]	Vel
Sigmoidal dose-response (variable slope)		0.000000	5405.00000
Best-fit values		1.000000e-009	13530.00000
BOTTOM	0.0	5.000000e-009	9527.00000
TOP	1.000	1.000000e-008	11000.00000
LOGEC50	-6.938	5.000000e-008	6906.00000
HILLSLOPE	-0.4029	1.000000e-007	5434.00000
EC50	1.153e-007	5.000000e-007	6365.00000
Std. Error		0.000001	3632.00000
LOGEC50	0.1666	0.000005	3223.00000
HILLSLOPE	0.06372	0.000010	2060.00000
95% Confidence Intervals		0.000020	1121.00000
LOGEC50	-7.322 to -6.554		
HILLSLOPE	-0.5499 to -0.2560	Con [M]	Vel
EC50	4.760e-008 to 2.793e-007	-9.000	1.000
Goodness of Fit		-8.301	0.704
Degrees of Freedom	8	-8.000	0.813
R ²	0.9185	-7.301	0.510
Absolute Sum of Squares	0.06558	-7.000	0.402
Sy.x	0.09054	-6.301	0.470
Constraints		-6.000	0.268
BOTTOM	BOTTOM = 0.0	-5.301	0.238
TOP	TOP = 1.000	-5.000	0.152
Data		-4.699	0.083
Number of X values	11		
Number of Y replicates	1		
Total number of values	10		
Number of missing values	1		

Figure C7. IC50 Determination of Compound 35.



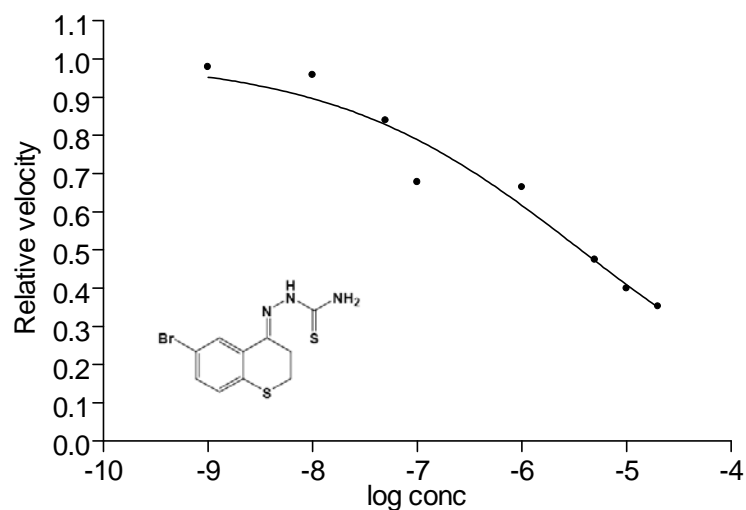
	Vel	Con [M]	Vel
Sigmoidal dose-response (variable slope)		0.000000	6253.00000
Best-fit values		1.000000e-009	6459.00000
BOTTOM	0.0	5.000000e-009	5264.00000
TOP	1.000	1.000000e-008	5575.00000
LOGEC50	-6.226	5.000000e-008	4928.00000
HILLSLOPE	-0.3986	1.000000e-007	3905.00000
EC50	5.937e-007	5.000000e-007	3939.00000
Std. Error		0.000001	2675.00000
LOGEC50	0.1676	0.000005	2480.00000
HILLSLOPE	0.05866	0.000010	2160.00000
95% Confidence Intervals		0.000020	439.50000
LOGEC50	-6.623 to -5.830		
HILLSLOPE	-0.5373 to -0.2598		
EC50	2.383e-007 to 1.479e-006	Con [M]	Vel
Goodness of Fit			0.968
Degrees of Freedom	7	-9.000	1.000
R ²	0.9351	-8.301	0.815
Absolute Sum of Squares	0.04767	-8.000	0.863
Sy.x	0.08253	-7.301	0.763
Constraints		-7.000	0.605
BOTTOM	BOTTOM = 0.0		
TOP	TOP = 1.000	-6.000	0.414
Data		-5.301	0.384
Number of X values	11	-5.000	0.334
Number of Y replicates	1	-4.699	0.068
Total number of values	9		
Number of missing values	2		

Figure C8. IC50 Determination of Compound 35.



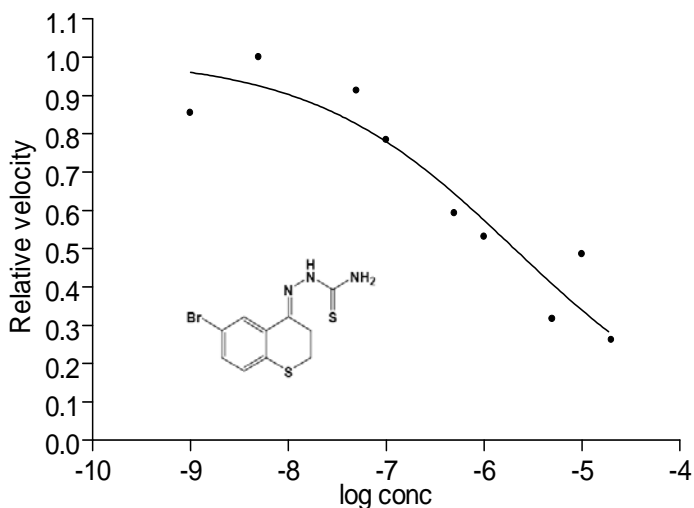
	Vel	Con [M]	Vel
Sigmoidal dose-response (variable slope)		0.000000	8721.0
Best-fit values		1.000000e-009	9389.0
BOTTOM	0.0	5.000000e-009	8082.0
TOP	1.000	1.000000e-009	5855.0
LOGEC50	-4.558	5.000000e-008	8550.0
HILLSLOPE	-0.3735	1.000000e-007	7932.0
EC50	2.769e-005	5.000000e-007	8108.0
Std. Error		0.000001	7829.0
LOGEC50	0.1905	0.000005	5945.0
HILLSLOPE	0.06355	0.000010	5721.0
95% Confidence Intervals		0.000020	4682.0
LOGEC50	-5.008 to -4.107		
HILLSLOPE	-0.5238 to -0.2232		
EC50	9.811e-006 to 7.815e-005	Con [M]	Vel
Goodness of Fit		-9.000	1.000
Degrees of Freedom	7	-8.301	0.861
R ²	0.9075		
Absolute Sum of Squares	0.01996	-7.301	0.911
Sy.x	0.05340	-7.000	0.845
Constraints		-6.301	0.864
BOTTOM	BOTTOM = 0.0	-6.000	0.834
TOP	TOP = 1.000	-5.301	0.633
Data		-5.000	0.609
Number of X values	11	-4.699	0.499
Number of Y replicates	1		
Total number of values	9		
Number of missing values	2		

Figure C9. IC50 Determination of Compound 39.



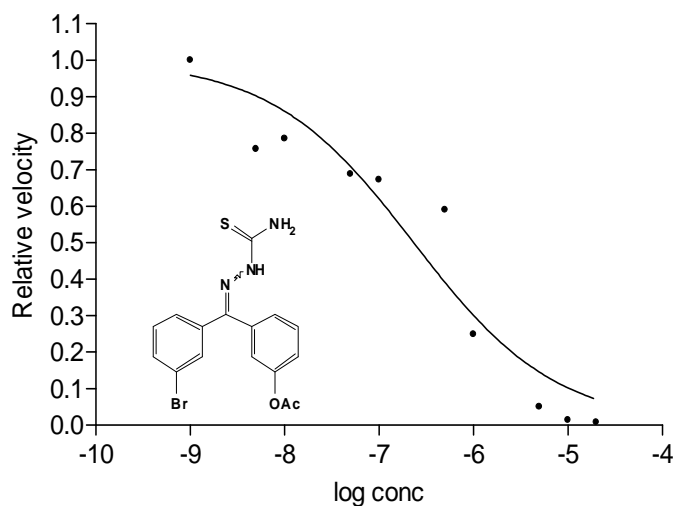
	Vel	Con [M]	Vel
Sigmoidal dose-response (variable slope)		0.000000	14620.0
Best-fit values		1.000000e-009	14320.0
BOTTOM	0.0	5.000000e-009	13020.0
TOP	1.000	1.000000e-008	14010.0
LOGEC50	-5.435	5.000000e-008	12270.0
HILLSLOPE	-0.3657	1.000000e-007	9908.0
EC50	3.669e-006	5.000000e-007	12270.0
Std. Error		0.000001	9711.0
LOGEC50	0.1301	0.000005	6939.0
HILLSLOPE	0.04823	0.000010	5830.0
95% Confidence Intervals		0.000020	5149.0
LOGEC50	-5.754 to -5.117		
HILLSLOPE	-0.4838 to -0.2477		
EC50	1.763e-006 to 7.637e-006	Con [M]	Vel
Goodness of Fit		-9.000	1.000
Degrees of Freedom	6		0.979
R ²	0.9539	-8.000	0.958
Absolute Sum of Squares	0.01938	-7.301	0.839
Sy.x	0.05683	-7.000	0.678
Constraints			
BOTTOM	BOTTOM = 0.0	-6.000	0.664
TOP	TOP = 1.000	-5.301	0.475
Data		-5.000	0.399
Number of X values	11	-4.699	0.352
Number of Y replicates	1		
Total number of values	8		
Number of missing values	3		

Figure C10. IC50 Determination of Compound 41.



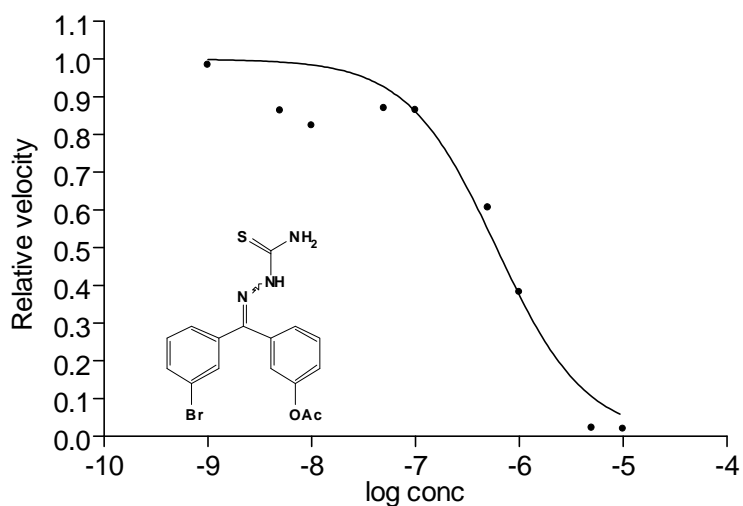
	Vel	Con [M]	Vel
Sigmoidal dose-response (variable slope)		0.000000	5584.0
Best-fit values		1.000000e-009	6611.0
BOTTOM	0.0	5.000000e-009	7737.0
TOP	1.000	1.000000e-008	5230.0
LOGEC50	-5.690	5.000000e-008	7060.0
HILLSLOPE	-0.4190	1.000000e-007	6066.0
EC50	2.041e-006	5.000000e-007	4587.0
Std. Error		0.000001	4106.0
LOGEC50	0.1704	0.000005	2451.0
HILLSLOPE	0.08042	0.000010	3759.0
95% Confidence Intervals		0.000020	2023.0
LOGEC50	-6.093 to -5.287		
HILLSLOPE	-0.6092 to -0.2288		
EC50	8.069e-007 to 5.161e-006	Con [M]	Vel
Goodness of Fit		-9.000	0.854
Degrees of Freedom	7	-8.301	1.000
R ²	0.8945	-7.301	0.912
Absolute Sum of Squares	0.05871	-7.000	0.784
Sy.x	0.09158	-6.301	0.593
Constraints		-6.000	0.531
BOTTOM	BOTTOM = 0.0	-5.301	0.317
TOP	TOP = 1.000	-5.000	0.486
Data		-4.699	0.261
Number of X values	11		
Number of Y replicates	1		
Total number of values	9		
Number of missing values	2		

Figure C11. IC50 Determination of Compound 41.



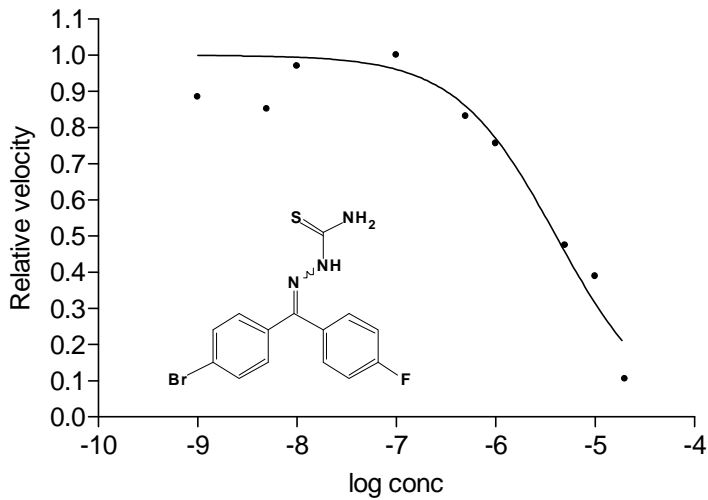
	Vel	Con [M]	Vel
Sigmoidal dose-response (variable slope)		0.000000	9777.00000
Best-fit values		1.000000e-009	11100.00000
BOTTOM	0.0	5.000000e-009	8400.00000
TOP	1.000	1.000000e-008	8709.00000
LOGEC50	-6.633	5.000000e-008	7635.00000
HILLSLOPE	-0.5781	1.000000e-007	7464.00000
EC50	2.328e-007	5.000000e-007	6550.00000
Std. Error		0.000001	2763.00000
LOGEC50	0.1635	0.000005	552.50000
HILLSLOPE	0.1136	0.000010	147.60000
95% Confidence Intervals		0.000020	80.81000
LOGEC50	-7.010 to -6.256		
HILLSLOPE	-0.8400 to -0.3162		
EC50	9.774e-008 to 5.545e-007	Con [M]	Vel
Goodness of Fit			0.881
Degrees of Freedom	8	-9.000	1.000
R ²	0.9216	-8.301	0.757
Absolute Sum of Squares	0.09504	-8.000	0.785
Sy.x	0.1090	-7.301	0.688
Constraints		-7.000	0.672
BOTTOM	BOTTOM = 0.0	-6.301	0.590
TOP	TOP = 1.000	-6.000	0.249
Data		-5.301	0.050
Number of X values	11	-5.000	0.013
Number of Y replicates	1	-4.699	0.007
Total number of values	10		
Number of missing values	1		

Figure C12. IC50 Determination of Compound 50.



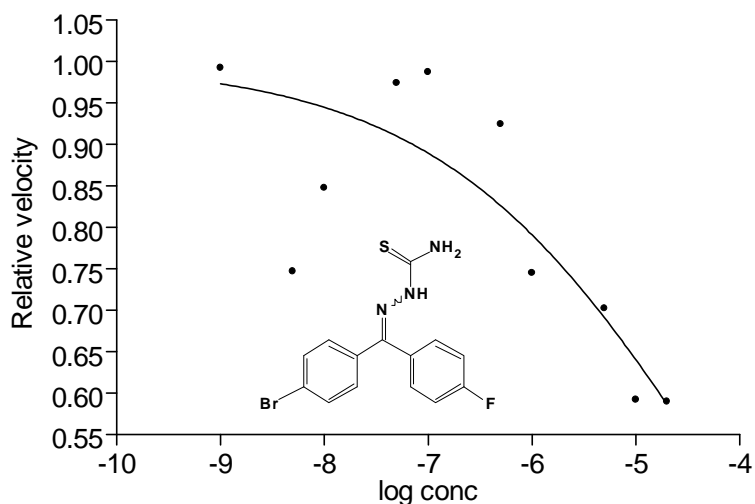
	Vel	Con [M]	Vel
Sigmoidal dose-response (variable slope)		0.000000	4763.00000
Best-fit values		1.000000e-009	4690.00000
BOTTOM	0.0	5.000000e-009	4114.00000
TOP	1.000	1.000000e-008	3922.00000
LOGEC50	-6.219	5.000000e-008	4144.00000
HILLSLOPE	-1.013	1.000000e-007	4122.00000
EC50	6.035e-007	5.000000e-007	2888.00000
Std. Error		0.000001	1821.00000
LOGEC50	0.1012	0.000005	106.20000
HILLSLOPE	0.2277	0.000010	95.43000
95% Confidence Intervals		0.000020	572.50000
LOGEC50	-6.459 to -5.980		
HILLSLOPE	-1.551 to -0.4743		
EC50	3.478e-007 to 1.047e-006	Con [M]	Vel
Goodness of Fit			1.000
Degrees of Freedom	7	-9.000	0.985
R ²	0.9491	-8.301	0.864
Absolute Sum of Squares	0.05739	-8.000	0.823
Sy.x	0.09054	-7.301	0.870
Constraints		-7.000	0.865
BOTTOM	BOTTOM = 0.0	-6.301	0.606
TOP	TOP = 1.000	-6.000	0.382
Data		-5.301	0.022
Number of X values	11	-5.000	0.020
Number of Y replicates	1		
Total number of values	9		
Number of missing values	2		

Figure C13. IC50 Determination of Compound 50.



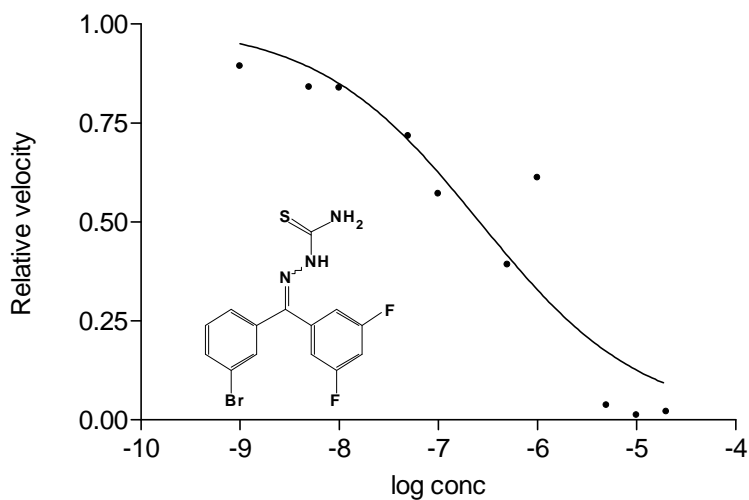
	Vel	Con [M]	Vel
Sigmoidal dose-response (variable slope)		0.000000	3024.00000
Best-fit values		1.000000e-009	6157.00000
BOTTOM	0.0	5.000000e-009	5928.00000
TOP	1.000	1.000000e-008	6755.00000
LOGEC50	-5.392	5.000000e-009	4658.00000
HILLSLOPE	-0.8633	1.000000e-007	6961.00000
EC50	4.059e-006	5.000000e-007	5787.00000
Std. Error		0.000001	5263.00000
LOGEC50	0.1028	0.000005	3300.00000
HILLSLOPE	0.1729	0.000010	2706.00000
95% Confidence Intervals		0.000020	726.50000
LOGEC50	-5.635 to -5.149		
HILLSLOPE	-1.272 to -0.4545		
EC50	2.320e-006 to 7.102e-006	Con [M]	Vel
Goodness of Fit		-9.000	0.884
Degrees of Freedom	7	-8.301	0.852
R ²	0.9291	-8.000	0.970
Absolute Sum of Squares	0.05266		
Sy.x	0.08673	-7.000	1.000
Constraints		-6.301	0.831
BOTTOM	BOTTOM = 0.0	-6.000	0.756
TOP	TOP = 1.000	-5.301	0.474
Data		-5.000	0.389
Number of X values	11	-4.699	0.104
Number of Y replicates	1		
Total number of values	9		
Number of missing values	2		

Figure C14. IC50 Determination of Compound 48.



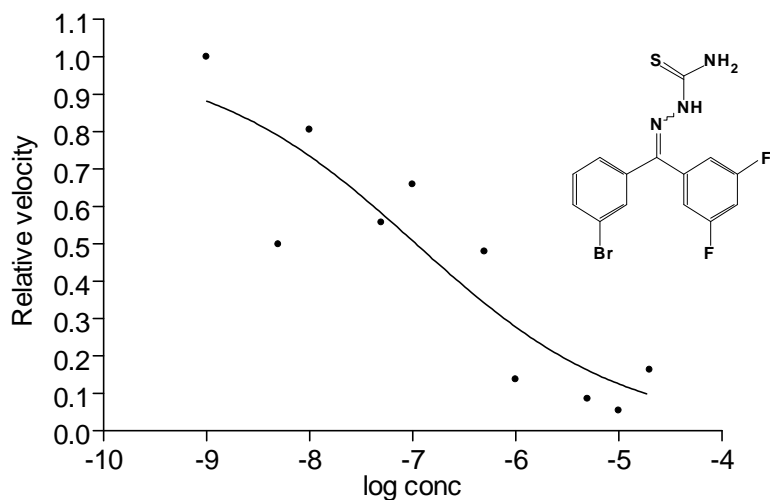
	Vel	Con [M]	Vel
Sigmoidal dose-response (variable slope)		0.000000	2963.00000
Best-fit values		1.000000e-009	2941.00000
BOTTOM	0.0	5.000000e-009	2213.00000
TOP	1.000	1.000000e-008	2512.00000
LOGEC50	-4.236	5.000000e-008	2886.00000
HILLSLOPE	-0.3278	1.000000e-007	2925.00000
EC50	5.810e-005	5.000000e-007	2739.00000
Std. Error		0.000001	2207.00000
LOGEC50	0.4974	0.000005	2081.00000
HILLSLOPE	0.1111	0.000010	1754.00000
95% Confidence Intervals		0.000020	1748.00000
LOGEC50	-5.383 to -3.089		
HILLSLOPE	-0.5841 to -0.07154		
EC50	4.142e-006 to 0.0008149		
Goodness of Fit		Con [M]	Vel
Degrees of Freedom	8	-9.000	1.000
R ²	0.6339	-8.301	0.993
Absolute Sum of Squares	0.08124	-8.000	0.848
Sy.x	0.1008	-7.301	0.974
Constraints		-7.000	0.987
BOTTOM	BOTTOM = 0.0	-6.301	0.924
TOP	TOP = 1.000	-6.000	0.745
Data		-5.301	0.702
Number of X values	11	-5.000	0.592
Number of Y replicates	1	-4.699	0.590
Total number of values	10		
Number of missing values	1		

Figure C15. IC50 Determination of Compound 48.



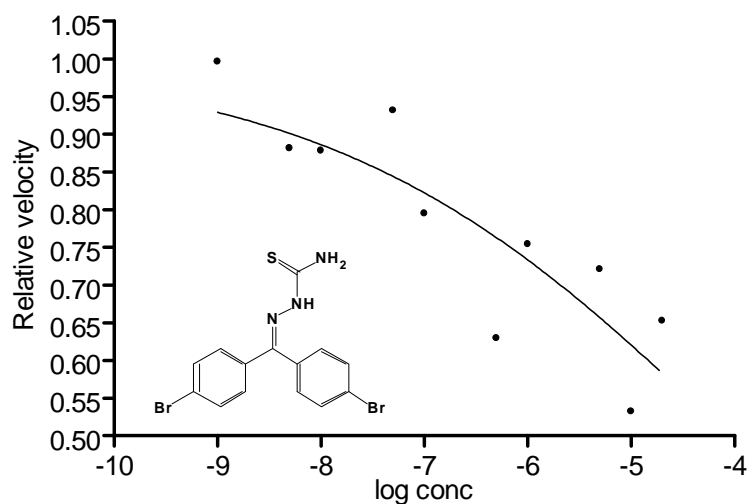
	Vel	Con [M]	Vel
Sigmoidal dose-response (variable slope)		0.000000	4815.00000
Best-fit values		1.000000e-009	4305.00000
BOTTOM	0.0	5.000000e-009	4049.00000
TOP	1.000	1.000000e-008	4037.00000
LOGEC50	-6.583	5.000000e-008	3453.00000
HILLSLOPE	-0.5316	1.000000e-007	2752.00000
EC50	2.614e-007	5.000000e-007	1888.00000
Std. Error		0.000001	2946.00000
LOGEC50	0.1960	0.000005	177.90000
HILLSLOPE	0.1176	0.000010	58.40000
95% Confidence Intervals		0.000020	101.60000
LOGEC50	-7.035 to -6.131		
HILLSLOPE	-0.8027 to -0.2604		
EC50	9.232e-008 to 7.404e-007	Con [M]	Vel
Goodness of Fit		-9.000	0.894
Degrees of Freedom	8	-8.301	0.841
R ²	0.8902	-8.000	0.838
Absolute Sum of Squares	0.1255	-7.301	0.717
Sy.x	0.1253	-7.000	0.572
Constraints		-6.301	0.392
BOTTOM	BOTTOM = 0.0	-6.000	0.612
TOP	TOP = 1.000	-5.301	0.037
Data		-5.000	0.012
Number of X values	11	-4.699	0.021
Number of Y replicates	1		
Total number of values	10		
Number of missing values	1		

Figure C16. IC50 Determination of Compound 49.



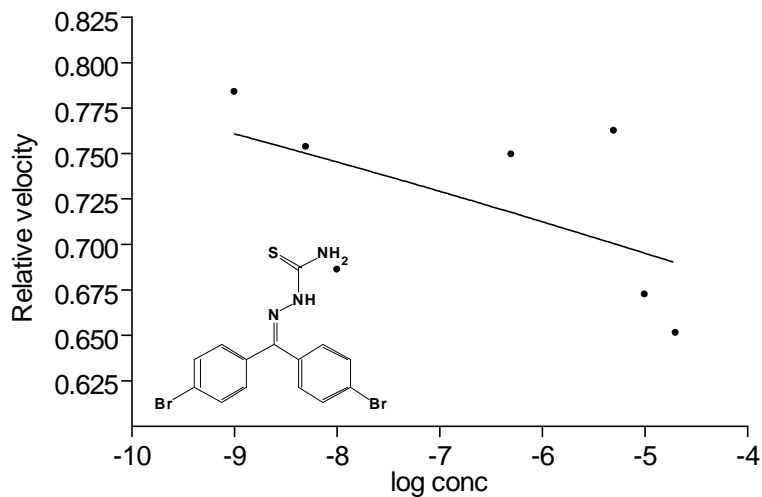
	Vel	Con [M]	Vel
Sigmoidal dose-response (variable slope)		0.000000	4107.00000
Best-fit values		1.000000e-009	4464.00000
BOTTOM	0.0	5.000000e-009	2226.00000
TOP	1.000	1.000000e-008	3594.00000
LOGEC50	-6.968	5.000000e-008	2485.00000
HILLSLOPE	-0.4290	1.000000e-007	2942.00000
EC50	1.077e-007	5.000000e-007	2140.00000
Std. Error		0.000001	611.70000
LOGEC50	0.2668	0.000005	381.80000
HILLSLOPE	0.1126	0.000010	240.90000
95% Confidence Intervals		0.000020	726.50000
LOGEC50	-7.583 to -6.353		
HILLSLOPE	-0.6886 to -0.1694	Con [M]	Vel
EC50	2.611e-008 to 4.440e-007		0.920
Goodness of Fit		-9.000	1.000
Degrees of Freedom	8	-8.301	0.499
R ²	0.8111	-8.000	0.805
Absolute Sum of Squares	0.1807	-7.301	0.557
Sy.x	0.1503	-7.000	0.659
Constraints		-6.301	0.479
BOTTOM	BOTTOM = 0.0	-6.000	0.137
TOP	TOP = 1.000	-5.301	0.086
Data		-5.000	0.054
Number of X values	11	-4.699	0.163
Number of Y replicates	1		
Total number of values	10		
Number of missing values	1		

Figure C17. IC50 Determination of Compound 49.



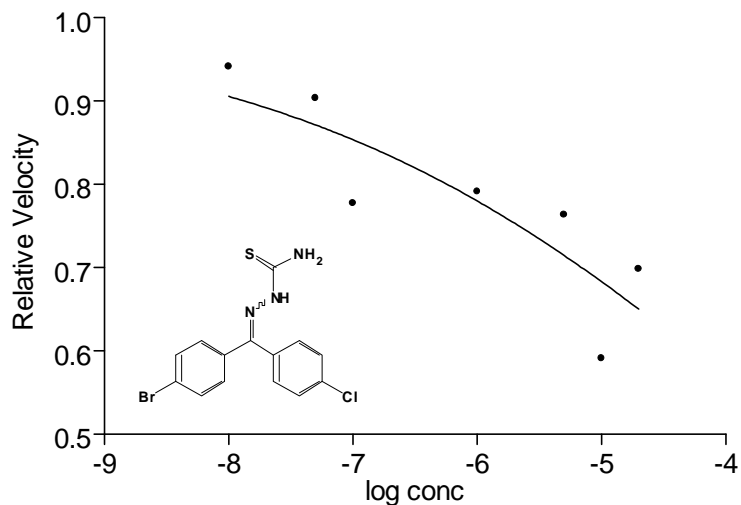
	Vel	Con [M]	Vel
Sigmoidal dose-response (variable slope)		0.000000	8228.00000
Best-fit values		1.000000e-009	8197.00000
BOTTOM	0.0	5.000000e-009	7255.00000
TOP	1.000	1.000000e-008	7228.00000
LOGEC50	-4.055	5.000000e-008	7667.00000
HILLSLOPE	-0.2260	1.000000e-007	6541.00000
EC50	8.816e-005	5.000000e-007	5180.00000
Std. Error		0.000001	6204.00000
LOGEC50	0.5203	0.000005	5931.00000
HILLSLOPE	0.05766	0.000010	4383.00000
95% Confidence Intervals		0.000020	5370.00000
LOGEC50	-5.255 to -2.855		
HILLSLOPE	-0.3590 to -0.09307	Con [M]	Vel
EC50	5.564e-006 to 0.001397		1.000
Goodness of Fit		-9.000	0.996
Degrees of Freedom	8	-8.301	0.882
R ²	0.7514	-8.000	0.878
Absolute Sum of Squares	0.04828	-7.301	0.932
Sy.x	0.07768	-7.000	0.795
Constraints		-6.301	0.630
BOTTOM	BOTTOM = 0.0	-6.000	0.754
TOP	TOP = 1.000	-5.301	0.721
Data		-5.000	0.533
Number of X values	11	-4.699	0.653
Number of Y replicates	1		
Total number of values	10		
Number of missing values	1		

Figure C18. IC50 Determination of Compound 46.



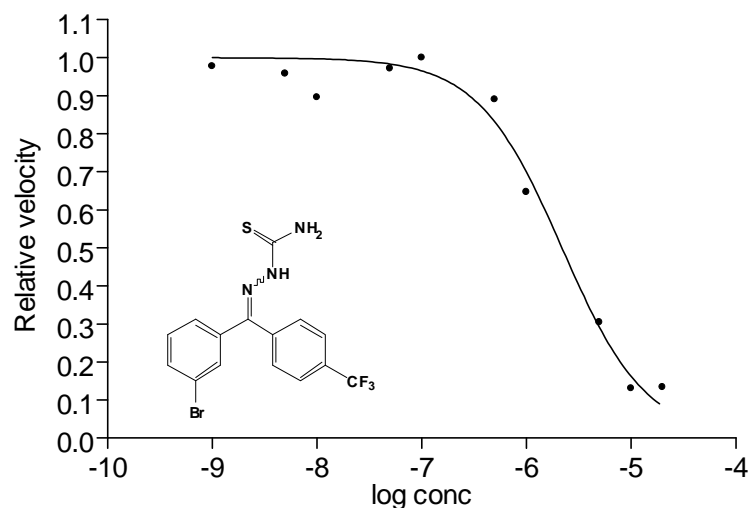
	Vel	Con [M]	Vel
Sigmoidal dose-response (variable slope)		0.000000	9757.00000
Best-fit values		1.000000e-009	8723.00000
BOTTOM	0.0	5.000000e-009	8387.00000
TOP	1.000	1.000000e-008	7636.00000
LOGEC50	4.920	5.000000e-009	11130.00000
HILLSLOPE	-0.03609	1.000000e-007	10860.00000
EC50	83138	5.000000e-007	8342.00000
Std. Error		0.000004	5350.00000
LOGEC50	7.631	0.000005	8485.00000
HILLSLOPE	0.02396	0.000010	7483.00000
95% Confidence Intervals		0.000020	7250.00000
LOGEC50	-14.70 to 24.54		
HILLSLOPE	-0.09770 to 0.02551	Con [M]	Vel
EC50	2.002e-015 to 3.453e+024		0.877
Goodness of Fit		-9.000	0.784
Degrees of Freedom	5	-8.301	0.754
R ²	0.3158	-8.000	0.686
Absolute Sum of Squares	0.01090		
Sy.x	0.04669		
Constraints		-6.301	0.750
BOTTOM	BOTTOM = 0.0		
TOP	TOP = 1.000	-5.301	0.762
Data		-5.000	0.672
Number of X values	11	-4.699	0.651
Number of Y replicates	1		
Total number of values	7		
Number of missing values	4		

Figure C19. IC50 Determination of Compound 46.



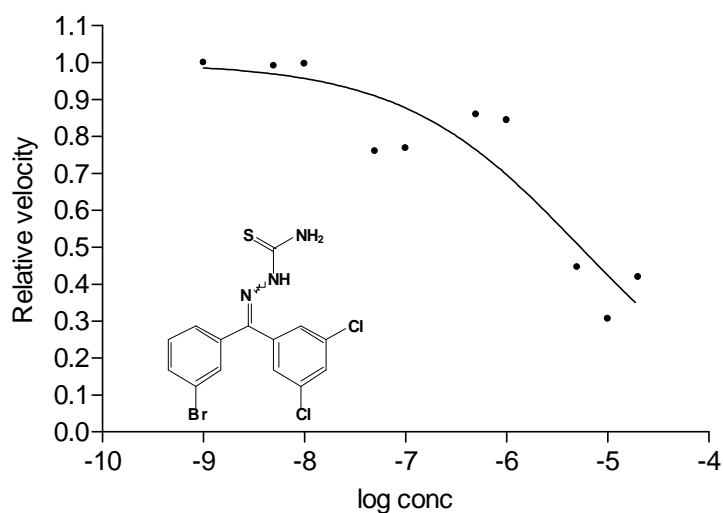
	Vel	Con [M]	Vel
Sigmoidal dose-response (variable slope)		0.000000	5898.00000
Best-fit values		1.000000e-008	4884.00000
BOTTOM	0.0	5.000000e-008	4006.00000
TOP	1.000	1.000000e-008	5552.00000
LOGEC50	-3.454	5.000000e-008	5328.00000
HILLSLOPE	-0.2159	1.000000e-007	4585.00000
EC50	0.0003520	5.000000e-007	3275.00000
Std. Error		0.000001	4668.00000
LOGEC50	0.7147	0.000005	4502.00000
HILLSLOPE	0.06793	0.000010	3486.00000
95% Confidence Intervals		0.000020	4119.00000
LOGEC50	-5.291 to -1.616		
HILLSLOPE	-0.3906 to -0.04129		
EC50	5.117e-006 to 0.02421		
Goodness of Fit		Con [M]	Vel
Degrees of Freedom	5		1.000
R ²	0.7447	-8.000	0.941
Absolute Sum of Squares	0.02145	-7.301	0.903
Sy.x	0.06549	-7.000	0.777
Constraints			
BOTTOM	BOTTOM = 0.0	-6.000	0.791
TOP	TOP = 1.000	-5.301	0.763
Data		-5.000	0.591
Number of X values	11	-4.699	0.698
Number of Y replicates	1		
Total number of values	7		
Number of missing values	4		

Figure C20. IC50 Determination of Compound 47.



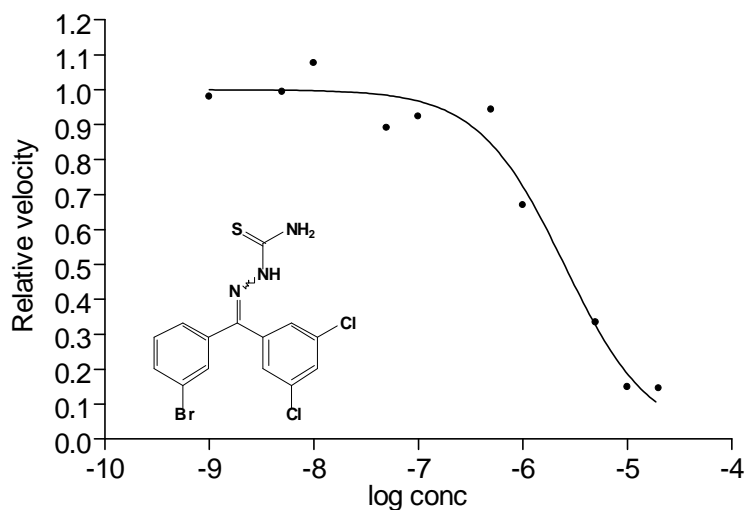
	Vel	Con [M]	Vel
Sigmoidal dose-response (variable slope)		0.000000	4640.00000
Best-fit values		1.000000e-009	4860.00000
BOTTOM	0.0	5.000000e-009	4765.00000
TOP	1.000	1.000000e-008	4454.00000
LOGEC50	-5.659	5.000000e-008	4833.00000
HILLSLOPE	-1.080	1.000000e-007	4972.00000
EC50	2.192e-006	5.000000e-007	4426.00000
Std. Error		0.000001	3216.00000
LOGEC50	0.06021	0.000005	1516.00000
HILLSLOPE	0.1264	0.000010	650.40000
95% Confidence Intervals		0.000020	665.20000
LOGEC50	-5.798 to -5.520		
HILLSLOPE	-1.371 to -0.7883	Con [M]	Vel
EC50	1.592e-006 to 3.018e-006		0.933
Goodness of Fit		-9.000	0.977
Degrees of Freedom	8	-8.301	0.958
R ²	0.9801	-8.000	0.896
Absolute Sum of Squares	0.02363	-7.301	0.972
Sy.x	0.05434	-7.000	1.000
Constraints		-6.301	0.890
BOTTOM	BOTTOM = 0.0	-6.000	0.647
TOP	TOP = 1.000	-5.301	0.305
Data		-5.000	0.131
Number of X values	11	-4.699	0.134
Number of Y replicates	1		
Total number of values	10		
Number of missing values	1		

Figure C21. IC50 Determination of Compound 44.



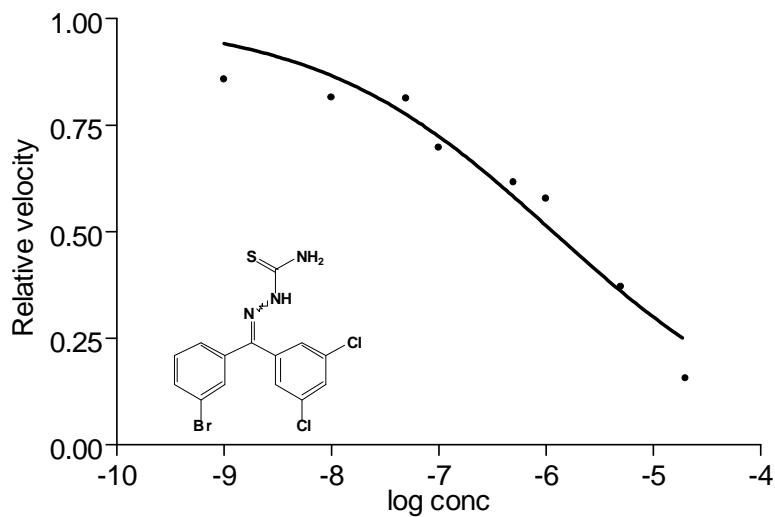
	Vel	Con [M]	Vel
Sigmoidal dose-response (variable slope)		0.000000	9653.00000
Best-fit values		1.000000e-009	10050.00000
BOTTOM	0.0	5.000000e-009	9963.00000
TOP	1.000	1.000000e-008	10020.00000
LOGEC50	-5.271	5.000000e-008	7635.00000
HILLSLOPE	-0.4937	1.000000e-007	7720.00000
EC50	5.362e-006	5.000000e-007	8638.00000
Std. Error		0.000001	8480.00000
LOGEC50	0.1894	0.000005	4483.00000
HILLSLOPE	0.1197	0.000010	3078.00000
95% Confidence Intervals		0.000020	4217.50000
LOGEC50	-5.707 to -4.834		
HILLSLOPE	-0.7696 to -0.2177		
EC50	1.961e-006 to 1.466e-005	Con [M]	Vel
Goodness of Fit			0.960
Degrees of Freedom	8	-9.000	1.000
R ²	0.8480	-8.301	0.991
Absolute Sum of Squares	0.09124	-8.000	0.997
Sy.x	0.1068	-7.301	0.760
Constraints		-7.000	0.768
BOTTOM	BOTTOM = 0.0	-6.301	0.860
TOP	TOP = 1.000	-6.000	0.844
Data		-5.301	0.446
Number of X values	11	-5.000	0.306
Number of Y replicates	1	-4.699	0.420
Total number of values	10		
Number of missing values	1		

Figure C22. IC50 Determination of Compound 51.



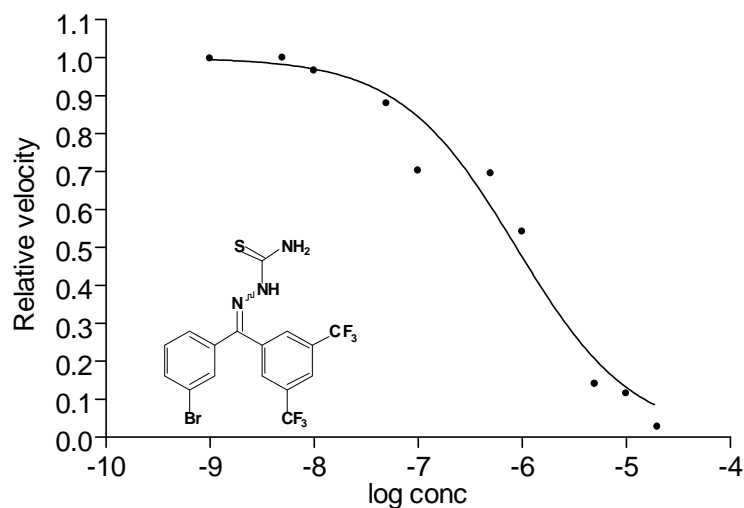
	Vel	Con [M]	Vel
Sigmoidal dose-response (variable slope)		0.000000	6880.0
Best-fit values		1.000000e-009	6743.0
BOTTOM	0.0	5.000000e-009	6838.0
TOP	1.000	1.000000e-008	7405.0
LOGEC50	-5.605	5.000000e-008	6128.0
HILLSLOPE	-1.055	1.000000e-007	6352.0
EC50	2.486e-006	5.000000e-007	6489.0
Std. Error		0.000001	4605.0
LOGEC50	0.07215	0.000005	2297.0
HILLSLOPE	0.1473	0.000010	1024.0
95% Confidence Intervals		0.000020	995.8
LOGEC50	-5.771 to -5.438		
HILLSLOPE	-1.395 to -0.7159		
EC50	1.695e-006 to 3.646e-006	Con [M]	Vel
Goodness of Fit			1.000
Degrees of Freedom	8	-9.000	0.980
R ²	0.9720	-8.301	0.994
Absolute Sum of Squares	0.03360	-8.000	1.076
Sy.x	0.06480	-7.301	0.891
Constraints		-7.000	0.923
BOTTOM	BOTTOM = 0.0	-6.301	0.943
TOP	TOP = 1.000	-6.000	0.669
Data		-5.301	0.334
Number of X values	11	-5.000	0.149
Number of Y replicates	1	-4.699	0.145
Total number of values	10		
Number of missing values	1		

Figure C23. IC50 Determination of Compound 51.



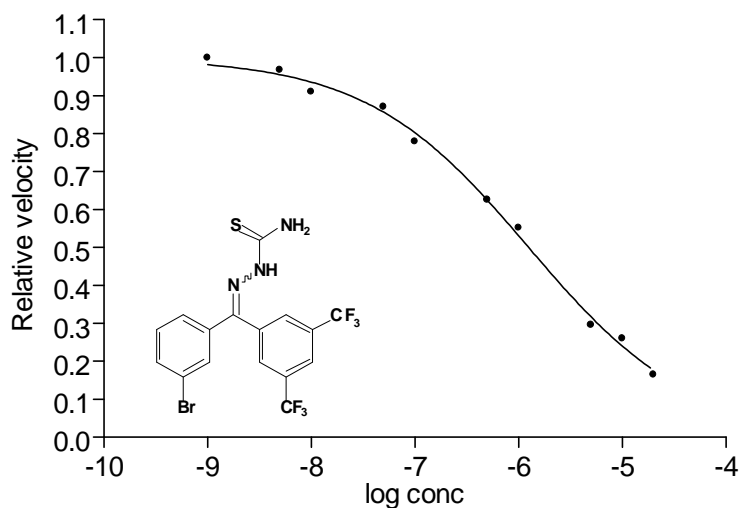
	Vel	Con [M]	Vel
Sigmoidal dose-response (variable slope)		0.000000	4659.00000
Best-fit values		1.000000e-009	3995.00000
BOTTOM	0.0	5.000000e-009	2812.00000
TOP	1.000	1.000000e-008	3799.00000
LOGEC50	-5.934	5.000000e-008	3788.00000
HILLSLOPE	-0.3934	1.000000e-007	3248.00000
EC50	1.164e-006	5.000000e-007	2868.00000
Std. Error		0.000001	2691.00000
LOGEC50	0.1356	0.000005	1727.00000
HILLSLOPE	0.05589	0.000010	3518.00000
95% Confidence Intervals		0.000020	726.50000
LOGEC50	-6.266 to -5.602	Con [M]	Vel
HILLSLOPE	-0.5302 to -0.2567		1.000
EC50	5.418e-007 to 2.498e-006	-9.000	0.857
Goodness of Fit			
Degrees of Freedom	6	-8.000	0.815
R ²	0.9397	-7.301	0.813
Absolute Sum of Squares	0.02512	-7.000	0.697
Sy.x	0.06471	-6.301	0.616
Constraints		-6.000	0.578
BOTTOM	BOTTOM = 0.0	-5.301	0.371
TOP	TOP = 1.000		
Data		-4.699	0.156
Number of X values	11		
Number of Y replicates	1		
Total number of values	8		
Number of missing values	3		

Figure C24. IC50 Determination of Compound 51.



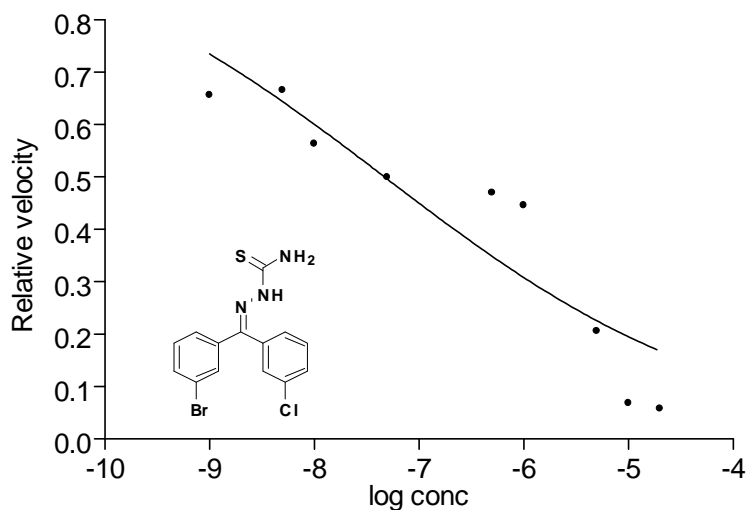
	Vel	Con [M]	Vel
Sigmoidal dose-response (variable slope)		0.000000	8913.0
Best-fit values		1.000000e-009	9581.0
BOTTOM	0.0	5.000000e-009	9603.0
TOP	1.000	1.000000e-008	9275.0
LOGEC50	-6.055	5.000000e-008	8443.0
HILLSLOPE	-0.7770	1.000000e-007	6747.0
EC50	8.813e-007	5.000000e-007	6676.0
Std. Error		0.000001	5199.0
LOGEC50	0.09096	0.000005	1350.0
HILLSLOPE	0.1120	0.000010	1105.0
95% Confidence Intervals		0.000020	262.9
LOGEC50	-6.265 to -5.845		
HILLSLOPE	-1.035 to -0.5188		
EC50	5.437e-007 to 1.429e-006	Con [M]	Vel
Goodness of Fit			0.928
Degrees of Freedom	8	-9.000	0.998
R ²	0.9696	-8.301	1.000
Absolute Sum of Squares	0.04034	-8.000	0.966
Sy.x	0.07101	-7.301	0.879
Constraints		-7.000	0.703
BOTTOM	BOTTOM = 0.0	-6.301	0.695
TOP	TOP = 1.000	-6.000	0.541
Data		-5.301	0.141
Number of X values	11	-5.000	0.115
Number of Y replicates	1	-4.699	0.027
Total number of values	10		
Number of missing values	1		

Figure C25. IC50 Determination of Compound 52.



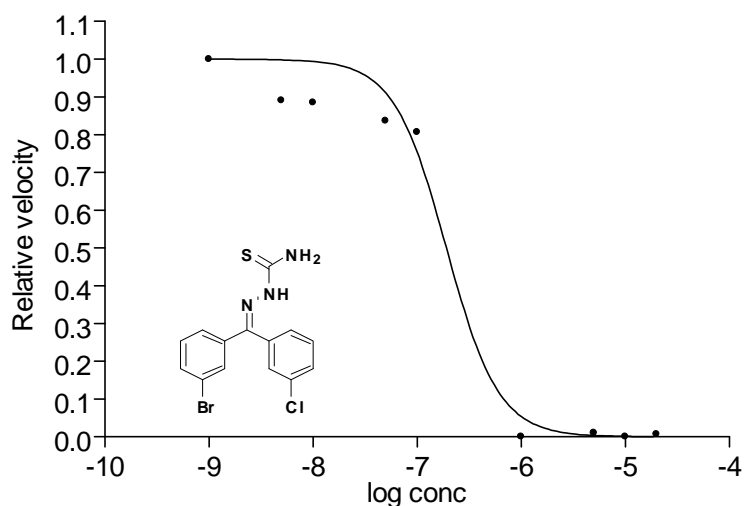
	Vel	Con [M]	Vel
Sigmoidal dose-response (variable slope)		0.000000	5191.0
Best-fit values		1.000000e-009	5266.0
BOTTOM	0.0	5.000000e-009	5098.0
TOP	1.000	1.000000e-008	4795.0
LOGEC50	-5.903	5.000000e-008	4587.0
HILLSLOPE	-0.5546	1.000000e-007	4103.0
EC50	1.251e-006	5.000000e-007	3293.0
Std. Error		0.000001	2906.0
LOGEC50	0.03117	0.000005	1555.0
HILLSLOPE	0.02133	0.000010	1368.0
95% Confidence Intervals		0.000020	866.6
LOGEC50	-5.975 to -5.831		
HILLSLOPE	-0.6037 to -0.5054		
EC50	1.060e-006 to 1.477e-006	Con [M]	Vel
			0.986
Goodness of Fit		-9.000	1.000
Degrees of Freedom	8	-8.301	0.968
R ²	0.9962	-8.000	0.911
Absolute Sum of Squares	0.003348	-7.301	0.871
Sy.x	0.02046	-7.000	0.779
Constraints		-6.301	0.625
BOTTOM	BOTTOM = 0.0	-6.000	0.552
TOP	TOP = 1.000	-5.301	0.295
Data		-5.000	0.260
Number of X values	11	-4.699	0.165
Number of Y replicates	1		
Total number of values	10		
Number of missing values	1		

Figure C26. IC50 Determination of Compound 52.



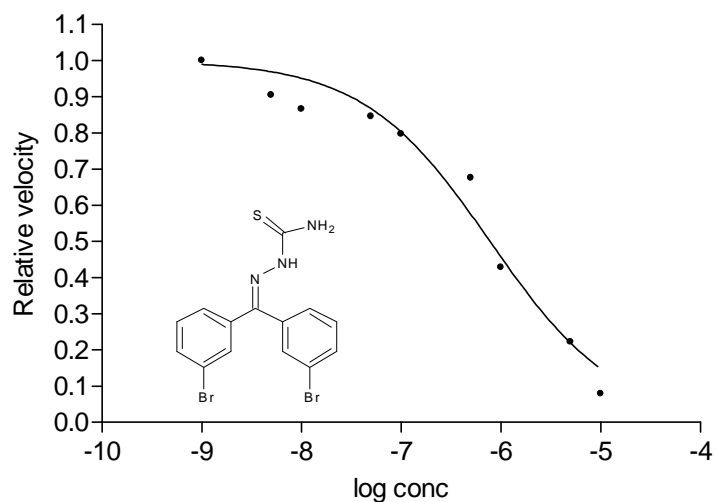
	Vel	Con [M]	Vel
Sigmoidal dose-response (variable slope)		0.000000	7838.0
Best-fit values		1.000000e-009	5147.0
BOTTOM	0.0	5.000000e-009	5221.0
TOP	1.000	1.000000e-008	4420.0
LOGEC50	-7.326	5.000000e-008	3917.0
HILLSLOPE	-0.2644	1.000000e-007	4419.0
EC50	4.716e-008	5.000000e-007	3688.0
Std. Error		0.000001	3496.0
LOGEC50	0.2753	0.000005	1614.0
HILLSLOPE	0.05340	0.000010	535.7
95% Confidence Intervals		0.000020	452.9
LOGEC50	-7.978 to -6.675		
HILLSLOPE	-0.3907 to -0.1381	Con [M]	Vel
EC50	1.053e-008 to 2.112e-007		1.000
Goodness of Fit		-9.000	0.657
Degrees of Freedom	7	-8.301	0.666
R ²	0.8419	-8.000	0.564
Absolute Sum of Squares	0.07037	-7.301	0.500
Sy.x	0.1003		
Constraints		-6.301	0.471
BOTTOM	BOTTOM = 0.0	-6.000	0.446
TOP	TOP = 1.000	-5.301	0.206
Data		-5.000	0.068
Number of X values	11	-4.699	0.058
Number of Y replicates	1		
Total number of values	9		
Number of missing values	2		

Figure C27. IC50 Determination of Compound 33.



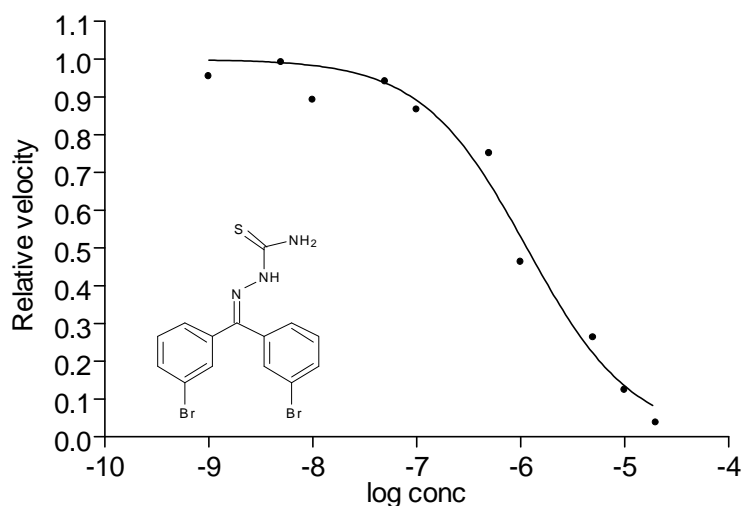
	Vel	Con [M]	Vel
Sigmoidal dose-response (variable slope)		0.000000	3075.00
Best-fit values		1.000000e-009	3572.00
BOTTOM	0.0	5.000000e-009	3183.00
TOP	1.000	1.000000e-008	3161.00
LOGEC50	-6.718	5.000000e-008	2988.00
HILLSLOPE	-1.732	1.000000e-007	2882.00
EC50	1.914e-007	5.000000e-007	3216.00
Std. Error		0.000001	0.00
LOGEC50	0.1181	0.000005	34.86
HILLSLOPE	0.5334	0.000010	0.00
95% Confidence Intervals		0.000020	24.46
LOGEC50	-6.997 to -6.439		
HILLSLOPE	-2.993 to -0.4706		
EC50	1.006e-007 to 3.643e-007	Con [M]	Vel
Goodness of Fit			0.861
Degrees of Freedom	7	-9.000	1.000
R ²	0.9801	-8.301	0.891
Absolute Sum of Squares	0.03461	-8.000	0.885
Sy.x	0.07031	-7.301	0.837
Constraints		-7.000	0.807
BOTTOM	BOTTOM = 0.0		
TOP	TOP = 1.000	-6.000	0.000
Data		-5.301	0.010
Number of X values	11	-5.000	0.000
Number of Y replicates	1	-4.699	0.007
Total number of values	9		
Number of missing values	2		

Figure C28. IC50 Determination of Compound 33.



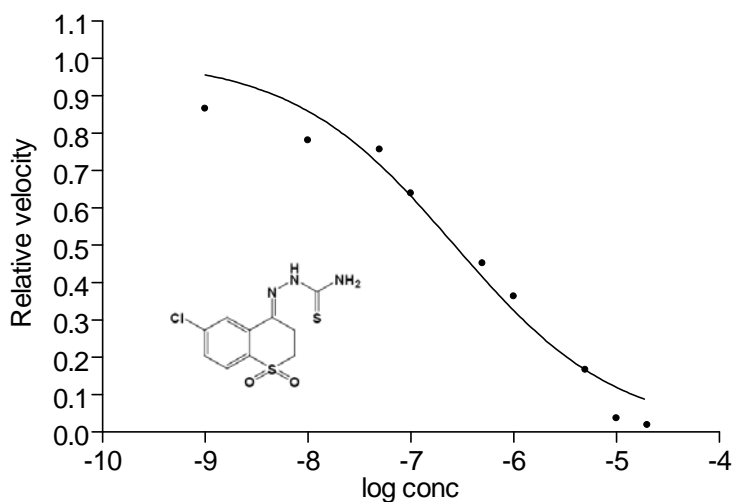
	Vel	Con [M]	Vel
Sigmoidal dose-response (variable slope)		0.000000	6673.00
Best-fit values		1.000000e-009	6881.00
BOTTOM	0.0	5.000000e-009	6225.00
TOP	1.000	1.000000e-008	5959.00
LOGEC50	-6.109	5.000000e-008	5821.00
HILLSLOPE	-0.6828	1.000000e-007	5486.00
EC50	7.783e-007	5.000000e-007	4650.00
Std. Error		0.000001	2947.00
LOGEC50	0.08811	0.000005	1525.00
HILLSLOPE	0.08976	0.000010	545.00
95% Confidence Intervals		0.000020	26.14
LOGEC50	-6.317 to -5.900		
HILLSLOPE	-0.8950 to -0.4705		
EC50	4.817e-007 to 1.258e-006	Con [M]	Vel
Goodness of Fit			0.970
Degrees of Freedom	7	-9.000	1.000
R ²	0.9673	-8.301	0.905
Absolute Sum of Squares	0.02788	-8.000	0.866
Sy.x	0.06311	-7.301	0.846
Constraints		-7.000	0.797
BOTTOM	BOTTOM = 0.0	-6.301	0.676
TOP	TOP = 1.000	-6.000	0.428
Data		-5.301	0.222
Number of X values	11	-5.000	0.079
Number of Y replicates	1		
Total number of values	9		
Number of missing values	2		

Figure C29. IC50 Determination of Compound 38.



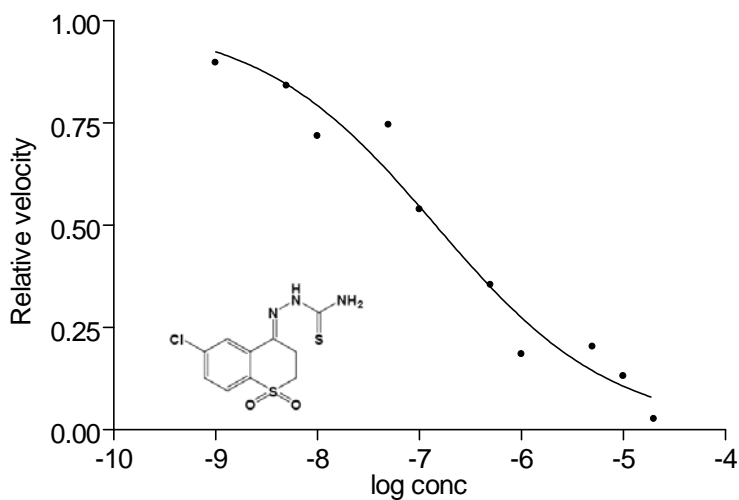
	Vel	Con [M]	Vel
Sigmoidal dose-response (variable slope)		0.000000	10170.00
Best-fit values		1.000000e-009	9712.00
BOTTOM	0.0	5.000000e-009	10090.00
TOP	1.000	1.000000e-008	9075.00
LOGEC50	-5.938	5.000000e-008	9570.00
HILLSLOPE	-0.8604	1.000000e-007	8815.00
EC50	1.153e-006	5.000000e-007	7640.00
Std. Error		0.000001	4711.00
LOGEC50	0.06827	0.000005	2679.00
HILLSLOPE	0.1017	0.000010	1261.00
95% Confidence Intervals		0.000020	378.90
LOGEC50	-6.096 to -5.781		
HILLSLOPE	-1.095 to -0.6259		
EC50	8.021e-007 to 1.656e-006	Con [M]	Vel
Goodness of Fit			1.000
Degrees of Freedom	8	-9.000	0.955
R ²	0.9797	-8.301	0.992
Absolute Sum of Squares	0.02520	-8.000	0.892
Sy.x	0.05613	-7.301	0.941
Constraints		-7.000	0.867
BOTTOM	BOTTOM = 0.0	-6.301	0.751
TOP	TOP = 1.000	-6.000	0.463
Data		-5.301	0.263
Number of X values	11	-5.000	0.124
Number of Y replicates	1	-4.699	0.037
Total number of values	10		
Number of missing values	1		

Figure C30. IC50 Determination of Compound 38.



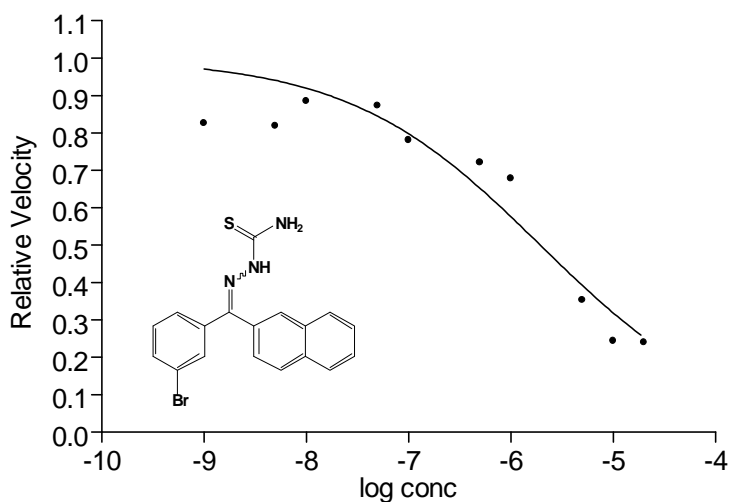
	Vel	Con [M]	Vel
Sigmoidal dose-response (variable slope)		0.000000	10170.00000
Best-fit values		1.000000e-009	8795.00000
BOTTOM	0.0	5.000000e-009	10130.00000
TOP	1.000	1.000000e-008	7937.00000
LOGEC50	-6.576	5.000000e-008	7684.00000
HILLSLOPE	-0.5507	1.000000e-007	6495.00000
EC50	2.657e-007	5.000000e-007	4584.00000
Std. Error		0.000001	3691.00000
LOGEC50	0.1030	0.000005	1690.00000
HILLSLOPE	0.06912	0.000010	370.30000
95% Confidence Intervals		0.000020	183.90000
LOGEC50	-6.819 to -6.332		
HILLSLOPE	-0.7142 to -0.3872		
EC50	1.516e-007 to 4.656e-007		
Goodness of Fit		Con [M]	Vel
Degrees of Freedom	7	-9.000	1.000
R ²	0.9646	-8.000	0.865
Absolute Sum of Squares	0.03026	-7.301	0.780
Sy.x	0.06574	-7.000	0.639
Constraints		-6.301	0.451
BOTTOM	BOTTOM = 0.0	-6.000	0.363
TOP	TOP = 1.000	-5.301	0.166
Data		-5.000	0.036
Number of X values	11	-4.699	0.018
Number of Y replicates	1		
Total number of values	9		
Number of missing values	2		

Figure C31. IC50 Determination of Compound 42.



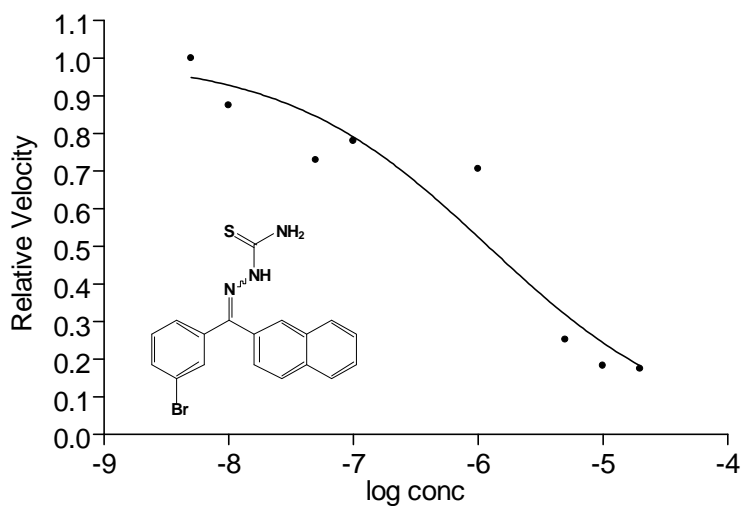
	Vel	Con [M]	Vel
Sigmoidal dose-response (variable slope)		0.000000	6497.00000
Best-fit values		1.000000e-009	5830.00000
BOTTOM	0.0	5.000000e-009	5462.00000
TOP	1.000	1.000000e-008	4665.00000
LOGEC50	-6.842	5.000000e-008	4843.00000
HILLSLOPE	-0.5026	1.000000e-007	3501.00000
EC50	1.439e-007	5.000000e-007	2298.00000
Std. Error		0.000001	1198.00000
LOGEC50	0.1062	0.000005	1318.00000
HILLSLOPE	0.05797	0.000010	847.80000
95% Confidence Intervals		0.000020	168.10000
LOGEC50	-7.087 to -6.597		
HILLSLOPE	-0.6363 to -0.3689	Con [M]	Vel
EC50	8.188e-008 to 2.530e-007		1.000
Goodness of Fit		-9.000	0.897
Degrees of Freedom	8	-8.301	0.841
R ²	0.9634	-8.000	0.718
Absolute Sum of Squares	0.03446	-7.301	0.745
Sy.x	0.06563	-7.000	0.539
Constraints		-6.301	0.354
BOTTOM	BOTTOM = 0.0	-6.000	0.184
TOP	TOP = 1.000	-5.301	0.203
Data		-5.000	0.130
Number of X values	11	-4.699	0.026
Number of Y replicates	1		
Total number of values	10		
Number of missing values	1		

Figure C32. IC50 Determination of Compound 42.



	Vel	Con [M]	Vel
Sigmoidal dose-response (variable slope)		0.000000	7281.00000
Best-fit values		1.000000e-009	6018.00000
BOTTOM	0.0	5.000000e-009	5964.00000
TOP	1.000	1.000000e-008	6444.00000
LOGEC50	-5.712	5.000000e-008	6359.00000
HILLSLOPE	-0.4630	1.000000e-007	5683.00000
EC50	1.940e-006	5.000000e-007	5253.00000
Std. Error		0.000001	4939.00000
LOGEC50	0.1496	0.000005	2568.00000
HILLSLOPE	0.07827	0.000010	1774.00000
95% Confidence Intervals		0.000020	1748.00000
LOGEC50	-6.057 to -5.367		
HILLSLOPE	-0.6435 to -0.2825		
EC50	8.765e-007 to 4.294e-006		
Goodness of Fit		Con [M]	Vel
Degrees of Freedom	8		1.000
R ²	0.9006	-9.000	0.827
Absolute Sum of Squares	0.06054	-8.301	0.819
Sy.x	0.08699	-8.000	0.885
		-7.301	0.873
Constraints		-7.000	0.781
BOTTOM	BOTTOM = 0.0	-6.301	0.721
TOP	TOP = 1.000	-6.000	0.678
Data		-5.301	0.353
Number of X values	11	-5.000	0.244
Number of Y replicates	1	-4.699	0.240
Total number of values	10		
Number of missing values	1		

Figure C33. IC50 Determination of Compound 53.



	Vel	Con [M]	Vel
Sigmoidal dose-response (variable slope)		0.000000	10070.00000
Best-fit values		1.000000e-009	5290.00000
BOTTOM	0.0	5.000000e-009	7215.00000
TOP	1.000	1.000000e-008	6312.00000
LOGEC50	-5.919	5.000000e-008	5261.00000
HILLSLOPE	-0.5342	1.000000e-007	5627.00000
EC50	1.204e-006	5.000000e-007	6151.00000
Std. Error		0.000001	5093.00000
LOGEC50	0.1753	0.000005	1816.00000
HILLSLOPE	0.1036	0.000010	1317.00000
95% Confidence Intervals		0.000020	1256.00000
LOGEC50	-6.348 to -5.490		
HILLSLOPE	-0.7878 to -0.2807	Con [M]	Vel
EC50	4.483e-007 to 3.234e-006	-8.301	1.000
Goodness of Fit		-8.000	0.875
Degrees of Freedom	6	-7.301	0.729
R ²	0.9220	-7.000	0.780
Absolute Sum of Squares	0.06017		
Sy.x	0.1001	-6.000	0.706
Constraints		-5.301	0.252
BOTTOM	BOTTOM = 0.0	-5.000	0.183
TOP	TOP = 1.000	-4.699	0.174
Data			
Number of X values	11		
Number of Y replicates	1		
Total number of values	8		
Number of missing values	3		

Figure C34. IC50 Determination of Compound 53.

APPENDIX D
DMEM components



Product Information

Dulbecco's Modified Eagle's Medium (DME)

Many modifications of Eagle's Medium have been developed since the original formulation appeared in the literature. Among the most widely used of these modifications is Dulbecco's Modified Eagle's Medium (DME). DME is a modification of Basal Medium Eagle (BME) that contains a four-fold higher concentration of amino acids and vitamins, as well as additional supplementary components. The original DME formula contains 1000 mg/L of glucose and was first reported for culturing embryonic mouse cells. A further alteration with 4500 mg/L glucose has proved to be optimal in cultivating certain cell types.

REFERENCES

1. Dulbecco, R. and Freeman, G. (1959). Plaque Production by the Polyoma Virus. *Virology*. 8, 396-397.
2. Smith, J.D., Freeman, G., Vogt, M. and Dulbecco, R. (1960). The Nucleic Acid of Polyoma Virus. 12, 185-196.
3. Morton, H.J., (1970). A Survey of Commercially Available Tissue Culture Media. *In Vitro*. 6, 89.
4. Rutzky, L.P. and Pumper, R.W., (1974). Supplement to a Survey of Commercially Available Tissue Culture Media (1970). *In Vitro*. 9, 468.

Formulations begin on next page.

	D 0422		D 2429	D 2554					
	[1X]	D 1152	[10X]	[10X]	D 2902	D 3656	D 5030	D 5280	D 5523
COMPONENT	g/L	g/L	g/L	g/L	g/L	g/L	g/L	g/L	g/L
INORGANIC SALTS									
CaCl ₂ •2H ₂ O	0.265	0.265	2.65	2.65	0.265	0.265	0.265	0.265	0.265
Fe(NO ₃) ₃ •9H ₂ O	0.0001	0.0001	0.001	0.001	0.0001	0.0001	0.0001	0.0001	0.0001
MgSO ₄	0.09767	0.09767	0.9767	0.9767	0.09767	0.09767	0.09767	0.09767	0.09767
KCl	0.4	0.4	4.0	4.0	0.4	0.4	0.4	0.4	0.4
NaHCO ₃	3.7	—	—	—	—	—	—	—	—
NaCl	6.4	4.4	64.0	64.0	6.4	6.4	6.4	6.4	6.4
NaH ₂ PO ₄	0.109	0.109	1.09	1.09	0.109	—	0.109	0.109	0.109
Succinic Acid	—	—	—	—	—	—	—	0.075	—
Sodium Succinate	—	—	—	—	—	—	—	0.1	—
AMINO ACIDS									
L-Arginine•HCl	0.084	0.084	0.84	0.84	0.084	0.084	0.084	0.084	0.084
L-Cystine•2HCl	—	0.0626	0.626	0.626	0.0626	0.0626	0.0626	0.0626	0.0626
L-Glutamine	—	0.584	—	—	0.584	0.584	—	—	0.584
Glycine	0.03	0.030	0.30	0.30	0.030	0.030	0.030	0.030	0.030
L-Histidine•HCl•H ₂ O	0.042	0.042	0.42	0.42	0.042	0.042	0.042	0.042	0.042
L-Isoleucine	0.105	0.105	1.05	1.05	0.105	0.105	0.105	0.105	0.105
L-Leucine	0.105	0.105	1.05	1.05	0.105	0.105	0.105	0.105	0.105
L-Lysine•HCl	0.146	0.146	1.46	1.46	0.146	0.146	0.146	0.146	0.146
L-Methionine	—	0.030	0.30	0.30	0.030	0.030	0.030	0.030	0.030
L-Phenylalanine	0.066	0.066	0.66	0.66	0.066	0.066	0.066	0.066	0.066
L-Serine	0.042	0.042	0.42	0.42	0.042	0.042	0.042	0.042	0.042
L-Threonine	0.095	0.095	0.95	0.95	0.095	0.095	0.095	0.095	0.095
L-Tryptophan	0.016	0.016	0.16	0.16	0.016	0.016	0.016	0.016	0.016
L-Tyrosine (free base)	—	—	—	—	—	—	—	0.072	—
L-Tyrosine•2Na•2H ₂ O	0.10379	0.10379	1.0379	1.0379	0.10379	0.10379	0.10379	—	0.10379
L-Valine	0.094	0.094	0.94	0.94	0.094	0.094	0.094	0.094	0.094
VITAMINS									
Choline Bitartrate	—	—	—	—	—	—	—	0.0072	—
Choline Chloride	0.004	0.004	0.04	0.04	0.004	0.004	0.004	—	0.004
Folic Acid	0.004	0.004	—	—	0.004	0.004	0.004	0.004	0.004
myo-Inositol	0.0072	0.0072	0.072	0.072	0.0072	0.0072	0.0072	0.0072	0.0072
Niacinamide	0.004	0.004	0.04	0.04	0.004	0.004	0.004	0.004	0.004
D-Pantothenic Acid•½Ca	0.004	0.004	0.04	0.04	0.004	0.004	0.004	0.004	0.004
Pyridoxal•HCl	—	0.004	—	—	0.004	0.004	0.004	0.004	0.004
Pyridoxine•HCl	0.004	—	0.04	0.04	—	—	—	—	—
Riboflavin	0.0004	0.0004	0.004	0.004	0.0004	0.0004	0.0004	0.0004	0.0004
Thiamine•HCl	0.004	0.004	0.04	0.04	0.004	0.004	0.004	0.004	0.004
OTHER									
D-Glucose	4.5	4.5	10.0	45.0	1.0	4.5	—	1.0	1.0
HEPES	—	5.958	—	—	—	—	—	—	—
Phenol Red•Na	0.0159	0.0159	0.159	0.159	—	0.0159	—	0.0093	0.0159
Pyruvic Acid•Na	0.11	—	1.1	1.1	0.11	—	—	0.11	0.11
ADD									
Glucose	—	—	—	—	—	—	1.0	—	—
L-Glutamine	0.584	—	0.584 (1X)	0.584 (1X)	—	—	0.584	0.584	—
L-Cystine•2HCl	—	—	—	—	—	—	—	—	—
L-Leucine	—	—	—	—	—	—	—	—	—
L-Lysine•HCl	—	—	—	—	—	—	—	—	—
L-Methionine	—	—	—	—	—	—	—	—	—
NaHCO ₃	—	3.7	3.7 (1X)	3.7 (1X)	3.7	3.7	3.7	3.7	3.7
NaH ₂ PO ₄	—	—	—	—	—	0.109	—	—	—
Phenol Red•Na	—	—	—	—	—	—	—	—	—
Pyruvic Acid•Na	—	—	—	—	—	—	—	—	—
Grams of powder required to prepare 1 L	N/A	17.4	N/A	N/A	10.0	13.3	8.3	9.6	10.0

	D 5546	D 5648	D 5671	D 5796	D 5921	D 6046	D 6171	D 6429	D 6546	D 7777
	[1X]	D 6655	[1X]	D 6780						
COMPONENT	g/L									
INORGANIC SALTS										
CaCl ₂ •2H ₂ O	0.265	0.265	0.265	0.265	0.265	0.265	0.265	0.265	0.265	0.265
Fe(NO ₃) ₃ •9H ₂ O	0.0001	0.0001	0.0001	0.0001	0.0001	0.0001	0.0001	0.0001	0.0001	0.0001
MgSO ₄	0.09767	0.09767	0.09767	0.09767	0.09767	0.09767	0.09767	0.09767	0.09767	0.09767
KCl	0.4	0.4	0.4	0.4	0.4	0.4	0.4	0.4	0.4	0.4
NaHCO ₃	3.7	—	3.7	3.7	3.7	3.7	3.7	3.7	3.7	—
NaCl	6.4	6.4	6.4	6.4	6.4	6.4	4.4	6.4	6.4	6.4
NaH ₂ PO ₄	0.109	0.109	0.109	0.109	0.109	0.109	0.109	0.109	0.109	0.109
Succinic Acid	—	—	—	—	—	—	—	—	—	—
Sodium Succinate	—	—	—	—	—	—	—	—	—	—
AMINO ACIDS										
L-Arginine•HCl	0.084	0.084	0.084	0.084	0.084	0.084	0.084	0.084	0.084	0.084
L-Cystine•2HCl	0.0626	0.0626	0.0626	0.0626	0.0626	0.0626	0.0626	0.0626	0.0626	0.0626
L-Glutamine	—	0.584	—	0.584	—	0.584	—	0.584	—	0.584
Glycine	0.030	0.030	0.030	0.030	0.030	0.030	0.030	0.030	0.03	0.030
L-Histidine•HCl•H ₂ O	0.042	0.042	0.042	0.042	0.042	0.042	0.042	0.042	0.042	0.042
L-Isoleucine	0.105	0.105	0.105	0.105	0.105	0.105	0.105	0.105	0.105	0.105
L-Leucine	0.105	0.105	0.105	0.105	0.105	0.105	0.105	0.105	0.105	0.105
L-Lysine•HCl	0.146	0.146	0.146	0.146	0.146	0.146	0.146	0.146	0.146	0.146
L-Methionine	0.030	0.030	0.030	0.030	0.030	0.030	0.030	0.030	0.030	0.030
L-Phenylalanine	0.066	0.066	0.066	0.066	0.066	0.066	0.066	0.066	0.066	0.066
L-Serine	0.042	0.042	0.042	0.042	0.042	0.042	0.042	0.042	0.042	0.042
L-Threonine	0.095	0.095	0.095	0.095	0.095	0.095	0.095	0.095	0.095	0.095
L-Tryptophan	0.016	0.016	0.016	0.016	0.016	0.016	0.016	0.016	0.016	0.016
L-Tyrosine (free base)	—	—	—	—	—	—	—	—	—	—
L-Tyrosine•2Na•2H ₂ O	0.10379	0.10379	0.10379	0.10379	0.10379	0.10379	0.10379	0.10379	0.10379	0.10379
L-Valine	0.094	0.094	0.094	0.094	0.094	0.094	0.094	0.094	0.094	0.094
VITAMINS										
Choline Bitartrate	—	—	—	—	—	—	—	—	—	—
Choline Chloride	0.001	0.001	0.001	0.001	0.001	0.001	0.001	0.001	0.001	0.001
Folic Acid	0.004	0.004	0.004	0.004	0.004	0.004	0.004	0.004	0.004	0.004
myo-Inositol	0.0072	0.0072	0.0072	0.0072	0.0072	0.0072	0.0072	0.0072	0.0072	0.0072
Niacinamide	0.004	0.004	0.004	0.004	0.004	0.004	0.004	0.004	0.004	0.004
D-Pantothenic Acid•½Ca	0.004	0.004	0.004	0.004	0.004	0.004	0.004	0.004	0.004	0.004
Pyridoxal•HCl	—	0.004	—	—	—	—	—	—	—	0.004
Pyridoxine•HCl	0.004	—	0.004	0.004	0.004	0.004	0.004	0.004	0.004	—
Riboflavin	0.0004	0.0004	0.0004	0.0004	0.0004	0.0004	0.0004	0.0004	0.0004	0.0004
Thiamine•HCl	0.004	0.004	0.004	0.004	0.004	0.004	0.004	0.004	0.004	0.004
OTHER										
D-Glucose	1.0	4.5	4.5	4.5	1.0	1.0	4.5	4.5	4.5	4.5
HEPES	—	—	—	—	—	—	5.958	—	—	—
Phenol Red•Na	0.0159	0.0159	0.0159	0.0159	—	0.0159	0.0159	0.0159	0.015	0.0159
Pyruvic Acid•Na	0.11	—	—	—	—	0.11	—	0.11	0.11	0.11
ADD										
Glucose	—	—	—	—	—	—	—	—	—	—
L-Glutamic	0.584	—	0.584	—	0.584	—	0.584	—	0.584	—
L-Cystine•2HCl	—	—	—	—	—	—	—	—	—	—
L-Leucine	—	—	—	—	—	—	—	—	—	—
L-Lysine•HCl	—	—	—	—	—	—	—	—	—	—
L-Methionine	—	—	—	—	—	—	—	—	—	—
NaHCO ₃	—	3.7	—	—	—	—	—	—	—	3.7
NaH ₂ PO ₄	—	—	—	—	—	—	—	—	—	—
Phenol Red•Na	—	—	—	—	—	—	—	—	—	—
Pyruvic Acid•Na	—	—	—	—	—	—	—	—	—	—
Grams of powder required to prepare 1 L	N/A	13.4	N/A	13.5						

REFERENCES

- (1) WHO Cell culture protocols. <http://www.who.int/vaccines/en/poliolab/webhelp/> (accessed 10/08, 2008).
- (2) Johnson, Sherida L and Maurizio Pellecchia *Current topics in medicinal chemistry* **2006**, *6*, 317-329.
- (3) Loser, R. *J. Med. Chem.* **2005**, *48*, 7688.
- (4) Berdowska, I.; Berdowska, I. *Clinica Chimica Acta* **2004**, *342*, 41.
- (5) Mohamed, M. M. *Nature Reviews: Cancer* **2006**, *6*, 764.
- (6) McGrath, M. E. *Annu. Rev. Biophys. Biomol. Struct.* **1999**, *28*, 181-204.
- (7) Amir Masoud Sadaghiani, Steven H.L. Verhelst, Vasilena Gocheva, Kimberly Hill, Eva Majerova, Sherman Stinson, Johanna A. Joyce, and Matthew Bogoy *Chemistry and Biology* **2007**, *14*, 499-511.
- (8) Hernandez, A.; Roush, W. *Current Opinion in Chemical Biology* **2002**, *6*, 459-465.
- (9) Lecaille, F., Kaleta, J., and Bromme, D. *Chem. Rev.* **2002**, *102*, 4459-4488.
- (10) Yang, Z.; Cox, J. L. *Cancer. Cell. Int.* **2007**, *7*, 8.
- (11) Brinker, A.; Weber, E.; Stoll, D.; Voigt, J.; Muller, A.; Sewald, N.; Jung, G.; Wiesmuller, K.; Bohley, P. *Eur. J. Biochem.* **2000**, *267*, 5085-5092.
- (12) D. Bromme; J. Kaleta *Curr. Pharm. Des.* **2002**, *8*, 1639-1658.
- (13) Eakin, A.; McGrath, M.; McKerrow, J.; Fletterick, R.; Craik, C. *J. Biol. Chem* **1993**, *268*, 6115-6118.
- (14) Engel, J.; Doyle, P.; Hsieh, I.; McKerrow, J. *J. Exp. Med.* **1998**, *188*, 725-734.
- (15) Du, X.; Guo, C.; Hansell, E.; Doyle, P. S.; Caffrey, C. R.; Holler, T. P.; McKerrow, J. H.; Cohen, F. E. *J. Med. Chem* **2002**, *45*, 2695-2707.
- (16) Kirchhoff, L. V.; Gam, A. A.; Gilliam, F. C. *Am. J. Med.* **82**, 1987, 915-920.
- (17) Paulino, M.; Iribarne, F.; Dubin, M.; Aguilera-Morales, S.; Tapia, O.; Stoppani, A. O. M. *Mini Reviews in Medicinal Chemistry* **2005**, *5*, 499-519.

- (18) Docampo, R. *Curr. Pharm. Des* **2001**, 7, 1157.
- (19) Morel, C. M.; Lazdins, J. Disease Watch: Chagas Disease. <http://www.who.int/tdr/dw/chagas2003.htm>(2007).
- (20) M. Sajid and J.H. McKerrow *Molecular & Biochemical Parasitology* **2002**, 120, 1-21.
- (21) Sajid, M.; McKerrow, J. H. *Molecular and Biochemical Parasitology* **2002**, 120, 1-21.
- (22) Lisa K. Minor, Ed.; In *Handbook of Assay Development in Drug Discovery*; Drug Discovery; Taylor & Francis: USA, 2006; Vol. 5.
- (23) Palermo, C.; Joyce, J. A. *Trends in Pharmacological Sciences*, **2008**, 29, 22-28.
- (24) Vikash K. Dubey, Monu Pande, Bishal Kumar Singh and Medicherla V. Jagannadham *African Journal of Biotechnology* **2007**, 6, 1077-1086.
- (25) Mosi, R.; Baird, I. R.; Cox, J.; Anastassov, V.; Cameron, B.; Skerlj, R. T.; Fricker, S. P. *J. Med. Chem.* **2006**, 49, 5262-5272.
- (26) Charron Martin and William M. Wright In M.K. Skinner and M.D.Griswold, Ed.; Sertoli *Cell Biology*; 2005; pp 121.
- (27) Turk Dusan and Guncar Gregor, *Biological Crystallography*. **2003**, 59, 2.
- (28) Smith, S.; Gottesman, M. *J. Biol. Chem.* **1989**, 264, 20487-20495.
- (29) Klose, A.; Zigrino, p. Denhofer, R.; Mauch, C.; Hunzelmann, N. *Anal Biochem* **2006**, 353, 57-62.
- (30) Chen, S. Modeling, Design, and Development of Potential Inhibitors of γ -Glutamylamine Cyclotransferase and Inhibitors of Cruzain as Therapeutic Agents for Chagas' Disease. Ph.D. dissertation. Baylor University, United States- Texas, 2008.
- (31) Yamamoto, y. *Current Protein and Peptide Science* **2002**, 3.
- (32) Lecaille, F.; Authie, E.; Moreau, T.; Serveau, C.; Gauthier, F. Lalmanach, G. *Eur. J. Biochem.* **2001**, 268, 2733-2741.
- (33) Fujishima, A. *FEBS Letters* **1997**, 407, 47.
- (34) Puzer, L. *Archives of Biochemistry and Biophysics* **2004**, 430, 274.
- (35) Thompson S.; Halbert S.; Bossard M; Tomaszek T.; Levy M.; Zhao B.; Smith B.; Abdel-Meguid‡ S.; Janson C.; D'Alessio K.; McQueney M.; Amegadzie B.; Hanning C.; DesJarlais R.; Briand J.; and Sarkar S. *PNAS* **1997**, 94, 14249-14254.

- (36) H. Kakegawa; T. Nikawa; K. Tagami; H. Kamioka; K. Sumitani; T. Kawata; M. Drobnic-Kosorok; B. Lenarcic; V. Turk, N. *FEBS Lett.* **1993**, *321*, 247.
- (37) Wood, W.; Huang, L.; Ellman, J. *J. Comb. Chem.* **2003**, *5*, 869-880.
- (38) Rukamp Brian and James C. Powers **2002**, *84*. 976-981
- (39) T. Schirmeister; A. Klockow *Mini Reviews in Medicinal Chemistry* **2003**, *3*, 585.
- (40) McGrath, M. E. *Annu. Rev. Biophys. Biomol. Struct.* **1999**, *28*, 28, 181-204.
- (41) Ishidoh, K.; Kominami, E. *FEBS Lett* **1994**, *352*, 281-284.
- (42) Tsuge, H. *Biochemical and Biophysical Research Communications* **1999**, *266*, 411.
- (43) Gauthier, J. Y.; Chauret, N.; Cromlish, W.; Desmarais, S.; Duong, L. T.; Falgueyret, J.; Kimmel, D. B.; Lamontagne, S.; Léger, S.; LeRiche, T.; Li, C. S.; Massé, F.; McKay, D. J.; Nicoll-Griffith, D. A.; Oballa, R. M.; Palmer, J. T.; Percival, M. D.; Riendeau, D.; Robichaud, J.; Rodan, G. A.; Rodan, S. B.; Seto, C.; Thérien, M.; Truong, V.; Venuti, M. C.; Wesolowski, G.; Young, R. N.; Zamboni, R.; Black, W. C. *Bioorganic & Medicinal Chemistry Letters*, **2008**, *18*, 923-928.
- (44) Frlan, R.; Gobec, S. *Curr. Med. Chem.* **2006**, *13*, 2309-2327.
- (45) Barrett, A. J.; Kirschke, H. In [41] *Cathepsin B, cathepsin H, and cathepsin L*; Laszlo Lorand, Ed.; Methods in Enzymology, Academic Press: 1981; Vol. Volume 80, pp 535-561.
- (46) Menard, R.; Carmona, E.; Takebe, S.; Dufour, E.; Plouffe, C.; Mason, P.; Mort, J. S. *J Biol Chem* **1998**, *273*, 4478-4484.
- (47) Jerala, R.; Erovnik, E.; Kidri, J.; Turk, V. *J. Biol. Chem.* **1998**, *273*, 11498-11504.
- (48) Nomura, T. **1997**, *230*, 143.
- (49) Kihara, M.; Kakegawa, H.; Matano, Y.; Murata, E.; Tsuge, H.; Kido, H.; Katunuma, N. *Biol. Chem.* **2002**, *383*, 1925-1929.
- (50) Barrett, A. J. *Trends Biochem Sci.* **1987**, *12*, 193-196.
- (51) Turk, V.; Turk, B.; Turk, D. *Embo J* **2001**, *20*, 4629-4633.
- (52) Freije, J.; Balbin, M.; Abrahamson, M.; Velasco, G.; Dalboge, H.; Grubb, A.; Lopez-Otin, C. *J. Biol. Chem* **1993**, *268*, 15737-15741.
- (53) Barrett, A. J. In *Proteolytic Enzymes: Serine and Cysteine Peptidases*. In *Meth.Enzymol*; Ed. Academic: San Diego, CA, 1994; Vol. 244, pp 461-700.

- (54) Werle, B. *Biol. Chem.* **1999**, 380, 1109.
- (55) Li, R.; Chen, X.; Gong, B.; Selzer, P.; Li, Z.; Davidson, E.; Kurzban, G.; Miller, R.; Nuzum, E.; McKerrow, J.; Fletterick, R.; Gillmor, S.; Craik, C.; Kuntz, I.; Cohen, F.; Kenyon, G. *Bioorganic & Medicinal Chemistry* **1996**, 4, 1421-1427.
- (56) Zuzarte-Luis, V.; Montero, J.; Kawakami, Y.; Izpisua-Melmonte, J.; Hurle, J. *Developmental Biology* **2007**, 301, 205-217.
- (57) Siles R.; Chen S.; Zhou M.; Pinney K.G.; Trawick M.L. *Bioorganic & Medicinal Chemistry Letters* **2006**, 16, 4405-4409.
- (58) T. Schirmeister; U. Kaeppler *Mini Reviews in Medicinal Chemistry* **2003**, 3, 361-373.
- (59) Friedrich, B.; Jung, K.; Lein, M.; Turk, I.; Rudolph, B.; Hampel, G.; Schnorr, D.; Loening, S. A. *Eur J Cancer* **1999**, 35, 138.
- (60) Nomura, T. *journal of medical investigation* **2005**, 52.
- (61) Katunuma, N.; Tsuge, H.; Nukatsuka, M.; Asao, T.; Fukushima, M. *Archives of Biochemistry and Biophysics* **2002**, 397, 305-311.
- (62) Colella, R.; Goodwyn, E.; Gopal, P. *Cancer Lett* **2002**, 185, 163-172.
- (63) James, I.; Marquis, R.; Blake, S.; Hwang, S.; Gress, C.; Ru, Y.; Zembryki, D.; Yamashita, D.; McQueney, M.; Tomaszek, T.; Oh, H.; Gowen, M.; Veber, D.; Lark, M. *Journal of Biological Chemistry* **2001**, 276, 11507-11511.
- (64) Falguyret, J. -.; Oballa, R. M.; Okamoto, O.; Wesolowski, G.; Aubin, Y.; Rydzewski, R. M.; Prasit, P.; Riendeau, D.; Rodan, S. B.; Percival, M. D. *J. Med. Chem.* **2001**, 44, 94-104.
- (65) Nishimura, F. *American Journal of Pathology* **2002**, 161.
- (66) Huang, I.; Jan Bosch, B.; Li, F.; Li, W.; Hoa Lee, K.; Ghiran, S.; Vasilieva, N.; Dermody, T.; Harrison, S.; Dormitzer, P.; Farzan, M.; Rottier, P. *Journal of Biological Chemistry* **2006**, 281, 3198-3203.
- (67) Gopal, P.; Rehman, R.; Chadha, K.; Qiu, M.; Colella, R. *Oncol Rep* **2006**, 16, 313 - 320.
- (68) Zhang, M.; Altuwaijri, S.; Yeh, S. *Oncogene* **2004**, 23, 3080-3088.
- (69) Hashimoto, Y.; Kondo, C.; Kojima, T.; Nagata, H.; Moriyama, A.; Hayakawa, T.; Katunuma, N. *Cancer Biother. Radiopharm.* **2006**, 21, 217-224.
- (70) Colella, R.; Jackson, T.; Goodwyn, E. *Biotech & Histochemi* **2004**, 79, 121-127.

- (71) Dalet-Fumeron, V.; Guinec, N.; and Pagano, M. *FEBS Lett.* **1993**, *251*, 332.
- (72) Kobayashi, H.; Moniwa, N.; Sugimura, M.; Shinohara, H.; Ohi, H.; and Terao, T. *Biochim. Biophys. Acta* **1993**, *55*, 1178.
- (73) Campo, E.; Munoz, J.; Miquel, R.; Palacin, A.; Cardesa, A.; Sloane, B. F.; and Emmert-Buck, M. R. *Am. J. Pathol.* **1994**, *145*, 301-309.
- (74) Himmelstein, B. P.; Canete-Soler, R.; Bernhard, E. J.; and Muschel, R. J. *J. Cell Sci.* **1994**, *107*, 477.
- (75) Mai, J.; Finley, R. L., Jr.; Waisman, D. M.; and Sloane, B. F. *J. Biol. Chem.* **2000**, *275*, 12806-12812.
- (76) Kos, J.; Werle, B.; Lah, T.; and Brunner, N. *International Journal of Biological Markers* **2000**, *15*, 84-89.
- (77) Stahl, A.; and Mueller, B. M. *J. Cell Biol.* **1995**, *129*, 335-344.
- (78) Visscher, D. W.; Sloane, B. F.; Sameni, M.; Babiarz, J. W.; Jacobson, J.; and Crissman, J. D. *Mod. Pathol.* **1994**, *7*, 76.
- (79) Sinha, A. A.; Gleason, D. F.; Deleon, O. F.; Wilson, M. J.; and Sloane, B. F. *Anat. Rec.* **1993**, *235*, 233.
- (80) Shah, P.; Myers, M.; Beavers, M.; Purvis, J.; Jing, H.; Grieser, H.; Sharlow, E.; Napper, A.; Huryn, D.; Cooperman, B.; Smith III, A.; and Diamond S. *Mol Pharmacol* **2008**, *74*, 34-41.
- (81) Que, X.; and Reed, S. L. *Clin. Microbiol. Rev.* **2000**, *13*, 196-206.
- (82) Scharfstein, J.; Schmitz, V.; Morandi, V.; Capella, M. M.; Lima, A. P.; Morrot, A.; Juliano, L.; and Muller-Esterl, W. *J. Exp. Med.* **2000**, *192*, 1289.
- (83) McGrath, M. E.; Eakin, A. E.; Engel, J. C.; McKerrow, J. H.; Craik, C. S.; Fletterick, R. J. *J. Mol. Biol.* **1995**, *247*, 251-259.
- (84) Tarleton, R.; Zhang, L. *Parasitology Today* **1999**, *15*, 94-99.
- (85) Urbina, J.; Docampo, R. *Trends in Parasitology* **2003**, *19*, 495-501.
- (86) Cazzulo, J. J. *Medicinal Chemistry Reviews - Online* **2005**, *2*, 495-503.
- (87) Cazzulo, J. J.; Stoka, V.; Turk, V. *Curr. Pharm. Des.* **2001**, *7*, 1143-1156.
- (88) Barrett, M.; Burchmore, R.; Stich, A.; Lazzari, J.; Frasc, A.; Cazzulo, J.; Krishna, S. *The Lancet* **2003**, *362*, 1469-1480.

- (89) Eakin, A.; Mills, A.; Harth, G.; McKerrow, J.; Craik, C. *J. Biol. Chem.* **1992**, *267*, 7411-7420.
- (90) Guedes, P. M. M.; Fietto, J. L. R.; Lana, M.; Bahia, M. T. *Anti-Infective Agents in Medicinal Chemistry* **2006**, *5*, 175-186.
- (91) Centers for Disease Control and Prevention Chagas Disease Fact Sheet. http://www.cdc.gov/NCIDOD/DPD/PARASITES/chagasdisease/factsht_chagas_disease.htm (accessed 09/06, 2007).
- (92) Center of Disease Control and Prevention Chagas Disease. <http://www.cdc.gov/chagas/factsheet.html> (accessed 08/29, 2008).
- (93) Tyler, K. M.; Engman, D. M. *Int. J. Parasitol* **2001**, *31*, 472-480.
- (94) Lalmanach, G.; Mayer, R.; Serveau, C.; Scharfstein, J.; Gauthier, F. *Biochem. J.* **1996**, *318*, 395-399.
- (95) Murta A. *Mol and Biochem. Parasitology* **1990**, *43*, 27-38.
- (96) Choe, Y.; Brinen, L. S.; Price, M. S.; Engel, J. C.; Lange, M.; Grisostomi, C.; Weston, S. G.; Pallai, P. V.; Cheng, H.; Hardy, L. W. *Bioorg. Med. Chem.* **2005**, *13*, 2141-2156.
- (97) Lecaille, F.; Kaleta, J.; Bromme, D. *Chem. Rev.* **2002**, *102*, 4459-4488.
- (98) voet and voet, Ed.; In wiley, Ed.; .
- (99) Fersht, A. In *In Structure and Mechanism in Protein Science: A guide to Enzyme Catalysis and Protein Folding*; Julet, M. r., Hadler, G. L., W. H. Freeman and Company: United States of America, 2003; .
- (100) Shao, Y. Application of a fluorometric high-performance liquid chromatographic assay for the evaluation of substrates for and inhibitors of transglutaminase. Ph.D. dissertation. Baylor University. United States- Texas, 1992.
- (101) Lightcap, E. S.; Silverman, R. B. *J. Med. Chem.* **1996**, *39*, 686-694.
- (102) Morrison, John F and Stone, Stuart R. *Comments on Molecular and Cellular Biophysics* **1985**, *2*, 347.
- (103) Lohse, A.; Hardlei, T.; Jensen, A.; Plesner, I.; and Bols, M. *Biochem. J.* **2000**, *349*, 211-215.
- (104) Fox, T.; de Miguel, e.; Mort, J.; and Storer, J. *Biochemistry* **1992**, *31*, 12571-12576.
- (105) Szedlacsek, S.E. and Duggleby, R.G *Meth. Enzymol* **1995**, *249*, 144.

- (106) Williams, J. W.; Morrison, J. F. *Meth. Enzymol* **1979**, *63*, 437-467.
- (107) Lipinski, C. *Advanced Drug Delivery Reviews* **1997**, *23*, 3.
- (108) Lindvall, M. K. *current pharmaceutical design* **2002**, *8*, 1673.
- (109) Katunuma, N. *FEBS Letters* **1999**, *458*, 6.
- (110) Vicik, R.; Busemann, M.; Baumann, K.; Schirmeister, T. *Current Topics in Medicinal Chemistry* **2006**, *6*, 331-353.
- (111) Radim Vicik, Verena Hoerr, Melanie Glaser, Martina Schultheis, Elizabeth Hansell, James H. McKerrow, Ulrike Holzgrabe, Conor R. Caffrey, Alicia Ponte-Sucre, Heidrun Moll, August Stichb and Tanja Schirmeistera *Bioorganic & Medicinal Chemistry Letters* **2006**, *16*, 2753.
- (112) Robichaud, J. *J. Med. Chem.* **2003**, *46*, 3709.
- (113) Nkemgu, J. *International Journal of Antimicrobial Agents* **2003**, *22*, 155.
- (114) Aguirre, G.; Cabrera, E.; Cerecetto, H.; Di Maio, R.; Gonzalez, M.; Seoane, G.; Duffaut, A.; Denicola, A.; Gil, M. J.; Martinez-Merino, V. *Eur. J. Med. Chem.* **2004**, *39*, 421-431.
- (115) Fujii, N.; Mallari, J. P.; Hansell, E. J.; Mackey, Z.; Doyle, P.; Zhou, Y. M.; Gut, J.; Rosenthal, P. J.; McKerrow, J. H.; Guy, R. K. *Bioorganic & Medicinal Chemistry* **2005**, *15*, 121-123.
- (116) Du, X.; Guo, C.; Hansell, E.; Doyle, P. S.; Caffrey, C. R.; Holler, T. P.; McKerrow, J. H.; Cohen, F. E. *J. Med. Chem.* **2002**, *45*, 2695.
- (117) Siles, R.; Chen, S.; Zhou, M.; Pinney, K.; Trawick, M. *Bioorganic & Medicinal Chemistry Letters* **2006**, *16*, 4405-4409.
- (118) Brak, K.; Doyle, P.; McKerrow, J.; and Ellman J. *J. Am. Chem. Soc.* **2008**, *130*, 6404-6410.
- (119) Siles, R. Design, synthesis, and biological evaluation of new anti-cancer nitrogencontaining combretastatins and novel cysteine protease inhibitors for the treatment of Chagas, Ph.D. dissertation Baylor University, United States - Texas, 2006.
- (120) ATCC. <http://www.atcc.org> (accessed 10/25, 2008).
- (121) Hulkower, K. **2000**, *267*, 4165.
- (122) Makkar, G.; Ng, N.; Yeung, W.; and Ho, P. *Hong Kong Med J* **2003**, *9*.
- (123) Peterson, G. L. *Analytical Biochemistry* **1979**, *100*, 201-220.

- (124) Elojeimy, S. *FEBS Letters* **2006**, 580, 4751.
- (125) Millipore Immunodetection: Application and Product Guide. www.millipore.com (accessed 02/12, 2007).
- (126) Donald Allison, R.; Purich, D. L. *Methods in Enzymology* **1979**, 63, 3-22.
- (127) Krupa, J. C. *Analytical Biochemistry* **2000**, 283, 99.
- (128) Nomura, T.; Fujishima, A.; Fujisawa, Y. *Biochemical and Biophysical Research Communications*, **1996**, 228, 792-796.
- (129) Santamaria, I.; Velasco, G.; Cazorla, M.; Fueyo, A.; Campo, E.; Lopez-Otin, C. *Cancer Res* **1998**, 58, 624-630.
- (130) Heidtmann, H.; Salge, U.; Havemann, K.; Kirschke, H.; Wiesmuller, K. *ONCOL RES* **1993**, 5, 441-451.
- (131) Elizabeth Hansell **2004**, 1-4.
- (132) Bradford, M. *Anal. Biochem.* **1976**, 72, 248-254.
- (133) Luis Sanchez TCA.
http://www.its.caltech.edu/~bjorker/Protocols/TCA_ppt_protocol.pdf (accessed 10/25, 2007).
- (134) <http://bh.sanofi-aventis.com/live/bh/medias/09A8DA30-E0C3-4699-A0CA-FF6006B552B2.gif> (accessed 10/16, 2007).
- (135) Cell invasion assay diagram. www.cellbiolabs.com (accessed 05/11, 2007).
- (136) <http://www.rsc.org/ej/P1/2001/b105117m/b105117m-fl.gif> (accessed 11/09, 2008)
- (137) United States patent application serial number 12/186,806, filed 13 June 2008.